Institut für Landtechnik
der Rheinischen Friedrich-Wilhelms-Universität Bonn

Modelling and Measurement of Soil Moisture Content Based on a Remote Sensing Method for Applications in Semi-Arid Tropics

Inaugural-Dissertation

zur

Erlangung des Grades

Doktor der Agrarwissenschaften
(Dr agr.)

der

Hohen Landwirtschaftlichen Fakultät

der

Rheinischen Friedrich-Wilhelms-Universität
zu Bonn

vorgelegt am 19 04 1999

von

M.Sc. Baanda A. Salim

aus

Morogoro, Tansania

Referent: Prof. Dr.-Ing. Peter Schulze Lammers
Korreferent: PD Dr.-Ing. Armin Rieser
Tag der mündlichen Prüfung: 18. Juni 1999

D 98

Bezugsquelle: Institut für Landtechnik
der Rheinischen Friedrich-Wilhelms-Universität Bonn
Nussallee 5
53115 Bonn

Vervielfältigt und gedruckt mit Unterstützung des Deutschen Akademischen Austauschdienstes.

Modelling and Measurement of Soil Moisture Content Based on a Remote Sensing Method for Applications in Semi-Arid Tropics

ABSTRACT

Soil moisture plays a very crucial role in land surface processes. It should therefore be monitored with the same accuracy and frequency as other important environmental variables. Two approaches are used for estimation of soil moisture content, namely, modelling and measurement, either in-situ or remote. Integration of modelling and measurements may provide the best solution towards estimation of soil moisture content

The utility of ground-based thermal infrared remote sensing method for the estimation of near-surface soil water content was tested under tropical semi-arid agricultural conditions in Morogoro, Tanzania, East Africa. Field experiments were conducted between January and August, 1997 at a bare soil site. Regression relationships between the daily maximum surface soil temperature minus air temperature (TDMax) and weighted-average soil water contents to different depths in the soil profile were developed based on the measured data. Better correlations were obtained for the top 0-5 and 0-15 cm layers of the soil, with coefficients of determination of 0.81 and 0.78, respectively. Use of "Normalized TDMax" as well as cloudness-cover-corrected "Normalized TDMax" (TDaMax) resulted in even better coefficients of determination (e.g., 0.95 for the 5 cm depth).

A physically based model of coupled flow of heat and water in the soil (SUAHEAT) was developed. The SUAHEAT model was tested by comparing its simulated soil water contents and soil temperatures with those measured at the bare soil site. Both qualitative as well as quantitative methods were used to evaluate the model performance, for the calibration and validation phases. For the calibration phase, the average values of the mean absolute difference (MAD) of soil water content were 0.06, 0.05, 0.05, and 0.03 m^3/m^3 for the 5, 15, 30, and 45 cm depths, respectively. The corresponding average values of the root mean square difference (RMSD) of soil water content were 0.07, 0.06, 0.05, and 0.03 m^3/m^3 for the same depths, respectively. As for the validation phase, the average MAD values of soil water content were 0.09, 0.05, 0.08, and 0.17 m^3/m^3 for the same depths, respectively. The corresponding average RMSD values for the same depths were 0.12, 0.08, 0.10, and 0.19 m^3/m^3, respectively. The unusually large errors (at the 45 cm depth) during the validation phase could be attributed to the overestimation of soil water content values during very wet conditions arising from the calibration equation used.

The performance of the model in the simulation of surface, near-surface, and profile soil temperatures was also both qualitatively and quantitatively evaluated. In the calibration phase, the MAD values were 2.8, 1.1, 0.5, and 0.3 °C for the 5, 15, 30, and 45 cm depths, respectively.

The corresponding RMSD values for the same depths were 3.5, 1.3, 0.6, and 0.4 °C, respectively. For the validation phase, the MAD values for the same depths were 2.3, 1.2, 0.7, and 0.4 °C, respectively. The corresponding RMSD values for the same depths were 2.7, 1.4, 0.8, and 0.5 °C, respectively. Generally, the errors obtained with the use of the SUAHEAT model are comparable to values obtained by other researchers elsewhere using similar models.

Integration of the model with remotely sensed surface soil water content and temperature data was effected through use of the initial profiles of soil water content and temperature. The initial profile data were derived from the regression relationships between TDMax and surface soil water content on the one hand, and between the surface and profile soil temperatures on the other, respectively. Model simulation results obtained using the remotely sensed initial conditions indicated that it is feasible to use remotely sensed data (one value of TDMax per day) to initialize the model. Similarly, extrapolation of the remotely sensed near-surface (0-5 cm depth) soil water content to values at greater depths in the soil profile was shown to be feasible.

Modelling and Measurement of Soil Moisture Content Based on a Remote Sensing Method for Applications in Semi-Arid Tropics

KURZFASSUNG

Bodenfeuchte spielt eine wesentliche Rolle bei den Prozessen in landwirtschaftlich genutzten Böden. Die Verfügbarkeit von Wasser sollte deshalb mit der gleichen Häufigkeit und Genauigkeit verfolgt werden, wie andere Umweltfaktoren Zwei generelle Ansätze werden für die Bestimmung der Bodenfeuchte angewendet, zum einen die Modellierung und zum anderen die Messung entweder in-situ oder kontaktlos (remote) Die Zusammenführung beider Methoden verspricht einen Fortschritt für die Bestimmung der Bodenfeuchte

Im Rahmen der Forschungsarbeiten wurde das Thermal-Infrarot als Sensorprinzip für die Bestimmung der Bodenfeuchte im Hinblick auf den Einsatz in tropisch semiariden Klimaten untersucht. Die Feldversuche wurden in Morogoro/ Tanzania (Ostafrika) in der Zeit von Januar bis August 1997 mit einer bodenbasierten Versuchsstation auf Boden ohne Bewuchs durchgeführt Es wurden Regressionsfunktionen aus den Meßdaten der täglichen Maximaldifferenz zwischen Bodenoberflächentemperatur und der Lufttemperatur (TDMax) und der gewichteten Bodenfeuchte verschiedener Bodenschichten errechnet. Für die Bodenschichten zwischen 0 - 5 cm und 0 - 15 cm wurden Bestimmtheitsmaß von 0,81 und 0,78 erreicht Die Einführung einer normalisierten täglichen Temperaturdifferenz (Normalized TDMax) führte zu besseren Korrelationen. Für die obere Bodenschicht von 5 cm wurde damit ein Bestimmtheitsmaß von 0,95 erreicht

Als ein weiterer Schwerpunkt der Forschungsarbeiten wurde ein physikalisch basiertes Simulationsmodell für den gekoppelten Wärme- und Wasserfluß (SUAHEAT) entwickelt. Die Ergebnisse des SUAHAET-Modells wurden für den Verlauf der Bodenfeuchte und der Temperatur im Boden mit den gemessenen Daten verglichen. Für die Kalibrierung und Validierung wurden zunächst qualitative und abschließend quantitative Methoden angewendet. Für die Kalibrierungsphase können als mittlere absolute Differenzen (MAD) für die Bodenfeuchte Werte von 0,06; 0,05; 0,05 und 0,03 m^3/m^3 für die Tiefen 5, 15, 30 und 45 cm angeben werden und als Standardabweichung (RMSD) 0,07; 0,06; 0,05 und 0,03 m^3/m^3. In der Validierungsphase wurden MAD-Werte von 0,09, 0,05, 0,08 und 0,017 m^3/m^3 und als Standarabweichung die Werte 0,12, 0,08; 0,10 und 0,19 m^3/m^3 für die dieselben Bodentiefen erreicht. Der hohe Fehler im Bereich der 45 cm Bodenschicht in der Validierungsphase wird der Überschätzung der Bodenfeuchte durch das Modell aufgrund der sehr feuchten Bodenverhältnisse in der Kalibrierungsphase zugeschrieben.

Die Simulationsergebnisse des Modells SUAHEAT bezüglich der Bodentemperaturen im Oberflächenbereich und der Temperaturprofile bis zur Bodentiefe von 45 cm wurden ebenfalls mit quantitativen und qualitativen Methoden bewertet In der Kalibrierungsphase wurden hier MAD-Werte von 2,8; 1,1; 0,5 und 0,3 °C für die Bodentiefen 5, 15, 30 und 45 cm erreicht Die Standardabweichungen betrugen 3,5; 1,3; 0,6 und 0,4 °C In der Validierungsphase waren die MAD-Werte 2,3; 1,2; 0,7 und 0,4 °C und die Standardabweichung erreichte Werte von 2,7; 1,4, 0,8; und 0,5 °C. Damit kann die Qualität der Simulationsergebnisse, die mit dem SUAHEAT-Programm berechnet wurden, in den Fehlerbereich anderer Forschungsarbeiten, in denen ähnliche Programme entwickelt wurden, eingeordnet werden.

Die Integration des Modells mit den durch Thermal-Infrarot ermittelten Daten bezüglich Bodenfeuchte und Bodentemperatur wurde durch Initialisierung mit den Anfangsprofilen erreicht. Die Simulationsergebnisse zeigen, daß es möglich ist, mit den berührungslos ermittelten Anfangswerten (ein Wert für TDMax pro Tag) das Modell zu initialisieren Gleichfalls führt die Extrapolation der berührungslos ermittelten Oberflächendaten für die Bodenfeuchte auf das Bodenfeuchteprofil zu einer ausreichenden Genauigkeit

ACKNOWLEDGEMENTS

I received a lot of assistance and support both materially and morally from quite a number of people both at the Institut fuer Landtechnik (IfL), University of Bonn in Germany and at the Sokoine University of Agriculture (SUA) in Tanzania. It is difficult to mention all of them by names. I would, however, like to express my heartfelt gratitude to the following

My supervisor, Prof. Dr.-Ing. Peter Schulze Lammers, for the untiring work of supervision, and moral and material support. His assistance in the English-to-German translation is also highly acknowledged. PD Dr.-Ing. Armin Rieser, my co-supervisor at the University of Bonn, for his untiring support. Dr. Peter Mtakwa, my local supervisor at SUA, for his assistance during my research work in Tanzania. All the staff at the IfL workshop, especially Mr. Dreesen, for the technical assistance they provided whenever requested. Ms Nilgül Karabulut and Ms Frauke Beeken for the painstaking work of English-to-German translation. Drs Peter Boeker, Lutz Damerow, and Gereon Broil for their moral and material support. The director of the IfL, Prof. Dr.-Ing. K.-H. Kromer, for his moral and material support. The director's secretary, Mrs. Effelsberg-Fussel, for her ever-charming character which never ceased to amuse me and actually made me feel at home in Germany. Prof. Dr.-Ing. M. Schätzke for his encouragement and never-ceasing fatherly care. He actually made me feel very much at home and ease in Germany. I will always remember his words "es ist verboten am Wochenende zu arbeiten" - meaning "it is not allowed to work during the weekends". Ms Sonntag, Prof. Schätzke's secretary, for her moral and material support. Emeritus Prof. Dr.-Ing. Brinkmann and his wife for their never-ceasing care and friendliness which helped rekindle my hopes at times of despair. My colleague Günter Römer and his family, with whom I had both academic and social discussions. My colleague Christoph Stephan and his family for their kindness. Mrs. Reinhardt, Mrs. Wolff, Mr. Johannes Niess and all staff members and colleagues at the IfL for their moral support and encouragement during the course of my studies. Staff members at the University library (ZBL), especially at the issue desk, for their assistance, friendliness, and understanding

The SACCAR-GTZ-SUA Project at the Department of Agricultural Engineering and Land Planning (DAELP), SUA for funding my studies and the DAAD in Bonn for administering the scholarship. I owe special thanks to Prof. Dr. V. Roenick, the project coordinator at the DAELP for his support. I also owe special thanks to Mrs. Birgitt Skailes, my official-in-charge at the DAAD in Bonn, for her care and support during all the period of my study and stay in Germany. My employer, SUA, for granting me an extended study leave, supporting and facilitating my research work in Tanzania. All the staff at the DAELP workshop for their technical support during my field experiments in Tanzania. The office of the head of DAELP for both material and logistical support. Messrs. Haruna Baanda, Bakari Baanda, Adam Baanda and Shaibu Mrope, without whose assistance and perseverance the research work in Tanzania wouldn't have come to fruition. Dr. Matthew Mulengera, for his assistance during my field experiments at SUA. Prof. B. Kayombo and Dr. H.O. Dihenga for lending me their laptop computer and for their advice. Dr. John Msuya, with whom I was in Germany, for his encouragement and words of advice. Lastly but in any case not least my dearest wife Zukra for bearing the burden of taking care of our family during my absence from home and for persevering the torture of separation. Our daughters Keja and Hawa for their understanding and persevering the absence of the fatherly care. They have always been a constant inspiration to me and a source of strength to my work. My parents and the rest of the family members for their support during my absence from home.

DEDICATION

Dedicated to my parents, who believed and still believe in the power of the pen I wouldn't have reached this far if it were not for their support and the Grace of Allah

TABLE OF CONTENTS

LIST OF FIGURES

LIST OF TABLES

LIST OF SYMBOLS (units as given in the text)

θ	volumetric soil water content
θ_{sat}	saturated soil water content
λ	thermal conductivity for the soil
$\theta_{wavg}(z,t)$	weighted-average soil water content
$\theta_z(t)$	profile soil water content
$\theta_{zmax}(t)$	bottom boundary volumetric soil water content
C	volumetric heat capacity
C_a	volumetric heat capacity of air
d	zero displacement height
E	evaporative flux
g	acceleration due to gravity
G	soil heaf flux
h	pressure head
H	sensible heat flux
H_o	saturation humidity of air at the soil surface
h_s	pressure head at the soil surface
H_s	humidity at the soil surface
$h_{wavg}(z,t)$	weighted-average pressure head
$h_z(t)$	profile pressure head
$h_{zmax}(t)$	bottom boundary pressure head
k	von Karman's constant
M	moisture availability
M_w	molar mass of water
r	aerodynamic resistance
r^2	coefficient of determination
R	gas constant
r_a	aerodynamic resistance
R_{dg}	daily global solar radiation
R_n	net radiation
r_s	soil resistance for water transport
T	temperature
T_a	air temperature
T_d	dewpoint temperature
T_s	soil surface temperature
$T_z(t)$	profile soil temperature
$T_{zmax}(t)$	bottom boundary soil temperature
u_a	wind speed
z	depth (or height)
z_a	measurement height for air temperature
z_m	measurement height for air temperature
z_{max}	maximum depth in the soil
z_{oh}	roughness length for sensible heat
z_{om}	roughness length for momentum

LIST OF ABBREVIATIONS

ALES	latent heat flux
DOY	Day of Year
GS	soil heat flux
GSCUM	cummulative soil heat flux
MAD	mean absolute difference
N	number of observations
PAVG	weighted-average pressure head
PSI	pressure head
RA	aerodynamic resistance
RMSD	root mean square difference
RN	net radiation
RS	bare soil resistance
SE	standard error
SEY	standard error for the estimation of Y
SH	sensible heat flux
SSE	residual sum of squares
SSR	sum of squares due to regression
SWC	soil water content
TD	soil surface temperature minus air temperature difference
TDa	equilibrium TD
TDaMax	daily maximum TDa
TDEW	dewpoint temperature
TDMax	daily maximum TD
THETA	soil water content
WAVG	weighted-average soil water content
WSPEED	wind speed
Z	depth
ZM	measurement height
ZO	surface roughness length

1 INTRODUCTION AND STUDY OBJECTIVES

1.1 Introduction

Greater understanding of the spatial and temporal dynamics of water under different soil conditions and cultural practices is required for the best use of available water resources while minimizing environmental pollution. There is an apparent continuous need for better methods to perform accurate, real-time, nearly continuous soil water measurements at specific soil depth intervals with minimal soil disturbance and covering large areas.

New developments in precision agriculture, remote sensing, surface and subsurface preferential water flow patterns, simulation models for soil-water-plant-atmosphere interrelationships over large areas and permanent watch of leakage from the waste material depositing sites will depend upon accurate *"ground truth"* data provided by independent real-time soil water content monitoring systems covering micro to large scale hydrobasins.

Soil water content is probably the most easily recognized tangible soil property. A number of hydrologic, biological and meteorological processes are controlled by the amount of water in the top metre of the earth's soil. Soil moisture in the top few centimetres governs the partitioning of rainfall into infiltration and surface runoff, the latter being the major source of flood flow in many streams and rivers. The rate of evaporation of water from soil is strongly dependent upon the amount of moisture near the soil surface. Transpiration and growth of crops and other plants depend upon the availability of water to the plant roots. Because a significant quantity of heat is absorbed when vaporization of liquid water occurs, the rates of evaporation and transpiration have a significant influence upon the energy balance of the surface of the earth. Therefore, soil moisture affects weather and climate by controlling the sensible and latent heat fluxes into the atmosphere. Analysis of the above-mentioned processes is often complicated by the extant variability of the soil moisture content both in space and time.

Despite the recognition of the importance of soil water content , our ability to measure and monitor it has been limiting to modelling efforts, especially at large spatial scales. Two approaches are used for estimation of soil moisture content, namely, modelling and

measurement, either in-situ or remote. All measurement methods rely on the dependence of some physical property of the soil upon its moisture content. In-situ measurements can yield highly accurate estimates of conditions at a particular site. However, since these estimates are based on relatively small volumes of soil, and since moisture content is highly variable in space and time, good estimates of the average moisture content of large areas require extensive and expensive observation.

Remote sensing methods, on the other hand, generally perform areal integration directly in the observation process. Their main disadvantage is their inability to sense beyond the surface (0 to 10 cm depth) soil layer. It is very important to recognize that in all remote sensing methods it is an intensity of electromagnetic radiation that is actually measured and from it physical characteristics or fluxes would have to be derived. In general the measured electromagnetic intensity depends upon many surface and atmospheric characteristics which almost invariably introduce uncertainties in the derived surface physical characteristics or fluxes. Remote sensing signals therefore contain significant statistical noise in them and in the values of moisture content inferred therefrom.

Modelling and measurement are both useful, though imperfect, techniques for the determination of the amount of moisture in the soil. It is reasonable to expect that a combination of these approaches, if feasible, would yield more accurate estimates of soil moisture than could be obtained from either approach alone. Therefore, a cost effective soil moisture monitoring program must utilize both approaches and not just one. An integrated system should be designed. The methods for measuring soil water content are continuing to evolve and improve. Advances in electronic technology and data logging capabilities have greatly strengthened the monitoring possibilities.

In order to enhance the utility of the remotely sensed soil moisture measurements to hydrological and agricultural applications, procedures and models are needed which will relate the profile moisture conditions to those of the surface zone. In other words, extrapolation of the surface measurements to the root-zone values is necessary. Empirical methods (based on statistical analysis and/or neural networks) may be used to achieve this goal. However, results obtained

using these methods are site specific. This means, therefore, that results obtained in a particular area cannot be transferred to another area under different climatic and soil conditions. Coupling of the remote sensing based surface measurements of soil moisture content with physically based models of heat and water flow provides a more flexible alternative

The importance of estimating the soil moisture and temperature profiles down to depths beyond the penetration reach of remote sensing radiometric observations has prompted numerous studies into this topic. Remote sensing observations (of microwave emission) may be used in conjunction with empirical formulae to estimate the surface soil water content $\theta(0)$ or matric potential $\psi(0)$. Sequential (passive microwave) observations together with empirical relations can be used to equate the emitted radiation to surface soil moisture The near-surface (0-5 cm depth) volumetric soil moisture values can then be used as the boundary conditions in a numerical model of soil water and heat flow in order to estimate the hydrologic conditions in an integrated depth within the soil column

Of the remote sensing methods, thermal infrared method offers a more cost-effective means of monitoring the Earth surface processes, including surface soil moisture content. This is because surface temperature can easily, directly, and accurately be measured The availability of small hand-held infrared thermometers makes this method even much more attractive for small-scale ground-based research However, measurement of the surface radiant temperature is complicated by the many physical factors that influence the observed temperatures. The utility of thermal remote sensing has been hampered by

the difficulty of calibration and correction of measured radiances to consistent physical properties,

the limited ability to estimate accurately the surface energy fluxes over complex terrain, which might consist of a mixture of vegetation (including forests), sloping surfaces, water bodies, bare soil and urban landscapes, and

the detection and removal of the effect of clouds

The use of remote sensing in the thermal infrared has, thus, (so far) not achieved operational status over the Earth's land surfaces. Inspite of all these deficiencies, the topic is of increasing importance as mankind's alteration of substantial areas of the globe produces effects on the local and global exchange of heat and moisture with the atmosphere. These factors ultimately control our physical environment and our ability to produce food and fibre to sustain ourselves. The thermal-infrared spectral region offers the best hope of monitoring global surface conditions on a regular cost-effective basis. Research in this technical discipline will improve our understanding of climatic processes near the Earth's surface. Many scientists are of the view that a multispectral approach to remote sensing, including thermal infrared temperature measurements, will prove to be essential (Carlson et al , 1995)

Substantial research and developmental efforts have in recent years been directed towards the estimation of surficial soil moisture status primarily using remote sensing data and then from airborne microwave radars and radiometers following an empirical correlative approach (Schmugge et al , 1978; Jackson and Schmugge, 1989; Perry and Carlson, 1988, Soares et al., 1987, Ijjas and Rao 1992; John, 1992, Shaha, 1995).

A few studies (Idso et al. 1975a; Van de Griend et al. 1985; Perry and Carlson 1988; Myhre and Shih, 1990; Saha, 1995) have shown the feasibility of using remotely sensed thermal infrared data collected through ground and airborne radiometers for estimating surface soil moisture. Soer (1980) developed a methodology for estimating root zone soil moisture using canopy surface temperatures derived from remotely sensed (airborne) thermal infrared data, with the aid of a soil-plant system-heat and moisture balance Tergra model (Soer 1977). Myhre and Shih (1990) used infrared thermometry to estimate soil water content for a sandy soil.

The importance of small-scale intensive field experiments aimed at further testing the utility of the thermal infrared method is evident. This is especially important in the developing countries where large-scale intensive field experiments, which normally involve a lot of financial investment, cannot be conducted due to limitations of financial resources. Most of the previous small-scale field experiments have been conducted under artificial conditions, in which case irrigation and/or lysimeters were used. The spatial and temporal variability of soil moisture

content as a result of the spatial (and temporal) variability of the soil physical, hydraulic, and thermal properties even at (spatial) scales of a few metres, necessitates the carrying out of such studies under natural field conditions. This is especially the case in the arid and semi-arid regions because of the extant surface heterogeneity. This study is therefore based on field experiments conducted under natural field conditions.

This study looks at the modelling and measurement of soil moisture content based on "ground" thermal infrared remote sensing measurement of surface soil temperature. The study was stimulated by the continuing need for development of methods for profile moisture estimation from remote sensing measurements of near-surface (0-5 cm depth) soil moisture content (see for example, Rawls and Jackson, 1997). The problems inherent in the remote sensing of soil moisture content could be overcome with an appropriate model that simulates the dynamics of water and heat movement in the soil. This study is therefore only an attempt towards addressing the problems, albeit on a small-scale basis. Notwithstanding its deficiencies, especially as far as detecting of near-surface soil moisture content is concerned, the thermal infrared remote sensing technique offers a more cost-effective means of repetitively monitoring of the states and fluxes of the surface of the Earth.

The main focus of the research was to study the relationship between the surface radiant temperature and near-surface soil water content under natural semi-arid agricultural conditions at field scale. Extrapolation of these surface measurements to root-zone values through coupling of field measurements with modelling approaches was the ultimate goal of the study bearing in mind the utility of subsurface soil water content values for agronomical applications. The use of the surface radiant temperature for estimation of the latent and sensible heat fluxes at the soil-atmosphere interface was also addressed. The relative cheapness of the thermal infrared sensors was the main drive towards the choice of the method.

1.2 Study objectives

The overall objective of this study was development of a model and an estimation method for soil water content based on a remote sensing method for applications in tropical semi-arid conditions. The specific objectives were:

- To develop a method of estimating soil water content using thermal infrared thermometer measurements on a bare soil surface.
- To describe the relationship between maximum soil surface-minus-air temperature differential (TDMax) and soil water cotent at different depths in the soil profile.
- To determine if soil water content estimation can be improved by using another term
- To study the feasibility of the method under tropical semi-arid conditions.
- To establish the depth to which soil water contents may be inferred from surface-minus-air temperature measurements under tropical semi-arid conditions
- To assess the effects of clouds on the sensor response under bare soil conditions.
- To couple field measurements with modelling approaches with the view of reducing the need for frequent field measurements.

1.3 Outline of the thesis

Chapter 2 treats the choice of the study area and in particular the semi-arid tropics (SAT). A brief review of the measurement methods for soil water content is dealt with in chapter 3. Future trends in the measurement methods for soil water content are also briefly covered in this chapter Chapter 4 handles in more detail the remote sensing techniques for the estimation of soil water content. Especially the thermal infrared technique is covered in a much more detail. Model formulation and theoretical treatment of the coupled flow of heat and water are handled in chapter 5. Description of the field experimental work including field sensor calibration is dealt with in chapter 6. Results and discussion are treated in chapter 7 and finally the thesis winds up with summary and conclusions in chapter 8. Recommendations for further research are also highlighted at the end of chapter 8.

2 CHOICE OF THE STUDY AREA

2.1 Introduction

The need for remote measurements of soil moisture is seldom more urgent than over regions experiencing severe drought. Rainfall is the most significant climatic factor that controls food production in the tropics, ranging from the extreme desertic zones to the tropical rainforests. Despite very high total rainfalls, drought in the seasonal tropics is a regularly occurring problem. Since these tropical areas have distinct wet-dry seasons, part of the year is not very productive for plant growth despite the favourable temperatures. In addition, whether or not there are wet-dry cycles to contend with, there is great variability in rain so that there may be exceedingly dry periods at unexpected times. This study was therefore deliberately carried out under tropical semi-arid conditions with the intention of further testing the utility of the thermal infrared method under those conditions. The method has been shown to give greatest sensitivity for low values of moisture availability ($M = \theta/\theta_{sat}$) (Carlson, 1984). Semi-arid areas probably offer the best chance of obtaining accurate surface soil moisture estimates from any of the available remote sensing techniques (Beven and Fisher, 1996).

2.2 The Semi-Arid Tropics (SAT)

2.2.1 General overview

Troll (1965) (as cited by El-Swaify et al., 1985) defines the semi-arid tropics (SAT) in the context of vegetation zone delineation as the region within the tropics where the mean monthly rainfall exceeds mean potential evapotranspiration during 2 to 7 months of the year. Within this region the areas where this excess lasts for 2 to 4.5 months are characterized by thorn Savannah vegetation and those where it lasts for 4.5 to 7 months are characterized by dry Savannah; these are called the dry SAT and wet-dry SAT, respectively.

Based on Troll's (1965) definition, the SAT comprise all or part of 48 countries on four continents (*see Fig. 2.1*). Of these countries all but Australia are less developed. The region covers much of the African continent stretching in a broad band from west to east below the Sahara desert, and including much of eastern and south-central Africa. In Asia it includes most of India (which contains the single largest SAT area of any country, nearly 9 % of the global total), northeastern Burma, and Thailand. Most of northern Australia, nearly all of Mexico, and large portions of Venezuela, Guyana, Surinam, French Guinea, Brazil, Paraguay, and Bolivia also lie within this region (Swindale, 1982 as cited by El-Swaify et al., 1985).

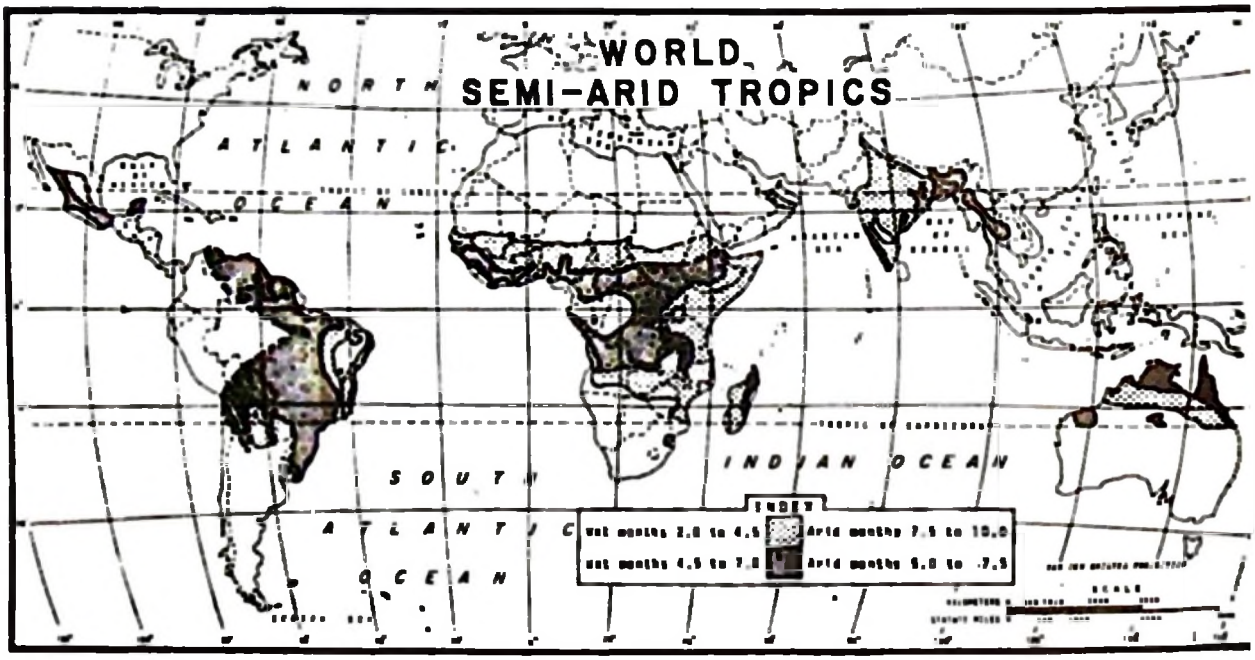

Fig. 2.1 Global distribution of the semi-arid tropics (SAT). Source: Ryan et al. (1974).

The total area of the SAT is estimated at about 19.6 million km² (Ryan, 1974 as cited by El-Swaify et al., 1985). Here, more than one billion, mostly impoverished, people live.

The important staple crops in the semi-arid tropics are sorghum (*Sorghum bicolor* (L.) Moench), pearl millet (*Pennisetum americanum* (L.) Leeke), pigeonpea (*Cajanus cajan* (L.) Millsp.), chickpea (*Cicer arietinum* L.), groundnuts (*Arachis hypogaea* L.), [and maize (*Zea mays* L.)]. More than about 50% of the respective crops are produced and consumed directly as human

food thus serving as the main source of carbohydrate, protein, and fat for people living in the SAT.

The most critical characteristic of the SAT from the agricultural utilization viewpoint is the definite seasonality of rainfall. Nearly 90 % of the rainfall is received during the summer: April to October in the northern hemisphere, and October to April in the southern hemisphere (Krishnan, 1975 as cited by El-Swaify et al , 1985) While rainfall seasonality seems clearly predictable, actual precipitation varies widely among various SAT locations and from year to year so that coefficient of variation (CV) values of 30 % or more are not uncommon. This variability also extends to the dates of rainfall arrival and withdrawal as well as its distribution within the rainy season Individual storm characteristics are also quite variable but, as a rule, a substantial portion of the total annual rainfall is accounted for by a few large, often intense, and highly erosive storms. For this, and other related reasons, SAT regions are generally considered to be of high potential erosion hazard (El-Swaify et al , 1982 as cited by El-Swaify et al., 1985). For rainfed agriculture, primary consideration is given to the duration of the effective rainfall period (and subsequently available soil water) which determines the successful establishment and sustainment of the cropping systems The classification of tropical climatic zones are usually based on the amount and seasonal distribution of rainfall.

The soil moisture regimes common to the tropics have been identified as udic, ustic, aridic and aquic (Sanchez, 1976 as cited by Thomas et al., 1984). The classification is based on the terminology and definition of U.S. Soil Taxonomy System (Soil Survey Staff, 1975 as cited by Thomas et al., 1984). The udic soil moisture regime implies that for most of the year water stress will not be a factor. This regime corresponds to the rainy or equatorial climate of the tropics and represents about 29 percent of the tropics. The ustic moisture regime describes soil conditions that have a definite dry season of several months and relates to the seasonal or monsoonal climates. This regime includes about one-third of the soils of the tropics. The aridic implies an even longer dry season than the ustic and relates to the dry desert climates. About 29 percent of the land area is aridic. Aquic moisture regimes are associated with poorly drained sites (Thomas et al., 1984).

The highest temperatures in the SAT are generally attained just before the onset of the rainy season. Prevailing temperatures and the fact that the mean annual values for solar radiation generally vary between 16 and 21 MJ/m²/day (Landsberg et al , 1963; Thompson, 1965 as cited by El-Swaify et al., 1985, see also Fig. 2.2) indicate that the SAT environments possess a high potential for year-round cropping. Actual utilization of this potential, however, is restricted by water unavailability during the non-rainy season. The availability of water is the controlling influence of the cropping sequence and date of planting in the SAT. Soil and crop management planning must be synchronized with the beginning and ending of the rainy season. The potential productivity of SAT soils is therefore closely correlated with moisture supplying potential and soil characteristics (Thomas et al., 1984). On certain soils, such as deep Vertisols, *in situ* profile storage is a reliable source of water during the rainy season and for extending the cropping period into the post-rainy season. For others, such as shallow Alfisols, profile water storage is so limited that supplemental irrigation is necessary after the rainy season and, indeed, frequently even during dry spells within the season. In any case, understanding the nature and characteristics of soils in the SAT is critical to formulating a successful strategy for their use and management under rainfed conditions. Table 2.1 gives the areal extent of different soil types in Tanzania.

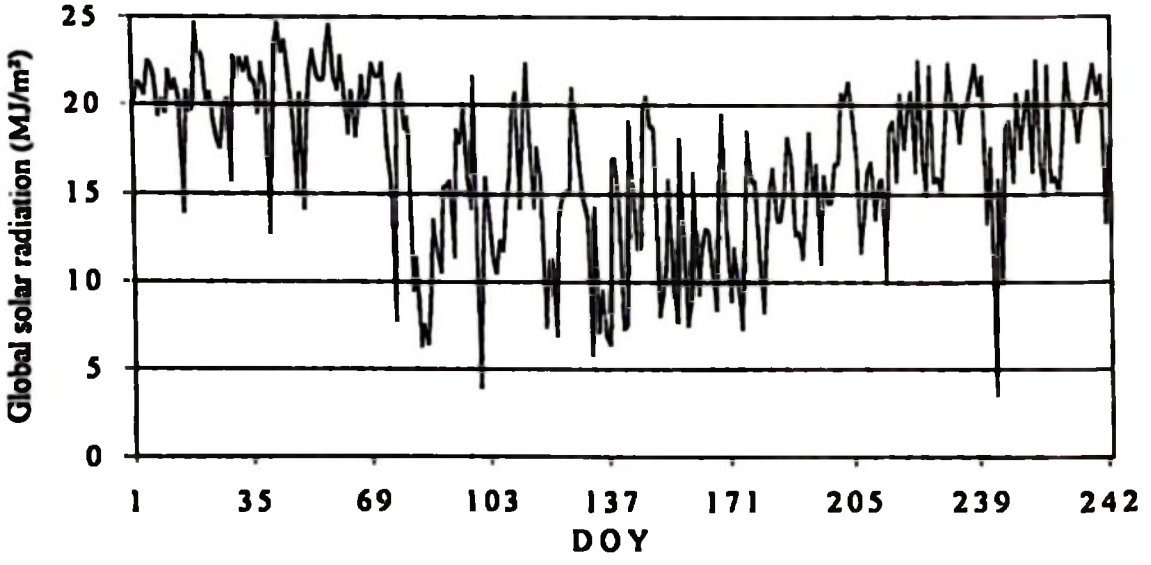

Fig. 2.2 Daily global solar radiation for SUA experimental site, Morogoro, Tanzania, January-September, 1997.

Table 2.1 Areal extent of different soil types in Tanzania (after De Pauw, 1984 as cited by Msanya and Magoggo, 1993)

Soil type	Area (mill. ha)	% proportion	Soil type	Area (mill. ha)	% proportion
Cambisols	23.3	28.2	Fluvisols	2 9	3 5
Ferralsols	12 5	15 1	Planosols	2.4	2.9
Vertisols	7.2	8 7	Phaeozems	1 7	2.1
Xerosols	5.9	7 1	Solonchaks	1 3	1.6
Lithosols	5 6	6 8	Andosols	1 3	1.6
Nitosols	4.8	5 8	Chernozems	0.9	1 1
Gleysols	4.7	5 7	Histosols	0.5	0.6
Arenosols	4.0	4 8	Solonetz	0.4	0.5
Luvisols	3.2	3.9	Regosols	0 06	0 07

Tanzania has a total area of about 945,000 km^2 and a population of over 24 million (Msanya and Magoggo, 1993) It extends from about 1.5 degrees south of the equator to about 12 degrees south. The country has a wide variety of landforms and climates; and it includes the highest and lowest parts of Africa, namely, the summit of Mount Kilimanjaro (about 5900 m above sea level) and the floor of Lake Tanganyika (about 358 m below sea level). The climate is mainly tropical, but the varying altitudes produce a corresponding range of temperature regimes from tropical to temperate. Rainfall is variable from place to place and is generally lower than might be expected for the altitude The distribution of the main land use types and farming (production) systems is determined largely by the agro-climatic and soil conditions Moisture availability and the management of soil water is considered one of the biggest constraints to crop production in Tanzania (Msanya and Magoggo, 1993).

2.2.2 The semi-arid regions and remote sensing

The arid and semi-arid regions represent a challenging area for research. In arid and semi-arid regions, relative extremes and large spatial and temporal gradients in water and energy balance components are encountered. Semi-arid and some agricultural environments exhibit strong surface heterogeneity, where high spatial and temporal variability of surface fluxes occur. In addition, semiarid rangelands contain ecosystems that are sensitive to climate anomalies and anthropogenic effects.

The arid and semi-arid regions are important for study, since they cover a large fraction of the globe, and a significant proportion of the human population depends on them for survival. Adverse climate change or surface degradation in these regions can have critical impacts on food and water supplies. Errors in remote sensing and flux modelling caused by ignoring the effects of surface heterogeneity are largest in these regions (Njoku et al., 1996). It is therefore imperative that an attempt be made to better understand the reciprocal relationship between the hydrological cycle and local and regional climate.

The urgency of such major environmental issues as desertification, soil erosion, deforestration, drought and locust plagues emphasizes the need for remote sensing and GIS technologies in Africa, although these sciences are only just beginning to be used (Tappan et al., 1991). The need for development of remote sensing and GIS-based studies in the developing countries is therefore apparent. Small-scale ground-based field experiments designed to address issues pertaining to the remote sensing of the Earth's surface and the applications thereof will definitely form a very good basis or starting point for disseminating the remote sensing knowledge in terms of its fundamental principles. The utility of ground truth data for calibration of spaceborne data also makes this kind of initiative a necessary step towards the long-term goal of obtaining and analysing spaceborne data.

2.3 Knowledge of soil moisture content and its importance

Soil moisture is one of the few directly observable hydrological variables that plays an important part in the water and energy budgets necessary for large scale hydrological as well as any soil-vegetation-atmosphere studies. The amount of water in the top metre of the earth's soil is a critical variable that controls a number of hydrologic, biological and meteorological processes. Soil moisture in the top few centimetres governs the partitioning of rainfall into infiltration and surface runoff, the latter being the major source of flood flow in many streams and rivers. The rate of evaporation of water from soil is strongly dependent upon the amount of moisture near the soil surface. Transpiration and growth of crops and other plants depend upon the availability of water to the plant roots. Because a significant quantity of heat is absorbed when vaporization of liquid water occurs, the rates of evaporation and transpiration have a significant influence upon the energy balance of the surface of the earth. Therefore, soil moisture affects weather and climate by controlling the fluxes of water and sensible heat into the atmosphere. Where soil moisture is high, evaporation will predominate, adding to atmospheric moisture content. Where it is low, the land surface will warm under the influence of radiational heating. Thus, it is not soil moisture which directly affects the atmosphere, but latent and sensible heat which is modulated by soil moisture (Dirmeyer and Shukla, 1993).

Soil moisture is difficult to quantify in terms of its effect on the atmosphere. Many other factors, such as vegetation, soil characteristics and ambient conditions alter the transfer of moisture from soil to the air. Also, soil moisture is very difficult to measure directly due to its heterogeneity at small scales. There has been no observational evidence that soil moisture anomalies in an otherwise unaltered surface can persist for time scales beyond a year, nor can they affect interannual climate. Yet changes in surface vegetation such as deforestration and desertification can change the value of surface soil moisture. They can also lead to changes in the surface roughness and albedo. These changes may then alter climate in significant ways. This may be the most important and ominous manifestation of soil moisture repercussions on climate.

The variability in time and space of the moisture content of the soil often complicates the analysis of many of the above-mentioned processes. Variations in time result from the dynamic nature of

the hydrological cycle, with periodic forcing at the annual and daily scales and with more random forcing due to the passage of weather systems. Variations in depth are intimately related to the temporal fluctuations in the atmospheric conditions. Generally, surface conditions respond to all frequencies of atmospheric changes. Deeper soil moisture responds more slowly, due to smoothing by the intervening surface layers (Milly & Kabala, 1986).

Measurement of water content in space and time is also important for modelling applications, monitoring hydrological water balance, measuring agricultural or forest water use efficiency, or monitoring changes in water content for irrigation scheduling The effective use of water content values for many applications, such as irrigation scheduling, depends on rapid, reproducible recovery of data from a number of representative locations (Topp et al., 1996).

2.4 The occurrence and significance of bare soils in the semi-arid regions

Bare soil surfaces occur for part of the year in all agro-climatological zones. Often, the lack of plant cover is the result of the adverse physical conditions of certain seasons. In the semi arid tropics, where arable land is often cultivated during a short growing season, drought and sometimes also high temperatures inhibit plant establishment and growth during the dry season. In semi-arid zones, rangeland may also be very sparsely vegetated for much of the year. Aside from these seasonal absence of vegetation, certain crops are cultivated in a manner that keeps most of the soil surface bare continuously. In some dry farming systems, rotation schemes that include a year fallow in order to store soil moisture for the next growing season can be found (ten Berge, 1990). There is a general concern that changes in the vegetation cover of the earth's surface will have an impact on climate, at least on a regional scale. Obviously bare soil represents one extreme in terms of vegetation cover. It is therefore important to know more about the soil-atmosphere interaction over bare land surfaces on a regional scale (ten Berge, 1990)

2.5 Bare soils and remote sensing

Remote sensing techniques have been used to study bare soils for nearly three decades now. These techniques provide information about a thin surface 'skin' of the soil, i e , a layer of a few tens of micrometers (thermal infrared) up to a few centimeters (microwaves). Being able to interpret surface signals quantitatively in terms of physical processes would greatly benefit the inventory of relevant time-dependent phenomena (ten Berge, 1990). Along with the development of remote sensing capabilities, there is a need to relate 'superficial' signals, as registered by remote sensors, to processes and conditions that have a practical significance. Two main approaches to this problem can be distinguished: correlation, and analysis based upon physical abstractions of reality (ten Berge, 1990).

In the first approach, the signal is directly correlated with the variable(s) of interest. Examples of such analyses are given by Idso et al. (1975a) (topsoil moisture and radiation temperature), Reginato et al. (1976) (evaporation and radiation temperature), ten Berge et al. (1983) (texture, moisture and radiation temperature), and Shih et al. (1986) and Myhre and Shih (1990) (soil water content and radiation temperature and other weather variables).

Alternatively, methods based on physical relations between fluxes and state variables (e.g. moisture content, temperature) in combination with relations between measured variables or derived parameters and the actual conditions of interest are employed (ten Berge, 1990). Examples of the latter type are models expressing thermal inertia in terms of soil moisture content and bulk density (e.g. Pratt & Ellyett, 1979). The procedures based on physical relations use the remotely measured course of a surface state variable as a starting point to calculate the desired surface flux or state variable and usually involve the balance concept (for mass or energy). If the goal is to obtain fluxes and soil state variables (profiles), straightforward physical models are often used, with the remotely sensed boundary conditions and known system parameters as input (as applied by e.g. Prevot et al. (1984) in calculations of the soil water regime, and by Hares et al. (1985) in monitoring the thermal regime of soil). If, on the other hand, system parameters (e.g. thermal inertia) and surface fluxes are sought, one encounters the so-called 'inversion' problem: now the measured course of a state variable must be used to infer

system parameters and fluxes. Then, analytical approximations to a balance equation can be used, e.g., to estimate evaporation and thermal inertia (Price, 1980).

3 MEASUREMENT OF SOIL MOISTURE CONTENT

3.1 Brief review of the measurement methods

For years researchers have sought an instrument for obtaining rapid, reliable, economical, and continuous measurements of soil water content that could be made in the field and laboratory. Measurements of soil water content are based upon the sensing of various properties of the water molecule. These include measurements of mass, response to radiation, thermal properties, and electrical properties. The relationship between these properties and moisture content is complex and involves both the pore structure and constituents of the soil solution. Therefore, no single universal technique will always provide a measure of the soil moisture content, rather, different techniques provide different information

Comprehensive reviews on the different estimation methods for soil water content already exist in the literature (e.g., Schmugge et al., 1980; Stafford, 1988; Topp et al., 1996). Two approaches are used for estimation of soil moisture content, namely, modelling and measurement, either in-situ or remote. The methods and instruments for estimating soil water content include gravimetric, tensiometers, gypsum blocks, Watermark sensors, neutron probes, and Time Domain Reflectometry (TDR). Schmugge et al. (1980) detail the advantages and disadvantages of the different estimation methods

Schmugge et al. (1980) and Myhre and Shih (1990) discussed the advantages and disadvantages of each conventional method. For example, to determine soil moisture by tensiometer, a soil water characteristic curve (water release curve) must be employed. Neutron probes are time-consuming to use, require access tubes, and must be calibrated for different soils (clay, sand, etc.). Gravimetric analysis of soil samples provides accurate soil moisture data, but the samples must be transported to a laboratory for analysis. Weighing soil lysimeters measure total soil moisture content for a given site, but this is not necessarily representative of the surrounding subsurface hydrology. As a group, the conventional field methods are limited by the fact that they provide point rather than areal values and therefore the values obtained are not necessarily representative of a large area. Furthermore, despite the fact that these point methods can be accurate, they are also time consuming (Shih and Jordan, 1992).

Remote sensing techniques (microwave and thermal infrared) offer the possibility of rapid and areal measurement of soil water content. However, these techniques can only estimate soil water content to depths of 5 to 20 cm (Schmugge, 1980; Schmugge et al., 1980, Stafford, 1988; Myhre and Shih, 1990). Thermal infrared technique has long been used for measurement of plant/soil surface temperatures for estimation of surface soil moisture and evaporation (Myhre and Shih, 1990; Carlson et al., 1990; Carlson et al., 1981; Kalma and Jupp, 1990; Taconet et al., 1995; Moran et al., 1996; Ben Asher et al., 1984; Ben Asher et al., 1983; Vleck and King, 1983; Woebbecke, 1994). Chapter 4 covers in detail the remote sensing techniques

Soil water and energy balance models can also be used to estimate soil water content. But these models require a lot of input data. The accuracy obtained using model simulations depends to a great extent on the the quality of the input data used. A lot of models of water and energy balance already exist in the literature (e.g., Arya et al., 1983; Camillo, et al., 1983; van de Griend and van Boxel, 1989; Bruckler and Witono, 1989, Witono and Bruckler, 1989). Soil water content is often one of the outputs of the complex models

3.2 Coupling of measurement with modelling

Both the in-situ and remote sensing methods as well as modelling approaches for the estimation of soil water content have disadvantages. It is apparent, then, that modelling and measurement are both useful, though imperfect, techniques for the determination of the amount of moisture in the soil. It is reasonable to expect that a combination of these approaches, if feasible, would yield more accurate estimates of soil moisture than could be obtained from either approach alone. Therefore, a cost effective soil moisture monitoring program must utilize both approaches and not just one. An integrated system should be designed. The coupling between modelling and measurement is further covered in chapter 4 in tackling the problem of inferring profile soil water content from surface measurements.

In tackling the problem of integration of models and remote sensing to estimate soil moisture, three points are pertinent. First, there is clearly information about soil moisture and evaporation

contained in measurements of surface temperature (based on thermal infrared technique), brightness temperature (based on passive microwave technique), and backscatter coefficient (based on active microwave technique). Second, there is virtually no dependence of most remotely sensed properties on the moisture content below the near-surface layer (estimated to lie between 5 to 20 cm) And third, remotely sensed information on near-surface moisture content and on surface temperature is noisy. This is due to measurement error and, in the case of moisture content, to imperfect functional relations between the moisture content and the measured quantity.

Therefore from the first point, all available observational data should be employed, when possible, for estimation of soil moisture. This underlines the need for a multispectral approach to remote sensing. From the second point, a simulation model is necessary to extrapolate surface information to greater depths. And from the third point, inferences of the surface state based on remote sensing should be combined with those of predictive simulation models for moisture and temperature in order to account for the errors inherent in both processes

3.3 Current and future developments

The methods for measuring soil water content are continuing to evolve and improve. Advances in electronic technology and data logging capabilities have greatly strengthened the monitoring possibilities. New soil moisture sensors are continuously being produced and tested. Better modelling techniques are being developed. The advent of new and better measurement techniques together with better modelling techniques will provide better ways of monitoring soil water content.

Probably of much interest is the proliferation of the use of neural networks in various research disciplines, e.g. remote sensing and hydrology. Neural networks have been used in predictions of soil moisture (Altendorf et al., 1992), soil thermal properties (Altendorf et al., 1992), soil hydraulic properties (e.g., Schaap and Leij, 1998; Schaap et al., 1998), pan evaporation (Bruton et al., 1998). The use of neural networks is thought to eventually lead to the development of a

stand-alone sensor that would provide an attractive alternative to the current methods of soil moisture measurement (Altendorf et al., 1992).

Possible use of noninvasive techniques based on electromagnetic induction for the measurement of soil water content has also been investigated (e.g., Sheets and Hendrickx, 1995; Kachanoski et al., 1988). Sheets and Hendrickx (1995) contend that electromagnetic induction has a great potential for quick detection of soil water content changes over large areas. Use of this technique, however, requires prior calibration, e.g., using neutron scattering technique (Sheets and Hendrickx, 1995).

4 REMOTE SENSING OF SOIL MOISTURE CONTENT

4.1 General overview

4.1.1 Introduction

Remote sensing is defined as acquisition of information about the condition and/or the state of a target by a sensor that is not in direct physical contact with it (Asrar, 1989). The sensor may be situated millimetres or kilometres away from the target (soil surface) (Stafford, 1988) The sensors that are currently used for this purpose are divided into two groups: active and passive systems.

The active sensors transmit a pulse of electromagnetic energy and then measure the backscattered return, which will be a function of the soil's reflectivity (Schmugge, 1990). The relationship between the transmitted and received signal is used to characterize the condition or state of the target. The most used active sensors are microwave radars Radars are specially useful in cloudy areas because some wavelengths of microwave radiations are not significantly attenuated by water droplets in the atmosphere. The Synthetic Aperture Radar (SAR) of the European Resources Satellite (ERS-1/SAR) is such a sensor category (Asrar, 1989;Su, 1996).

On the other hand, the passive sensors do not generate or transmit a signal. These detect and record the natural electromagnetic energy reflected and/or emitted from a target. The magnitude and shape of the signal are indicators of the condition and state of the target. Examples of passive sensors are photographic cameras, vidicon cameras, scanning radiometers, pushbrooms, and spectrometers (Asrar, 1989;Su, 1996). Radiometers observe the variations in the thermal emission from the soil resulting from emissivity changes (Schmugge, 1990).

4.1.2 Remote sensing platforms

The sensor systems currently used in remote sensing of the Earth's surface can be classified in different ways. This classification can be based on the mode of operation of the sensors, their spectral characteristics, and/or the platform on which the sensor is deployed. If classified

according to the last approach, the sensors can be divided into ground-based, airborne, and spaceborne systems (Asrar, 1989). Most of the ground-based sensors (radiometers) operate basically on the same principles as the airborne or spaceborne sensors, except that they measure the reflected or emitted energy from the surface over different wavelength regions of the electromagnetic spectrum (Asrar, 1989). Four remote sensing platforms are of interest for hydrological studies. First are the ground observation platforms, e.g., masts, towers Second are the balloons, used up to altitudes of about 30 km. Third are the airplanes These are used for topographic survey, hazard monitoring and disaster assessment (e g flooding and associated effects). Piloted aircrafts operate up to altitudes of about 15 km. And fourth are the satellites, consisting of low altitude polar orbiting satellites (800-1500 km) and high altitude equatorial orbiting satellites at geostationary altitudes (35400 km).

4.1.3 Consideration of spectral bands and their spatial and temporal resolution for hydrological application of remotely sensed data

For hydrological studies, three characteristics of remotely sensed data have to be considered. First is the spectral band, that is, the measured physical quantity (visible or infrared reflectance, thermal or microwave emission, as well as backscattering property) Second is the spatial resolution. And third is the temporal resolution. A detailed knowledge of the radiation responses of different classes and types of phenomena is fundamental both for choosing appropriate sensors and for interpreting remotely sensed data (Colwell, 1983, Engman and Gurney, 1991).

4.1.4 Physical considerations of remote sensing

Electromagnetic radiation is the means by which electromagnetic energy is propagated in the form of waves. This is of great significance for remote sensing because it is an energy form which can travel either through a medium (e.g water and atmosphere) or a vacuum (e.g. space). Radiation is emitted from all bodies with temperatures above absolute zero and is characterized by a signal whose configuration is determined by the physical characteristics of its source. This

signal is usually described in terms of wavelength and frequency. **Fig. 4.1** shows the electromagnetic spectrum

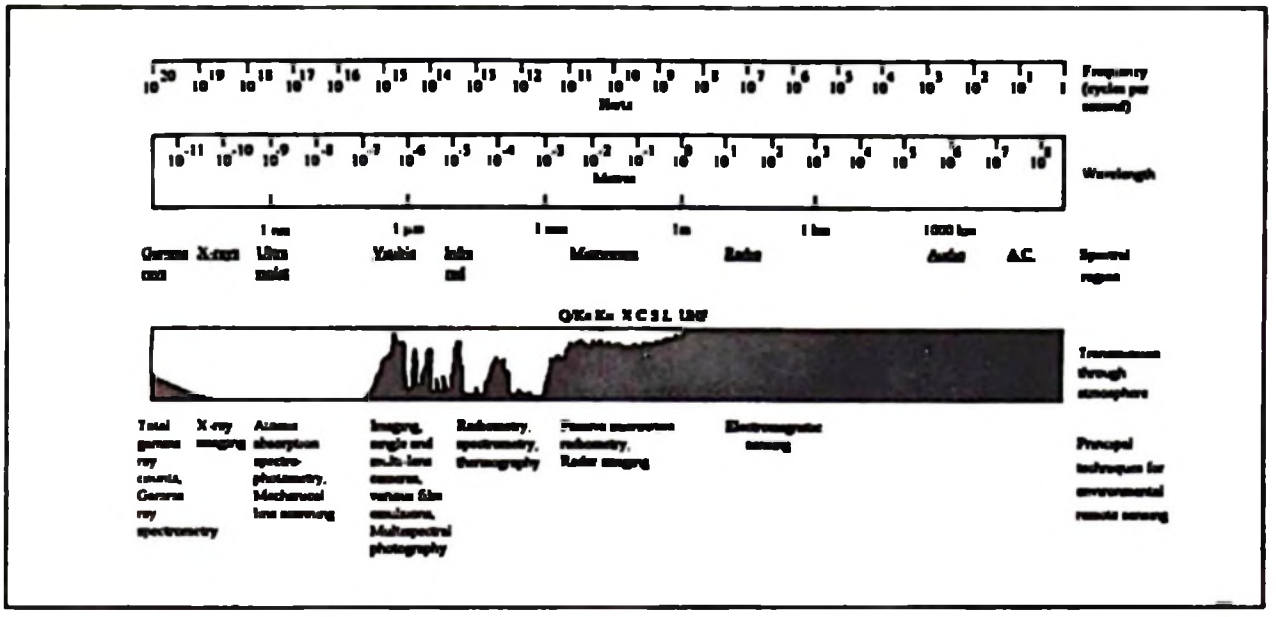

Fig. 4.1 The electromagnetic spectrum Source: Barret and Curtis, 1992

Some electromagnetic radiation properties are related to wavelength. The smaller the wavelength, the greater the energy. The higher the temperature of an object, the greater the total energy emitted and the shorter the peak wavelength emitted; which are statements of the Planck's law and Wien's law of elecromagnetic radiation, respectively. Futhermore, the interaction of energy with matter is wavelength dependent.

4.1.5 Hydrological application of remotely sensed data

The advent of better remote sensing techniques has greatly enhanced our ability to conduct areal measurements of hydrological parameters and variables, in combination with conventional point measurements. Applications of remotely sensed data in hydrological studies of precipitation, evapotranspiration, soil moisture and groundwater as well as catchment characteristics have received more and more attention. Comprehensive reviews have been presented by (Rango

(1987, 1990), Schultz (1988, 1989), Barrett (1989, 1990), Schultz and Barrett (1989), Engman and Gurney (1991), Haefner and Pampaloni (1992), and Kuitinnen (1992).

Evapotranspiration: Despite the fact that evapotranspiration cannot be measured directly by remote sensing techniques, some parameters and variables necessary in calculating evapotranspiration based on energy budget equation can be estimated with remotely sensed data in the visible and thermal infrared regions of the electromagnetic spectrum. Determination of evapotranspiration requires knowledge of the incoming solar radiation, surface albedo, surface temperature, land use and vegetation cover. Inspite of the fact that many studies (Menenti, 1983; Miller and Millis, 1989; Nieuwenhuis, 1986a,b; Ottlé et al., 1989; Rosema, 1981, 1986, 1990; Serafini, 1987; Seguin et al., 1990; Lagouarde, 1991, Feddes et al., 1993) have been conducted, there is still no operational method for determining evapotranspiration based on remote sensing techniques.

Soil moisture: As already mentioned in chapter one, conventional methods for soil moisture determination are both time and labour consuming and limited to point measurements. Remote sensing techniques offer the possibility of collecting areally distributed near-surface soil moisture. Extending these surface measurements to the root zone (usually less than one metre deep) can significantly reduce the errors in hydrological simulation of soil moisture as well as provide the necessary information required for agricultural applications. Remote sensing measurements of near-surface (0 - 5 cm depth) soil moisture are based on:

i. measuring bare soil reflectance in the visible and near infrared regions which provides only a poor indication of soil moisture due to the fact that the soil reflectance is also heavily influenced by soil texture and soil colour. The presence of vegetation poses another problem for this technique,
ii. measuring surface temperature in the thermal infrared region,
iii. measuring the brightness temperature in the passive microwave region, and
iv. measuring the backscattering coefficient with active microwave sensors.

4.2 Microwave remote sensing of soil moisture

Four characteristics of microwave remote sensing make it theoretically very effective for soil moisture determination. Firstly, due to the large difference between dielectric constant of water and that of dry soil. Secondly, due to the negligible atmospheric effects in the wavelength range suitable for soil moisture sensing Thirdly, due to its independence of solar illumination conditions. And fourthly, due to its ability of partially penetrating vegetation canopy (Su, 1996).

Passive microwave. This technique is based on the measurement of the brightness temperature in the passive microwave region In this technique the distinct difference of the dielectric constant of water (about 80) and that of dry soil (about 3 to 5) is utilized for determining soil water content of the top soil layer of about 5 cm (Schmugge, 1985; Jackson, 1993). Because the attenuation of the microwave radiation increases with increasing vegetation this technique is also limited to low vegetation area (Schmugge et al., 1986, Wang et al., 1990)

Theory of microwave radiometry. A microwave radiometer measures the thermal emission from the surface and at these wavelengths (i.e., low frequencies) the intensity of the observed radiation is proportional to the product of the thermodynamic temperature of the soil and the surface emissivity (Rayleigh-Jeans approximation to the Planck radiation law, **Eq. 4.1**) (Schmugge, 1990). This product is commonly called the brightness temperature (T_B) and is given by the product of the emissivity and the physical temperature of the near-surface layer of the soil.

$$T_B = eT_{soil} \tag{4.1}$$

where e is the emissivity, and

T_{soil} is the physical temperature of the soil in °C.

For a radiometer at some height above the ground, atmospheric effects must be included, yielding the equation

$$T_B = \tau[RT_{sky} + (1 - R)T_{soil}] + T_{atm} \tag{4.2}$$

where R is the surface reflectivity,

τ is the atmospheric transmission,

T_{atm} is the atmospheric temperature in K.

This situation is represented schematically in the Fig. 4.2 (Schmugge, 1990). The first term is the reflected sky brightness, which depends on the atmospheric conditions and frequency. T_{sky} typically varies between 5 to 10 K for the normal range of atmospheric conditions. The third term is the direct atmospheric contribution and is about 5 K. The atmospheric transmission will typically be about 99 % so the only term remaining is the emission from the soil, that is, the second term as the main contributor to T_B. Thus Eq. (4.2) reduces to Eq. (4.1).

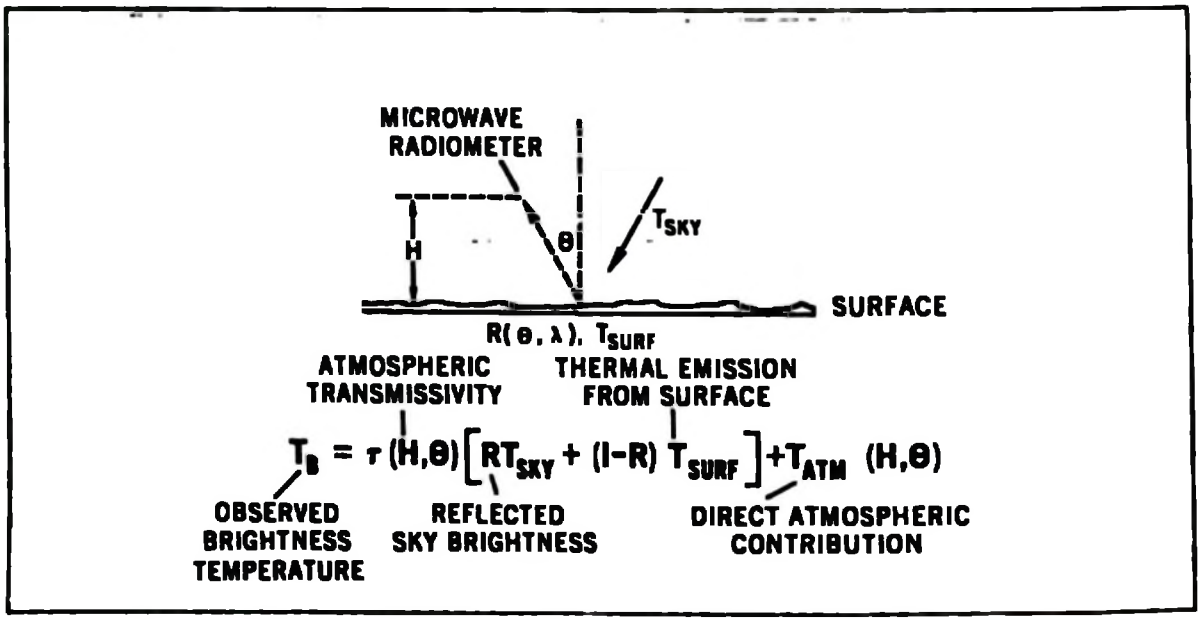

Fig. 4.2 Scheme of the sources of microwave radiation observed by a radiometer at a height h and an angle θ. Source: Schmugge, 1990.

This is true for isothermal soil; however, when there are variations of soil temperature with depth, the factor eT_{soil} is replaced by the integral:

$$T_B = e\int^0 T(z)\alpha(z)\int^0 \exp[-\alpha(z')dz']dz \qquad (4.3)$$

where $T(z)$ is the temperature at the depth z in the soil in K, and

$\alpha(z)$ is the absorptivity at the depth z in the soil; depends on the moisture content at z.

The integral essentially gives the intensity of the upwelling thermal radiation from the soil and is a weighted-average of the soil temperature over the electromagnetic skin depth of the soil. The factor e, the emissivity, gives the fraction of this upwelling radiation that is transmitted into the air and it is this factor that shows the primary sensitivity to the soil moisture content. The thickness of the layer at the surface whose dielectric properties determine the emissivity, e, is the critical factor. This thickness determines the soil moisture sampling depth for microwave sensors.

An early theoretical study of the radiative transfer in a soil by Wilheit (1978) (as cited by Schmugge, 1990) has shown that this depth is only of the order of a few tenths of a wavelength thick, or about 2 to 5 cm at the 21-cm wavelength. This result has been confirmed by the experimental work of Newton et al. (1982) and Wang (1987) (as cited by Schmugge, 1990).

Active microwave: An active microwave sensor or radar sends out a pulse of microwave radiation and then measures the intensity of the radiation reflected back to it. The intensity of this reflected signal is described by the backscattering coefficient (σ^0 - sigma zero). The active microwave technique for estimation of the surface soil water content is based on the measurement of the backscattering coefficient. Many research projects are being conducted in developing techniques for measuring near-surface soil moisture in this area. Progress has been made with regard to the choice of microwave frequency, elimination of influence of soil roughness as well as vegetation cover (e.g., Ulaby et al., 1978, 1984; Van Oevelen et al., 1996). Van Oevelen et al. (1996) conducted an analysis of the errors involved in determination of areal soil water content by means of active microwave remote sensing. The heterogeneity of the surface parameters was considered to be one of the main source of errors in soil moisture estimation.

4.3 Thermal infrared remote sensing

4.3.1 General overview

Quantitative interpretation of remotely sensed thermal-infrared data are complicated by the many physical factors that influence observed temperatures. Both the daily average surface temperature and day-to-night temperature range are greatly influenced by the ability of the surface to support evaporation, or in the case of vegetation, evapotranspiration. This effect generally may be ascribed to a surface soil water content factor, or to a resistance to evapotranspiration, e.g., a stomatal resistance in the case of vegetation. The radiation balance at the surface is affected by the moisture in the atmosphere which modifies downward radiation. The transfer of sensible heat from ground to atmosphere is affected by the temperature of air near the ground. Local air-temperature measurements are required for highly accurate interpretation of thermal measurements. Air temperature can generally be estimated reasonably well from conventional ground-based meteorological data. A major effect on the exchange of sensible and latent heat with the atmosphere is produced by both the surface wind speed and surface roughness. This difficult problem becomes even more complex when vegetative surfaces are considered. In addition, atmospheric humidity influences the magnitude of the moisture flux exchange between the Earth's surface and the atmosphere.

The day-to-night temperature changes observed by remote-sensing instruments are affected by the heat-storing capacity of soil. This factor is of some importance in dry areas, but of rather less significance in moist areas, where evapotranspiration decreases the energy available to drive a large day-to-night temperature cycle. Surface albedo determines the fraction of the sun's energy that is available to drive evaporation and near-surface heat storage. Surface emissivity, integrated over wavelength, affects radiative heat loss to the atmosphere, whereas emissivity in the atmospheric window influences the interpretation of measured radiance in terms of physical temperatures. Topography, i.e., attitude with respect to the sun, and openness or sheltering from the wind, modify the nominal energy balance of a flat surface.

4.3.2 Terminology

Introduction The temperature of complex surfaces such as soils and vegetation canopies can be estimated by indirect measurements of thermal radiance. An infrared thermometer (IRT) measures the thermal radiance that is coming from a surface within its instantaneous field-of-view (IFOV) and in some finite wavelength band. In the case of homogeneous surfaces in thermal equilibrium, the definition of surface temperature is not ambiguous and surface temperature can be measured by radiometry. With respect to heterogeneous surfaces which are not in thermal equilibrium within the corresponding IFOV of a radiometer, the definition of surface temperature is ambiguous and careful analysis of the measurement procedure has to be done. For example, the temperature indicated by an infrared thermometer pointed at a bare soil surface is a measure of the local equilibrium resulting from conduction into the soil, convection of heat and water from the surface, and broadband (3 - 100 μm) radiative exchange at the surface. In this case an infrared thermometer measures only the radiation emitted and reflected into the instrument in a narrow wavelength band from the IFOV and from a specific angle. The "surface" in this example is not easily defined, so it is not surprising that terminology related to "surface temperature" is vague (Norman and Becker, 1995). Furthermore, confusion arises due to the fact that the relationship between temperature measured by such a radiometer and the temperature used to calculate the sensible heat or evaporation fluxes is not obvious. The need for a consistent set of terminology is therefore apparent. The following paragraph attempts to define the various temperature terms that have been used in thermal infrared remote sensing.

Definitions Various terms such as "canopy temperature", "surface temperature", and "skin temperature" have been used in the literature and attempt has been made to identify more precise meanings for various terms (Norman et al., 1995) (see Appendix 10). The temperature definitions can be classified into three categories: kinetic temperature, radiative temperature, and aerodynamic temperature. The kinetic temperature, which might be referred to as the "true" temperature, is defined thermodynamically in terms of the kinetic energy of molecules. The radiative temperature usually is derived from a measurement of thermal radiance or flux density and represents a balance of radiative fluxes; it can be closely related to the true temperature of the radiating surface but is influenced by surface properties and external radiation sources. This

radiative temperature may depend on wavelength considerations of the sensor and directionality (directional versus hemispherical). The aerodynamic temperature is an effective temperature that is derived from a surface energy balance or extrapolation of the air temperature profile to the canopy displacement height, and it may not actually exist or be measurable except for smooth surfaces (Norman et al., 1995).

4.3.3 Theoretical background

Introduction: Temperature measurement can be divided into two categories: contact and noncontact. Contact thermocouples and thermometers are the most prevalent in temperature measurement applications. They must contact the target as they measure their own temperature and they are relatively slow responding. Noncontact temperature sensors measure infrared (IR) energy emitted by the target, have fast response, and are commonly used to measure moving and intermittent targets, targets in a vacuum, and targets that are inaccessible due to hostile environments, geometry limitations, or safety hazards.

Principles of infrared thermometry: An infrared thermometer measures temperature by detecting the infrared energy emitted by all materials which are at temperatures above absolute zero, (0 K). Infrared radiation is part of the Electromagnetic Spectrum and occupies frequencies between visible light and radio waves. The IR part of the spectrum spans wavelength from 0.7 μm to 1000 μm. Within this wave band, only frequencies of 0.7 μm to 20 μm are used for practical, everyday temperature measurement. IR energy travels in straight lines from the source and can be reflected and absorbed by material surfaces in its path. In the case of most solid objects which are opaque to the human eye, part of the IR energy striking the object's surface will be absorbed and part will be reflected. Of the energy absorbed by the object, a proportion will be re-emitted and part will be transmitted internally. These phenomena collectively contribute to what is referred to as the emissivity of the object or material.

Materials which do not reflect or transmit any IR energy are known as blackbodies and are not known to exist naturally. However, for the purpose of theoretical calculation, a true blackbody

is given an emissivity value of 1.0.

Different kinds of materials and gases have different emissivities, and will therefore emit IR at different intensities for a given temperature. The emissivity of a material or gas is a function of its molecular structure and surface characteristics. It is not generally a function of colour unless the source of the colour is a radically different substance to the main body of material. In addition to molecular structure and surface condition, a third factor affecting the apparent emissivity of a material or gas is the wavelength sensitivity of the sensor, known as the sensor's spectral response. As stated earlier, only IR wavelengths between 0.7 μm and 20 μm are used for practical temperature measurement. Within this overall band, individual sensors may operate in only a narrow part of the band, such as 0.78 to 1.06, or 4.8 to 5.2 μm.

Theoretical basis for IR temperature measurement: The important formulas upon which infrared temperature measurement is based are:

Kirchoff's law: Which states that when an object is at thermal equilibrium, the amount of absorption will equal the amount of emission.

$$a(\lambda) = e(\lambda)$$

where a is the absorption,
e is the emission, and
λ is the wavelength in m

Stephan Boltzmann law: The hotter an object becomes the more infrared energy it emits.

$$W = \epsilon\sigma T^4$$

where W is flux intensity in $W\ m^{-2}$,
ϵ is the emissivity,
σ is the Stephan Boltzmann constant ($5.67 \times 10^{-8}\ W\ m^{-2}\ K^{-4}$), and
T is the absolute temperature in K.

Wien's displacement law: The wavelength at which the maximum amount of energy is emitted becomes shorter as the temperature increases.

$$\lambda_{max} = 2897/T \ \mu m$$

Planck's equation: Describes the relationship between spectral emissivity, temperature and radiant energy.

$$W_\lambda = C_1 \epsilon_\lambda [\lambda^5 (\epsilon^{\frac{C_2}{\lambda T}} - 1)]^{-1}$$

where ϵ_λ is the emissivity at wavelength λ,
W_λ is the radiant energy,
C_1 and C_2 are constants.

4.3.4 Use of infrared thermometry

The use of infrared thermometry for measurement of plant/soil surface temperatures for estimation of surface soil moisture and evaporation has long been practiced (e.g., Moran et al., 1996; Taconet et al., 1995, Evett et al., 1994; Woebbecke, 1994; Myhre and Shih, 1990; Carlson et al., 1990; Kalma and Jupp, 1990; Ben Asher et al., 1984; Ben Asher et al., 1983; Vleck and King, 1983; and Carlson et al., 1981). Smith et al. (1986) (as cited by Campbell and Norman, 1990) conducted a field study to investigate the effect of various meteorological variables on their ability to predict canopy-air temperature differences. They found that both vapour deficit and net radiation were important in determining the magnitude of the temperature difference.

Within the last decade, several commercial IR thermometers, with associated environmental measurement capabilities, have become available (Boissard et al., 1990; Campbell and Norman, 1990). The availability of these instruments has given rise to a number of research programs that use thermal data to obtain information about the growth and condition of plant canopies.

Considerable research has also been done using the daily maximum surface plant minus air temperature difference as a means of determining the plant water stress (e.g., Soer, 1980; Moran et al., 1994,). Theoretical and empirical work by Jackson et al. (1981) and Idso et al. (1981), respectively, provide a method for calculating a crop water stress index (CWSI). Gardner et al. (1992a, 1992b) detail the necessary sampling procedures and interpretation of infrared thermometry data for the determination CWSI. The use of the infrared thermometry method in the field is restricted by the presence of clouds. Pennington and Heatherly (1989) describe a method of correcting the measured canopy minus air temperature difference (TD) for rapidly changing solar radiation.

Remotely sensed spectral measurements can provide an indirect means of deriving geophysical quantities required as inputs to hydrological models (Moran et al , 1994). Satellite- and ground-based measurements of surface reflectance and temperature have been related to critical model requirements, such as soil moisture (Idso, et al., 1975a). Furthermore, surface temperature and reflectance have been combined with ground-based meteorological data to directly evaluate surface energy fluxes, such as net radiation and evaporation (Jackson et al., 1977 as cited by Moran et al , 1994) These relations are generally semiempirical and often site-specific, so they must be reevaluated for application to new geographic regions and different ecosystems (Moran et al., 1994).

4.3.5 Using infrared thermometry to estimate near-surface soil water content

Numerous field studies have provided evidence of relations between near-surface moisture content and the behaviour of surface temperature (Vleck and King, 1983; Cihlar, 1980; Idso et al., 1975a, b; Heilman and Moore, 1980, Reginato et al., 1976; ten Berge et al., 1983). Based on literature, the dynamics of surface temperature have been expressed in terms of diurnal amplitude of surface temperature, or in terms of difference between maximum surface and maximum air temperature, or in terms of maximum surface minus air temperature difference, or momentary values have simply been used. The resulting empirical relations could, however, never be generalized to yield dependable formulas.

Moran et al. (1994) found significant relations between the surface minus air temperature (T_s - T_a) difference and measurements of soil moisture content (for vegetation-covered rangeland), though the shape differed from that previously published for bare soil (Idso et al., 1975a). They also found that the relation between daily evaporation rate and measurements of (T_s- T_a) and daily net radiation was similar to that derived previously for irrigated pasture and dryland shortgrass but differed from that derived for irrigated wheat.

However, the method of inferring soil water content from thermal infrared temperatures suffers a certain credibility due to the lack of direct comparisons between soil water content and surface thermal infrared temperatures. Inspite of the tantalizing indications that infrared ground temperatures are sensitive to soil moisture, there still exists a grave difficulty in the interpretation of the infrared signal. Central to the problem is the inability to determine the extent to which the temperature signal reflects the substrate moisture pattern or factors other than soil moisture, such as surface roughness, albedo, conductivity, vegetation cover, etc. Few comparisons have been made between infrared temperatures and substrate water contents over a region (Perry and Carlson, 1988).

Soil water content and surface soil minus air temperature can be related through the soil thermal property referred to as the "thermal inertia". The amplitude of the diurnal range of surface temperature for the soil is a function of both internal and external factors. The internal factors are thermal conductivity (K) and heat capacity (C), where $P = (KC)^{\frac{1}{2}}$ defines what is known as "thermal inertia". The external factors are primarily meteorological - solar radiation, air temperature, relative humidity, cloudiness, wind, etc. The combined effect of these external factors is that of the driving function for the diurnal variation of surface temperature. Thermal inertia, then, is an indication of the soil's resistance to this driving force. Since both the heat capacity and thermal conductivity of a soil increase with an increase of soil moisture, the resulting diurnal range of surface temperature will decrease. By measuring the surface soil temperature, the amount of soil water content in the soil can therefore be inferred.

Another process which has a direct or indirect relation to the variation of the surface soil temperature is soil evaporation. As soil water becomes limiting, the ability of the soil to supply

water for evaporation decreases which in turn has the effect of raising the surface soil temperature. The variation in soil evaporation is therefore directly or indirectly linked to the variation in soil water content.

Despite the fact that there is a relation between thermal inertia and surface soil water content, the use of this method has, however, been shown to be unattractive (ten Berge, 1990). Alternatively, several researchers (e.g , Nieuwenhuis, 1985; Stroosnijder et al , 1984; Smith and Newton, 1983; Entekhabi et al., 1994) have attempted to use physical models combined with remotely sensed flux boundary conditions.

A number of algorithms are currently available to infer soil moisture from surface temperature data. The approach is to invert an air-soil interface energy budget model with which surface temperature can be simulated. The evaporation and soil heat storage terms in these models are formulated in various ways which are either directly or indirectly dependent on soil moisture (Wetzel and Woodward, 1987); e g , the models of Carlson et al. (1981); Price (1980); Deardorff (1978); Lin, 1980; Camillo et al. (1983); and Choudhury and Idso (1984). Chanzy and Bruckler (1993) address the significance of soil surface moisture with respect to daily bare soil evaporation.

Little work has been done using the surface soil-minus-air temperature difference as an indicator of soil water content (Myhre and Shih, 1990), especially as far as inferring the profile soil water contents from the surface plant/soil temperature measurements in dryland is concerned. There is therefore a need to further test this method under different climatic and soil conditions. Myhre and Shih (1990) developed regression equations relating weighted-average soil water contents (W_{AVG}) and daily (maximum) plant minus air temperature/soil minus air temperature (TDMax) for different soil profile depths. Other terms were also used in place of TDMax.

The following general formula was used to calculate the weighted-average soil water contents to different depths in the soil profile (Wu et al., 1997).

$$W_{AVG} = [\frac{1}{2}(Z_1 - Z_0)\theta_1 + \sum_{i=1}^{n-1} \frac{1}{2}(Z_{i+1} - Z_{i-1})\theta_i + \frac{1}{2}(Z_n - Z_{n-1})\theta_n]/(Z_n - Z_0)$$

where Z is depth downward (m), and θ_i is volumetric water content at depth Z_i. Z_n is the depth of the profile. An illustration of this method is presented in subsection 5.6.2 of chapter 5 for the case of SUA field experiments.

4.4 Extraction of remote sensing information

4.4.1 The information extraction problem

Deriving information about the Earth's surface using measurements made with a sensor that is not in direct contact with it is a complex task. The success of the task depends on the nature of the interactions of radiation from a source with the (soil) surface, the atmosphere and the sensor itself, as well as the position of the sensor relative to the source. Information may be extracted either directly or by inference, or may be assimilated into a physical model of the process under study. The number of variables which can be measured directly, however, is very small. For the land surface it is only possible to make three measurements directly from remotely sensed data, namely, topography, albedo and surface temperature (depending on a variety of limiting assumptions). In contrast, the inference route can potentially yield a number of Earth surface measurements and is therefore worthy of further consideration (Danson et al., 1995).

4.4.2 Approaches to solving the inference problem

The extraction of information on surface properties from remotely sensed data is a fundamental research problem. Two main solutions to this problem are available, namely, empirical approach and theoretical approach. In the empirical approach an algorithm to relate the remotely sensed data to the ground surface variable is developed. As for the theoretical approach an analytical model is used and implies an understanding of the physics under consideration.

The empirical approach: The empirical approach in its purest form involves the derivation of a statistical relationship between the remotely sensed data and a given class of objects or a

calibration relationship between the remotely sensed data and the variable of interest. This approach does not require an understanding of the physics of the surface interaction mechanisms and can be easy to determine using statistical techniques. However, the empirical approach is usually informed, to some degree, by knowledge and theory. The main attraction of the empirical approach is that it is easy to apply; the main limitation is that the algorithms derived are generally specific to the conditions at the time the measurements were obtained.

Neural networks. A new empirical approach using neural networks provides a powerful alternative to the "statistical" methods. Here, the neural network is able to "learn" the form of the relationships between sets of input and output parameters. The technique has been applied successfully for image classification and for retrieving surface properties from remotely sensed data.

Theoretical approach. In the theoretical approach an analytical model of the interaction between solar radiation and the surface is derived. These models vary in complexity and computational requirements but they all involve parameterization of the surface by a set of variables which describe its optical, thermal or microwave properties.

4.5 Inferring profile soil moisture content from surface measurements

Estimates of soil moisture content in the root-zone or in the top metre is important for many agricultural and hydrological applications. Conventional methods for soil moisture determination are both time and labour consuming and extremely difficult to make at regional scale. These methods are impractical for frequent observations; moreover, as they are point measurements, the area they represent is questionable owing to the spatial variability of the soil (Ragab, 1995). Remote (microwave) sensing on the other hand offers one possible way to measure soil moisture over large areas. However, remote sensing methods (microwave) can only provide an estimate of soil moisture for the top 10 cm layer. The use of near-surface soil moisture to estimate root zone soil moisture is still a continuing question in soil water remote sensing (e.g., Newton et al., 1983; Rawls and Jackson, 1997). Very few attempts to extrapolate this value to estimate the

root-zone or the top 1 m soil moisture content have been reported Ragab (1992) and Kostov and Jackson (1993) reviewed the possible approaches. They can be classified into four types: regression, knowledge-based, inversion and combination of remote sensing data with soil water balance models. A dynamic rather than static approach to the solution of the problem has been recommended (Newton et al., 1983).

4.5.1 Knowledge-based approach

The knowledge-based approach uses a priori information on the hydrological behaviour of soils together with surface observations to predict the profile moisture content. Reutov and Shutko (1986) (as cited by Ragab, 1995) used an approach that combines microwave radiometry and a priori knowledge of soil's hydrophysical parameters to estimate the moisture profile. This approach has been used by Mkrtchjan et al. (1988) (as cited by Ragab, 1995) to produce maps of the top 1 m soil moisture content for 15 agricultural fields. Kondratyev et al. (1977), Jackson (1980) and Jackson et al (1987) (as cited by Ragab, 1995) used a method based on the assumption that the soil profile attains hydraulic equilibrium at some stage. At equilibrium the hydraulic potential, defined as the sum of gravity and pressure potential, becomes equal at all depths.

If the soil moisture at the soil surface is known, its matric potential can be derived from the soil moisture-soil matric potential relationship. Having obtained the matric potential of this surface layer, the matric potential of the other layers can be calculated. The soil moisture-soil matric potential relationship can then be used to obtain the soil moisture of the soil profile. The hydraulic equilibrium works best in the absence of appreciable surface fluxes such as evaporation and precipitation and therefore works better at predawn time.

4.5.2 Statistical methods

Regression analysis This approach is based on developing a regression equation by which it is possible to calculate the profile moisture content from surface moisture content as reported by Zotova and Geller (1985) and Jackson et al. (1987) (as cited by Ragab, 1995). Such an approach is usually based on data for typical soil and land use conditions. These equations usually have low coefficients of determination, R^2 , and cannot be extrapolated from one location to another (Ragab, 1995).

Time series analysis A time series consists of a collection of observations made sequentially in time. Time series methods have been increasingly used in hydrologic investigations and water quality management in the past two decades (Hipel et al., 1977, Hipel, 1985; Zetterqvist, 1991 as cited by Wu et al., 1997). Several researchers have applied time series models to describe the field soil water regime. Nash et al. (1991) (as cited by Wu et al., 1997) used autocorrelation and cross-correlation analyses to examine the relationship between soil water content and rainfall distribution.

Based on the hydrologic balance equation and Richards equation, Parlange et al. (1992) (as cited by Wu et al., 1997) developed a first-order autoregressive Markovian model to estimate the soil water regime in the top 1.05 m of the soil profile. The predicted water storage in the soil profile was close to that measured by the neutron probe. Hipel et al. (1977) (as cited by Wu et al., 1997) discussed key aspects of time series modelling in hydrology and water quality studies.

A transfer function model in the time domain is an input-output filter-type model that is constructed according to the stochastic properties of two related time series. In the analysis, processes and mechanisms governing the reactions are not considered. At the end, observations of one time series (input) may be used to estimate the outcome of another time series (output). When a transfer function model is employed in estimation, the model parameters are a linear combination of observations made in previous time periods.

Wu et al. (1997) conducted a study to estimate soil water fluctuations in the field regime by using time-series-based models Some of their specific objectives were to develop models to predict water contents at deeper soil depths from the water contents measured at a shallower depth of the same profile; and to use time series models to predict the water storage in a soil profile by soil water measurements made at a single soil depth

The advantage of time series modelling is that it is a dynamic approach, i.e., predictions are based on the most recent observations (Wu et al., 1997). The disadvantage of this approach is that it requires site-specific calibration, and time series models usually produce systematic errors. However, calibration is also required in general for process-based models (Wu et al., 1997). In principle, the model based on data measured on a pedon scale is applicable to locations within the distance of spatial correlation length. For locations outside of the spatial correlation length, new models must be established based on data collected from the location (Wu et al., 1997).

4.5.3 Inversion methods

The inversion method uses representative soil moisture and temperature profiles and an inversion algorithm to calculate the profile soil moisture (Entekhabi et al., 1994) The method is relatively new and its accuracy depends on how representative the equations used in the algorithm are of the real situation (Ragab, 1995).

4.5.4 Integration with modelling

Various studies have shown that surface temperature (estimated from space) can be used to infer surface fluxes such as evapotranspiration and soil moisture content by the use of a surface model describing the exchanges between the soil, the vegetation and the atmosphere, (e.g., Carlson et al., 1981; Taconet et al., 1986; Ottlé et al., 1996).The soil water balance models adapted to use the remote sensing data can produce information on soil moisture in addition to the other components of the soil water balance (Ragab, 1995) Generally, soil water balance models differ

in their degree of complexity in depicting the system they represent. The accuracy of the output depends largely on the accuracy of the input. The remotely sensed soil moisture data can be used in these models as input, to update and calibrate (Ragab, 1995)

The possibility of using such information in water balance models was explored by Prevot et al. (1984), Bernard et al. (1986), Ottlé et al. (1989), Ottlé and Vidal-Madjar (1994), and Ragab (1995) Ottlé and Vidal-Madjar (1994) used a one-dimensional, soil-vegetation-atmosphere (SVAT) model. The model is described in several papers (Taconet et al., 1986; BenMehrez et al., 1992a, 1992b; Ottlé and Vidal-Madjar, 1994). The model calculates the surface fluxes, the surface temperature and the surface soil moisture by solving simultaneously the energy budget equation for the bare soil surface and above the canopy. An adequate partitioning of the incident energy fluxes between the vegetation and the soil is assumed as well as knowledge of the daily variation of the atmospheric forcing and the physical characteristics of the soil and of the vegetation

4.6 Continuous operational system for estimation of root-zone moisture

Ragab (1995) explored the possibility of using the above described methods on an operational basis using remotely sensed observations. Ragab (1995) carried out a study to develop and evaluate a system to estimate soil moisture content in the root-zone using active microwaves from the European Remote Sensing Satellite, ERS-1, to measure moisture content in the top 10 cm of the soil profile. The system consists of an initialization phase, which provides surface and root-zone moisture contents as initial values for the dynamic phase of a soil water balance model. The initial value for surface moisture can be either a remotely sensed or a measured value. The surface moisture value for a given day is in turn used to derive the initial value of the root-zone (profile soil) moisture (contents) for the same day. This can be obtained either from an empirical relationship for drying or wetting conditions, or during drying conditions alone.

A proper operational system to estimate profile soil moisture from remotely sensed near-surface soil moisture requires a proper integration between the remotely sensed information and

modelling. In this study a relatively more comprehensive coupled soil heat and water flow model (SUAHEAT) was used to integrate near-surface soil water content derived from remotely sensed soil surface temperature and modelling (see Fig. 4.3). Detailed description of the SUAHEAT model is covered in chapter 5. The measured infrared temperature or TDMax can be used to derive the profile soil temperatures using regression analysis. Similarly, using an empirical relationship between TDMax and the near-surface soil water content, initial profile soil water contents can be derived from the near-surface soil water content measurements. Both the profile soil temperatures and profile soil water contents are required to initialize the SUAHEAT model. The use of the SUAHEAT model offers a possibility of variable soil profile depth, i.e., the soil profile depth could be 0-5, 0-10, 0-15, ..., 0-60 cm or even to greater depths.

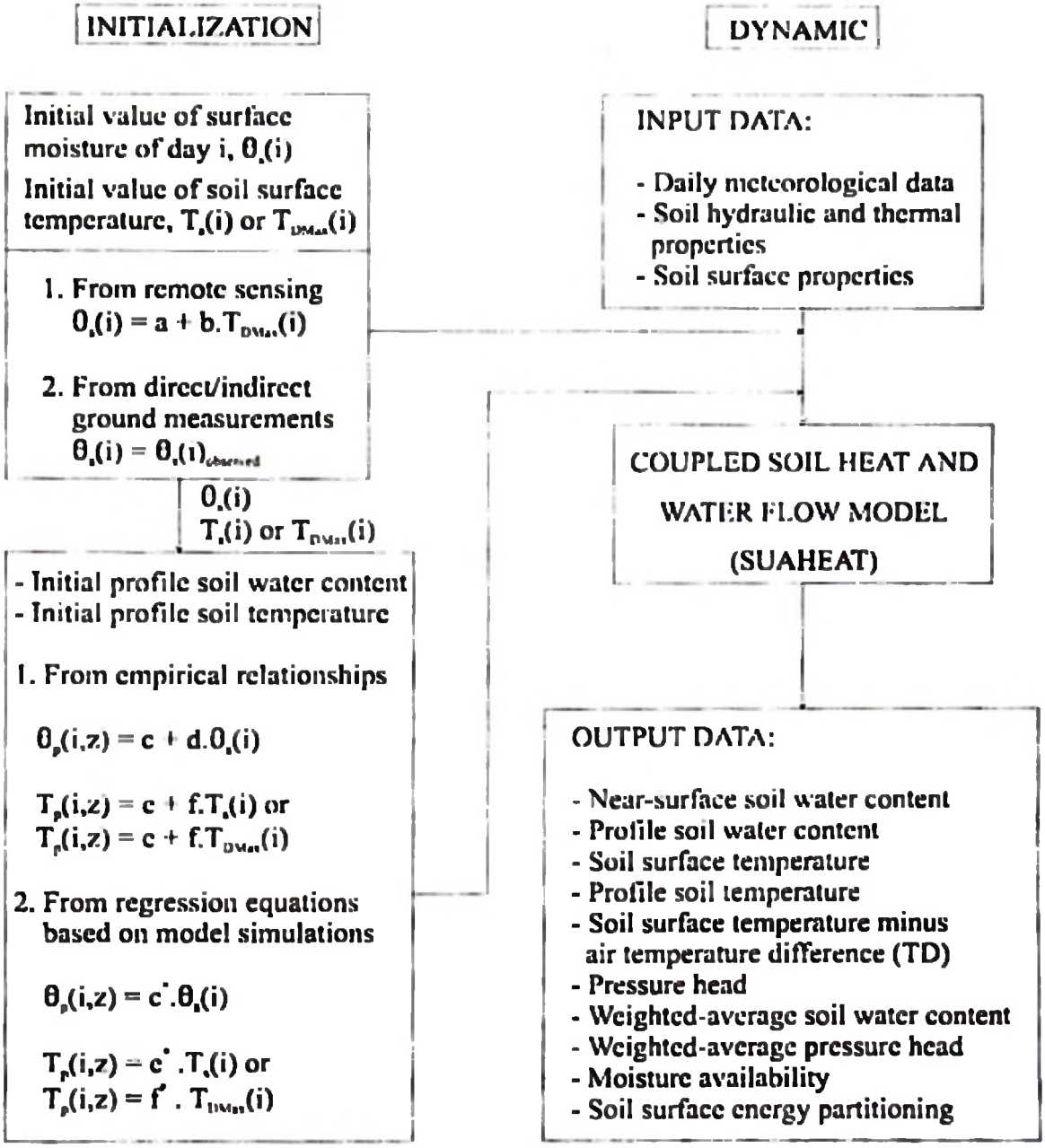

Fig. 4.3 A continuous operational system for estimation of profile soil water content.

In Fig. 4.3, $\theta_s(i)$ is the near-surface soil water content for day i,
$T_s(i)$ is the soil surface temperature corresponding to $\theta_s(i)$,
$T_{DMax}(i)$ is the maximum soil surface temperature minus air temperature difference corresponding to $\theta_s(i)$,
$\theta_s(i)_{observed}$ is the observed (measured) near-surface soil water content,
$\theta_p(i,z)$ is the profile soil water content for day i and depth z,
$T_p(i,z)$ is the profile soil temperature for day i and depth z, and
a, b, c, d, e, f, c^*, e^*, and f^* are constants.

5 THEORY AND MODELLING OF HEAT AND WATER FLOW IN THE SOIL

5.1 Coupled transport processes in unsaturated porous media

5.1.1 General overview

Coupled flow of heat and water in the soil is a complex subject. In this study, more emphasis was therefore put on the formulation of the model building blocks rather than a detailed theoretical treatment of the subject matter Comprehensive treatment of the subject matter can however be found in the literature (e.g., Parlange et al., 1998; Mohanty et al., 1998) Recent literature (e.g., Parlange et al., 1998) has underlined the need for further measurements of coupled heat and moisture transport in diurnally-heated soils. The advent of more accurate instruments coupled with modelling of the simultaneous flow of heat and water in the soil will definitely attempt to provide answers to the many questions about the complex movement of heat and water in unsaturated soil near the land-atmosphere interface, particularly under arid and semiarid conditions.

5.1.2 Theory of coupled transport processes in unsaturated porous media

Unsaturated soil can be described as a complex porous medium that is composed of the three phases. solid particles, liquid water and gaseous air. The solid phase consists of a large number of mineral and organic particles of different sizes and shapes. The liquid water phase contains dissolved inorganic and organic solutes.The gaseous phase is composed of nitrogen, oxygen, carbon dioxide, organic vapours and water vapour.The fractions of each phase change spatially and temporally.The phases interact strongly with each other, and each of the phases has a too complex geometry to be known completely.

Transport of liquid water, of air, of compounds dissolved in liquid water, of water vapour (as part of the air phase), and of heat are the relevant transport processes in the unsaturated zone under field conditions.

Transport of liquid water: Water moves due to potential gradients from high to low potential. If a unit mass of water is transported from its reference state to another equilibrium state, the required work is called the total potential of the water at the new state. The reference state (of zero potential) is usually taken to be pure, free water at atmospheric pressure, a temperature of 20 °C and a certain geodetic height.

Potential gradient can be expressed either as work per unit mass or work per unit volume of water. In the former case, potential gradient attains the units of J/kg (i.e., Nm/kg). In the latter case, potential gradient assumes the units of pressure [i.e., $Nm/m^3 = N/m^2$ = Pascal (Pa)]. For convenience, potential is often expressed as the equivalent height of a water column, in units of length [m]. In porous media, the total potential can be defined as the sum of gravitational potential, matric potential, pneumatic potential, and osmotic potential. Temperature influences the matric, pneumatic, and osmotic potentials. In addition, temperature influences liquid water transport due to the change of hydraulic conductivity with temperature. The gravitational potential increases with increasing distance from the centre of the earth, and is quantified by the geodetic height above a datum.

The matric potential is a potential that only water in a porous medium (or in fine capillaries) has. It is related to the adhesive and cohesive forces of water, solid particles and soil air and quantifies how strong water is attracted by the solid particles. The matric potential of water at atmospheric pressure, e.g., directly at the water table, is defined to be zero. Work is required to transport soil water that is attracted by solid particles to a state where it is not in contact with solid particles and at atmospheric pressure; therefore, matric potential is a negative number. Matric potential increases with water content, i.e., it becomes less negative.

The term suction is a synonym for the absolute value of matric potential. When the pressure of water is higher than the atmospheric pressure, which only occurs under saturated conditions, the term "matric potential" is replaced by the term "pore water pressure potential", which is always a positive number. Matric potential reflects the phenomena of both adsorption of water at the surfaces of the solid particles and capillarity. Capillarity involves pressure differences across curved water-air interfaces under surface tension, whereas adsorption occurs due to short-

distance interactions between water, solute and solid. Capillarity is more important than adsorption at high matric potentials, but it is not clear below which matric potential value adsorption becomes dominant (Milly and Eagleson, 1980).

The pneumatic potential of water is caused by pore gas pressure being different from external gas pressure; the higher the pressure in the pore gas adjacent to the water, the higher the pneumatic potential. External or atmospheric pressure is defined to be zero. The osmotic potential is caused by solutes in the soil water. It is defined as the pressure to which a pool of pure water must be subjected in order to be in equilibrium through a semipermeable (i e., permeable to water molecules only) membrane with a pool containing a solution identical in composition with the soil water. The osmotic potential is proportional to solute concentration (and temperature) and is negative or zero.

Water flow due to temperature gradients: Temperature gradients are considered to be indirect driving forces of liquid water transport. At constant soil water content, matric potential changes with temperature (Philip and de Vries, 1957). This could be attributed to the fact that surface tension of water changes with temperature (Briggs, 1897).

Transport of heat: Transport of heat in the soil occurs through conduction, convection and radiation; in that order of importance (de Vries, 1975). Temperature gradients are necessary for heat conduction to take place. Convection of heat takes place when a fluid or any other matter (water, water vapour, air) and with it its heat content is transported. Latent heat is transported by the vapour and released at condensation. Radiation is of electromagnetic nature, but only important in large, dry pores at high temperatures (de Vries, 1975) or at the soil surface. Conductive heat flux in the soil is mostly orders of magnitude larger than convective heat flux. The soil thermal conductivity depends on the volume fractions of the soil constituents (the different minerals, liquid water, and air) and their geometries (de Vries, 1958). Soil thermal conductivity is known to increase with quartz and soil water contents as well as with bulk density (Farouki, 1986).

Coupled transport of liquid water, water vapour and heat in unsaturated soils: Soil water movement in unsaturated soils has been extensively studied for many years. Most of the studies have been conducted under isothermal conditions, which neglect water movement in response to temperature gradients. In arid and semiarid regions, where temperature gradients can be very large, transfer of water from warmer to cooler regions may have a significant effect on soil water status, especially in near-surface horizons. Prediction of water content for these areas may be in error if the effects of temperature gradients are not considered (Bach, 1992).

Incorporation of temperature components into theoretical or numerical models, however, greatly complicates analysis. In some cases, neglecting thermal effects may not cause significant errors in estimation of soil water movement. It is therefore important that theoretical and numerical models that incorporate simultaneous water movement and heat flow be tested and validated with experimental data (Bach, 1992).

Philip and Vries (1957) presented a theory to describe coupled water and heat flow in soil. Van Bavel and Hillel (1975, 1976), Sophocleous (1979), Milly (1982), Bristow et al. (1986), and Nassar and Horton (1989a, b) expanded and/or used the theory to calculate heat and water flow in soil. In many cases, heat flow by radiation, convection, and conduction is modelled by the conduction equation alone (Hanks et al., 1971, Wierenga and De Wit, 1970; Gupta et al., 1981; Horton et al., 1984a, b; Parton, 1984, Persaud and Chang, 1984). Apparent thermal properties rather than real thermal properties (Jackson and Kirkham, 1958) are assumed to account for both conductive and non-conductive heat flow. Many investigators have modelled soil heat transfer in two dimensions (Takakura et al., 1971; Jury and Bellantuoni, 1976a, b; Davis, 1977; Mahrer and Katan, 1981; Mahrer, 1982; Horton et al., 1984a, b; Horton, 1989; Benjamin et al., 1990; Kluitenberg and Horton, 1990).

Milly and Eagleson (1980, 1982) and Milly (1982, 1984) developed a comprehensive numerical model for simultaneous moisture and heat flow using a matric-head-based equation formulation instead of the water-content-based formulation of Philip and de Vries. They tested the model against analytical solutions and measured data for several simplified cases and found that the model performed well under these conditions. However, no tests were performed in which the

full moisture- and heat-flow model was compared with experimental data that measured water movement under the influence of both water-content and temperature gradients.

Other studies (e.g., Entekhabi et al., 1994) have neglected vapour flow for simplification purposes and therefore considered liquid phase only. In some cases, the coupling between the heat and moisture equations has been solely through the thermal properties of the soil. In this study the coupling of the flow equations has been further enhanced by taking into account the temperature dependence of both the pressure head and unsaturated hydraulic conductivity functions.

5.2 The surface energy balance

Explicit initial conditions and the lower boundary conditions of soil temperature and water content must be specified before equations (5.37) and (5.50) can be solved. In this model, an energy partitioning method can be used to determine the thermal and hydraulic upper boundary conditions. Equations (5.37) and (5.50) are coupled by way of the surface boundary conditions. The surface evaporative flux depends in part on the soil surface temperature while the soil surface temperature is likewise influenced in part by the evaporative flux. The surface boundary conditions are determined implicitly by solving a set of temperature-dependent equations. The equations are physically based and describe the partitioning of energy at the soil surface (Horton, 1989).

5.2.1 Energy partitioning at the soil surface

The central equation that sets boundary conditions to both the soil and the atmosphere is the energy balance equation of the soil surface (see Fig. 5.1):

$$R_n - H - LE - G = 0 \tag{5.1}$$

where R_n is net radiation flux (positive downward) in Wm^{-2},

H is sensible heat flux (positive upward) in Wm^{-2},

LE is latent heat flux (positive upward) in Wm^{-2}, and

G is soil heat flux into the soil (positive downward) in Wm^{-2}

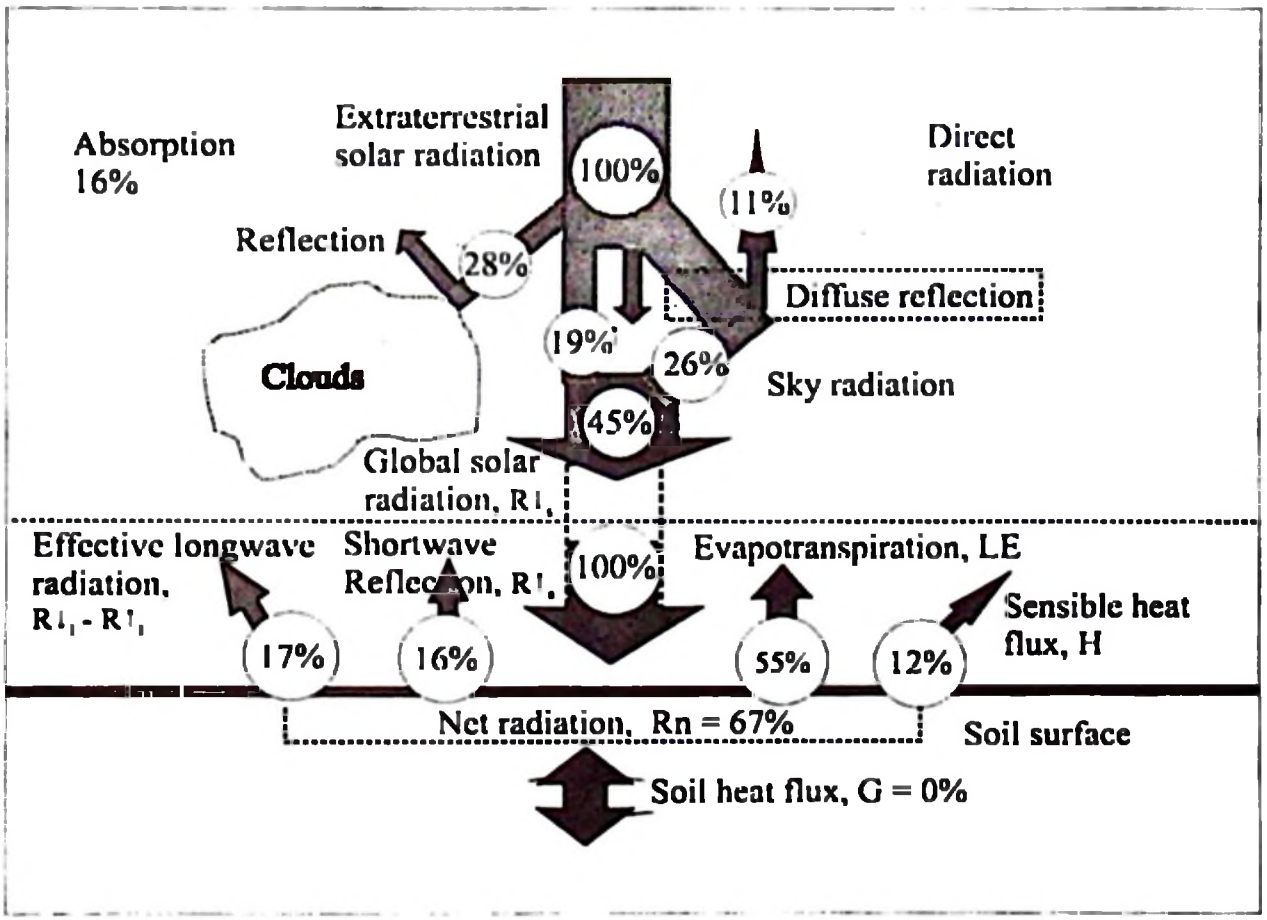

Fig 5.1 Typical distribution of the radiation components and energy partitioning at the soil surface for a summer day (Jury, 1991).

The net radiation flux is the result of incoming and outgoing radiation fluxes

$$R_n = (1 - \alpha) R_g + (1 - \alpha) R_l - \epsilon\sigma(T_s + 273.16)^4 \qquad (5.2)$$

where R_g is the measured global radiation in Wm^{-2},

R_l is the longwave sky irradiance in Wm^{-2},

T_s is the soil surface temperature in °C,

a is the soil surface albedo (soil's reflection coefficient for shortwave radiation),

α is the soil's reflection coefficient for longwave radiation,

ϵ is the emissivity of the soil (soil's emission coefficient),

σ is the Stefan-Boltzmann constant in $Wm^{-2}\,°K^{-4}$.

For longwave radiation at the soil surface, the sum of ϵ and α equals 1, so Eq. (2) can be written as:

$$R_n = (1 - a)R_g + \epsilon(R_l - \sigma(T_s + 273.16)^4) \qquad (5.3)$$

5.2.2 Shortwave radiation terms

Global radiation: Measured values of global radiation are used for direct computation of net radiation on the bare soil surface Global radiation as a function of time, R_g, is described as (Van Bavel and Lascano, 1979)

$$R_g = (R_{dg}/D_L)\sin[(t - S_n + D_L/2)\pi/D_L] \qquad (5.4)$$

where R_g is global radiation in $W\,m^{-2}$,

R_{dg} is the input daily global radiation in $J\,m^{-2}$,

D_L is the input day length in s,

S_n is the input solar noon time in s, and

t is the time of day in s

Albedo: Many state variables such as superficial soil water content are not directly measurable by the spaceborne or airborne sensors (Bastiaanssen, 1991). Only a correlation analysis between measured signals and ground truth data may bring solutions. Out of all hydro-meteorological variables, only surface temperature can be directly measured. The surface albedo can be measured indirectly by means of spectral reflectance satellite data (Menenti et al., 1989a as cited by Bastiaanssen, 1991). A relationship between surface albedo and surface temperature exists. Satellite observations and field measurements under completely different climatological

conditions and with different length scales have shown that albedo and surface temperature are mutually related (e.g., Menenti et al., 1989b and Bastiaanssen, 1990 as cited by Bastiaanssen, 1991). The slope of the surface temperature expressed as a function of surface albedo has usually two different signs: a negative sign occurs at radiation controlled surface temperature, i.e., no evaporation. A positive sign occurs at evaporative controlled surface temperatures, i e., wet areas (Menenti et al., 1989b as cited by Bastiaanssen, 1991).

Albedo of bare soil has been reported to depend on solar elevation Generally albedo for bare soils reaches a maximum at incidence angles ranging from 70 to 80 degrees. Cloud cover has also been reported to affect soil albedo. Surface roughness, mineral composition, and organic matter content are known to have strong effects on albedo. Clearly of much interest is the marked effect of soil moisture on soil albedo A linear dependence of albedo on volumetric water content has been reported in the literature (e.g , Idso et al., 1975, ten Berge, 1990) In this study, a linear relationship between albedo, a, and volumetric soil moisture content, θ, has been adopted following ten Berge (1990):

$$a(\theta) = a_{wet} + ((\theta_{crit} - \theta)/\theta_{crit})(a_{dry} - a_{wet}) \qquad (5.5)$$

where θ_{crit} is the moisture content below which albedo starts increasing during drying A θ_{crit} value of 0.25 was assumed. For a_{wet} and a_{dry} , 0 08 and 0.15, respectively, were assumed. Other values can, however, be inputed in the model program Table 5.1 shows albedo values for wet and dry soils.

Table 5.1 Albedo values for wet and dry soils (after Idso & Reginato, 1974 as cited by ten Berge, 1990).

Soil type	Wet	Dry	Source
Dune sand	0.24	0.37	Buttner & Sutter, 1935
Arenosa sand	0.22	0 38	Graser & Bavel, 1982
Yuma sand	0.18	0.42	Gold & ben Asher, 1976
Williams loam	0 14	0.26	Aase & Idso, 1975
Avondale loam	0.14	0.30	Idso et al., 1975
Tippera clay loam	0.14	0.23	Kalma & Badham, 1972
Swifterbant silt loam	0.13	0.31	ten Berge, 1985
Grey soil	0.11	0.27	Kondrat'ev, 1954
Red-brown clay loam	0 10	0.20	Piggin & Schwertfeger, 1973
Sandy loam	0.10	0 17	Feddes, 1971
Oudelande sandy loam	0.08	0.20	van der Heide & Koolen, 1980
Clay	0.08	0 14	Feddes, 1971
Black soil	0.08	0.14	Kondrat'ev, 1954

5.2.3 Longwave radiation terms

Sky radiation: Thermal sky radiation or, more accurately, the incoming longwave radiant flux density or longwave irradiance (W m^{-2}), constitutes an important term in the surface energy balance. In practice, the longwave radiation is often taken to be a function of air temperature at screen height (1.5 m). The longwave irradiance, R_l , can be estimated following Van Bavel and Hillel (1976) from the following form of Brunt's formula:

$$R_l = \sigma(T_a + 273.16)^4 [0.605 + 0.048(1370H_v)^{0.5}] \quad (5\,6)$$

where T_a is the air temperature in °C, and

H_a is the air humidity in kg m^{-3}, all of which are measured inputs.

The expression in square brackets in **Eq. (5.6)** is the apparent emissivity of the atmosphere, $\epsilon_a(0)$, for cloudless sky. The emissivity $\epsilon_a(0)$ depends in principle on the distribution of temperature, water vapour and carbon dioxide in the lower atmosphere. Since about half the radiation comes from the lowest 100 m, the $\epsilon_a(0)$ is therefore strongly correlated with screen temperature.

The apparent emissivity of the atmosphere increases with increasing air temperature because of the strong correlation between air temperature and the total water content of the atmosphere. The apparent emissivity of the atmosphere can be related to the precipitable water, w. Alternatively, based on the knowledge that w is well correlated with the square root of the mean vapour pressure at screen height, e (mbar) (e g , Monteith, 1973), the apparent emissivity can as well be related to the mean vapour pressure. In this study, the following expression was assumed (see also **Eq. 5.6**)

$$\epsilon_a(0) = 0.605 + 0.048(e)^{0.5} \qquad (5.6a)$$

A mean air temperature of 24.0 °C was assumed in the conversion of e (mbar) to H_a (kg m^{-3}) in **Eq. (5.6)**. It is to be borne in mind that the expression given in **Eq. (5.6a)** is empirical and applicable only to particular climatic conditions

The air ambient humidity, H_a , (kg m^{-3}), is determined using dewpoint temperature, T_d, as follows:

$$H_a = 1.323 \exp[17.27\, T_d/(T_d + 237.3)]/(T_a + 273.16) \qquad (5.7)$$

Surface emittance: The longwave radiation leaving the surface (apparent emittance) consists of the terms emittance and reflection. Planck's law for black body radiation expressses the spectral radiance in a direction normal to the surface, $R_{n\lambda}$, as a function of wavelength and absolute

temperature. Applying Lambert's cosine law, the spectral emittance R_λ is found by integrating the radiance over a hemisphere. Finally, integrating R_λ over the whole wavelength interval yields the emittance. The well known Stefan-Bolzmann law expresses this radiant flux density as

$$R_e = -\epsilon\sigma(T_s + 273.16)^4 \qquad (5.8)$$

where R_e is the emittance in W m^{-2},

σ is the Stefan-Bolzmann constant (5.67×10^{-8}) in W m^{-2} $°K^{-4}$,

T_s is the temperature of the emitting body in °C, and

ϵ is the emissivity.

The emissivity ϵ is introduced as a reduction factor for non-black bodies, and is equal to the absorption factor for the corresponding wavelengths (Kirchhoff's law) For the present case, the soil is assumed to be a grey (ϵ independent of λ) body with a flat, homogeneous surface, obeying Lambert's law.

In order to be able to determine the physical surface temperature by means of thermal infrared remote sensing, knowledge of the thermal emissivity of natural surfaces is necessary. The importance of the remote measurement of surface temperature derives from the fact that the surface temperature is a dominant factor controlling the exchange processes between the Earth's surface and the atmosphere and forms one of the basic measurements in energy balance applications using thermal infrared remote sensing (Van de Griend et al., 1985, Van de Griend and Van Boxel, 1989; Van de Griend et al., 1991)

Thermal emissivity is defined as the ratio of radiation emitted by a body at a thermodynamic temperature T to the blackbody radiation at the same temperature. Emissivity is wavelength dependent and can be given as

$$\epsilon_\lambda = R(\lambda,T)/B(\lambda,T) \qquad (5.9)$$

where R is the actual surface radiance, and

B is the blackbody radiance, both at wavelength interval λ and thermodynamic temperature T_s.

The emissivity is needed in remote sensing to derive the physical temperature of the surface from the observed outgoing longwave radiation. Ignoring atmospheric influences and reflected thermal infrared radiation, the outgoing longwave radiation from the surface is given by

$$R = \int_{\lambda_1}^{\lambda_2} \epsilon(\lambda) L_\lambda(T_s) d\lambda \qquad (5.10)$$

where R is the emitted longwave radiation in the wavelength domain (λ_1 - λ_2),

$\epsilon(\lambda)$ is the spectral thermal emissivity of the surface,

λ is the wavelength in m,

T is the absolute temperature in °K, and

$L_\lambda(T_s)$ is the Planck function, given by

$$L_\lambda(T_s) = C_1 \lambda^{-5} \{\exp(C_2 / (\lambda T)) - 1\}^{-1} \qquad (5.11)$$

where $C_1 = 3.74 \times 10^{-16}$ W m^{-2} and $C_2 = 1.4388 \times 10^{-2}$ mK.

Differences in soil texture, mineral composition, organic and moisture content, and differences in vegetation cover have been reported to be the determining factors for the significant variation in the emissivity of terrestrial surfaces (ten Berge, 1990; Van de Griend et al., 1991). Knowledge of field emissivity is of special importance in remote sensing studies in semiarid regions because of the large differences to be found in such environments. A more detailed treatment of the subject matter can be found in the literature (e.g., ten Berge, 1990, Van de Griend et al., 1991; Schmugge et al., 1991; Salisbury and D'Aria, 1992; Norman et al., 1995 (and literature cited therein)). Tables 5.2 and 5.3 summarize emissivity values for different surfaces.

In this study, soil surface emissivity, ϵ, is treated as a function of soil moisture content using the empirical relationship (ten Berge, 1990)

$$\epsilon(\theta) = \epsilon_{dry} + (\theta/\theta_s)(\epsilon_{wet} - \epsilon_{dry}) \quad (5.12)$$

where θ_s is the soil moisture content at saturation. Values of 0.90 and 0.94 were assumed for the ϵ_{dry} and ϵ_{wet}, respectively.

Table 5.2 Soil emissivity values (after ten Berge, 1990)

Soil type	ϵ		λ (m)	Source
	dry	wet		
Coarse silica sand	0.914	0.936	8-12	Buettner & Kern, 1965
White sand	0.890	0.925	10.4-11	Schurer, 1975
Plainfield sand	0.900	0.940	8-12	Fuchs & Tanner, 1968
Avondale loam	0.967	0.980	8-13	Idso & Jackson, 1969 and Conaway & van Bavel, 1967
Swifterbant silt loam	0.910	0.940	8-14	ten Berge, 1986

Table 5.3 Emissivity of different surfaces (after Van de Griend et al., 1991)

Surface Type	Emissivity	
	Mean (8-14 µm)	Standard Deviation
Bare soil (loamy sand)	0.914	0.011
Sorghum, 10% coverage of bare soil	0.940	0.006
Grass (partly covered)	0.956	0.013
Dicotyledonous plants (Solanaceae), almost complete cover	0.985	0.005
Grass, almost complete cover (Gramineae eragrostic)	0.985	0.006
Open grass, partly covered (Gramineae eragrostic)	0.949	0.008
Tall grass, complete cover (0.25 m high)	0.958	0.003
Shrub, partly covered (Rhygozum brevispinosum)	0.952	0.009
Shrub, partly covered (Euclea undulata)	0.976	0.008
Shrub, complete cover (Euclea undulata)	0.986	0.006

5.3 Transport of heat fluxes in the atmospheric boundary layer

5.3.1 Exchange at the surface

From equation (5.1), the sensible and latent heat fluxes constitute the other components of the energy balance equation of the soil surface which sets boundary conditions to both the soil and the atmosphere. The sensible heat flux H can be written as a transport equation, consisting of a driving force, the soil-air temperature gradient (T_s - T_a), and a turbulent diffusion resistance for heat transport r_{ah} (s m^{-1})

$$H = \rho c_p \frac{T_s - T_a}{r_{ah}} \tag{5.13}$$

where ρ is the density (kg m^{-3}) and c_p is the specific heat (J kg^{-1} K^{-1}) of moist air

The turbulent diffusion resistance r_{ah} is a function of wind velocity u (m s^{-1}), the stability of the atmosphere just above the soil surface, and of the nature of the surface structure. Under conditions of neutral stability ($T_s \approx T_a$), r_{ah} can be expressed as a function of only wind velocity and roughness of the surface

$$r_{ah} = \frac{\ln[(z - d)/z_{om}]\ln[(z - d)/z_{oh}]}{k^2 u} \tag{5.14}$$

where z is the elevation reference level in the atmosphere (m) (where wind velocity and air temperature are recorded), d is the zero displacement (m) (assumed to be equal to zero for bare soil surface), k is Von Karman's constant (here taken to be 0.4), z_{om} is the roughness length for momentum (m), and z_{oh} is the roughness length for sensible heat (m). In this study, z_{om} and z_{oh} are assumed to be equal. Eq. (5.14) therefore reduces to

$$r_{ah} = \frac{\ln[z/z_o].\ln[z/z_o]}{k^2 u} \tag{5.15}$$

When evaporation is reduced through drying of the soil, soil temperature will rise and unstable conditions will come into being. Due to temperature-induced differences in air density, vertical mass as well as heat transport will increase. For such conditions, Businger et al. (1971), and Dyer (1967) derived semiempirical mass and heat transport formulas, based on the use of the Monin-Obukhov length L (m) as a measure for stability (Monin and Obukhov, 1954):

$$L = \frac{-u_*^3 \rho c_p T_a}{kgH} \tag{5.16}$$

where u_* is the friction velocity (m s^{-1}) and g is the acceleration due to gravity (9.813 m s^{-2})

The friction velocity, u_*, can be derived from the wind profile equation

$$u = \frac{u_*}{k}\left(\ln\left(\frac{z}{z_o}\right) - P_1\right) \tag{5.17}$$

Similarly, the temperature profile equation is given as

$$T_a = T_1 + \frac{T_*}{k}\left(\ln\left(\frac{z}{z_o}\right) - P_2\right) \tag{5.18}$$

where T_* is the friction potential temperature, assuming that the potential temperature at the 2 m measurement height equals the actual air temperature; P_1 and P_2 are stability correction functions as given below.

The friction velocity, u_*, and the friction potential temperature, T_*, are related by Eq. (5.19).

$$T_* = \frac{H/(\rho c_p)}{u_*} \tag{5.19}$$

Under unstable conditions ($T_s > T_a$ and L negative), r_{ah} can be expressed as (cf. Paulson, 1970)

$$r_{ah} = \frac{(\{\ln[z/z_o] - P_1\}.\{\ln[z/z_o] - P_2\})}{k^2 u} \quad (5.20)$$

where P_1 and P_2 are functions of L according to

$$P_1 = 2\ln(\frac{1+x}{2}) + \ln(\frac{1+x^2}{2}) - 2\arctan(x) + \frac{\pi}{2} \quad (5.21)$$

$$P_2 = 2\ln(\frac{1+x^2}{2}) \quad (5.22)$$

where:

$$x = (1 - 16\frac{z}{L})^{0.25} \quad (5.23)$$

For stable conditions ($T_s < T_a$ and L positive), the formulas established by Webb (1970) can be used. According to Businger et al. (1971), a value of 4.7 was adopted for the constant in these formulas.

$$r_{ah} = \frac{(\{\ln[z/z_o] + 4.7[z/L]\}.\{\ln[z/z_o] + 4.7[z/L]\})}{k^2 u} \quad (5.24)$$

for $L > z$;

$$r_{ah} = \frac{(\{\ln[z/z_o] + 4.7 + 4.7\ln[z/L]\}.\{\ln[(z/z_o] + 4.7 + 4.7\ln[z/L]\})}{k^2 u} \quad (5.25)$$

for $0 < L \leq z$;

The latent heat flux LE can be expressed as a transport equation,

$$LE = \frac{\rho c_p}{\gamma} \frac{e_a - e_c^*}{r_{ah} + r_s} \qquad (5.26)$$

where γ is the psychrometric constant in Pa K^{-1},

e_a is the water vapor pressure in the air in Pa,

e_a^* is the saturated water vapor pressure of air at a temperature T_a in Pa, and

r_s is the soil resistance for water vapor transport in sm^{-1}.

In this study the stability correction functions were not taken into account However, the computer program provides for such an option whereby a user can choose an appropriate indicator to be able to include the stability correction functions in the model simulations. For the results presented in this work, therefore, simple formulations of the sensible and latent heat fluxes at the soil surface were adapted. The latent and sensible heat fluxes at the surface of the soil are calculated by using the equations

$$E = (H_s - H_a)/(1000\, r_a) \qquad (5.27)$$

$$L = 2.49463 \times 10^9 - 2.247 \times 10^6\, T_s \qquad (5.28)$$

$$LE = L \,.\, E \qquad (5.29)$$

$$H = (T_s - T_a)\, C_a / r_a \qquad (5.30)$$

where E is the evaporative flux in m s^{-1} ,

L is the latent heat of vaporization in J m^{-3} (Forsythe, 1964),

r_a is the aerodynamic boundary layer resistance in s m^{-1} ,

C_a is the volumetric heat capacity of air in J $°C^{-1}$ m^{-3} ,

H_s is the humidity of air at the soil surface in kg m^{-3} , and

H is the sensible heat flux in W m^{-2}.

The aerodynamic boundary layer resistance, r_a , is calculated according to Van Bavel and Hillel (1976) as

$$r_a = [\ln (z_m / z_o)]^2 / (k^2 . W_s) \quad (5.31)$$

where z_o is the roughness length in m,

W_s is the wind speed in m s^{-1},

k is von Karman's constant,

z_m is the measurement height (2 m in this study) in m.

Various studies (e.g., Ottlé and Vidal-Madjar, 1994) have shown that surface temperature (estimated from space) can be used to infer surface fluxes such as evaporation and soil moisture by using a rough surface model, provided the measurements are made around the maximum daily value (Carlson et al., 1981, Taconet et al , 1986). Evaporation is a parameter that varies with time and the estimation of the surface fluxes from surface temperature measurements can only be made under cloudless sky conditions (Ottlé and Vidal-Madjar, 1994) This poses some difficulty in direct assimilation of evaporation in hydrologic models. It is preferable to estimate the soil humidity in the soil layer contributing to the evaporation. This parameter is less variable with time (Ottlé and Vidal-Madjar, 1994). The surface temperature (estimated from ground-based infrared thermometer measurements) permits the estimation of the surface soil humidity over the soil surface which can be finally assimilated in the soil heat and water flow model

The humidity of air at the soil surface, H_s , depends not only upon the surface temperature, but also on the surface water content. If H_o is the saturation humidity at the surface temperature, w_1 the water content of the surface layer, and h (m water column) the pressure potential associated with this value, the humidity of the soil surface, H_s , is calculated from the equation

$$H_s = H_o \exp[h/46.97 (T_s + 273.16)] \quad (5.32)$$

where H_o is the saturated humidity at the soil surface in kg m^{-3} , and

h is the soil water pressure head in m.

Relative humidity, $RH = H_s / H_o = \exp(M_w g h / (R(T_s + 273.16)))$ (Kimball et al., 1976)

where M_w, molar mass of water = 0.018 in kg mol^{-1},

R, gas constant = 8.314 in J mol^{-1} K^{-1},

g, acceleration due to gravity = 9.81 in m s^{-2}.

Air absolute humidity, H_{abs} (g cm^{-3}) = (217e)/(T+273.16), where e = vapour pressure in mbar, or H_s (kg m^{-3}) = (0.217e)/(T+273.16).

The saturated humidity, H_o, of the air at the soil surface is calculated by using the following equation suggested by Murray, 1967:

$$H_o = 1.323 \exp[17.27 T_s/(237.3 + T_s)]/(T_s + 273.16) \quad (5.33)$$

Note that h always has a negative value, so that, e.g., if h = -100 m, then the relative humidity (H_s / H_o), at T_s = 30 °C equals 0.993. This approach is approximate in that it assumes that the water content of the surface layer (0.01 m) is equal to that of the very surface.

Evaporation and surface temperature - introduction of a surface resistance term: The assumption of equality of the aerodynamic resistances, r_E and r_H, for exchange of latent and sensible heat, respectively, between the surface and the air at reference height is only justified for crop evaporation, where foliage surface and stomatal cavities are almost at identical temperatures, and the stomatal cavities are saturated (Choudhury, 1989) However, it is less readily justified for a drying soil, because of temperature and moisture gradients within the soil (Fuchs and Tanner, 1967; Choudhury and Monteith, 1988 as cited by Choudhury, 1989). Camillo and Gurney (1986) found that the introduction of a surface resistance in a detailed soil-physics model improved agreement with the observed soil evaporation and surface temperature.

A surface resistance, r_s, was therefore introduced in the expression for the evaporative flux, E, as follows:

$$E = (H_s - H_a)/(1000(r_a + r_s)) \quad (5.34)$$

Surface resistance is an additional aerodynamic resistance to water vapour flux in series with r_a, which reduces evaporation below potential rates (at potential rates $r_s = 0$). For a bare soil, r_s accounts for extra resistance to evaporative loss at the soil surface that results as the surface layers dry.

Many expressions for r_s as a function of near-surface soil water content θ_s have been reported in the literature (e.g , Daamen and Simmonds, 1996). Since θ_s can be sensed remotely, the functional relationships between r_s and near-surface soil water content offer an attractive option of estimating evaporation. In this study the following expression was adopted following Kondo et al. (1990) (as cited by Daamen and Simmonds, 1996)

$$r_s = (3 \times 10^{10})(\theta_{sat} - \theta_s)^{16.6} \quad s\,m^{-1} \tag{5.35}$$

where θ_s is soil water content of the 0- to 20-mm surface layer and θ_{sat} is saturated soil water content.

The influence of surface roughness: The roughness length, z_0, appears in the expression for the aerodynamic boundary layer resistance, r_a , (same as in Eq. (5.31)) thus

$$r_a = [\ln (z_m / z_0)]^2 / (k^2 . W_z) \tag{5.36}$$

Clearly, the surface roughness has a strong influence on the exchange processes. Since a precise value of z_0 cannot be specified for remote sensing purposes, an approximate classification containing four classes is suggested (Seguin and Itier, 1983) (see Table 5.4).

Table 5.4 Values of surface roughness length, z_0 , for different surfaces (Seguin and Itier, 1983)

z_0 (mm)	Surface type
1	Smooth bare soil
1 - 10	Bare soil, grass, pastures, etc.
10 - 100	Wheat, tall crops, shrubs, etc.
100 - 1000	Orchards, forests

Ten Berge (1990) obtained z_o values ranging between 0.02 and 0.15 mm for unvegetated surfaces. Values up to 0.9 mm were occasionally determined in the study. In this study a 1 mm z_o value was assumed for the smooth bare soil.

5.4 Flow of heat in the soil

In many instances, heat flow by convection, radiation, and conduction is modelled by the conduction equation alone. Apparent thermal properties rather than actual thermal properties are assumed to account for both conductive and non-conductive heat flow (Horton, 1989). To predict heat flow in soils, investigators have used either process-oriented or semi- or non-process-oriented methods. Process-oriented models of heat flow are based upon physical principles and generally consist of partial differential equations that require detailed initial boundary inputs; e.g., the numerical models presented by Van Bavel and Hillel (1976), Lascano and Van Bavel (1983), and Horton et al. (1984b). The semiprocess-oriented models of heat flow are partly based upon physical principles but generally require some regression relationships that are site specific. Nonprocess-oriented models are generally site specific regression-type relationships used to estimate soil temperature at a particular depth (Horton, 1989).

5.4.1 Heat flow model

Remote sensing in the thermal-infrared spectral region is more complicated than in the visible near-infrared and the microwave (Price, 1989). This is because thermal-infrared measurements imply a value of *temperature*, which in turn pertains to the *heat* stored in objects. Observations of the Earth's surface are therefore complicated by factors that are unique to this spectral interval (Price, 1989):

(i) The temperature of an object depends on its past history as well as present conditions because objects are capable of storing and then releasing heat.

(ii) At the Earth's surface, heat energy is gained or lost by radiation as well as through exchange of sensible and latent heat (evaporation) with the atmosphere.

Although thermal infrared measurements can provide estimates of the temperature at the surface of the soil being viewed, the resulting temperature values are seldom of interest by themselves. Instead, relationship between temperatures and physical properties at the soil's surface is sought. The observed temperatures are affected by the prevailing conditions at the time and location of the measurement. Qualitative interpretation of the values of temperatures obtained can be made through general knowledge of the prevailing conditions. More precise inference of surface properties, however, requires additional information about the surface and the local atmospheric conditions and processing of these data by means of a model according to the result desired (Price, 1989). The heat-flow equation, which describes the behaviour of temperature in the soil, is the starting point for a quantitative description. Together with a surface boundary condition, the heat-flow equation relates observed surface temperatures to the energy flux exchanged with the atmosphere (Price, 1989).

Soil heat transfer is frequently considered as a one-dimensional (vertical) process. This is justifiable in the case under consideration because generally surface-temperature variations extend only to a depth of some tens of centimetres over a day, or a few metres over the course of a year. Both distances are so small that effects of horizontal variability are negligible and one-dimensional treatment is satisfactory. However, certain circumstances cause two- or three-dimensional soil heat flow to occur (e g., incomplete surface cover by plants or mulches, buildings, pipelines or other buried heat sources, and ridges or other nonuniformities in surface configuration). In this study, a one-dimensional vertical coupled heat and water flow is considered.

An equation describing conductive heat transfer in a vertical one-dimensional system is:

$$C\frac{\partial T}{\partial t} = \frac{\partial}{\partial z}(\lambda \frac{\partial T}{\partial z}) \qquad (5.37)$$

where C is the volumetric heat capacity in J $°C^{-1}$ m^{-3} ,

T is the temperature in °C,

t is the time in s,

z is the depth (positive downward) in m, and

λ is the thermal conductivity in W m^{-1} $°C^{-1}$.

For remote-sensing applications, this equation is solved to yield T_s at the soil's surface. The solution of the above equation requires a surface boundary condition, which may be provided either by specification of the value of temperature as a function of time at the surface z = 0 or else by a condition on the surface energy flux This latter condition requires specification of the value of the ground heat flux G at the surface as covered under subsection 5.4.2.

In the presence of a temperature gradient in a moist soil, heat transfer takes place by convection in addition to conduction. For the present case, Eq. (5.37) is used to describe heat transfer by making λ the apparent thermal conductivity rather than the real thermal conductivity; thus, convective heat transfer is not explicitly modelled In a moist soil, λ depends on the soil water content, which can vary with both depth and time

5.4.2 Soil heat flux

The heat flux into the soil is proportional to the temperature gradient and the heat conductivity in the soil (Soer, 1980),

$$G = -\lambda \frac{\partial T}{\partial z} \tag{5.38}$$

where G is the soil heat flux in W m^{-2} ,

λ is the thermal conductivity for soil surface in W m^{-1} $°C^{-1}$, and

$\partial T/\partial z$ is the vertical soil temperature gradient at the soil surface in °C m^{-1}.

The soil temperature gradient generally increases when the soil temperature increases, but heat conductivity decreases at increasing surface temperatures because an increase in surface temperature usually results from a lower water content of the soil The variables R_n, LE, H, and G in Eq. (5.1) are all functions of the unknown soil surface temperature Before the soil surface temperature can be calculated, the right-hand side of Eq. (5.38) must be estimated numerically. The following approximation (Chung and Horton, 1987) is used in the present model,

$$G = -\lambda\left[\frac{T_2 - T_s}{\Delta z}\right] + (T_s - T_1)C\frac{\Delta z}{2\Delta t} \qquad (5.39)$$

where T_s is the surface temperature for the present time step in °C,

T_1 is the surface temperature from the previous time step in °C,

T_2 is the soil temperature from the previous time step for the node at vertical position 2 in °C,

Δz is the vertical spatial increment in m,

C is the volumetric heat capacity for the soil surface layer in J °C^{-1} m^{-3}, and

Δt is the time step increment in s.

The above equation approximates the soil heat flux density by adding a term that estimates soil heat flux at a depth of $\Delta z/2$ and a term that estimates the change in heat stored in the soil above $\Delta z/2$.

The value of T_s is solved at each numerical time step by Eq. (5.1) (by using Eq. (5.2), (5.29), (5.30), and (5.39) to describe R_n, LE, H, and G, respectively), using a bisector root-finding algorithm (James et al., 1977). The predicted soil surface temperature, T_s, from the energy balance partitioning is used as the upper-boundary condition. The soil-water evaporative flux is also predicted at each time step as a result of the surface energy partitioning.

5.4.3 Parameters

A recurring problem in all the research dealing with remote sensing of soil moisture is accounting for the effects of soil properties, i.e., soil moisture/matric potential and soil moisture/unsaturated hydraulic conductivity or matric potential/unsaturated hydraulic conductivity relations. Similarly, realistic simulations of physical processes require not only adequate mathematical formulations but also reasonable and representative parameter values Coupled soil heat and water flow in soils requires a few highly nonlinear parameters which are themselves functions of dependent variables, i e, matric potential and temperature. The soil water characteristic curve (section 5 5.2) relates the liquid water content to the matric potential and influences both liquid water and water vapour movements. Of great importance is the unsaturated hydraulic conductivity function (section 5.5.3). Predictive models of the thermal properties of soils, thermal conductivity and heat capacity, are presented in sections 5 4.3.1 and 5.4.3.2, respectively. The soil thermal properties are expressed as functions of soil water content Because of the difficulty involved in measurements of both soil hydraulic and thermal properties, more and more use of predictive models is becoming a common feature especially in modelling works.

Thermal conductivity of soils Soil thermal conductivity is defined following the approach of de Vries (1963), Cass et al. (1984), Campbell (1985), and Daamen and Simmonds (1996). Consider that the bulk soil matrix consists of air, water, quartz solid, and nonquartz solid in fractions

p_a, p_w, p_q, and p_{nq}, respectively ($p_a + p_w + p_q + p_{nq} = 1$, $p_w = \theta$).

Soil thermal conductivity, λ (W m^{-1} °C^{-1}), is then described by

$$\lambda = C_1 + C_2\theta - (C_1 - C_4)\exp[-(C_3\theta)^{C_5}] \qquad (5.40)$$

where

$$C_1 = \frac{0.57+1.73p_q+0.93p_{nq}}{1.0-0.74p_q-0.49p_{nq}} - C_2\theta_{sat} \quad (5.41)$$

$$C_2 = 2.8(p_q + p_{nq})\theta_{sat} \quad (5.42)$$

$$C_3 = \theta_{sat} + \frac{2.6\theta_{sat}}{(f_c)^{1/2}} \quad (5.43)$$

$$C_4 = 0.03 + 0.7(p_q + p_{nq})^2 \quad (5.44)$$

$$C_5 = 4 \quad (5.45)$$

f_c is the fraction of soil particles with diameter < 2 μm (the clay fraction), and θ_{sat} is the saturated soil water content.

Volumetric heat capacity of soils: The volumetric heat capacity C of a soil is defined as the change in heat content of a unit bulk volume of soil per unit change in temperature. Its SI units are joules per cubic metre per degree. As such, C depends on the composition of the soil's solid phase (the mineral and organic constituents present), bulk density, and the soil's soil water content (see Table 5.5) (Hillel, 1980).

The value of C can be calculated by addition of the heat capacities of the various constituents, weighted according to their volume fractions as given by de Vries (1975),

$$C = \sum p_s C_s + p_w C_w + p_a C_a \quad (5.46)$$

Here, p denotes the volume fraction of each phase: solid (subscripted s), water (w), and air (a).

The solid phase includes a number of components, subscripted i, such as various minerals and organic matter. The C value for water, air, and each component of the solid phase is the product of the particular density and specific heat per unit mass

(i.e., $C_w = \rho_w c_{mw}$, $C_s = \rho_s c_{ms}$, $C_i = \rho_i c_{mi}$).

Thus, Eq. (5.46) can be simplified as follows:

$$C = p_m C_m + p_o C_o + p_w C_w \tag{5.47}$$

where subscripts m, o, w refer to mineral matter, organic matter, and water, respectively.

Note that $p_m + p_o + p_w = 1 - p_a$, and the total porosity $p = p_a + p_w$. The volume fraction of water p_w can also be designated as θ.

Knowing the approximate average values of C_m , C_o , and C_w (0.46, 0.60, and 1.0 cal/g. respectively), Eq. (5.47) can further be simplified to give

$$C = 0.46 p_m + 0.60 p_o + p_w \tag{5.48}$$

Table 5.5 Densities and volumetric heat capacities of soil constituents (at 10 °C) and of ice (at 0 °C)

	Density, ρ	Heat capacity, C
Constituent	(kg/m³)	(J/m³ K)
Quartz	2.66×10^3	2.0×10^6
Other minerals (average)	2.65×10^3	2.0×10^6
Organic matter	1.3×10^3	2.5×10^6
Water (liquid)	1.0×10^3	4.2×10^6
Ice	0.92×10^3	1.9×10^6
Air	1.25	1.25×10^3

In this study the soil volumetric heat capacity (J $°C^{-1}$ m^{-3}) is determined following De Vries (1963) as,

$$C = (1 - \theta_s)\ 1.92 \times 10^6 + 4.18 \times 10^6\ \theta \qquad (5.49)$$

where θ_s is the saturated water content (assumed equal to the total porosity, p) for the specific soil. Eq. (5.49) is merely a conversion of Eq. (5 48) to SI units.

5.5 Flow of water in the soil

An equation describing water movement in a one-dimensional medium (Haverkamp et al., 1977; Horton, 1989) is:

$$F\frac{\partial h}{\partial t} = \frac{\partial}{\partial z}[K(h)(\frac{\partial h}{\partial z} - 1)] \qquad (5.50)$$

where F is the specific water capacity, $d\theta/dh$, in m^{-1}, which represents the slope of the soil moisture characteristic curve,

θ is the volumetric water content in $m^3\ m^{-3}$,

h is the soil water pressure head in m,

K is the hydraulic conductivity in m s^{-1} , and

z is the vertical distance positive downward in m.

In this study the thermal liquid flow is assumed to be insignificant, as demonstrated by Milly (1984) (as cited by Chung and Horton, 1987) for most soil water contents except very wet conditions.

5.5.1 Soil hydraulic properties

Soil hydraulic properties are required to fully understand and predict water movement in the soil. Soil hydraulic properties include the soil water characteristic curve (the relation between

volumetric water content [θ] and pressure head [h]), θ(h), and hydraulic conductivity. Numerical solutions of the flow and transport problems in the vadose zone are the most important approaches to predict quantitatively the dynamic behaviour of the system. Modelling of unsaturated flow and transport of water in the soil usually requires accurate and complete information about the unsaturated hydraulic properties for the proper functioning of the model

Unsaturated hydraulic properties can be determined using either direct or indirect methods. Direct determination of the hydraulic properties both in the laboratory and in the field are time consuming and are limited by the uncertainty in the estimated hydraulic parameters, especially for field methods. Bearing in mind the limitations of the direct methods of determination of hydraulic properties, various efforts have been made to relate hydraulic conductivity and the soil water characteristic curve to easily determined soil physical properties. This approach results in indirect methods (Shao and Horton, 1998). The use of pedotransfer functions (PTFs) as an alternative to the direct methods has proliferated over the last two decades. PTFs estimate the hydraulic properties through correlation with more easily measured or widely available soil parameters (Schaap et al., 1998).

Several attempts have already been made to address the limitations of both the direct and indirect methods of determination of soil hydraulic properties. Shao and Horton (1998) developed an integral method for estimating soil hydraulic properties based on the Richard equation of water flow in soils. Using the integral method the soil water characteristic curve could be measured within several days as compared to several weeks by using pressure plate apparatus. Schaap et al. (1998) reported on the use of neural-network-based PTFs. Compared with traditional PTFs, neural networks have the advantage of not requiring a priori model concept (Schaap et al., 1998).

5.5.2 Soil water characteristics

Introduction: Soil water content and matric potential are functionally related to each other, and the graphical representation of this relationship is termed the soil-moisture characteristic curve.

As mentioned in subsection 5.5.1, soil water characteristic curves are difficult to measure in the field, hence methods are needed to relate easily measured soil physical properties to soil water retention characteristics (Rawls et al., 1991). Tables A7.3 and A7.5 in Appendix 7 give, respectively, the estimation equations for the Brooks and Corey parameters, and soil water retention and hydraulic conductivity relationships, according to Rawls and Brakensiek (1989).

Parameterization: The process of fitting a function (curve) to the simultaneously measured volumetric water content and matric potential values is referred to as parameterization. The van Genuchten (1980) parameterization scheme of the water retention function of soils has over the last decade been used by many researchers. In this study soil water characteristics and specific water capacity are described by empirical equations presented by van Genuchten (1980) as follows

$$\theta = \theta_r + (\theta_s - \theta_r)\left[\frac{1}{1 + (\alpha_1 h)^n}\right]^{1-\frac{1}{n}} \qquad (5.51)$$

$$C(\theta,h) = (n-1)(\theta_s - \theta_r)\frac{\left[1 - \left(\frac{\theta - \theta_r}{\theta_s - \theta_r}\right)^{\frac{n}{n-1}}\right]}{h} \qquad (5.52)$$

where θ_s and θ_r are saturated and residual water contents, h is the absolute value of the pressure head, and α_1 and n are nonlinear regression parameters describing the shape of the soil-water characteristic curve. In this study, hysteresis effects are not taken into account.

Temperature dependence: Matric potential is known to increase with increasing temperature at constant soil water content. Similarly, soil water content decreases with increasing temperature at constant matric potential. Matric potential reflects on the one hand the air-water interface forces, capillarity, and on the other the attraction of water by the grain surfaces. Philip and de Vries (1957) proposed, therefore, that matric potential increases with temperature because the surface tension decreases with temperature.

In this study the temperature dependence of the matric potential (pressure head) has been taken into account by including a "temperature correction factor" based on the temperature-dependent air/water interfacial tension. The air/water interfacial tension (N/m) can be determined as follows (Witono and Bruckler, 1989):

$$\sigma_{aw}(T) = [(-0.15301(T+273.16)) + 117.528] \cdot 10^{-3} \qquad (5.53)$$

where T is temperature in °C.

The generalized soil water potential (pressure head) can then be determined as follows (Witono and Bruckler, 1989):

$$h(\theta,T) = [\sigma_{aw}(T)/\sigma_{aw}(T_0)]h(\theta) \qquad (5.54)$$

where T_0 is a reference temperature in °C. The term $[\sigma_{aw}(T)/\sigma_{aw}(T_0)]$ on the right-hand-side (RHS) of Eq. (5.54) is the "temperature correction factor" for the matric (pressure) head function. A reference temperature, T_0, of 28.75 °C was used in this study

5.5.3 Unsaturated hydraulic conductivity

The hydraulic conductivity of a soil decreases with its water saturation, because the empty pores can no longer contribute to flow. The decrease depends on the pore size distribution, expressed by the water retention curve, and the connections between the pores (Mualem, 1976a). Often, unsaturated hydraulic conductivity is expressed as a function of matric potentials instead of water content because, firstly, matric potential can be measured much more easily than water content and, secondly, simulation models use matric potential (pressure head) as a dependent variable

Generally, the unsaturated hydraulic conductivity function is soil specific and changes with the dry density of the soil. In this study, hysteresis of the unsaturated hydraulic conductivity as a function of water content is neglected (cf. Mualem, 1976b).

Parameterization: In this study hydraulic conductivity is described by an empirical equation presented by van Genuchten (1980) as follows:

$$K(h) = K_s \frac{[1 - (\alpha_1 h)^{n-1}[1 + (\alpha_1 h)^{\frac{1-n}{n}}]]^2}{[1 + (\alpha_1 h)^n]^{\frac{n-1}{2n}}} \qquad (5.55)$$

where K_s is the saturated hydraulic conductivity, h is the absolute value of the pressure head, and α_1 and n are nonlinear regression parameters describing the shape of the soil-water characteristic curve. The above equation is the combined van Genuchten-Mualem model based on the Mualem (1976a) unsaturated hydraulic conductivity model and the van Genuchten (1980) analytical parameterization of the water retention curve.

Temperature dependence: The hydraulic conductivity as a function of matric potential is subject to two counteracting effects. Firstly, hydraulic conductivity decreases because the amount of water held at a given matric potential decreases as temperature increases. Secondly, hydraulic conductivity increases because the viscosity of water, μ, decreases. Therefore, hydraulic conductivity as a function of matric potential may increase or decrease with temperature.

In this study, the temperature effect on the hydraulic conductivity has been taken into account by including a "temperature correction factor" based on the temperature-dependent soil water viscosity. The soil water viscosity ($m^2 s^{-1}$) can be determined as follows (Witono and Bruckler, 1989):

$$\mu(T) = 1.0681 \times 10^{-3} \exp[-0.02372 (T + 273.16)] \qquad (5.56)$$

where T is temperature in °C.

The generalized hydraulic conductivity ($m s^{-1}$) can then be determined as follows (Witono and Bruckler, 1989):

$$K(h,T) = [\mu(T_0)/\mu(T)]K(h) \qquad (5.57)$$

where T_0 is a reference temperature in °C. The term $[\mu(T_0)/\mu(T)]$ on the RHS of Eq. (5.57) is the "temperature correction factor" for the unsaturated hydraulic conductivity function. A reference temperature, T_0, of 28.75 °C was used in this study.

5.5.4 Surface infiltration

Infiltration is the term applied to the process of water entry into the soil, generally by downward flow through all or part of the soil surface (Hillel, 1980). Water may enter the soil through the entire surface uniformly, as under ponding or rain, or it may enter the soil through furrows or crevices. It may also move up into the soil from a source below (e.g., a high water table). The rate of this process, relative to the rate of water supply, determines how much water will enter the root zone, and how much, if any, will run off.

Infiltration rate: The infiltration rate is defined as the volume flux of water flowing into the profile per unit of soil surface area (Hillel, 1980). This flux, with units of velocity, has also been referred to as infiltration velocity. For the special condition wherein the rainfall rate exceeds the ability of the soil to absorb water, infiltration proceeds at a maximal rate, which Horton (1940 as cited by Hillel, 1980) called the soil's infiltration capacity. Hillel (1971) proposed the term infiltrability to designate the infiltration flux resulting when water at atmospheric pressure is made freely available at the soil surface.

Darcy's equation for vertical flow is

$$q = -K\frac{dH}{dz} = -K\frac{d}{dz}(h - z) \qquad (5.57a)$$

where q is the flux, H the total hydraulic head, h the pressure head, z the vertical distance from the soil surface downward (i.e., the depth), and K the hydraulic conductivity. At the soil surface, $q = i$, the infiltration rate. In an unsaturated soil, h is negative and can be expressed as a suction head ψ. Hence,

$$q = K\frac{d\psi}{dz} + K \qquad (5\ 57b)$$

5.6 Estimating near-surface soil water content from infrared thermometry (IRT) measurements

5.6.1 Basic equations

Remotely-sensed estimates of soil moisture are averages in space and depth. If these estimates are to be compared to ground-truth data or modelled data, the latter have to be averaged over the same depth. Two methods for extracting near-surface soil volumetric water contents from IRT measurements were considered in this study.

1. The simplest method involves direct extraction of volumetric water content estimates from classical "TDMax/volumetric water content" regression lines. "Normalized TDMax" can also be used in place of TDMax. Assuming that

$$TDMax = a\theta_{0\text{-}x} + b \qquad (5.58)$$

where TDMax is the daily maximum soil surface temperature minus air temperature difference in °C;

$\theta_{0\text{-}x}$ is the volumetric water content between the soil surface (0) and the depth (x) in $m^3\ m^{-3}$;

a slope of the regression line in $°C/(m^3\ m^{-3})$,

b intercept of the regression line in °C.

The volumetric water content, $\theta_{0\text{-}x}$, can be directly estimated from the TDMax values. The x value generally varies between 1 and 10 cm.

2. The second method is derived from the first one and leads theoretically to precise near-surface soil water content estimates. This method is an adaptation of the theoretical equations developed by Bruckler et al. (1988) based on microwave measurements. In this study it was assumed that for a given soil different empirical calibration lines between the TDMax and volumetric water content calculated for several arbitrary soil depths (0-1, 0-2, ..., 0-10 cm, for example) were available In the following equations the subscript "1" refers to the first regression line (corresponding to the first layer), and the subscript n to the last. The symbols a and b correspond to the slope and intercept of the regression lines, respectively, whereas the notation $\theta_{i,i+1}$ and TDMax corresponds to the mean volumetric water content between the depths i and i+1 and the maximum infrared minus air temperature difference, respectively. The following set of equations were thus obtained:

$$\begin{aligned} a_1\theta_{0,1} + b_1 &= TDMax \\ a_2\theta_{0,2} + b_2 &= TDMax \\ &\cdot \\ &\cdot \\ &\cdot \\ a_n\theta_{0,n} + b_n &= TDMax \end{aligned} \qquad (5.59)$$

It was further assumed that an obvious set of relationships between the ($\theta_{0,1}$, $\theta_{0,2}$, ..., $\theta_{i-1,i}$, ..., $\theta_{n-1,n}$) were available

$$\begin{aligned} \theta_{0,1} &= \alpha_{11}\,\theta_{0,1} \\ \theta_{0,2} &= \alpha_{21}\,\theta_{0,1} + \alpha_{22}\,\theta_{1,2} \\ &\cdot \\ &\cdot \\ &\cdot \\ \theta_{0,n} &= \alpha_{n1}\,\theta_{0,1} + \ldots + \alpha_{nn}\,\theta_{n-1,n} \end{aligned} \qquad (5.60)$$

where the α_{ij} coefficients are dimensionless weighting factors that account for the

elementary thickness of soil layers chosen during the water content sampling procedure. Inserting Eq. (5.60) in Eq. (5.59) and recombining, Eq. (5.61) was obtained in a matrix form:

$$[a\alpha]\{\theta\} = \{TDMax - b\} \tag{5.61}$$

which is a linear set of equations to be solved in terms of $\{\theta\}$:

$$\begin{aligned} a_1\alpha_{11}\{\theta_{0,1}\} &= TDMax - b_1 \\ a_2\alpha_{21}\{\theta_{0,1}\} + a_2\alpha_{22}\{\theta_{1,2}\} &= TDMax - b_2 \\ &\vdots \\ a_n\alpha_{n1}\{\theta_{0,1}\} + a_n\alpha_{n2}\{\theta_{1,2}\} + \ldots + a_n\alpha_{nn}\{\theta_{n-1,n}\} &= TDMax - b_n \end{aligned} \tag{5.62}$$

Thus calculations using Eq. (5.62) provide an estimation of the entire water content profile from layer 1 to layer n, and a procedure of extrapolation as far as the soil surface (z = 0) may easily provide the estimated water content at the soil surface. It is to be noted that for the water content profile estimation, only one measurement of TDMax is necessary, but several calibration lines (a_i , b_i) are necessary, one for each arbitrary soil layer.

5.6.2 Calculation of the weighted-average soil water content

The following general formula was used in this study to calculate the weighted-average soil water content between the soil surface (0) and the various depths (z or x) (Wu et al., 1997)

$$W_{AVG} = [\frac{1}{2}(Z_1 - Z_0)\theta_1 + \sum_{i=1}^{n-1}\frac{1}{2}(Z_{i+1} - Z_{i-1})\theta_i + \frac{1}{2}(Z_n - Z_{n-1})\theta_n]/(Z_n - Z_0) \tag{5.63}$$

where Z is depth downward (m), θ_i is volumetric water content ($m^3\ m^{-3}$) at depth Z_i , Z_n is the depth of the profile (m), and W_{AVG} is the weighted-average soil water content (m^3/m^3) of the soil

profile which is equivalent to θ_{0-z} expressed in subsection 5.6.1.

Myhre and Shih (1990) used the soil water content to the 15-cm depth as the water content at the soil surface and derived the average soil water contents to the subsequent depths based on the general formula given above. They then developed relationships between the average soil water contents to various depths and the surface soil minus air temperature difference (TD) to a maximum depth of 90 cm.

In a similar manner, the following equations for the determination of the weighted-average soil water contents to various depths were derived for the case of the SUA field experiments. Soil water contents (soil water potentials) were measured up to the 60-cm depth, i.e., at 5, 15, 30, 45, and 60 cm depths.

In this case $Z_0 = 0$ cm; $Z_1 = 5$ cm, $Z_2 = 15$ cm,
$Z_3 = 30$ cm; $Z_4 = 45$ cm; $Z_5 = 60$ cm.

Therefore

$$W_{AVG5} = [\tfrac{1}{2}(5 - 0)\theta_5 + \tfrac{1}{2}(5 - 0)\theta_5] / (5 - 0) = \theta_5 \qquad (5.64)$$

$$W_{AVG15} = [\tfrac{1}{2}(5 - 0)\theta_5 + \tfrac{1}{2}(15 - 0)\theta_5 + \tfrac{1}{2}(15 - 5)\theta_{15}]/(15 - 0) = \tfrac{2}{3}\theta_5 + \tfrac{1}{3}\theta_{15} \qquad (5.65)$$

$$W_{AVG30} = [\tfrac{1}{2}(5 - 0)\theta_5 + \tfrac{1}{2}(15 - 0)\theta_5 + \tfrac{1}{2}(30 - 5)\theta_{15} + \tfrac{1}{2}(30 - 15)\theta_{30}](30 - 0) = \tfrac{1}{3}\theta_5 + \tfrac{5}{12}\theta_{15} + \tfrac{1}{4}\theta_{30} \qquad (5.66)$$

Similarly

$$W_{AVG45} = \tfrac{2}{9}\theta_5 + \tfrac{5}{18}\theta_{15} + \tfrac{1}{3}\theta_{30} + \tfrac{1}{6}\theta_{45} \qquad (5.67)$$

and

$$W_{AVG60} = \frac{1}{6}\theta_5 + \frac{5}{24}\theta_{15} + \frac{1}{4}\theta_{30} + \frac{1}{4}\theta_{45} + \frac{1}{8}\theta_{60} \qquad (5.68)$$

In this case W_{AVG} are the average soil water contents to the respective depths in $m^3 m^{-3}$, and

θ_i are the soil water contents at the respective depths in $m^3 m^{-3}$.

The general equation above is used to calculate the weighted-average soil water content and pressure head values in the model program The simulated values at each horizon are used to calculate the weighted-average values for the entire profiles for each output time interval, e.g , after every one hour. It is to be noted, however, that in the model program the values of Z are determined by the spatial step size. In this study a spatial (depth) step size of 5 cm was used and therefore with Z_0 set equal to 0 (zero), Z_1 equals 5, Z_2 equals 10, and so on, thus providing a variable soil profile depth.

5.7 Correction for changing solar radiation in the simulated temperature difference (TD)

An attempt was made to correct the simulated soil surface temperature minus air temperature difference (TD) values for the changing solar radiation. In this case net radiation was used as a surrogate for solar radiation because solar radiation was not simulated. To correct for the effects of changing solar radiation in the simulation of the soil surface minus air temperature (TD), the following procedure was used (Pennington and Heatherly, 1989)

i. A regression analysis was applied between the simulated net radiation values and the simulated TD values.

ii. A net radiation value, Rneq, which would correspond to an equilibrium TDmi was calculated as follows using the TDm and Rnm regression function for a particular day.

$$Rneqi = (TDmi\text{-}1)\ S \tag{5.69}$$

where TDmi is TDm of i simulation output;
I is intercept of Rnm and TDm function;
S is slope of Rnm and TDm function;
Rneqi is Rn which would give an equilibrium TD of TDmi.

iii. A total potential change in TD when Rn changes to Rnmi from Rneqi was calculated as shown below. Rneq(i-1) is used as the reference point to calculate the magnitude of potential change in TDm(i-1) with change in Rn to Rnmi using the slope of the TDm and Rnm function.

$$DTDi = (Rnmi - Rneq(i\text{-}1))xS \tag{5.70}$$

where Rnmi is simulated Rn for i simulation output;
DTDi is potential total change in TD when Rn changes from Rneq(i-1) to Rnmi

iv. Assume that TD changes by 30% of DTDi in TIME1, the time that elapse from i-1 to the i simulation output. Add 70% of DTDi to TDmi to calculate the TD that would result if TD were in equilibrium at Rnmi.

$$TDai = 0.7\ x\ DTDi + TDmi \tag{5.71}$$

where TDai is equilibrium value of TD at Rnmi,
TIME1 is the output time interval in s.

The computer program offers the possibility of calculating both the slope and intercept of the regression equations for the model simulated net radiation and TD as well as the net radiation and the equilibrium value of TD, TDa. This offers the possibility of using the TDa values for determining the relationship between the TDa and surface soil water content.

5.8 Numerical implementation

To be able to solve the partial differential equations (**Eqs. 5.37 and 5.50**) for both heat and water flow, the equations need to be discretized with respect to space and time in order to turn them into a system of algebraic equations that can be solved numerically. Finite difference methods have been used by various researchers (e g , Haverkamp et al., 1977, Chung and Austin, 1987; Celia et al., 1990; Doell, 1996). The finite difference method has been proven to be just as flexible as the finite element method with respect to spatial geometry, especially as far as the one-dimensional solution domain is concerned. Also, the solution of the Richards equation requires a diagonal matrix which happens to be inherent in the finite difference approximation (Celia et al., 1990, Doell, 1996).

Either explicit or implicit finite difference methods can be used to solve **Eqs. (5.37) and (5.50)** numerically. The explicit, finite difference approximations to the partial differential equations are easily programmed for computer solution. However, the stability criteria sometimes require small incremental time steps and, thus, large amounts of computation time. The implicit finite-difference method does not have stability criteria and generally requires less computer time when modelling heat and water flow in soils. This is the case even though programming the implicit method is more difficult, conceptually, than the straightforward explicit method (Horton , 1989).

5.8.1 Discretization

In this study the implicit finite-difference method has been used for both the heat and water flow equations. The implicit, finite difference equation for **Eq. (5.37)** is:

$$\frac{T_i^{n+1} - T_i^n}{\Delta t} = \frac{\alpha_{i+1/2}^{n+1/2}(T_{i+1}^{n+1} - T_i^{n+1}) - \alpha_{i-1/2}^{n+1/2}(T_i^{n+1} - T_{i-1}^{n+1})}{(\Delta z)^2} \qquad (5.72)$$

where i is the depth index,

n is the time step index,

α is the thermal diffusivity, which is thermal conductivity divided by volumetric heat capacity, and

z is the depth that increases downward.

The internodal thermal diffusivities can be estimated by either the arithmetic mean or geometric mean of the diffusivities at the two adjacent nodes. In this study, the arithmetic mean is used.

In Eq. 5.72, the unknown temperature at node i at time (n + 1) is expressed in terms of unknown temperatures at time (n + 1). Therefore, T_i^{n+1} cannot explicitly be solved for. One implicit equation can be generated at each node by Eq. (5.72). Then, a system of equations that must be solved simultaneously is obtained. The system of equations provide a tridiagonal matrix, which can be solved efficiently by using a particular form of the Gaussian elimination method known as the Thomas algorithm (Remson et al., 1971; Press et al., 1988 p. 40).

The finite difference equation for water flow (Eq. (5.50)) can be formulated similarly. The solution process is the same as for the heat flow. A numerical approximation of Eq. (5.50) is:

$$\left(\frac{h_i^{n+1} - h_i^n}{\Delta t}\right) F_i^{n+1/2} = K_{i-1/2}^{n+1/2}\left(\frac{\beta(h_{i-1}^n - h_i^n) + \alpha(h_{i-1}^{n+1} - h_i^{n+1}) + \Delta z}{(\Delta z)^2}\right) - K_{i+1/2}^{n+1/2}\left(\frac{\beta(h_i^n - h_{i+1}^n) + \alpha(h_i^{n+1} - h_{i+1}^{n+1}) + \Delta z}{(\Delta z)^2}\right) \qquad (5.73)$$

where i is a depth index,

n is a time index,

h is the soil water pressure head at position (or depth i) and time n,

Δt is the finite time increment ($t^{n+1} - t^n$),

Δz is the finite depth increment ($z_{i+1} - z_i$),

$F_i^{n+1/2}$ is the specific water capacity, $d\theta/dh$, at depth i averaged over Δt,

$K^{n+1/2}_{i-1/2}$ is K_h averaged across depth i and i-1, and

$K^{n+1/2}_{i+1/2}$ is K_h averaged across depth i and i+1 at Δt.

The coefficients α and β are used to allow for different approximations of h across the time interval, subject to the restriction that $\alpha + \beta = 1$. It is to be noted that the values h^n constitute the initial (known) values, and h^{n+1} is not known, but will be computed at the end of the time interval. If β is set at 1 and $\alpha = 0$, then the computation can be made with known values of h^n on the right-hand side of Eq. (5.73), but the size of Δz and Δt increments must be small, and much computation is required. However, the numerical solution is quite simple. An equation is written for each depth increment and values of h^{n+1} are found for each depth. These values are taken as the new initial conditions and the process is repeated.

However, if $\alpha = \frac{1}{2}$ to 1 and $\beta = \frac{1}{2}$ to 0, there is no restriction on the size of the Δt and Δz increments. A set of m equations with m unknowns results (m is the number of depth increments), which calls for a procedure to solve simultaneous equations. Fortunately, a very efficient method is available, the tri-diagonal matrix solution (Press et al., 1988, p. 40). Using this scheme decreases computation time, and places no restrictions on the time and depth increments.

In this study, the coefficients α and β were assigned values of 1 and 0, respectively. The resulting numerical equation is given as follows.

$$\left(\frac{h_i^{n+1} - h_i^n}{\Delta t}\right) F_i^{n+1/2} = K_{i-1/2}^{n+1/2}\left(\frac{h_{i-1}^{n+1} - h_i^{n+1} + \Delta z}{(\Delta z)^2}\right) - K_{i+1/2}^{n+1/2}\left(\frac{h_i^{n+1} - h_{i+1}^{n+1} + \Delta z}{(\Delta z)^2}\right) \qquad (5.74)$$

The above numerical equation corresponds to Model 3 of Haverkamp et al. (1977); an implicit discretization with explicit linearization of K and F. Different researchers (e.g., van Keulen and van Beek, 1971; Feddes et al., 1978; Haverkamp and Vauclin, 1979; Raes, 1982, Hornung and Messing, 1983; Zaidel and Russo, 1992) presented differing views as to the use of either the geometric or arithmetic mean in calculating the interblock hydraulic conductivity. In some cases the geometric mean has been shown to lead to the smallest weighting errors (Doell, 1996). The use of the arithmetic mean as it has been done in this study is somehow a simplification and therefore subject to greater weighting errors. However, it is assumed that the magnitude of the weighting errors would not excessively affect the general solutions of the equations. The interblock hydraulic conductivity is therefore calculated as follows:

$$K_{i-1/2}^{n+1/2} = \frac{K_i^{n+1/2} + K_{i-1}^{n+1/2}}{2} \tag{5.75}$$

$$K_{i+1/2}^{n+1/2} = \frac{K_{i+1}^{n+1/2} + K_i^{n+1/2}}{2} \tag{5.76}$$

5.8.2 Computer program description

The principal structure and logical components of the computer program for calculating heat and water flow are described by a flow chart, as shown in Fig A1.1 in Appendix 1. Table A1.1 in Appendix 1 gives the user manual for the SUAHEAT program. The computer program is written in FORTRAN 77. The program listing is shown in Appendix 3. Data processing program listings are shown in Appendix 4. The model uses the implicit, finite difference method to solve the soil heat and water flow equations as described in the previous sections and summarized in Fig. (5.2). Users can choose appropriate indicators from several options for flow type (either heat flow only, or heat and water flow), soil type, initial condition type, and boundary condition type

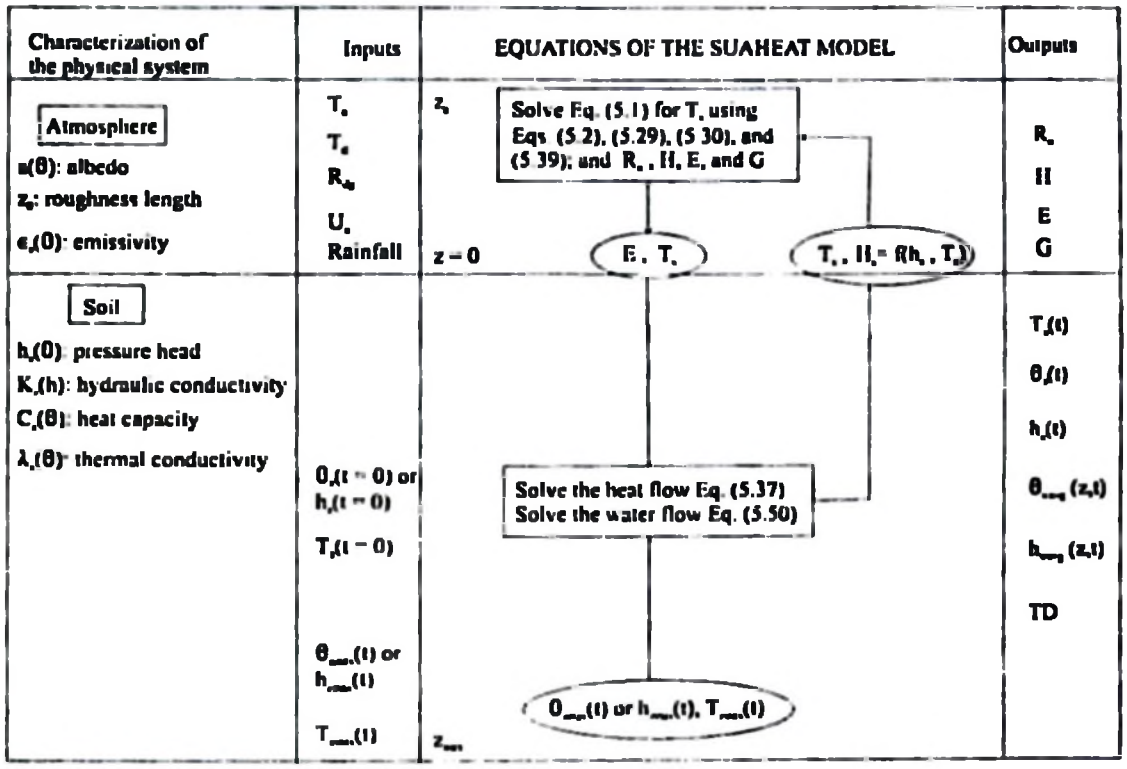

Fig. 5.2 Scheme of the SUAHEAT model. The top boundary conditions are calculated from the energy balance at the soil surface.

In Fig. (5.2)

T_s	is the soil surface temperature,
H_s	is the humidity at the soil surface,
h_s	is the pressure head at the soil surface,
$\theta_{zmax}(t)$	is the bottom boundary volumetric soil water content,
$T_{zmax}(t)$	is the bottom boundary soil temperature,
$h_{zmax}(t)$	is the bottom boundary pressure head,
$T_z(t = 0)$	is the initial profile soil temperature,
$h_z(t = 0)$	is the initial profile pressure head,
$\theta_z(t = 0)$	is the initial profile soil water content,
T_a	is the air temperature,
T_d	is the dewpoint temperature,
R_{dg}	is the daily global solar radiation,
u_a	is the wind speed,
R_n	is the net radiation,
H	is the sensible heat flux,

E	is the evaporative flux,
G	is the soil heaf flux,
$T_z(t)$	is the profile soil temperature,
$h_z(t)$	is the profile pressure head,
$\theta_z(t)$	is the profile soil water content,
TD	is the soil temperature minus air temperature difference,
$\theta_{avg}(z,t)$	is the weighted-average soil water content,
$h_{avg}(z,t)$	is the weighted-average pressure head,
z_a	is the measurement height for air temperature,
z	is the depth, and
z_{max}	is the maximum depth in the soil.

When heat flow is considered alone, the model skips over the water flow portion of the program. Measured values, or explicit or implicit expressions, can be used to describe the boundary conditions. A user must provide input information for the upper boundary conditions. For explicit, boundary-condition input data, a user must provide the temperature or water content values (at regular intervals) and the total number of inputs per day. With this input, the program uses a step function approach to adjust the boundary values to constant time steps throughout a day. If a user has daily maximum and minimum surface-temperature values available, then a sine function option can be used to describe the soil surface boundary condition. The surface energy partitioning method can be used to determine the soil surface temperature and evaporation rate if weather input data are available. The required weather inputs for this program are daily global radiation, maximum and minimum daily air temperatures, maximum and minimum daily dewpoint temperatures, average daily wind speed, and rainfall. The weather inputs are assumed to be measured at a height of 2 m above the ground. When a user chooses the surface-energy partitioning method to describe the upper-boundary condition for heat flow, the choice also provides the upper-boundary water flow condition. When the energy partitioning method is used for the boundary condition, the soil surface temperature is assumed to be equal to the air temperature during a rainfall period. The model is set up for bare soil with no plants.

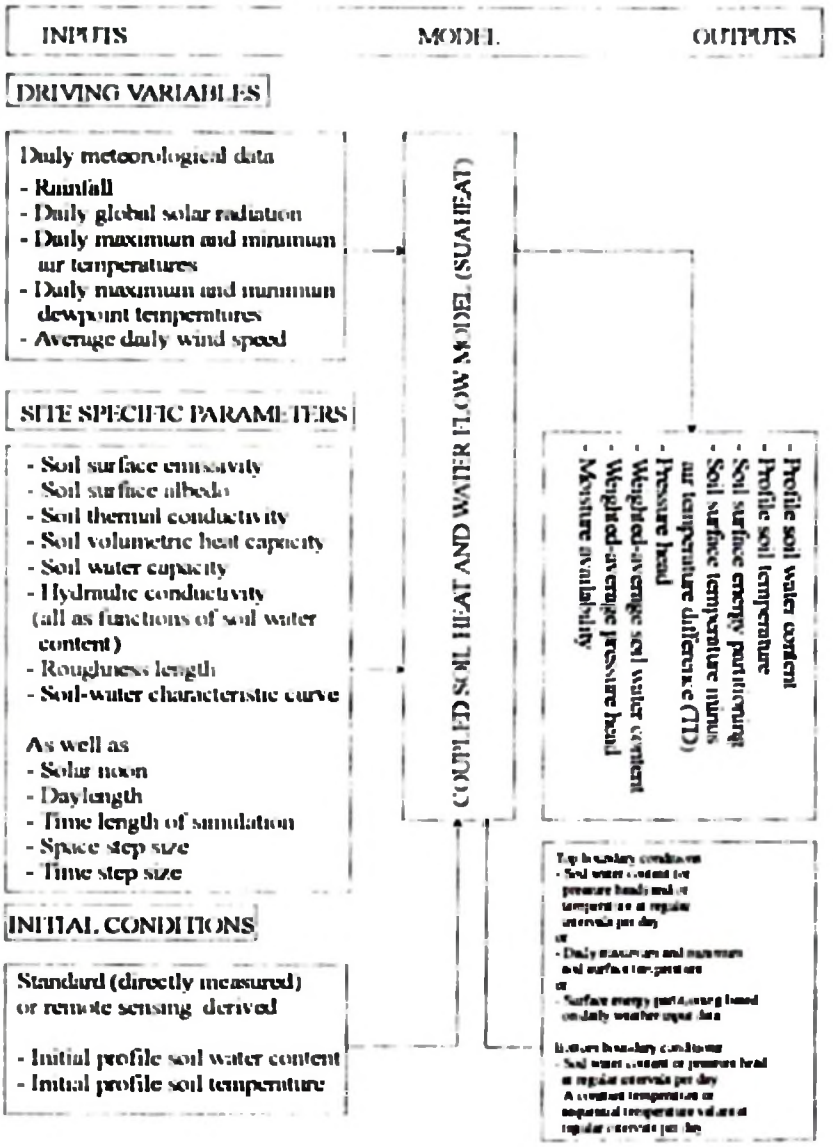

Fig. 5.3 Required input variables and parameters and the outputs from the SUAHEAT model.

Soil parameters required as inputs include soil surface emissivity, soil surface albedo, soil thermal conductivity, soil volumetric heat capacity, soil water capacity, and hydraulic conductivity, all as functions of water content, roughness length, and the soil-water characteristic curve. A few general inputs are also required to run the computer program. These inputs include solar noon, daylength, time length of simulation, Δz, and Δt. **Fig. 5.3** summarizes the required input variables and parameters and the ouputs from the SUAHEAT model.

The weather inputs are used in conjunction with empirical expressions to describe weather conditions as a function of time. In the current state of the computer program, global radiation as a function of time is described as (cf. Van Bavel and Lascano, 1979)

$$R_g = (9/16)\pi (R_{dg}/D_L) \sin[(t - S_N + D_L/2)\pi/D_L] \quad (5.77)$$

where R_g is global radiation in W m^{-2},

R_{dg} is the input daily global radiation in J m^{-2},

D_L is the input day length in s,

S_N is the input solar noon time in s, and

t is the time of day in s.

Air temperature, T_a, as a function of time is described as

$$T_a = [(T_{max} + T_{min})/2] + [(T_{max} - T_{min})/2] \sin(\omega t + \pi) \quad (5.78)$$

where T_{max} and T_{min} are the input daily maximum and minimum air temperatures in °C, and

ω is the angular frequency (7.272×10^{-5}) in rad s^{-1}.

The dewpoint temperature, T_d, as a function of time is described as

$$T_d = [(T_{dmax} + T_{dmin})/2] + [(T_{dmax} - T_{dmin})/2] \sin(\omega t + \pi) \quad (5.79)$$

where T_{dmax} and T_{dmin} are the input daily maximum and minimum dewpoint temperatures in°C.

If dewpoint temperature data are not available, but instead relative humidity and air temperature data are available, the following method (Campbell Scientific Inc., 1996) can be used to calculate dew point temperature from relative humidity and air temperature data as has been done in this study.

$$T_{dc} = (C_3 * \ln(V_p/C_1))/(C_2 - \ln(V_p/C_1)) \quad (5.80)$$

where $C'_1 = 0.61078$

$C'_2 = 17.558$

$C'_3 = 241.88$

T_{dc} is the calculated dewpoint temperature in °C,

V_p is the vapour pressure (kPa) calculated from $V_p = RH*S_{vp}/100$,

RH is the relative humidity in %,

S_{vp} is the saturation vapour pressure (kPa) calculated using Instruction 56 of the CR10 Campbell Scientific Inc (CSI) datalogger from the measurements of RH and air temperature (T_a).

Equation (5.80) is an inversion of a version of Tetens' equation optimised for dewpoints in the range -35 to 50 °C (Campbell Scientific Inc., 1996). The values of T_{dmax} and T_{dmin} can then be obtained from the T_{dc} values in Eq. (5.80)

In the current state of the computer program, the wind speed is assumed to be constant throughout the day. All required soil parameters are described by various equations in the current state of the computer program. The expressions for the soil surface emissivity, soil surface albedo, soil thermal conductivity, soil volumetric heat capacity; soil water characteristics, hydraulic conductivity, and specific water capacity are as given in the model formulation treated in the various sections of this chapter.

5.8.3 Computer model validation

The performance of a numerical model should be evaluated to examine its validity because any numerical scheme may introduce instability, truncation, and round-off errors. A model is valid only if the approximate solution is satisfactorily accurate or close to the exact solution, if one exists. The accuracy of a model is also dependent on its convergence and stability. Convergence is satisfied when the approximate solution approaches the exact solution while step sizes of the spatial and temporal discretization approach zero. A model is said to be stable if the amplification of the error is restricted or has a finite limit as computation marches forward in time.

The validity of a model can be tested by comparing the numerical solution with either an analytical solution, if it is available, or observed data. In this study comparison between the model simulated state variables (i.e., soil water content and soil temperature) and their corresponding observed values was used to test the validity of the model. Results and discussion of the model evaluation, calibration, and validation are presented in chapter 7.

5.8.4 Evaluation criteria of model performance

Several evaluation criteria were used to test the model performance. Both qualitative and quantitative procedures were used to evaluate the model by comparing the model simulated and observed data over space and time. The qualitative procedures consisted of visually comparing the observed (measured) and model simulated data over space and time. The quantitative procedures involved the use of statistical analysis. Fox (1981) (as cited by Durar et al., 1995) identified two general types of quantitative measures for the evaluation of model performance, namely, measures of correlation and measures of difference. The coefficient of determination (r^2) has been widely used as a quantitative index of correlation between measured (observed) and model simulated data. It generally describes the proportion of the total variance explained by the model. However, several researchers (Willmott, 1981, 1982; Robinson and Hubbard, 1990) have expressed strong reservations about the use of the coefficient of determination alone in model performance analysis. The main problem is that the magnitudes of r^2 are not consistently related to the accuracy with which the model simulates the observed data. The observed and model simulated variables may also not conform to the assumptions that are prerequisites to the application of regression analysis. Fox (1981) recommended the use of mean absolute error (MAE) (also referred to as mean absolute difference (MAD) (Anderson et al., 1996)) as a difference measure in model performance analysis. Similarly, Willmott (1981) contended that MAE or MAD is among the best overall measures of model performance. The mean absolute error (difference), which describes the average absolute deviation between model simulated and observed data, is defined as follows:

$$MAD = \frac{1}{N}\sum_{i=1}^{N} |P_i - O_i| \qquad (5.81)$$

where P and O are the paired model simulated and observed values of the variable of interest at a given time, respectively, and N is the total number of observations (Durar et a., 1995). The root mean square difference (RMSD) (Anderson et al., 1996) (also referred to as standard error of estimate (SE) (Clemente et al., 1994)) is another quantitative measure used in evaluation of model performance. The root mean square difference is defined as follows:

$$RMSD = [\frac{1}{N}\sum_{i=1}^{N} (P_i - O_i)^2]^{1/2} \qquad (5.82)$$

6 FIELD EXPERIMENTS

6.1 General overview

A major limitation to the utility of water and energy balance simulation models is the availability of data, both in terms of quality and quantity. The accuracy of model simulations depends to a great extent on the accuracy and temporal resolution of input data. Carrying out of field experiments under suitable climatic and soil conditions required for model calibration and validation is therefore very crucial. The interdependence between modelling and measurement makes either one incomplete without the other. An integrated measurement scheme consisting of both measurement and modelling is therefore advisable in any field measurement exercise.

The measurements covered in this chapter are also used for model calibration and validation in chapter 7. Detailed discussion of the results is therefore presented in chapter 7. Simulation using the SUAHEAT model requires specification of both initial and boundary conditions as well as soil thermal and hydraulic properties. The initial conditions are provided by the profiles of the state variables, i.e., soil temperature and soil moisture content or matric potential (pressure head). The incoming solar radiation, rainfall, air temperature, relative humidity or dewpoint temperature, and wind speed at a given measurement height above the soil surface are the driving variables. Soil surface energy balance based on the weather data provides for the top boundary conditions. The measured soil water contents (or matric potentials) and soil temperatures at a given depth below the soil surface provide the lower boundary conditions. The radiative, thermal and hydraulic properties of the soil are expressed as functions of known state variables and system parameters.

6.1.1 Errors

Model calibration and validation based on the comparison of model simulations and observations entail some uncertainties, both in measurements and in simulations, and these must be known. The term 'uncertainty' refers to the possible deviation of a measured value at some point in the field from the actual value at a particular location for which a prediction is made. Sources of error in the measurement can be attributed to calibration errors and violation of certain

assumptions underlying the experimental method In this study, (quarter-hourly or hourly) averaged values of most of the measured variables were used for analysis. Calibration errors were, however, not explicitly taken into account in the respective calculations or analyses. Error levels for the various sensors used have been covered in the respective sections. Errors arising from spatial variability of soil physical properties are also worth a mention. Detailed treatment of the errors arising from spatial variability is however beyond the scope of this work

6.2 General characteristics of the study area

The study area is located near Morogoro town, Tanzania (see map) It is part of the Sokoine University of Agriculture (SUA) farm. It lies at latitude 6°50'20"S and longitude 37°39'20"E at an elevation of 525.8 m above mean sea level (msl) The SUA farm is bordered on the east by the town, to the south-east by the Uluguru mountains and to the north-west by Lugala Hills. The farm covers an area of approximately 2,300 ha

Kaaya (1989) did a soil survey of part of the SUA farm including the current study area. The geological survey of Morogoro (Sampson et al , 1961 as cited by Kaaya et al., 1994) indicates that the study area is covered mostly by red and reddish brown soils. Most of the geomorphological features of the SUA farm have been described by Mpepo (1986) (as cited by Kaaya et al , 1994). The farm has a saucer-like shape as it is surrounded by the Uluguru mountains rising up to a height of over 2,000 m above sea level (a.s.l.), and the Mindu mountains and Lugala hills, of 1,200 m and 820 m a.s.l , respectively. The overall study area (which includes the current study area) lies on undulating slopes to almost flat land at an altitude of 480 m to 600 m a.s.l (Kaaya et al., 1994) Typical relief at the research plot were : undulating, north of Uluguru mountains, upper slope from an interfluve, 1.6° - 2.3° (eastern aspect) - level to gently sloping

Fig 6.1 Map of Tanzania showing the location of the study area

There has been some conflicting statements about the characterization of the climate of the study area. The climate of the study area has been documented by Msanya (1980) and Moberg et al (1982) (as cited by Kaaya et al., 1994) and Kaaya (1989) According to Kaaya et al (1994), the climate at SUA farm is of a sub-humid tropical type. The area experiences two rainfall peaks in a year, with short and lighter rains lasting from November and January with the peak in December. A short, dry period in mid-January or February follows afterwards. The long and heavier rains last from March to May with the peak period in April The onset and distribution of the rainfall are irregular and unreliable (Kaaya et al., 1994)

Based on 15-years (1971-1986) of weather data, Kaaya et al. (1994) found out that the mean monthly temperature varies between 21.4 °C and 21.3 °C in June and July, respectively, and 26.4 °C in November to February. The mean monthly maximum temperature ranges from 27.5 °C, during the coldest months, to 32 0 °C, during the hottest months. The mean monthly minimum temperature ranges from 15 1 °C, during the coldest months, to 21.5 °C, during the hottest months. Kaaya et al. (1994) obtained a mean annual air temperature of 24.4 °C for the period considered. The average soil temperature was estimated as 25.4 °C, by adding 1 °C to the mean annual air temperature (after Soil Survey Staff, 1975) and, thus, the soil temperature regime is isohyperthermic (Kaaya et al., 1994).

Nearly all the vegetation in the farm has been disturbed by man through cultivation. The local vegetation is mainly grassland dominated by *Andropogon spp.*, Hyparrhenia spp. and *Themeda* spp. Cultivation of maize and sorghum is the main land use in the study area. All the crops are grown under rainfed conditions. Land use and vegetation at the research plot were fallow (grass covered), very few shrubs, planted trees and sisal on the field boundary.

6.3 Soil survey, laboratory analysis and soil classification

Despite the fact that detailed soil survey of the SUA farm including the current study area was previously conducted (Kaaya, 1989), a soil profile was excavated to characterize the soil of the research plot. This was necessary bearing in mind the spatial variability of soil physical properties that may exist even within a sampling area as small as several square metres. Soil colour was determined using Munsell Colour Charts (Munsell Color Company, 1954). Both disturbed and undisturbed soil samples were collected from each horizon for physical characterization in the laboratory. Results of the soil survey are given in Table A7.4, Appendix 7. Standard laboratory methods were employed. Texture was determined by Bouyoucos hydrometer method (Day, 1965) after dispersion with Na-hexametaphosphate. Bulk density was determined using the core method (Blake, 1965). Laboratory analysis was carried out to determine soil texture, bulk density, particle density, and particle size distribution. The soil at the experimental site, hereby referred to as Getini site, has been classified as sand clay loam (Kaaya, 1989; Makungu, 1991;

and Thadei, 1992) with the following average composition: sand 63.6%, silt 6.2%; and clay 30.2%. However, the soil of the experimental plot was classified as clay with the following average mechanical composition: sand 38%, silt 7%; and clay 55%. The field was under maize crop and uncropped for two and five years, respectively.

6.4 Field experimental layout

A 25 x 25 m research plot was fenced according to the World Meteorological Organization (WMO) recommendations. About 10 x 10 m (grass-covered) was reserved for the installation of the automatic weather station (AWS) and other sensors and the rest of the plot (bare soil) was left for carrying out other measurements. The bare part of the plot was initially ploughed to about 10 cm depth and the soil smoothed and allowed to consolidate itself after the start of the rains. The soil surface was levelled both manually and by rolling the moist soil after ploughing. The field was kept continuously bare for the whole period of the experiment by manually uprooting the weeds at their earliest time of emergence. Use of herbicides was avoided on environmental protection grounds. Detailed (time-series) observations of the soil state as well as weather variables were carried out. This took place between January and early August, 1997. Equipment and sensor installation in the field is covered in subsection 6.5.2 (see also Figs 6.2 and 6.3). The field experiment was conducted on a relatively small scale because of time and budget constraints.

6.5 Field measurements

6.5.1 General overview of measurement and instrumentation principles

PC data acquisition and control: The term ***data acquisition*** can simply be stated as the collection of information that describes a given situation. Computers play an important role in data acquisition. Computers provide high speed, accuracy, flexibility, adaptability, consistency, reliability and mass storage. However, most real-world signals (temperature, pressure, flow, speed, intensity, position, etc.) cannot be read directly by digital computers.

These parameters are represented by analog signals distinguished by their continuum of levels, while computers recognize only digital (off/on) levels. Therefore, a translation product is required. Data acquisition and control products *translate* real-world signals into a format that digital computers can accept. And, they can generate analog and other signals from digital computer instructions. In this way, data acquisition and control systems bridge the gap between the computer and the real world.

Data acquisition and control hardware can be classified by the method used to interface it with the PC. external bus products, which interface with the PC via a serial (RS-232, RS-422), IEEE-488, or parallel communications port; and internal bus products, which connect directly to the PC bus. The external bus system has the following advantages: it allows remote operation, offers reduced PC load, and offers support for distributed systems. The advantages of internal bus systems are: high speed, low cost, and smaller size.

Data conversion principles: Typically, data acquisition systems include analog-to-digital (A/D) converters, multiplexers, sample/holds, amplifiers, counter/timers, and other, more specialized, elements. The analog input system performs the function of converting analog signals into a corresponding digital format. The analog-to-digital converter (A/D) transforms the original analog information into computer-readable data (a digital binary code). In addition to the A/D converter, several other components may be required to obtain optimum performance. These can include a sample/hold, an amplifier, a multiplexer, timing and synchronization circuits, and signal conditioning elements. The amplitude of analog signals can vary over a very wide range. Signals from common transducers are between 50 μV and 10 V. Yet, most A/D converters perform best when their inputs are in the range of 1 to 10 V. Therefore, many systems include an amplifier to boost low-level signals to the desired amplitude.

Differential inputs are especially useful for measuring low-level signals. Most analog input systems have provisions for configuring the input multiplexer and amplifier for either single-ended or differential use. Analog signals can be configured as either single-ended or differential inputs. Single-ended inputs all share a common return or ground line. Only the high ends of the signals are connected through the multiplexer to the amplifier. This arrangement works well for

high-level signals when the difference in ground potential is relatively small. Problems arise when there is a large difference in ground potentials. This is usually caused by current flow (a ground loop) through the ground conductor.

A differential arrangement allows both the noninverting (+) and the inverting (-) inputs of the amplifier to make connections to both ends of the actual signal source. In this way, any ground-loop-induced voltage appears as a common-mode signal and is rejected by the differential properties of the amplifier. While differential connections can greatly reduce the effects of ground loops, they consume the equivalent of two single-ended inputs.

The multiplexer (Mux) is simply a switch arrangement that allows many input channels to be serviced by one amplifier and one A/D converter. Software or auxiliary hardware can control this switch to select any one channel for processing at a given time. Because the amplifier and A/D converter are shared, the channels are read sequentially, causing the overall speed of the system to be reduced.

Signals and transducers: Signals are often described as being either analog, digital or pulse. They are defined by how they convey useful data. Attributes such as amplitude, state, frequency, pulse-width, and phase can represent data. While all signals can be assumed to be changing with time, analog signals are the only ones that convey information within their incremental amplitude variations. In Instrumentation and control applications, most analog signals are in the range of -10 V to +10 V or 4 -to- 20 mA. Digital and pulse signals have binary amplitude values; that is, they are represented by only two possible states - low and high. While low and high states can be represented by any voltage level, transistor-transistor-logic (TTL) levels are most often used. TTL levels are approximately 0 V and 5 V. The actual allowable ranges for TTL signals are:

Low level = 0 V to 0.8 V
High level = 2.0 V to 5.0 V

Digital signals are sometimes called *discrete* signals. Pulse signals are similar to digital signals in many respects. The distinction lies in their time-dependent characteristics. Information can be

conveyed in the number of state transitions or in the rate at which the transitions occur. Rate is referred to as frequency (pulses per second).

Transducers: An electrical transducer is a combination of a sensor element with a conversion element or process which produces an electrical signal (output) dependent on the magnitude of the sensed quantity. A sensor responds to the quantity to be measured. Transducers play a vital role in the data acquisition and control system. It is the transducer that makes the transition between the physical and electrical world. Data acquisition and control can involve both input and output signals. Input signals can represent force, temperature, flow, displacement, count, speed, level, pH, light intensity, etc. Output signals can control valves, relays, lamps, horns, motors, and so on.

The electrical equivalents produced by input transducers are most commonly in the form of voltage, current, charge, resistance or capacitance. These basic signals can further be converted into voltage signals by the process of signal conditioning. This is important because the interior blocks of the data acquisition and control system can only deal with voltage signals. A brief description of some of the transducers used in this study is given below.

Thermocouples: Many different types of thermocouples, using different combinations of metal alloys, are in use. For convenience, alphabetic letter designations have been given to the most common. These include:

Type J - Iron-Constantan (Fe-C) - Lowest cost, highest sensitivity, moderate accuracy. Should not be used above 760 °C because of severe decalibration.

Type K - Chrome-Alumel (Ch-Al) - Moderate cost, moderate sensitivity, low accuracy, *high temperature range*. Can be used to 1372 °C due to its high resistance to oxidation.

Type T - Copper-Constantan (Cu-C) -Moderate cost, moderate sensitivity, high accuracy. *Very useful at low temperatures*. Because one lead

is copper, cold-junction compensation is not required when making differential temperature measurements with two back-to-back thermocouples.

Thermocouples are low in cost and rugged. In general, accuracy is limited to about *1 to 3 percent* due to material and manufacturing variations. Most thermocouples require several seconds The type T thermocouple was used in this study.

Thermistors: Thermistors are generally more accurate than thermocouples, yielding ± 0.1 °C under some conditions. The physically small size and high nominal resistance are significant advantages. Small size yields a fast response, while the high resistance makes any error, due to lead-wire resistance, small.

These units can be used from -50 to +100 °C In addition to the limited temperature range, attention must be given to the fragile nature of these devices Careful mounting and handling must be used to avoid accuracy-destroying stress or catastrophic crushing

Resistance sensors: A resistance sensor is usually measured as part of a Wheatstone bridge circuit. Transducer excitation, as well as provisions for the insertion of bridge-completion components, can be provided on signal terminating panels. While both voltage and current excitation can be used, current excitation is generally more desirable This is because current excitation provides a more linear output response, making the data interpretation easier. Bridge-completion resistors should be of very high precision (typically 0 05%). Stability is actually the most important characteristic of the bridge-completion elements. The Watermark sensors and gypsum blocks used in this study are resistance sensors.

Wiring and noise considerations: Signals entering a data acquisition and control system include unwanted noise. The signal-to-noise ratio and the specific applications determine the extent of the severity of the problem. In general, it is desirable to minimize noise to achieve high accuracy. Digital signals are relatively immune to noise because of their discrete (and high-level) nature. In contrast, analog signals are directly influenced by relatively low-level disturbances.

6.5.2 Equipment and sensor installation

Choosing the location: The objective of any data collection exercise is to obtain data that is accurate, reliable and representative. Accuracy and reliability depend mostly on the correct selection and use of sensors. Data representativeness refers to the extent to which the values recorded are typical of the site or location in which the sensors are placed. Automatic weather stations (AWS) are often used to provide local meteorological measurements that otherwise could only be obtained from a "standard" meteorological site In this case the AWS should be exposed in a similar way to the instruments on the standard site, i e , over a short grass surface that is level and not shielded by trees or buildings

The effects of varying environmental conditions There are three ways in which local conditions such as moisture or the presence of vegetation can affect the measurements taken by an AWS. These are the clothesline effect, the leading edge effect, and the oasis effect

The clothesline effect: The clothesline effect in its simplest form describes the effect of air passing from dry, unvegetated surfaces to moist, vegetated surfaces and the consequent effect on vapour gradients and heat transfer This should be carefully considered when siting an AWS in crops or near trees when the wind direction is mostly towards the vegetation.

The leading edge effect: This effect occurs when air moves over a surface that differs in temperature, moisture content, roughness or some other characteristics from an adjacent surface The line of discontinuity is known as the leading edge As air passes over the leading edge its characteristics gradually adjust to the new surface. This internal boundary layer varies in vertical extent with distance from the leading edge A transitional zone exists where the air is modified but not adjusted to the new surface. These effects become most pronounced when advection (horizontal air flow) is strongest. There are no universally accepted figures for the height of this internal boundary layer as it is influenced by the nature of the surface and extent of any advection.

The oasis effect: The oasis effect occurs when an isolated moisture source is surrounded by an otherwise arid region. If the wind direction is such that moist air is drawn from the surface of the water body (or other water source such as a glacier or area of vegetation), then the relative humidity measurements do not represent the general conditions in the region.

Obstructions: Whenever possible, the AWS should be located away from windbreaks or shelterbelts. Several zones have been identified upwind and downwind of a windbreak in which the airflow is unrepresentative of the general speed and direction. Eddies are generated in the lee of the windbreak and air is displaced upwind of it. The height and depth of these affected zones varies with the height and to some extent the density of the obstacle.

Generally, a structure disturbs the airflow in an upwind direction for a distance of about twice the height of the structure, and in a downwind direction for a distance of about six times the height. The airflow is also affected to a vertical distance of about twice the height of the structure. Ideally, therefore, the AWS should be located outside this zone of influence in order to obtain representative values for the region. In order to ensure that accurate data were obtained, the choice of the experimental site took into consideration all the factors described above. Detailed information including the results of the soil survey which was conducted prior to the commencement of field measurements is presented in **Table A7.4 Appendix 7**.

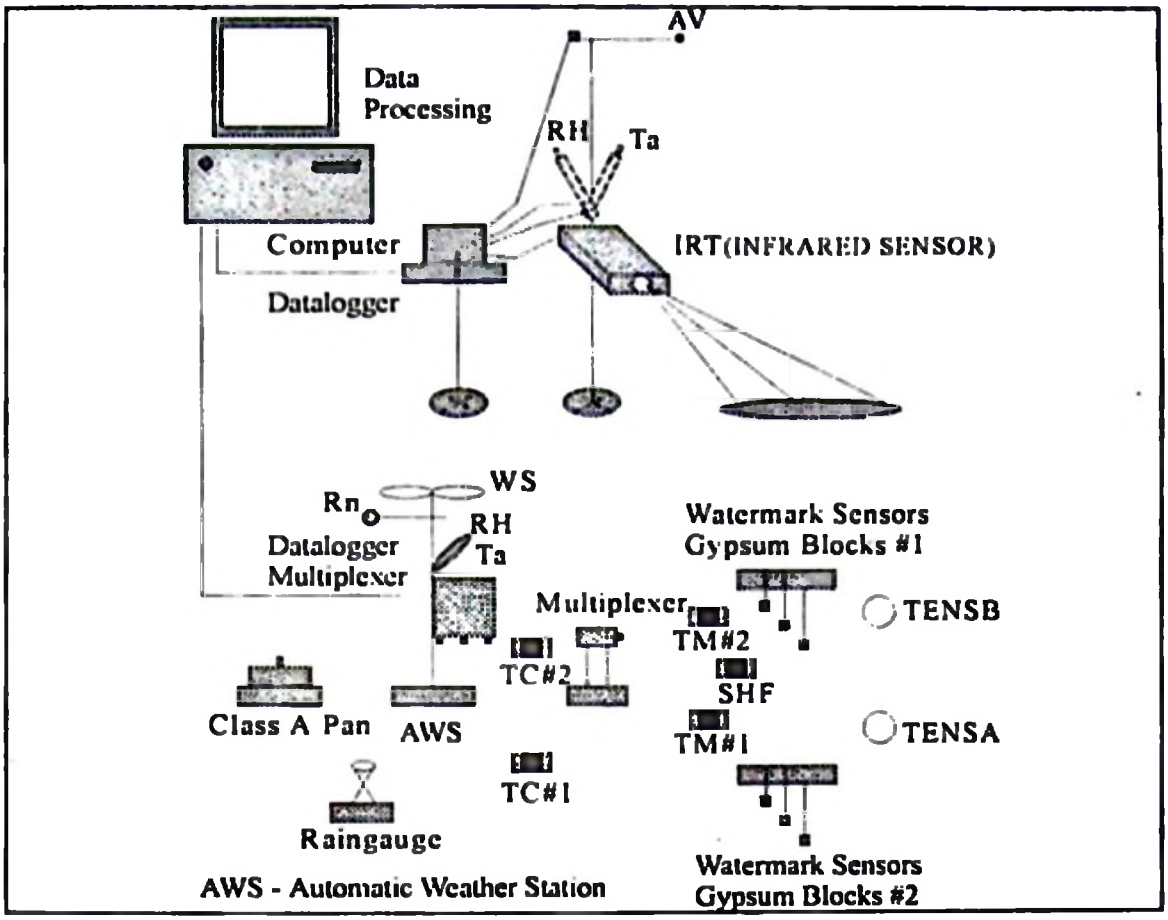

Fig. 6.2 Experimental arrangement and field layout - side elevation.

NB: All sensors with cables not shown were measured by the datalogger and multiplexer except for the tensiometers TENSA and TENSB.

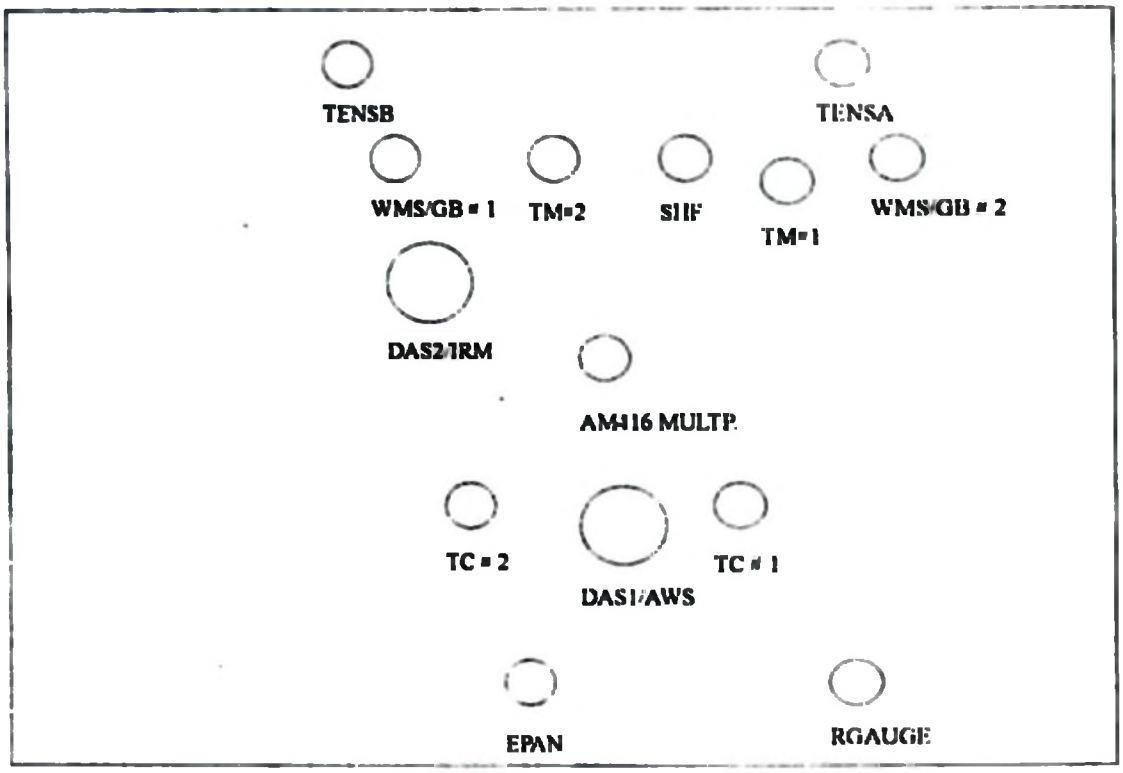

Fig. 6.3 Field experimental layout and positioning of different equipment/sensors - plan view, not to scale (cf. Fig. 6.2).

KEY:

TENSA	-	Tensiometer Group A - Manually read
TENSB	-	Tensiometer Group B - Manually read
WMS/GB # 1	-	Watermark Sensors/Gypsum Blocks Group 1 - CR10/AM416
WMS/GB # 2	-	Watermark Sensors/Gypsum Blocks Group 2 - CR10/AM416
TM#1	-	Thermistor Temperature Probe 107 #1 - CR10
TM#2	-	Thermistor Temperature Probe 107 #2 - CR10
SHF	-	Heat Flux Sensor - CR10/AM25T
TC # 1	-	Thermocouples Group 1 - CR10/AM25T
TC # 2	-	Thermocouples Group 2 - CR10/AM25T
EPAN	-	Clas A Pan with a Pressure Transducer - CR10/AM25T
RGAUGE	-	ARG100 Tipping Bucket Raingauge - CR10
AM416 MULTP.	-	AM416 Relay Multiplexer for soil moisture sensors - CR10

DAS1/AWS - Data Acquisition System 1/Automatic Weather Station consisting of the following sensors/equipment.

- AM25T Solid State Multiplexer for thermocouple or voltage sensors
- CR10 Measurement and Control Module (MCM)
- Q-7 Net Radiometer - CR10/AM25T
- 05103-5 RM Young Wind Monitor - CR10
- HMP35AC Temperature and Relative Humidity Probe with URS1 Unaspirated Radiation Shield - CR10

– ATW2 2m Aluminium Tower and Grounding Kit

- Solar Panel for battery charging
- ENC 12/14 White GRP Enclosure with PS12E-ALK 12V Alkaline Power Supply or lead-acid battery

DAS2/IRM - Data Acquisition System 2/Infrared Measurements consisting of the following sensors/instruments.

- A small hand-held data acquisition system (ALMEMO)
- Thermal infrared sensor
- Air temperature sensor
- Air temperature/relative humidity sensor
- Air velocity sensor.

•• Indicates sensor connection, either directly to the CR10 MCM or to the multiplexers, AM416 or AM25T.

Installation of Data Acquisition System 1 (DAS1/AWS): The DAS1/AWS is as shown in Figs. 6.2 and 6.3 with the respective datalogger-sensor or datalogger-multiplexer-sensor connections.

Tower Assembly: A hole 0.5 m by 0 5 m square by 0 5 m deep was excavated in the ground in the position where the 2m tower was erected. The three steel legs (supplied with the tower) were secured to the base of the aluminium tower using the bolts provided. The tower and legs were

placed in an upright position in the centre of the hole. Concrete mixture was poured into the hole and the tower was checked for uprightness using a spirit level.

System Assembly: System assembly was done after the base had set. The ENC 12/14 Enclosure was attached to the tower at a height of about 0.5 m from the ground. Sensors were then mounted on the tower at appropriate heights. The AM416 Multiplexer was placed on a wooden stool (see Fig. 6.2). The evaporation pan was placed on a wooden base constructed according to the required specifications (see Fig. 6.2). Some sensors were connected directly to the CR10 Measurement and Control Module (MCM) and others were connected through the Multiplexers, AM416 and AM25T.

Grounding: The tower and datalogger were grounded with copper-covered steel spikes. Two spikes were used

Power supply: The measurement system was powered by a 12V lead-acid battery. A 10W solar panel (SOP10/X Solarex Solar Panels) was used to charge the lead-acid battery.

Programming: Because of the non-standard configuration of the system used in this study, it was necessary to develop own program for the measurement of the datalogger and multiplexers. The programming was done using the Edlog, the program editor module of the PC208E Datalogger Support Software (Campbell Scientific Inc. (CSI)). The program was downloaded to the datalogger from the PC at the beginning of the measurements. It is to be borne in mind that the existence of the program in the datalogger requires continuous presence of power. The program is lost in the event of power failure in the datalogger and must be redownloaded. Measurements of the different sensors were made every five minutes and data storage done every fifteen minutes. Additionally, storage of hourly and daily data was done. A link between the PC and the datalogger was set using the SC32A opto-isolated interface. Final storage data from the CR10 MCM were automatically collected using the GraphTerm terminal emulator program (CSI). The GraphTerm terminal emulator program offers real time graphical monitoring capability. Data were collected (downloaded to the computer) once or twice every day.

Installation of Data Acquisition System 2 (DAS2) The DAS2 is as detailed in **Figs. 6.2 and 6.3** with the respective connections. A wooden mast and a wooden stool for holding the sensors and equipment, respectively, were constructed. The ALMEMO hand-held data acquisition system was put on the wooden stool. Because of the fear of the DAS2 and the sensors being damaged through exposure to rain, the DAS2 was put in place early in the morning (around 0800 h) and removed late in the evening (around 1800 h) every day. Essentially measurements were carried out during the daytime when conditions allowed, i.e., mostly in the absence of rain. Measurements were carried out regardless of whether a day was mostly cloudy or mostly cloud-free. This provided a comprehensive data set both for testing of the infrared thermometry method for estimation of near-surface soil water content as well as for model calibration and validation presented in chapter 7.

6.5.3 Description of the measurements carried out

Net radiation: Net radiation was measured using a Q-7 Net Radiometer (CSI) at a 1.6 m height. The Q-7 Net Radiometer is a high-output thermopile sensor which measures the algebraic sum of incoming and outgoing all-wave radiation (i.e. short-wave and long-wave components). Incoming radiation consists of direct (beam) and diffuse solar radiation plus long-wave irradiance from the sky. Outgoing radiation consists of reflected solar radiation plus the terrestrial long-wave component. The sensor has 60 junctions with low electrical resistance (4 ohms nominal) to reduce susceptibility to noise. The calibration factors are 9.30 $Wm^{-2}mV^{-1}$ (for positive values), and 11.73 $Wm^{-2}mV^{-1}$ (for negative values). The sensor has a time constant of approximately 30 s, and its spectral response is 0.25 to 60 μm.

Most sensors which measure long wave radiation are subject to some degree of error caused by moving air cooling the windows of the sensor. The sensor was therefore programmed with a dynamic wind speed correction. Net radiation was measured every five minutes by the CR10 MCM and average, maximum, and minimum values stored every 15 minutes. This radiation flux was used for model calibration and validation. Measured net radiation will be further treated in chapter 7 together with model simulations. Daily global radiation data were obtained from a neighbouring weather station.

Rainfall: Rainfall was measured using an ARG100 tipping bucket raingauge (CSI). The manufacturer's calibration factor for the gauge was 0.199 mm/tip. The gauge was mounted on a concrete paving slab using through-bolts. Sand was added underneath the slab to level the gauge. Additionally, a spirit level was placed across the rim of the assembled gauge. The sensor was automatically measured every five minutes by the CR10 MCM and data storage of the total rainfall was done every 15 minutes.

Pan evaporation: Potential evaporation was measured using a Class A Pan. Measurements of the water depth in the pan were effected using a pressure transducer which was measured by the CR10 MCM every five minutes and data storage done every 15 minutes. The transducer has a stainless steel diaphragm that is deflected by change in hydrostatic pressure with respect to atmospheric pressure. The sensor was suspended in a column of water (in the evaporation pan). As the level of water above the transducer reduces (due to evaporation) the mV output reduces linearly. The stainless steel diaphragm is mounted in a steel block. Two machined holes at the side allow water to enter the transducer. The sensor has a sensitivity of 0.0100 V/mm and non-linearity of 0.3544%. The measurement range is 0 - 200 mm with hysteresis of less than 0.1% and temperature coefficient of less than 0.1 % /°C. The sensor has a zero offset of 0.248 V. Simultaneous measurements of the water depth were done every day at around 0900 h using a graduated scale in order to calibrate the sensor. The evaporation pan was filled up with water to within about 2.54 cm of top. Refilling of the evaporation pan to within about 2.54 cm of top was done each time the level of water in the pan dropped down to about 5 cm.

Soil heat flux: Soil heat flux density was measured using a HFT-3 Soil Heat Flux Plate (CSI). The HFT-3 Soil Heat Flux Plate is a heat flow transducer designed to measure heat flow in soils. The thermopile is encapsulated in high thermal conductivity epoxy to prevent ground potential pickup. The sensor has a calibration factor of 34.0 Wm^{-2} mV^{-1}, a resistance of about 2 ohms, and a thermal conductivity of about 1.22 $Wm^{-1}K^{-1}$. Soil heat flux density was measured at 0.05 m depth and corrected for the difference in the specific heat conductivity of plate and soil and for the change in heat storage in the soil layer between 0.00 and 0.05 m, using the soil temperature at a depth of 0.02 m (van den Berg, 1989; Mayocchi and Bristow, 1995). The soil heat flux density measurement using the HFT-3 plate was supplemented by temperature profile technique

of estimation of soil heat flux density (Horton and Wierenga, 1983).

Air temperature and relative humidity Air temperature and relative humidity were measured at 1 6 m screen height using a HMP35AC Temperature and Relative Humidity (RH) Probe (CSI). The probe contains a Vaisala capacitive relative humidity sensor and a precision thermistor. The probe was housed in a URS1 radiation shield (CSI) The temperature sensor has a measurement error of about ± 0 2 °C in the range 0 °C to 60 °C. The RH sensor has a measurement range of 0 to 100 % RH and a measurement error of about ± 0 1 % RH. The sensors were automatically measured every five minutes by the CR10 MCM and data storage done every 15 minutes.

Additional air temperature measurement at 1 6 m height was made using an ALMEMO hand-held instrument This was measured simultaneously with the surface soil radiant temperature The air temperature sensor (TK 127 - Ahlborn GmbH, Germany) has maximum range of 500 °C and a response time of 0 8 s The measurement interval was 2 5 minutes and averaged readings of the variables were stored in the DAS2 datalogger.

Wind speed and direction. Wind speed and direction were measured at 2 m height using a 05103-5 Wind Monitor (CSI) The wind speed sensor is a 18 cm diameter 4-blade helicoid propeller moulded of polypropylene The sensor has a measurement range of 0 to 60 m/s and a gust survival of 100 m/s The transducer is a centrally mounted stationary coil, with a 2 kΩ nominal DC resistance. The transducer output is an AC sine wave signal induced by rotating magnet on propeller shaft. The sensor has an output frequency of 3 cycles per propeller revolution (0.098 m/s per Hz)

The wind direction sensor is a balanced vane with a 38 cm turning radius. The sensor has a measurement range of 360° mechanical, and 355° electrical (5° open). The transducer is a precision conductive plastic potentiometer with 10 kΩ resistance (± 20%) and 0.25% linearity. The sensors were automatically measured every five minutes by the CR10 MCM and data storage done every 15 minutes.

Soil water content: Soil water content at various depths were determined gravimetrically. Soil samples were taken using an auger to the depth of 60 cm in steps of 5 cm. Immediately after augering the soil samples were sealed in plastic bags to avoid loss of soil moisture to the atmosphere. The soil samples were taken to the laboratory for determination of soil moisture content. Samples were weighed to determine the wet mass They were then dried in an oven at 105 °C for 24 hours. The samples were then reweighed to determine the dry mass. The gravimetric soil moisture content was then determined as follows:

$$\theta_{m,wet} = \frac{m_w - m_d}{m_d} \times 100 \qquad (6\,1)$$

where $\theta_{m,wet}$ is the gravimetric soil moisture content in weight %,

m_w is the wet mass of the soil in g,

m_d is the dry mass of the soil in g.

Volumetric soil moisture content was determined by multiplying the gravimetric soil moisture content by the bulk density. The bulk density was simultaneously determined with gravimetric soil moisture content using cored soil samples of known volume

Matric potential: For the measurement of matric potential, Watermark sensors and gypsum blocks were installed at 5, 15, 30, 45, and 60 cm depths at two separate locations in the experimental field. Tensiometers were also installed at 15, 30, 45, and 60 cm depths. The tensiometers were read manually four times daily at 0900, 1200, 1500, and 1800 h, except for the days when weather conditions did not allow

Watermark Sensors: The Watermark soil moisture sensors (models 257 and 253) are solid state, electrical resistance sensors which provide a convenient method of estimating soil water potential in the 0.1 to 2 bar (10 to 200 kPa) range The sensors consist of two concentric electrodes buried in a reference matrix material. The matrix material is surrounded by a thin stainless-steel mesh. The sensors can be left in the soil all year. An internal gypsum tablet buffers against the salinity levels found in irrigated soils.

The model 253 is supplied with two green leads from Watermark. These leads are connected directly to the H and L inputs on the AM416 Multiplexer. A 1 kΩ precision resistor has to be connected at the datalogger to complete the half bridge measurement. Details of connection can be found in the instruction manual delivered with the sensors.

The sensor is excited by an AC signal and its resistance measured by the datalogger as shown below in tabular form for the CR10 datalogger. The ratio of signal voltage to excitation voltage is used to calculate the sensor resistance as follows

$$U_s / U_x = R_s / (R_s + R_f) \qquad (6.2)$$

where

U_s is signal voltage in mV,

U_x is excitation voltage in mV,

R_s is sensor resistance in kΩ, and

R_f is fixed bridge resistor in kΩ.

The sensor resistance and soil temperature are used to calculate soil water potential based on a calibration equation.

Datalogger	Excitation	Range Code	Full Scale Range
CR10	250 mV	14	±250 mV

Gypsum blocks. Gypsum soil moisture blocks (models 227 and 223) provide a convenient method of estimating soil water potential. The Delmhorst cylindrical block is composed of gypsum cast around two concentric electrodes which confine current flow to the interior of the block, greatly reducing potential ground loops. Gypsum located between the outer electrode and the soil creates a buffer against salts which may affect the electrical conductivity and hence the calibration of the block. Individual calibrations are required for accurate readings of soil water potential. Model 223 was used in this study. Connections and measurement are similar to the model 253 Watermark sensor described above.

A total of ten Watermark sensors were used in the measurements These plus ten gypsum blocks were connected to one multiplexer. Both the Watermark sensors and gypsum blocks were subjected to several wetting-drying cycles before final installation in the field as recommended by the manufacturers. A pit was dug for the installation of Watermark sensors and gypsum blocks at each of the two locations. At each depth, a Watermark sensor and a gypsum block sensor were installed 15 cm apart adjacent to each other. This was done in order to compare the two types of sensors, bearing in mind the fact that the two type of sensors are complementary in their measurement ranges.

In order to study the effect of soil variability, each measurement of matric potential at a particular depth in the soil was replicated at least twice. More replications were not possible due to the limitation of the respective sensors

Soil temperature : Soil temperature was measured using the 107 Thermistor Temperature Probes and thermocouple wires (type T) (CSI). The thermocouple wires have a measurement error of about + 0.01 °C in the temperature range 20 °C to 50 °C. The thermistor probes are designed for measuring temperatures in the range - 40 °C to +56 °C. The thermistor probes have a measurement error of about ± 0 2 °C.

The thermocouple wires were installed at 5, 15, 30, and 45 cm depths as recommended by the WMO (Buchan, 1991) at two separate locations in the field. Two thermistor temperature probes were used for the measurement of soil temperature at the 5 cm depth. Thus there were a total of four measurement locations at the 5 cm depth in the field.

A pit was dug for the installation of thermocouple wires. The thermocouple wires were routed down to the bottom of the installation pit along one side of the pit and up along the opposite side until a desired installation depth was reached This was necessary to avoid any water flowing along the wires coming to the tip of the wires and therefore causing erroneous measurements. The thermocouple wires were installed horizontally at each depth. Again the sampling depth for the temperature measurements was limited to the upper 50 cm from the soil surface.

Additionally soil temperatures were measured during the day at various points in the field at 5, 10, 15, and 30 cm depths using (mercury-in-glass) portable soil thermometers, with two to three replications at each of the measurement depths. The portable soil thermometers have a measurement range of -10 to +50 °C and contained in rugged brass case with stem graduated at 5, 10, 15, 20, and 30 cm to enable measurement at various depths. The mercury thermometer temperature data were used for calibration of the thermocouples and thermistors.

The thermocouples and thermistor probes were measured by the CR10 MCM every five minutes and data stored every fifteen minutes. The mercury thermometers were read manually every 30 minutes during daytime and values entered in data sheets. In order to study the effect of soil variability, each measurement of soil temperature at a particular depth in the soil was replicated at least twice. More replications were not possible due to the limitation of the respective sensors.

Soil surface radiant temperature Soil surface radiant temperature was measured using an infrared thermometer (IRT1) (Ahlborn GmbH, Germany) with a Field of View (FoV) of about 15° (300 mm target diameter at 1 m distance) at a height of 1.2 m from the ground at an angle of 45° to the horizontal. This sensor has a measurement range of -30 °C to +70 °C and a resolution of 0.1 °C. The linearization accuracy of the sensor is given as 0.05 K ± 0.05% of the measured value. Analog output of sensor is 10 mV/°C. Response time is 250 s. The accuracy of the sensor is less than 1.5 % of the measurement range, i.e., ± 1.5 °C. The sensor is equipped with chopper compensation. The emissivity value can be adjusted

Another infrared thermometer (IRT2) (FR 260 MV- Ahlborn GmbH, Germany) was used for random check of the surface soil temperature in the vicinity of the area of measurement. The IRT2 has a measurement range of -18 °C to +260 °C and a resolution of 0.1 °C. The sensor output is 1 mV/°C. The accuracy of the sensor is ± 2% of the measured value or ± 2 °C. The response time of the sensor is 1 s. The sensor is also equipped with chopper compensation. The emissivity value can be adjusted. Both the IRTs measure in the 8-14 μm spectral range. The IRT1 broke down in the middle of the experimental period and therefore the IRT2 was used in place of the IRT1 for the rest of the measurement period.

Field-saturated hydraulic conductivity: Field soil saturated hydraulic conductivity was determined using the Model 2800K1 Guelph Permeameter (GP) (Soilmoisture Equipment Corp , USA). The GP theory, apparatus, procedures for its use, and example calculations are given in detail in Reynolds et al. (1985) and Reynolds and Elrick (1986) The operating instructions also detail the procedures for carrying out the measurements. Briefly, the GP method provides simultaneous, in-situ measurements in the vadose (unsaturated) zone of field-saturated hydraulic conductivity, K_{fs}, sorptivity, S, and the hydraulic conductivity (K) - pressure head (ψ) relationship, $K(\psi)$.

Determination of soil thermal properties: Soil heat capacity was determined using de Vries (1963) method (ten Berge, 1990) from the measurement of soil moisture content and soil texture. Soil thermal conductivity was determined using the de Vries (1963, 1975) method (ten Berge, 1990) from the conductivities of the individual components based on the measurement of soil moisture and soil texture.

Determination of soil physical properties: Soil samples were augered from the field for the determination of soil physical properties. These were taken to the laboratory for analysis to determine soil texture, bulk density, porosity, specific gravity, and particle size distribution. Cored samples of known volume were used for the determination of bulk density and soil water content. Soil sampling was done to the 60 cm depth with two replications for each of the depth for a particular day on which sampling was done. Tables A7.1 and A7.2 in Appendix 7 detail the results of the soil analysis.

Determination of soil surface roughness: Soil surface roughness was determined by estimation method. The soil surface was assumed to be smooth after performing several rolling operations on it.

6.5.4 Field calibration of sensors

Correction of measured infrared temperature for emissivity and temperature of the environment: Equation (6.3) was used to correct the measured infrared temperature for emissivity and temperature of the environment as recommended by the manufacturer of the thermal infrared sensors. Air temperature, which was measured simultaneously with the infrared temperature of the surface of the soil, was used as the temperature of the environment in this case. This provided a continuous monitoring of the temperature of the environment. A soil emissivity value of 0.95 was used

Let T_s = soil surface temperature (temperature of the object of interest) in °C,

ϵ = emissivity of the bare soil surface,

T_m = infrared measured temperature in °C, and

T_a = air temperature in °C

then

$$T_s = \frac{1}{\epsilon}(T_m - T_a) + T_a \qquad (6.3)$$

Calibration of Watermark soil moisture sensors for soil matric potential and temperature

Temperature calibration: Normalizing measured block resistance (R_m, kΩ) obtained at temperature T_m (°C) to a reference resistance (R_r, kΩ) at temperature T_r (°C) was accomplished using (Spaans and Baker, 1992)

$$R_r = R_m [1 + a (T_m - T_r)] \qquad (6.4)$$

Campbell and Gee (1986) reported a = 0.03 as a typical value for resistance blocks. The manufacturer of the Watermark block lists a = 0.018. Spaans and Baker (1992) obtained 0.024 as a value for a from their data with T_r = 25 °C.

Matric potential calibration: Spaans and Baker (1992) used tensiometers to calibrate the Watermark sensors in a greenhouse and in a laboratory. Calibrations were conducted in two different soils. Measured block resistances were corrected for temperature according to Eq. (6.4).

For the SUA field experiments, tensiometers were also used to calibrate the Watermark sensors in the field. Tensiometers were installed at 15, 30, 45, and 60 cm depths at two locations in the experimental field. The tensiometers were read manually four times daily at 0900, 1200, 1500, and 1800 h, except for days when this was not possible.

The following calibration equation (McCann et al 1992) was used for the Watermark sensors in calculating resistance:

$$R = \alpha[\frac{S}{\beta}]^a[1 + k(18 - T)] \qquad (6.5)$$

After rearranging the Eq. (6.5), the soil water potential, S, was calculated as follows:

$$S = \beta\,[\frac{R}{\alpha[1 + k(18 - T)]}]^{1/a} \qquad (6.6)$$

where

R is sensor resistance in kΩ,

S is soil water potential in -kPa,

T is soil temperature in °C,

and α, β, a, and k were statistically determined and have the values of:

α = 0.93,

β = 2.1,

a = 0.8,

k = 0.03.

In Eq. (6.6), the electrical conductance (1/R) of the sensor is assumed to be directly proportional to its liquid content The relationship between conductance and soil water potential is modelled after Brooks-Corey equation, which relates soil water content to soil water potential (Brooks and Corey, 1966) Using this form of equation, conductivity is analogous to soil water content.

Calibration of soil temperature sensors: Mercury thermometer measured temperature data were used to calibrate the thermocouples and thermistors This was done at the beginning of the field experiments All the thermocouple wires and thermistors were installed at the 5 cm depth in the field The eight thermocouple wires were installed at one location, whereas the two thermistors were installed at another two different locations closeby. These sensors were measured every five minutes using the data acquisition system (DAS1) and data stored every 15 minutes. Simultaneously, soil temperature measurements were manually effected using the mercury thermometers at 12 different locations scattered all over the field at the 5 cm depth The mercury thermometers were manually read every 30 minutes during the daytime and data entered in data sheets Average values of the mercury thermometer data as well as the sensor data were used for the calibration purpose

Calibration of air temperature sensors Air temperature data measured by DAS1 were compared with measurements of air temperature from a nearby weather station located about 20 m away from the experimental field A good correlation between the two sets of measurements was observed.

6.6 Correction for changing solar radiation in the measurement of temperature difference (TD)

An attempt was made to correct the measured TD values for the changing solar radiation. In this case net radiation was used as a surrogate for solar radiation because high temporal resolution solar radiation data were not measured. To correct for the effects of changing solar radiation in the measurement of the soil surface minus air temperature (TD), the following procedure (Pennington and Heatherly, 1989) as illustrated in Fig 6.4 was used·

i. A regression analysis was applied between the average quarter-hourly measured net radiation values and the the TD values.

ii. A net radiation value, Rneq, which would correspond to an equilibrium TDmi was calculated as follows using the TDm and Rnm regression function for a particular day.

$$Rneqi = (TDmi-I)/S$$

where Tdmi is TDm of i measurememt,
I is intercept of Rnm and TDm function,
S is slope of Rnm and TDm function, and
Rneqi is Rn which would give an equilibrium TD of TDmi.

iii. A total potential change in TD when Rn changes to Rnmi from Rneqi was calculated as shown below. Rneq(i-1) is used as the reference point to calculate the magnitude of potential change in TDm(i-1) with change in Rn to Rnmi using the slope of the TDm and Rnm function.

$$DTDi = (Rnmi - Rneq(i-1))xS$$

where Rnmi is measured Rn for i measurement,
DTDi is potential total change in TD when Rn changes from Rneq(i-1) to Rnmi.

iv. Assume that TD changes by 30% of DTDi in the 15 minutes that elapse from i-1 to the i measurement. Add 70% of DTDi to TDmi to calculate the TD that would result if TD were in equilibrium at Rnmi.

$$TDai = 0.7 \times DTDi + TDmi$$

where TDai is the equilibrium value of TD at Rnmi.

Using the linear relationship between Rnm and TDa, the calculation of TD at a reference Rn is:

$$TDri = [(Rnr - Rnmi)xS] + TDai$$

where Tdri is TDi at reference Rn.

The average day time (within the period of measurement) net radiation was used as a reference for each day.

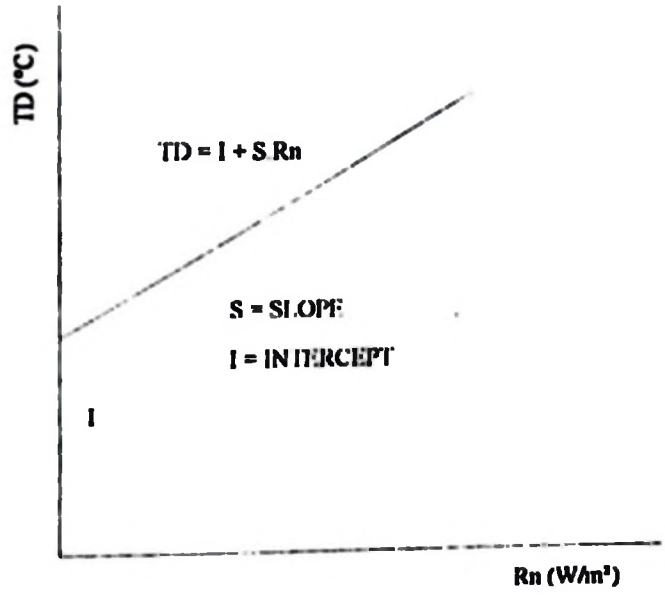

Fig. 6.4 Illustration of the above used procedure.

7 RESULTS AND DISCUSSION

7.1 Prevailing conditions during the experimental period

7.1.1 Introduction

As mentioned in chapters one and four, quantitative interpretation of remotely sensed thermal-infrared data is complicated by the many physical factors that influence observed temperatures. The following subsections address briefly the prevailing conditions during the course of the experiment as reflected by the various measured variables.

7.1.2 Solar radiation

Fig. 7.1 shows the variation of the the measured daily global solar radiation during the experimental period. As can be seen, the global radiation ranged between around 2 and around 25 MJ/m^2. Low solar radiation values could be attributed to the fact that the experimental period was frequented by rainfall and cloud cover.

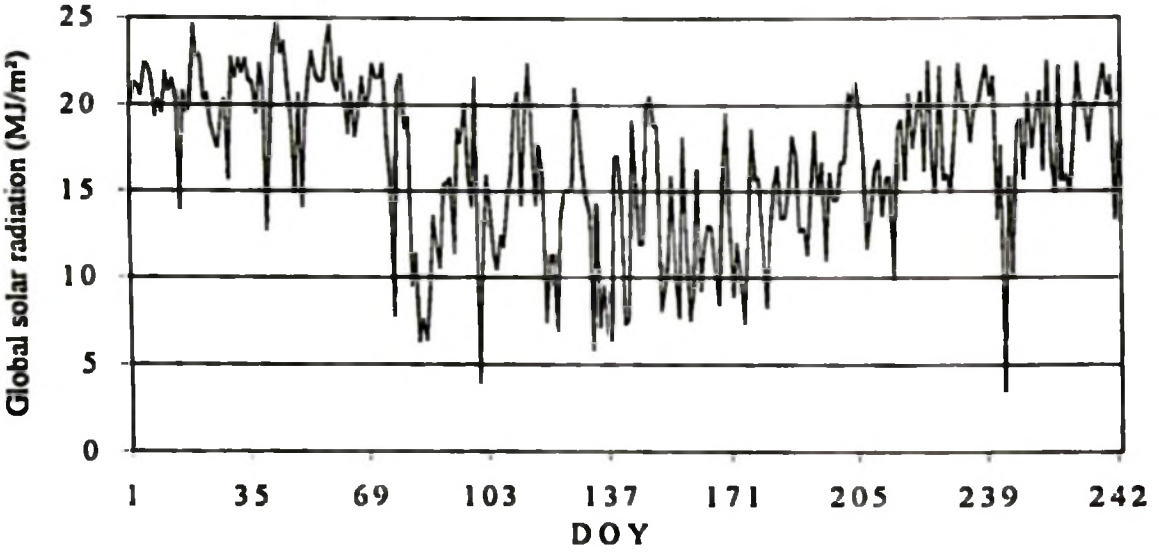

Fig. 7.1 Measured daily global solar radiation at the experimental site, January - September, 1997.

7.1.3 Sunshine hours

Fig. 7.2 shows the measured sunshine hours during the experimental period. As can be seen, sunshine hours ranged between 0 to around 10. The experimental period was frequented by rains with intermittent dry spells.

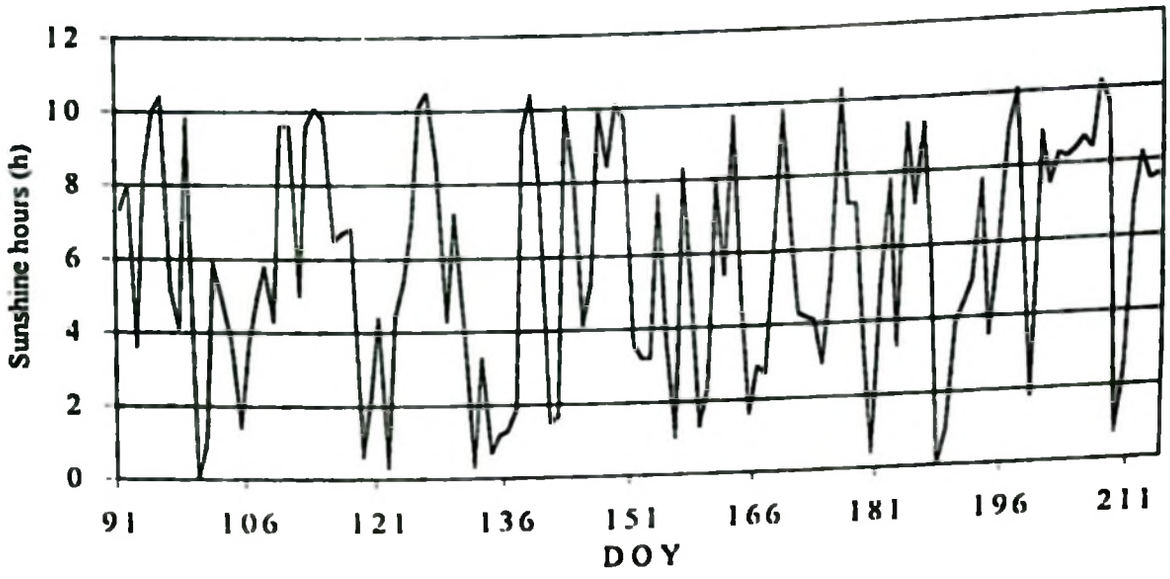

Fig. 7.2 Measured sunshine hours at the experimental site.

7.1.4 Net radiation

A typical quarter-hourly variation of the measured average, maximum, and minimum net radiation is shown in **Fig. 7.3.** The daily variation of the average, maximum, and minimum measured net radiation during the experimental period is shown in **Fig. 7.4**. As can be seen from **Fig. 7.4,** the daily net radiation ranged from about -60 to 900 W/m^2 during the experimental period, with daily average values ranging from about -60 to 200 W/m^2. This is not surprising because of the frequent occurrences of rainfall and clouds. However, higher values of net radiation are to be expected during mostly sunny and clear-sky days in this part of the world.

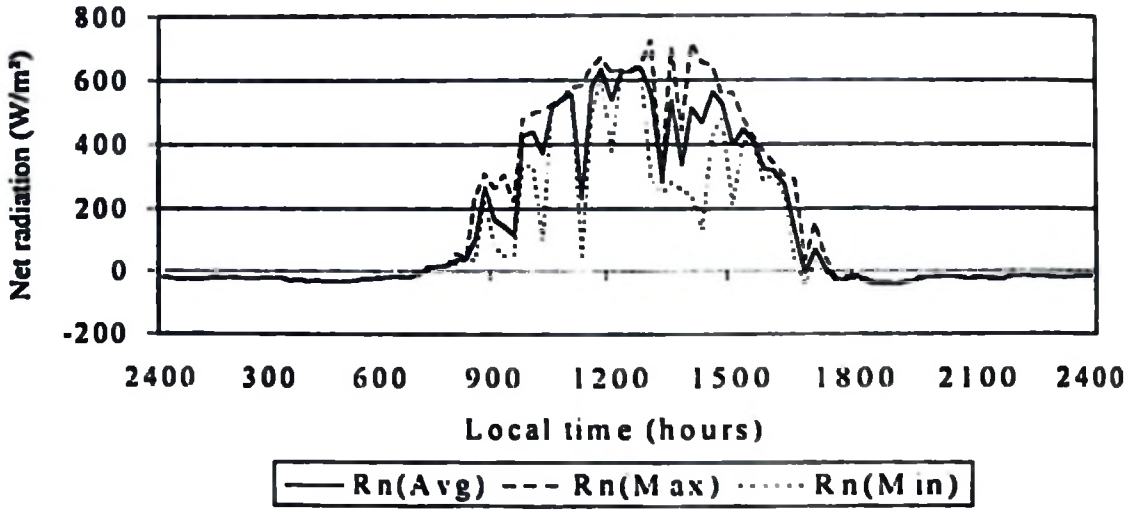

Fig. 7.3 Quarter-hourly variation of measured average, Rn(Avg), maximum, Rn(Max), and minimum, Rn(Min), net radiation at the experimental site (DOY 150, 1997).

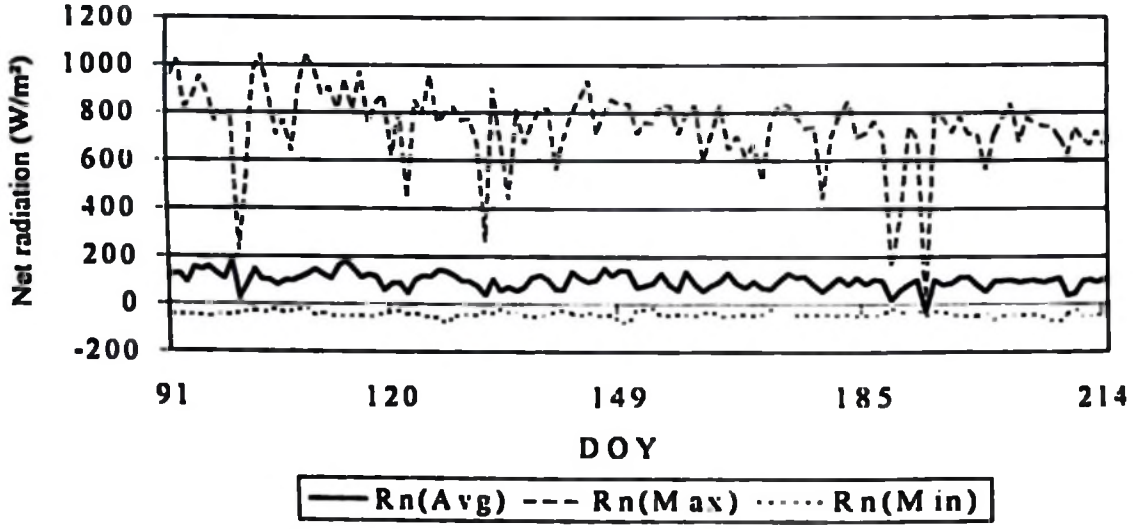

Fig. 7.4 Daily variation of measured average, Rn(Avg), maximum, Rn(Max), and minimum, Rn(Min), net radiation at the experimental site.

7.1.5 Soil heat flux

Assuming that conduction is the predominant heat transfer mechanism in homogeneous soils, combination of Fourier's law

$$G_s = -\lambda \frac{\partial T}{\partial z} \tag{7.1}$$

with a sinusoidal behaviour of the surface temperature T_s yields the relation between surface heat flux G_s, the angular frequency ω and the amplitude of the surface temperature wave T_{sA} (van Wijk, 1963):

$$\int_{t_1}^{t_2} G_s(t)dt = T_{sA}\sqrt{(\omega\lambda C)} \int_{t_1}^{t_2} \sin(\omega t + \frac{\pi}{4})dt \tag{7.2}$$

Thermal inertia is defined as $P \equiv (\lambda C)^{1/2}$. The "thermal inertia approach" for estimation of soil water content basically combines remote measurements of T_s with estimates of G_s (t) to solve Eq. (7.2) for P. If the interest is to estimate soil moisture content, this thermal property is subsequently translated into volumetric moisture content. Such a translation requires specific soil information, primarily on bulk density as well as mineralogical composition. Fig. 7.5 shows the daily variation of the average measured soil heat flux during the experimental period. The soil heat flux values range from about -20 W/m² to 20 W/m², with an average value of about 0 to 5 W/m².

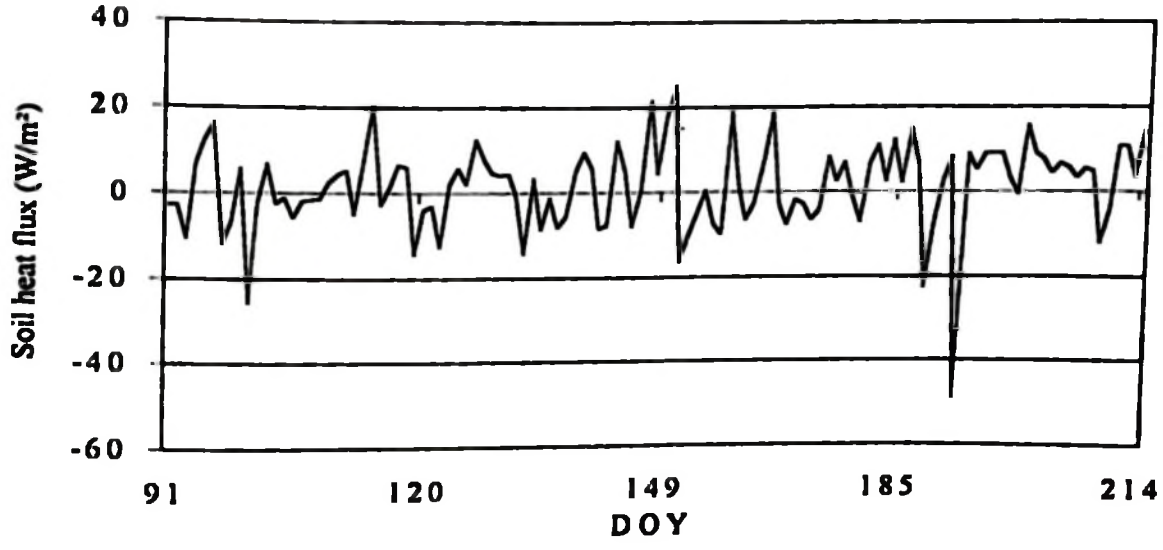

Fig. 7.5 Daily variation of measured average soil heat flux at the experimental site.

7.1.6 Air temperature

Air temperature can generally be estimated reasonably well from conventional meteorological data. The daily variations of the measured average, maximum, and minimum air temperatures during the experimental period are shown in Fig. 7.6.

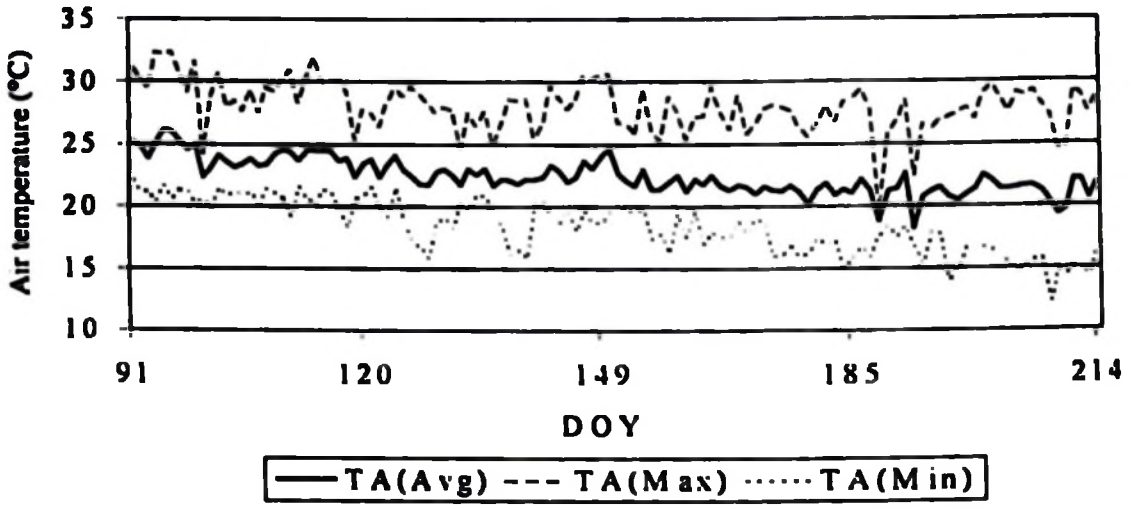

Fig. 7.6 Daily variation of measured average, TA(Avg), maximum, TA(Max), and minimum, TA(Min), air temperature at the experimental site.

Daily average air temperatures ranged from about 18 to 26 °C. Maximum air temperatures ranged from about 20 to 32 °C, and minimum air temperatures from about 12 to 22 °C.

7.1.7 Wind speed

Due to the fact that the aerodynamic resistance to sensible heat transfer decreases with increasing wind speed, previous works (O'Toole and Hatfield, 1983) have found that canopy temperature measured with an Infrared Thermometer (IRT) declined with increasing wind speed. This effect is small for wind speeds above 2.5 m s^{-1} since aerodynamic resistance decreases slowly with increases in wind speed above 2.5 m s^{-1} (Howell et al., 1986). The results of these findings are assumed to apply for the case of bare soil surface in this study. During the course of the field experiments, and as can be seen from the graphs in Figs 7.7 to 7.9, maximum wind speeds occurred in the late afternoons or evenings for most of the time. In very few days did maximum wind speeds exceed the 2.5 m s^{-1} limit during the noon and early afternoon hours, a time period during which TDMax occurred. Instantaneous wind speed measurements were also used for the dynamic wind speed correction for the measurement of net radiation.

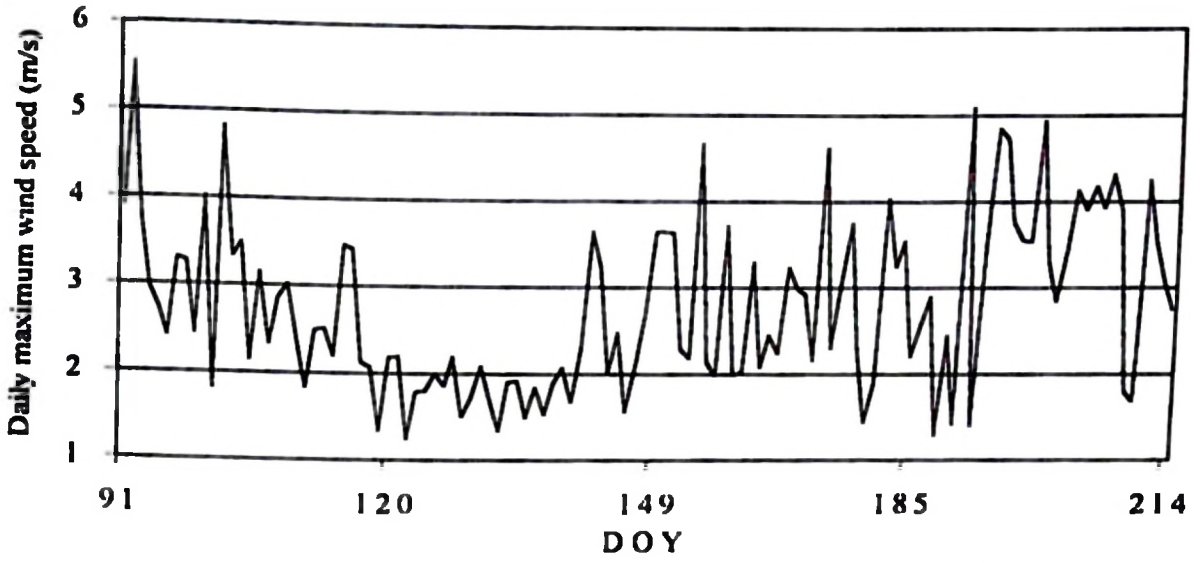

Fig 7.7 Daily variation of measured maximum wind speed at the experimental site.

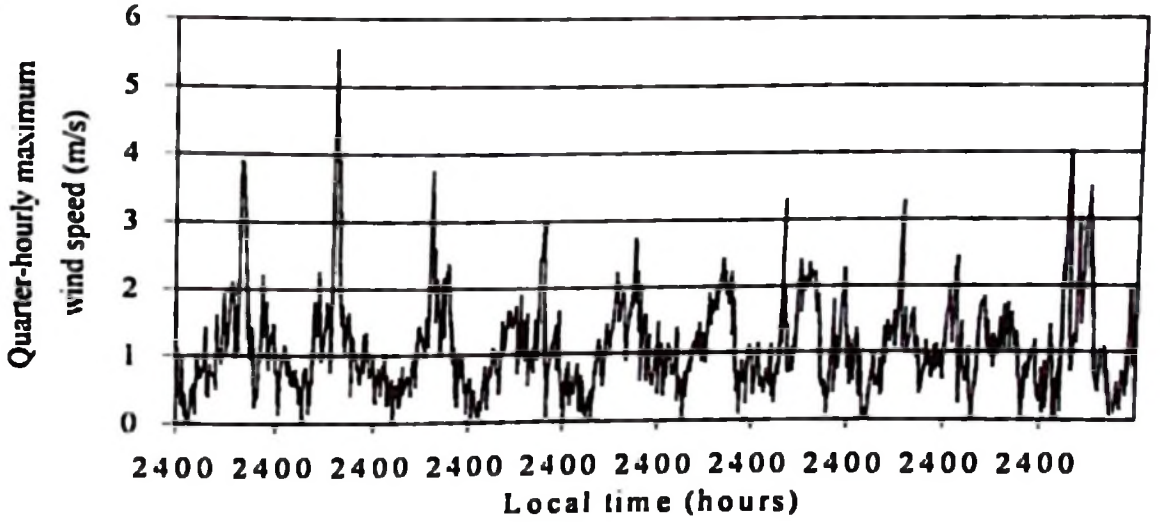

Fig 7.8 Quarter-hourly variation of measured maximum wind speed for DOY 91 to DOY 100 at the experimental site.

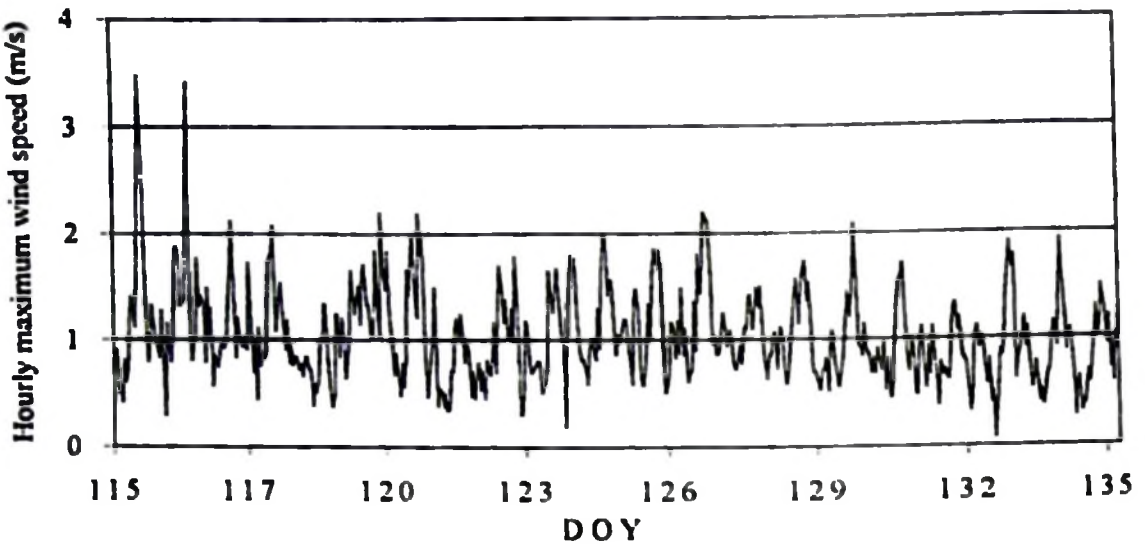

Fig. 7.9 Hourly variation of measured maximum wind speed for DOY 115 to DOY 135 at the experimental site.

7.1.8 Relative humidity

In **Fig. 7.10** the daily variations of the average, maximum, and minimum measured relative humidity during the experimental period are shown. The average relative humidity ranged from about 65 to 95%. The maximum relative humidity ranged from about 90 to 100%, whereas the minimum relative humidity ranged from about 35 to 90%. As can be seen from the graph, high relative humidities did prevail during the whole period of the experiment

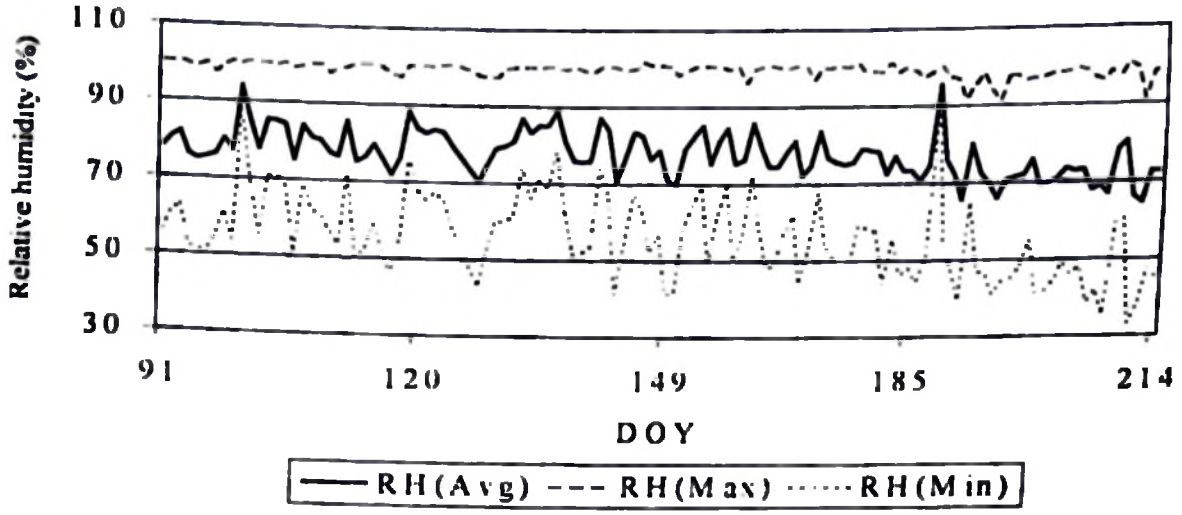

Fig. 7.10 Daily variation of measured average, RH(Avg), maximum, RH(Max), and minimum, RH(Min), relative humidity at the experimental site.

7.1.9 Vapour pressure deficit

The variation of the daily average vapour pressure deficit for the whole period of the experiment is shown in Fig. 7.11. The experimental period was frequented by relatively low average vapour pressure deficits

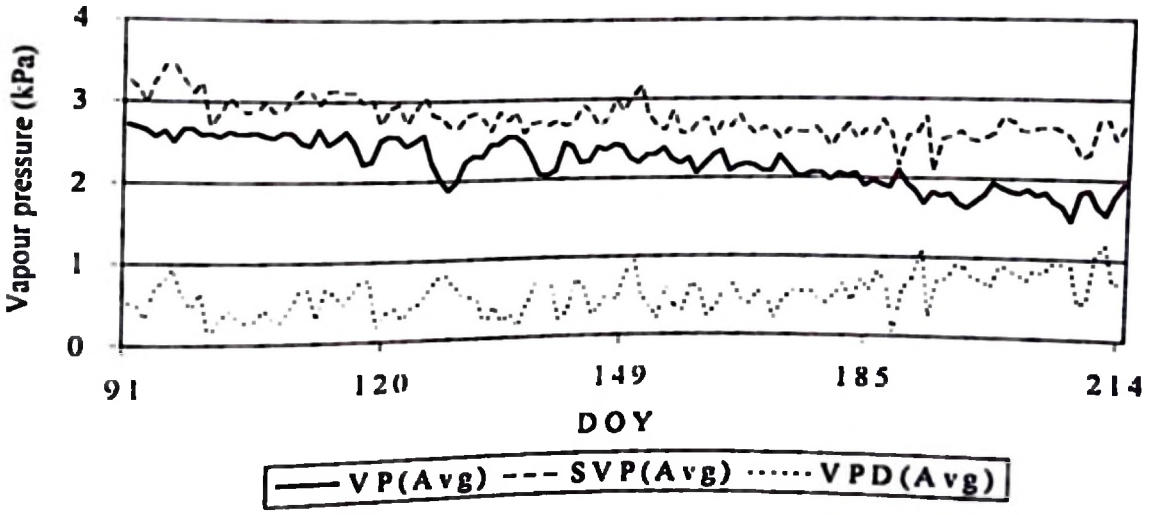

Fig 7.11 Daily measured vapour pressure (VP), saturated vapour pressure (SVP), and vapour pressure deficit (VPD) at the experimental site.

7.1.10 Soil surface radiant temperature

Fig.7.12 shows the temporal variation of the surface soil radiant temperature T(IRT) together with simultaneously measured air temperature, TA (NiCr). The difference between IRT and AT is also shown in the figure. As can be seen from the figure, there are fluctuations in both the surface soil radiant and air temperatures in response to the rapid changes in solar radiation. Clearly this is one of the mostly cloud-free days. While the surface soil radiant temperature is very sensitive to the rapid fluctuations in solar radiation, the air temperature is not comparably sensitive. In order to keep track of the changing solar radiation, a highly sensitive sensor is therefore required for the measurement of the surface soil radiant temperature.

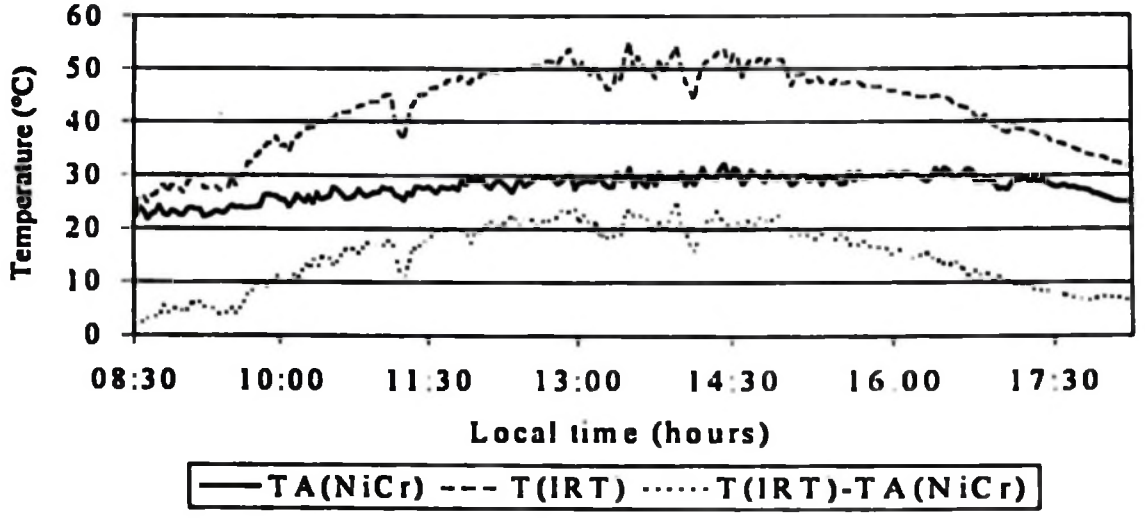

Fig. 7.12 Daytime variation of the surface soil radiant temperature, T(IRT), air temperature, TA(NiCr), and the difference, T(IRT)-TA(NiCr), for a typical nearly cloud-free day (DOY 150, 1997).

The measurement interval used in this study of 2.5 minutes does to some extent help to reveal the effect of changing solar radiation on the measurement of both surface soil radiant and air temperatures. Because solar radiation was not measured in this study (daily values were obtained from a nearby weather station), net radiation was used as a surrogate for solar radiation in trying to associate the changes in solar radiation with the fluctuations observed in the measured surface soil radiant and air temperatures. Clearly more time-intensive measurements of both solar radiation (net radiation) and infrared and air temperatures would be desirable to be able to study in more detail the effects of clouds, as reflected by changing solar radiation, on the measured infrared and air temperatures (see also subsection 7.2.4).

7.1.11 Profile soil temperatures

Although soil surface radiant temperature (see subsection 7.1.10) plays a central role in many of the surface processes, the course of soil temperature at various depths below the surface is of more general agronomic interest Information on temperatures in the top few centimetres of soil may be relevant to the characterization of conditions for germination and root growth Such information could also be valuable for predicting pest development To obtain estimates of subsurface soil temperatures, a measured course of surface temperature could be combined with a model describing heat transport in the soil.

Soil temperature, though a function of array of soil and atmospheric parameters, can be relatively easily measured by either ground or remote methods (see also subsection 7 1.10). Most often the soil and atmospheric parameters, such as soil water content, evaporation, air temperature, net radiation are difficult and expensive to measure It is possible to estimate soil water content and evaporation from the measurements of soil temperature. The extent of the accuracy in such estimations may depend upon the accuracy of our prior understanding of the nature of variation and structure of soil temperature over space.

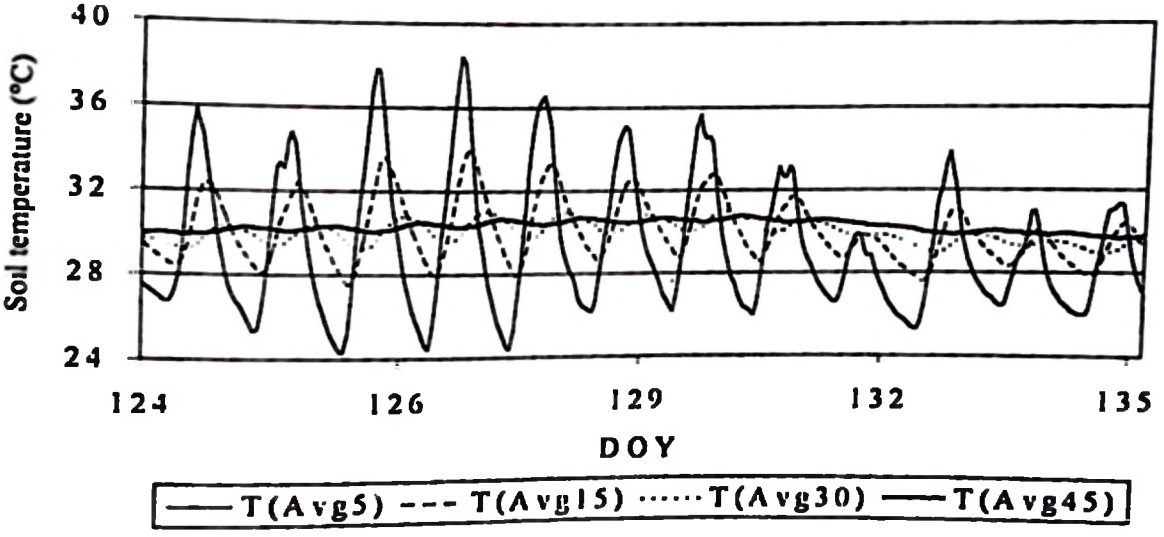

Fig. 7.13 Diurnal variations of the measured average soil temperatures at the 5, 15, 30, and 45 cm depths for DOY 124 to DOY 135.

Figs 7.13 and 7.14 show the diurnal variations of the measured average soil temperatures for different depths in the soil during selected days of the experimental period. Simultaneous measurements of soil temperatures were necessary for the correction of the resistance readings of the temperature-dependent gypsum blocks and Watermark sensors. Temperature

measurements were also necessary for the calibration and validation of the model. Soil temperatures measured using mercury thermometers in different depths in the soil were used for calibration of the thermistor and thermocouple sensors. Calibrated average values for each depth were used for further analysis; for the correction of measured Watermark sensor resistances, correction of the measured gypsum block resistances, and for model calibration and validation.

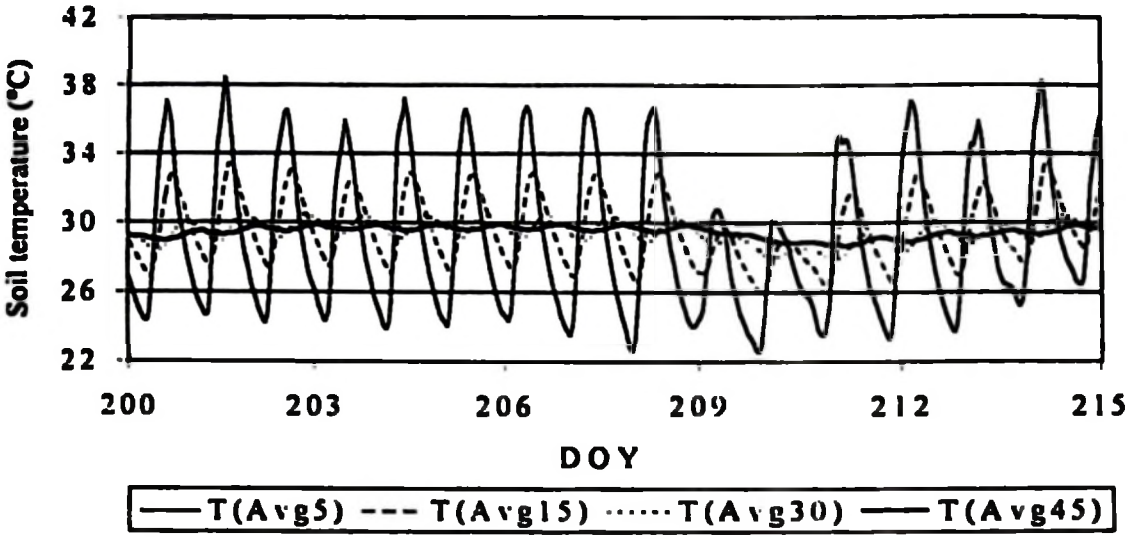

Fig. 7.14 Diurnal variations of the measured average soil temperatures at the 5, 15, 30, and 45 cm depths for DOY 200 to DOY 215.

A nearly sinusoidal variation can be observed from the diurnal variations of the soil temperatures at different depths. Soil temperatures at the 5 cm depth exhibit marked variations in response to the rapid changes in the weather parameters A similar trend is shown by the soil temperatures at the 15 cm depth, although at lower amplitudes. Soil temperatures at the 30 and 45 cm depths show low-amplitude diurnal variations, with the soil temperatures at the 45 cm depth almost remaining constant with time. A clear phase shift can also be observed with increase in depth. Spatial variability of the measured soil temperatures was also observed for certain measurement depths.

7.1.12 Pan evaporation

The pan evaporation sensor was calibrated against manually measured water levels in the pan. The pan evaporation sensor performed very well and could follow very well the changes in water levels in the pan.

Evaporation losses from the soil surface were estimated using FAO method (Doorenbos, 1977). The soil evaporation (E_{soil}) was estimated using the following formula:

$$E_{soil} = K_c ET_o = K_c K_p E_{pan}$$

where E_{pan} = pan evaporation in mm/day,
K_p = pan coefficient read out from Table 18 (Doorenbos, 1977),
K_c = "soil" coefficient read out from Fig. 6 (Doorenbos, 1977),
ET_o = "Potential evapotranspiration".

Table A5.1 in Appendix 5 summarizes the calculated "potential evapotranspiration" and the estimated soil evaporation "Potential evapotranspiration" ranged from about 0.1 to 5.2 mm per day. The estimated soil evaporation ranged from about 0.1 to 3.6 mm per day. On average, the estimated soil evaporation was about 1.5 mm per day for those days falling within the rain recurrence interval of about seven days.

7.1.13 Precipitation

The experimental period was frequented by rainfall especially during the months of April and May. **Fig. 7.15** shows rainfall events during the experimental period. Maximum daily rainfall was about **65 mm** during the experimental period. A total of about ***580 mm*** of rain did fall during the whole period of the experiment, January to end of July, 1997. Accurate measurement of rainfall inputs is necessary in the knowledge of the spatial variability of soil moisture in the field.

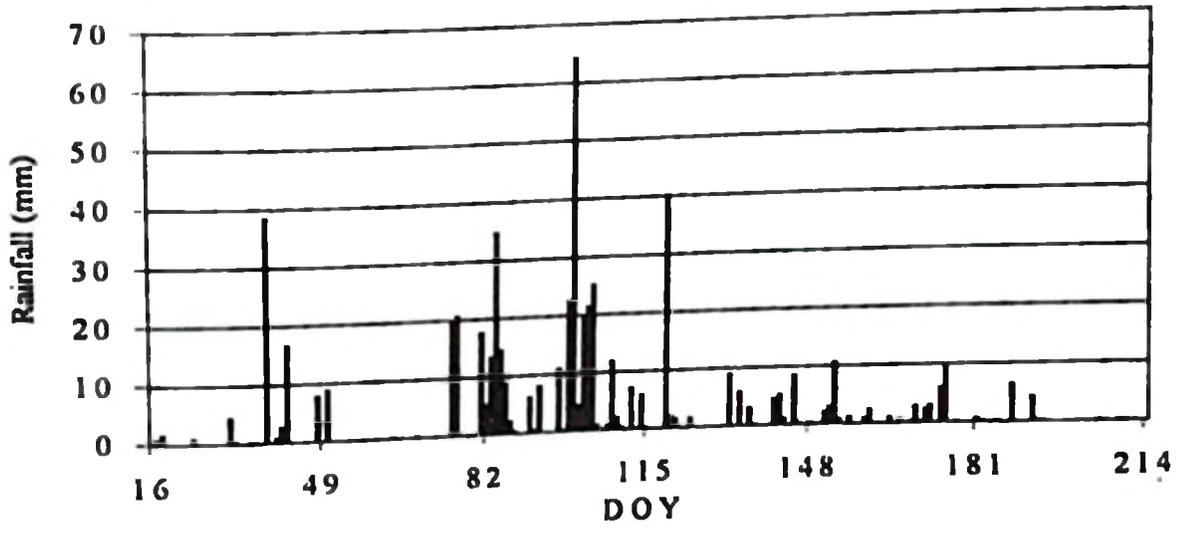

Fig. 7.15 Daily measured rainfall at the experimental site (DOY 16 to 215, 1997).

7.1.14 Soil water content

Considerable difference in drying rate was noticed from the measurements of soil water potential in the two measurement locations equipped with gypsum blocks and Watermark sensors. This was especially the case for the uppermost 5-cm layer of the soil profile. Spatial variability in the readings of the matric potential was observed from the two measurement locations. This posed some difficulty in using the mean soil water content (derived from the measurements of the matric potential) for each depth as the representative value of the soil water content. **Figs. 7.16 and 7.17** show the variations of the hourly derived average soil water content values for the Watermark sensors and the gypsum blocks, respectively, for the different depths. Gypsum block values were used beyond the 200-kPa matric potential value and the Watermark sensors were used in the 10 to 200 kPa range As can be seen from **Figs 7.16 and 7.17**, the Watermark sensors are more sensitive in the low soil water content range as compared to the gypsum blocks.

7.1.15 Matric potential

As can be seen from **Figs 7.18 and 7.19**, there is a clear diurnal variation of the measured matric potential (matric suction) in response to the diurnal variations of the soil temperature. The Watermark sensors are more sensitive at low matric (potential) suction values as compared to the gypsum blocks. There is some difference in the readings obtained from each of the sensors of the same type (gypsum blocks or Watermark sensors) for the two measurement locations, identified by, for example, MP(WM#2) and MP(WM#7). This could be attributed to the inherent soil variability under natural soil conditions resulting in different values of matric suction. The variability between sensors could also be the reason for the discrepancy in the values obtained. However, measurements made by the same type of sensors show a high degree of correlation for the two measurement locations.

It is to be borne in mind that any existence of substantial temperature changes (at any depth), as shown in this example for the 15 cm depth, leads to temperature gradients Moisture in the soil will move rapidly in response to these temperature gradients. Reliable measurement of either suction or soil moisture under such conditions is extremely difficult, partly because of the rapidity of changes, but also because the soil will be switching from the draining side of the moisture retention curve to the wetting side at least once a day. Under such conditions the normal assumption of a non-hysteretic moisture retention curve becomes invalid. Daily averaging of the obtained readings effectively filters out the variations observed in the tension during the day. Of practical importance is the cautious use of gypsum blocks or Watermark sensors close to the soil surface. Not only is the block or sensor affected by temperature, but temperature gradients in the soil will also drive soil moisture movement due to evaporations and re-condensation. These effects will be seen by the blocks.

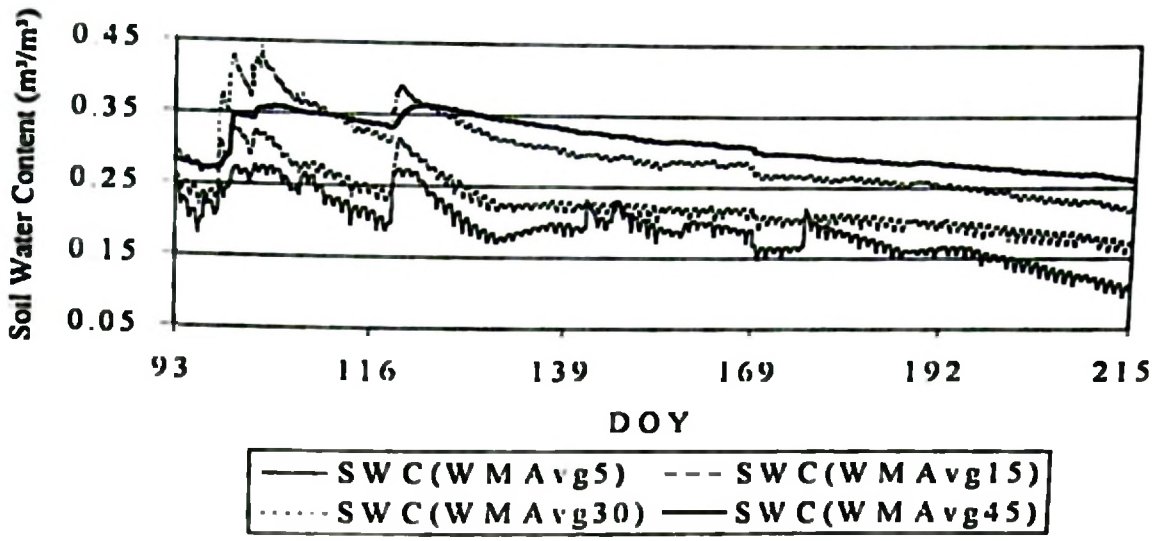

Fig 7.16 Soil water content (SWC) derived from the Watermark sensor measurements at the 5, 15, 30, and 45 cm depths

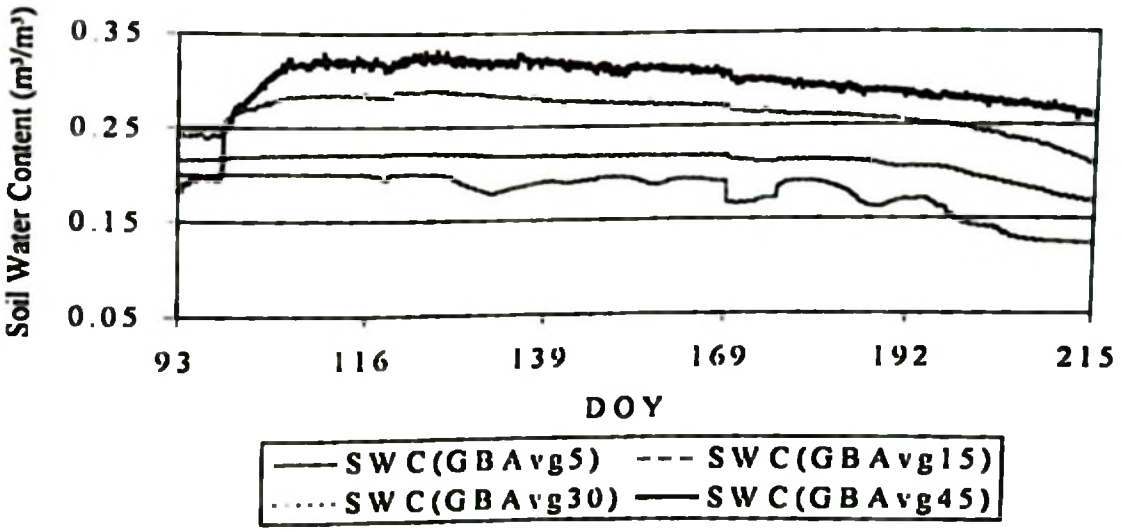

Fig 7.17 Soil water content (SWC) derived from the Gypsum block measurements at the 5, 15, 30, and 45 cm depths

Comparison of derivation methods for soil water content: Derivation of soil water content from measured matric potential requires use of a soil water characteristics curve, i.e., a curve relating soil water content to matric potential. The van Genuchten (1980) curve is very

commonly used, but this requires provision of several fitting parameters. Extensive usage of pedotransfer functions has of late become common in determining the van Genuchten fitting parameters using easily measured soil physical properties. Pedotransfer functions relate the soil hydraulic properties to soil data available from soil surveys. These have been developed to estimate empirically soil water retention and conductivity characteristics (Cosby et al., 1984).

In this study, van Genuchten fitting parameters were determined using soil texture data (see Tables A7.1 and A7.3 in Appendix 7). The measured matric potential data were then fit in the van Genuchten curve to determine soil water content. Soil water content data so obtained were calibrated using gravimetric soil water content data. At the same time, measured sensor resistances were also used to derive soil water content. Based on the apparent linear relationship between sensor conductance (reciprocal of resistance) and volumetric water content, calibration equations were derived expressing soil water content in terms of sensor conductance. Figs 7.20 to 7.23 show the comparisons between pedotransfer functions derived soil water contents and sensor conductance derived soil water contents. It is worthwhile to note that the use of pedotransfer functions alone without calibration with gravimetrically measured soil water content data tends to overpredict the soil water content values. This is especially important if the soil water content data are to be used for model calibration or validation. The extent of the error involved should therefore be taken into account.

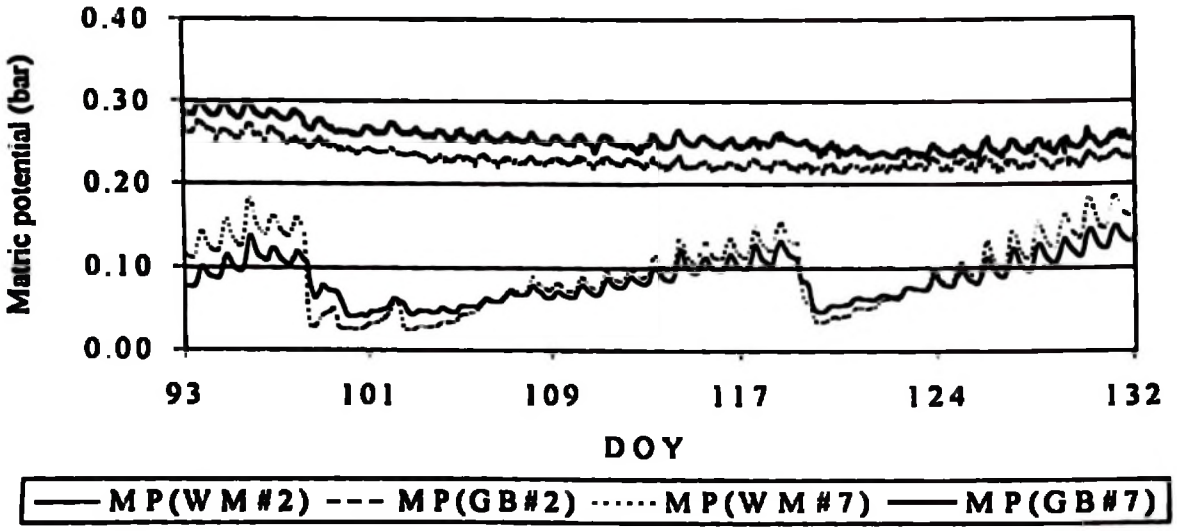

Fig. 7.18 Spatio-temporal variation of the measured matric potential (MP) (suction) at the 15 cm depth - beginning of the field experiment. Comparison between Gypsum blocks (GB#..) and Watermark sensors (WM#..).

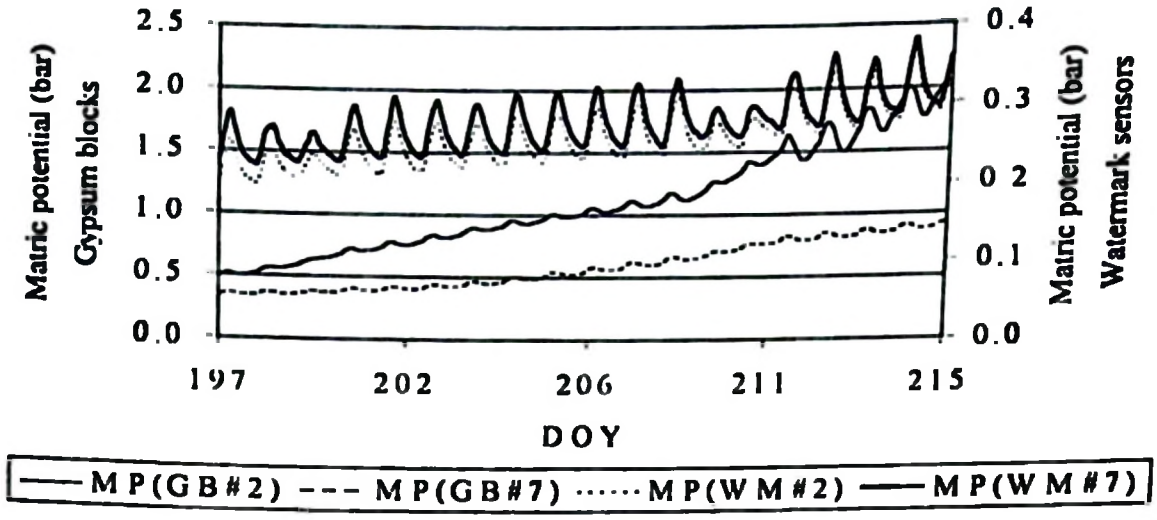

Fig. 7.19 Spatio-temporal variation of the measured matric potential (MP) (suction) at the 15 cm depth - end of the field experiment. Comparison between Gypsum blocks (GB#...) and Watermark sensors (WM#...).

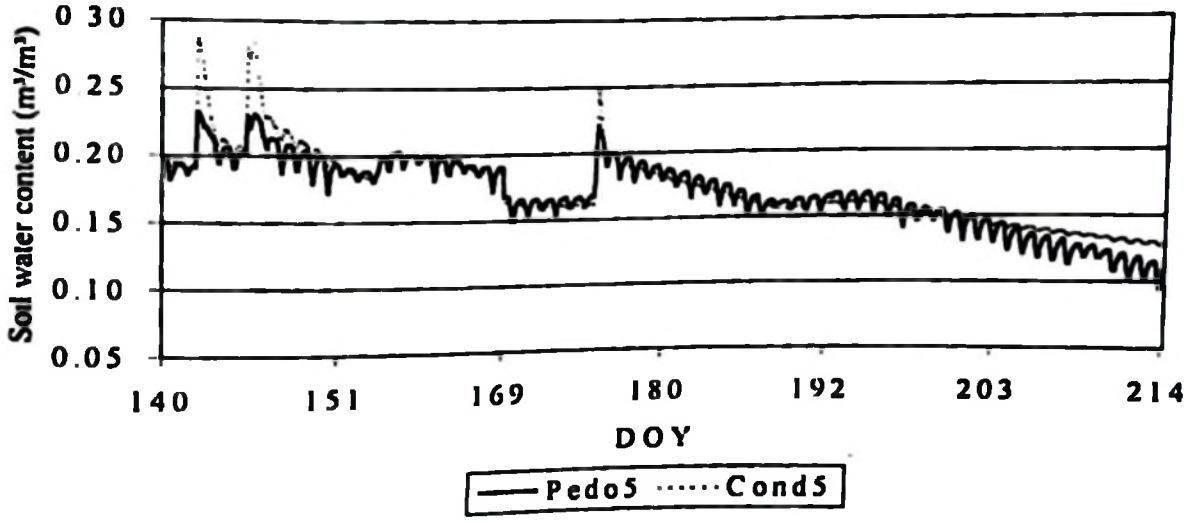

Fig. 7.20 Comparison between pedotransfer functions derived soil water content (Pedo5) and sensor conductance derived soil water content (Cond5) at 5 cm depth.

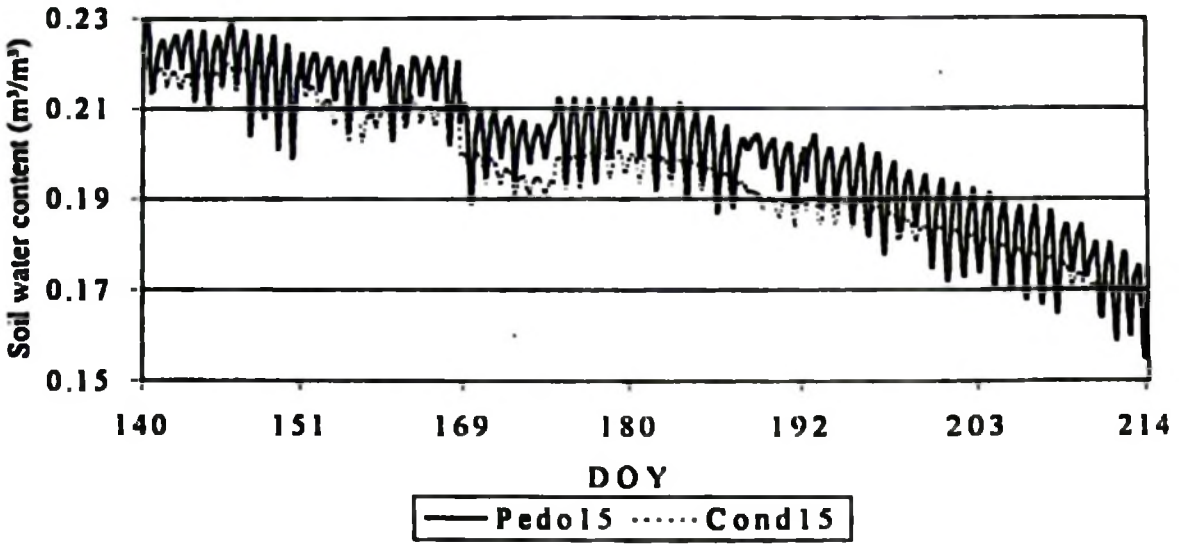

Fig.7 21 Comparison between pedotransfer functions derived soil water content (Pedo15) and sensor conductance derived soil water content (Cond15) at 15 cm depth

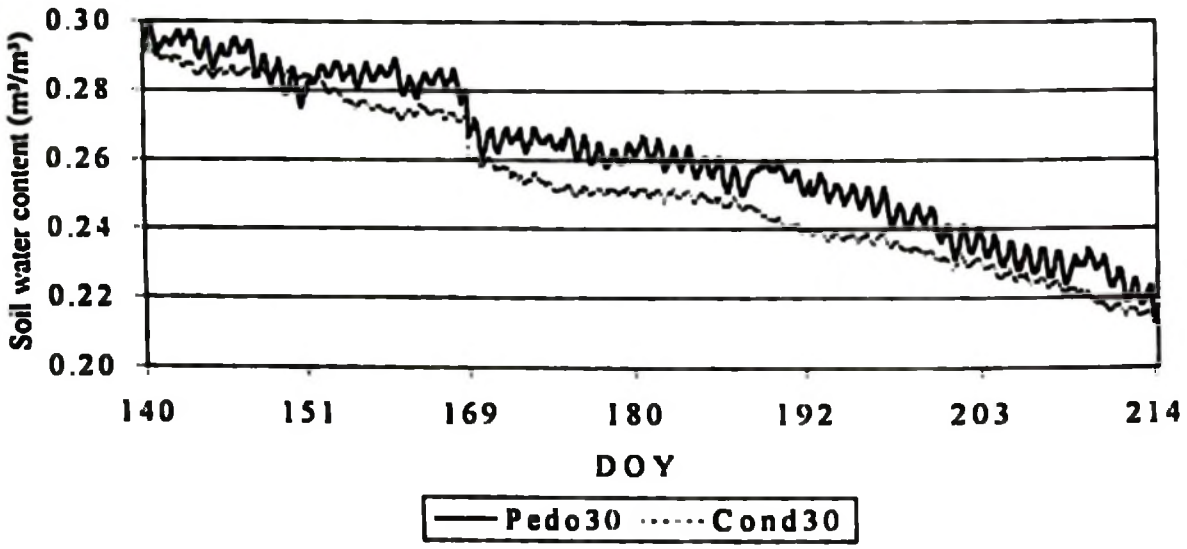

Fig 7.22 Comparison between pedotransfer functions derived soil water content (Pedo30) and sensor conductance derived soil water content (Cond30) at 30 cm depth

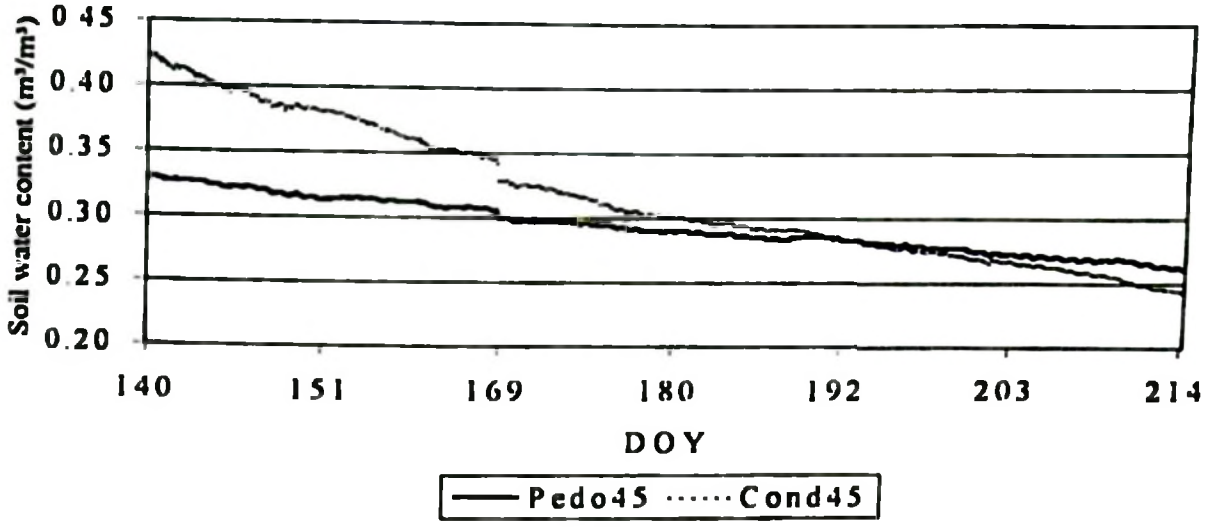

Fig 7 23 Comparison between pedotransfer functions derived soil water content (Pedo45) and sensor conductance derived soil water content (Cond45) at 45 cm depth.

7.2 Estimation of near-surface soil moisture using infrared thermometry

7.2.1 Establishing suitable time for the measurement of surface soil minus air temperature under tropical semi-arid conditions

Similar to other research findings (e.g., Myhre and Shih, 1990) obtained under different environmental conditions, it was found in this study that the surface bare soil temperatures were always greater than the air temperatures from around 0800 to around 1830 h local time (LT). This was the time period during which the temperature measurements were carried out. **Fig. 7.12** shows a typical daytime variations of infrared surface soil temperatures, air temperatures and the infrared minus air temperature difference (TD). It was also found that the optimum time for the measurement of soil surface minus air temperature was between 1200 to 1400 h LT during which the maximum surface soil minus air temperature (TDMax) occurred.

7.2.2 Use of maximum surface soil minus air temperature differential (TDMax) as estimator of soil moisture content

Remotely-sensed estimates of soil moisture are averages in space and depth. If these estimates are to be compared to ground-truth data or modelled data, the latter have to be averaged over

the same depth. Depth weighted-averages of the gravimetrically determined soil water contents were therefore calculated using the method outlined under subsection 5.6.2 of chapter 5. This was done because of the relative better accuracy of the gravimetrically determined soil water content data. Soil water content data derived from matric potential measurements using the gypsum blocks and Watermark sensors were used in other sections, for calibration and validation of the model.

Fig. 7.24 shows the graph of the weighted-average soil water content to the 5 cm depth versus TDMax. Despite data insufficiency especially in the middle region of the graph, a general linear trend is depicted by the graph.

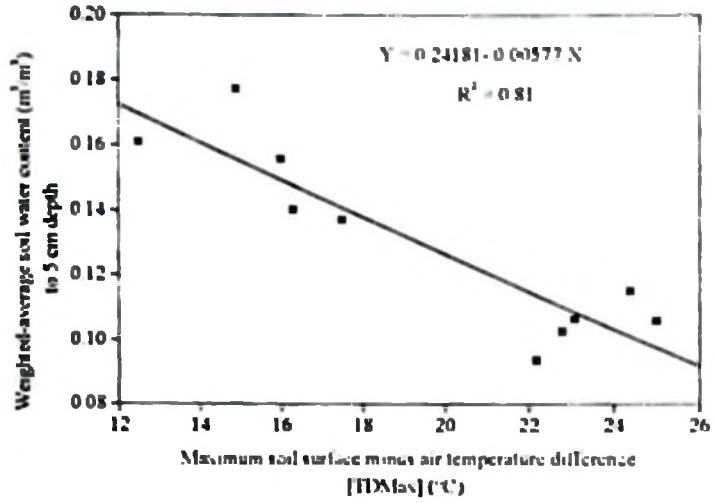

Fig. 7.24 Weighted-average soil water content to the 5 cm depth vs TDMax.

Similarly, **Fig. 7.25** shows the graph of the weighted-average soil water content to the 15 cm depth versus TDMax. Similar trends were observed to the other depths. Generally good correlations between the measured weighted-average soil water contents and TDMax were observed to the different depths. The correlation coefficients decrease with depth, which is to be expected. The simple linear correlation coefficients are significant at the 1% level of significance. About 81%, 78%, 64%, 63%, and 70%, respectively, of the variations in the weighted-average soil water contents for the 0-5, 0-15, 0-30, 0-45, and 0-60 cm depths are accounted for by the respective linear functions of TDMax. The relatively high R^2 values obtained is also indicative of the closeness between the estimated regression lines and the observed points. **Table A11.1 in Appendix 11** gives a detailed statistical analysis of the relationships, using either TDMax or the average of five daily maximum readings (A5MR), for the different depths in the soil.

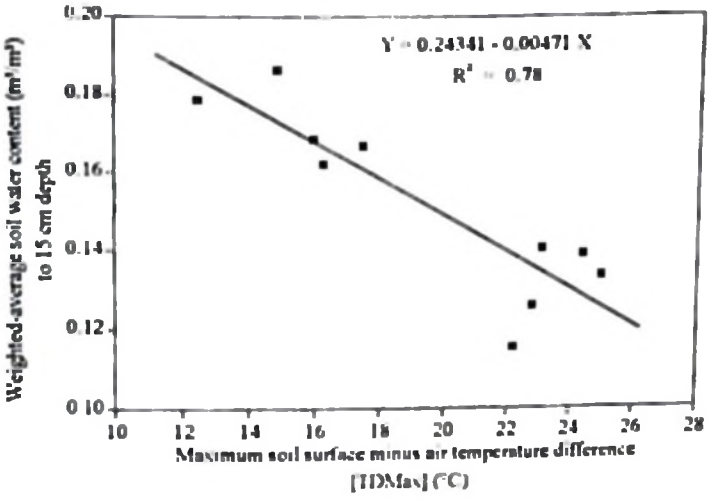

Fig. 7.25 Weighted-average soil water content to the 15 cm depth vs TDMax.

In order to establish the depth to which thermal infrared remote sensing can effectively be used for estimation of near-surface soil water content under tropical semi-arid conditions, it was necessary to carry out a depth sensitivity test. Based on the results presented so far, it would seem reasonable to assume that the thermal infrared method can be used to estimate soil water contents to the depth of about 15 cm. Better correlations between (weighted-average) soil water content and TDMax can be obtained to the 15 cm depth and these decrease with depth.

7.2.3 Use of net radiation - TDMax/RnDT

In an attempt to take into account the effects of clouds, net radiation was used as a surrogate for solar radiation to correct for the effects of changing solar radiation at the finest temporal resolution possible. This was done because net radiation was observed at a smaller temporal resolution (15 minutes) as compared to solar radiation data which were available only at a daily temporal resolution. Other works (e.g., Myhre and Shih, 1990) used solar radiation data. The TDMax was divided by the average daytime net radiaton (RnDT) to obtain the "Normalized TDMax". **Fig. 7.26a** shows the graph of volumetric water content versus TDMax for the 5 cm depth. Use of the "Normalized TDMax" is illustrated in **Fig. 7.26b**. When compared to the use of TDMax alone (see **Fig. 7.26a**), it can be seen that the use of "Normalized TDMax" (see **Fig. 7.26b**) does improve the correlation coefficient to some extent. It is to be noted however that the soil water content data used in this example were derived from the measured matric potential data (selected during the drying period, DOY 192 to DOY 214). Clearly, more representative results would have been obtained if more accurate soil water content data were used.

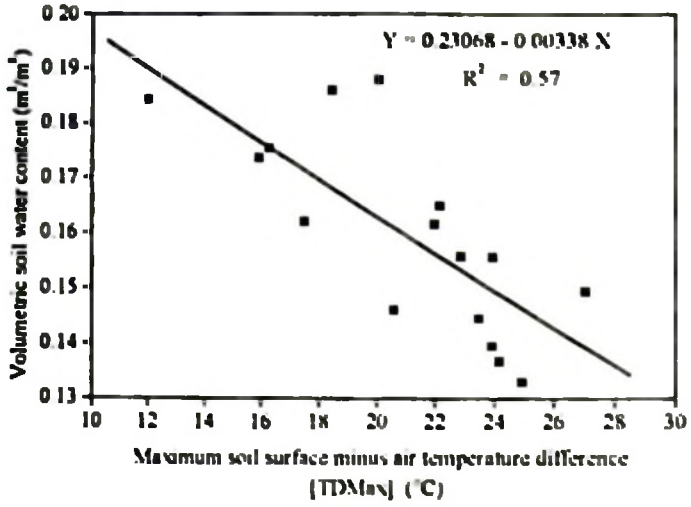

Fig. 7.26a Volumetric water content vs TDMax for the 5 cm depth.

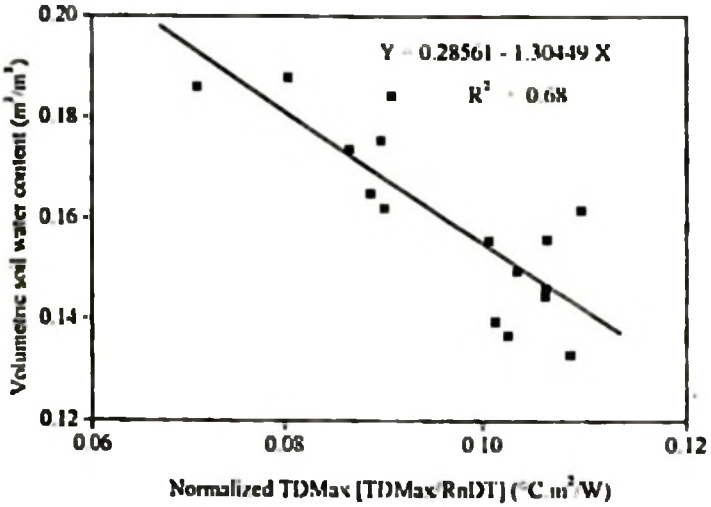

Fig. 7.26b Volumetric water content vs. TDMax/RnDT for the 5 cm depth

7.2.4 Influence of cloud cover - improvement of the relationships

Further to the use of "Normalized TDMax" as covered under section 7.2.3, an attempt was made to study the relationship between net radiation and the surface soil minus air temperature differential (TD) on a daily basis. Fig 7.27 shows a graph of TD versus net radiation for DOY 208. An equilibrium temperature difference (TDa) was calculated for each day as outlined under section 6.6 of chapter 6. Table A6.1 in Appendix 6 shows a summary of the calculated daily

maximum TDa for the whole measurement period. A graph of TDa versus net radiation for the same DOY 208 is shown in Fig. 7.28. Compared to Fig. 7.27, it can be seen that the use of TDa does considerably improve the regression coefficients. Figs 7.29 and 7.30 show the graphs of soil water content versus "Normalized maximum equilibrium temperature difference (Normalized METD)" (TDaMax/RnDT), where RnDT is the average daytime net radiation. Substantial improvement in the regression coefficients can be observed from the graphs. Fig. 7.31 shows an example of a quarter-hourly variation of the measured average, maximum, and minimum net radiation for DOY 138. Fig. 7.32 shows daytime surface soil radiant temperature, air temperature, and surface soil -minus- air temperature difference variations on a typical cloudy day (DOY 138). A small section of Fig. 7.32 is further analysed as shown in Fig. 7.33. From Fig. 7.33, it is reasonable to assume that there is a potential change in the temperature difference (TD) of about 30% within roughly 10 to 15 minutes of the occurrence of an intervening cloud cover. This underlines the need for exercising of care in effecting the measurement of the temperature difference during intermittent occurrences of cloud covers. Please note that the time scale in Fig. 7.33 is given in hours expressed in decimal point format.

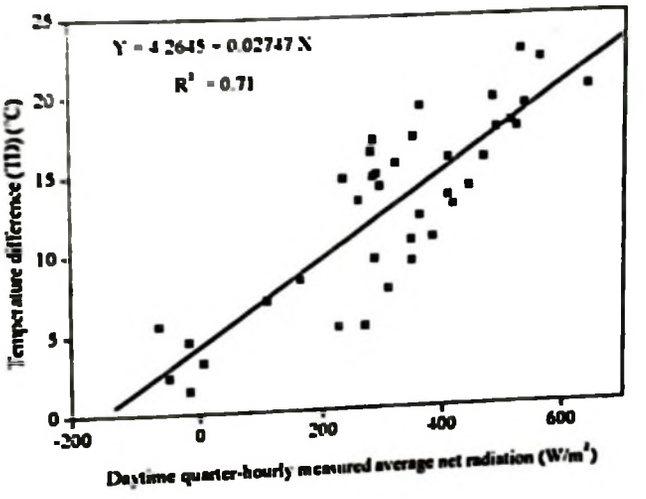

Fig. 7.27 Soil surface minus air temperature difference (TD) vs. net radiation (DOY 208, 1997).

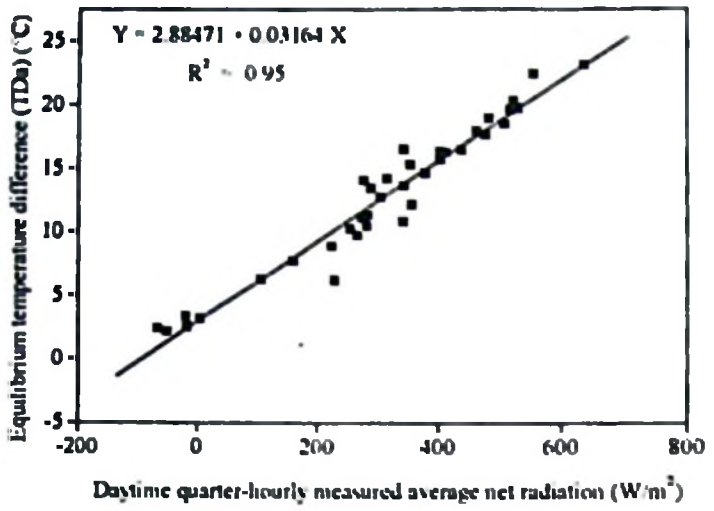

Fig. 7.28 Equilibrium temperature difference (TDa) vs. net radiation (DOY 208, 1997).

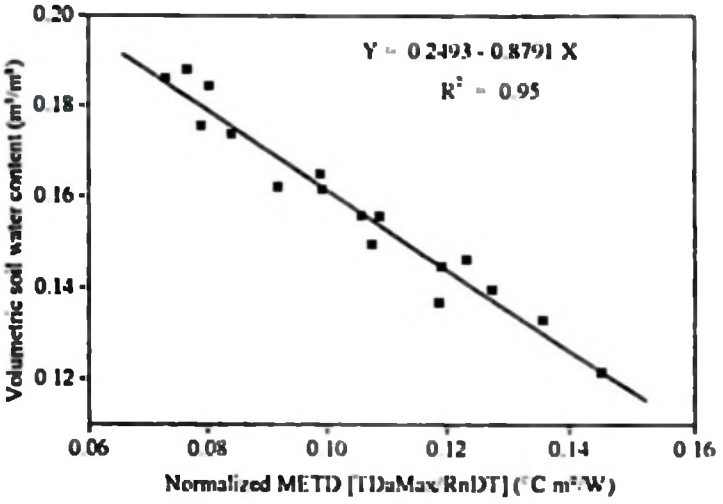

Fig. 7.29 Volumetric water content vs. Normalized METD for the 5 cm depth.

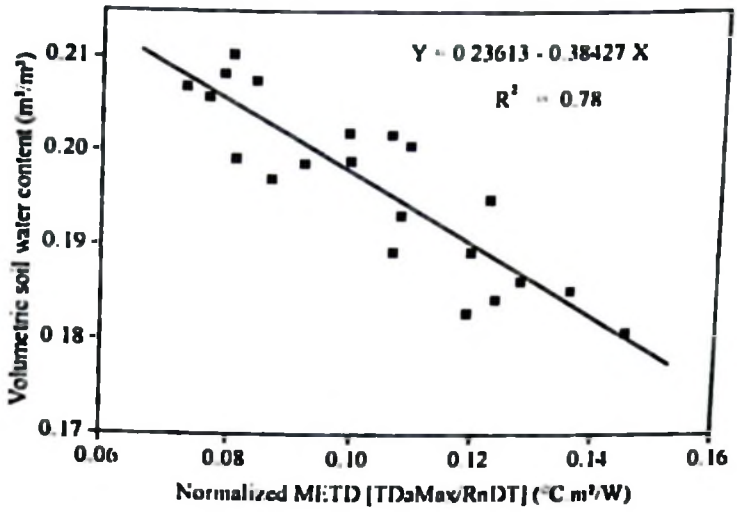

Fig. 7.30 Volumetric water content vs. Normalized METD for the 15 cm depth.

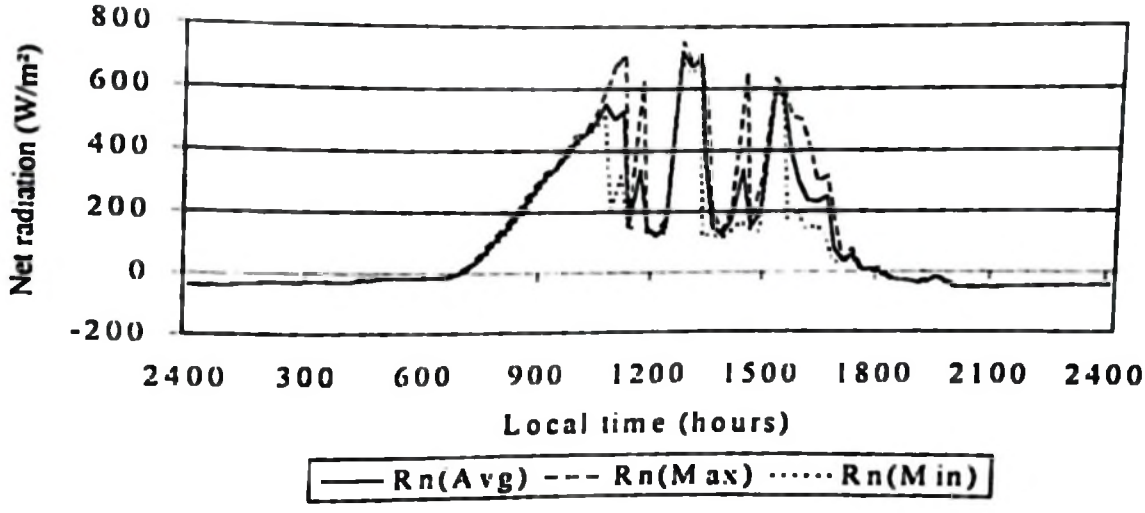

Fig. 7.31 Quarter-hourly variation of measured average, Rn(Avg), maximum, Rn(Max), and minimum, Rn(Min), net radiation (DOY 138, 1997).

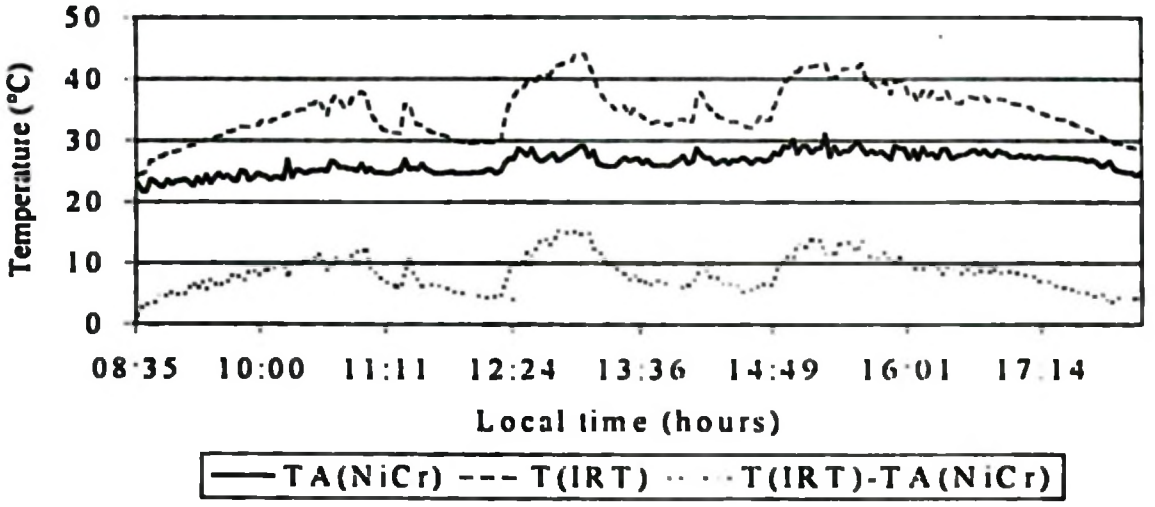

Fig. 7.32 Daytime variation of measured soil surface radiant temperature, T(IRT), air temperature, TA(NiCr), and their difference, T(IRT)-TA(NiCr), (DOY 138, 1997).

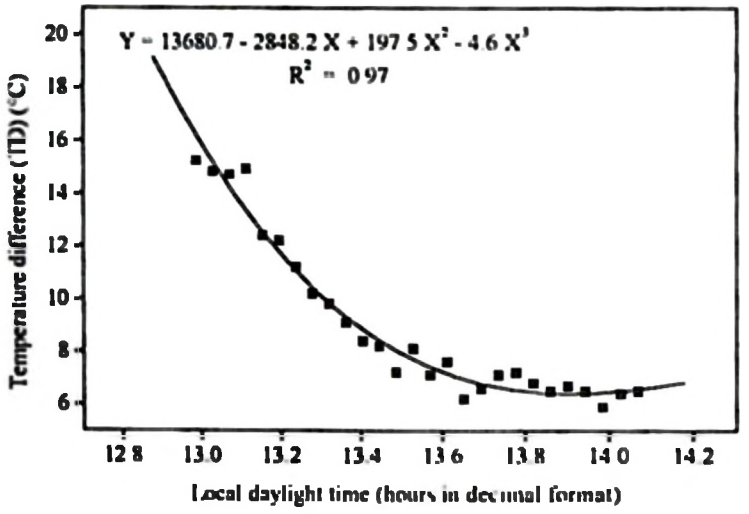

Fig.7.33 Typical effect of rapid change of solar radiation on the measurement of temperature difference (TD) - DOY 138

7.2.5 Inferring of profile soil moisture content from near-surface measurements

7.2.5.1 Empirical methods based on statistical analysis

Fig. 7.34 shows the graph of weighted-average soil water content to the 5 cm depth versus the weighted-average soil water contents to the 15 cm depth. As can be seen, there is a reasonably high correlation between the average soil water content to the 5 cm depth and that to the 15 cm depth in the soil profile. **Table 7.1** gives a summary of the coefficients of determination. Generally the coefficients of determination for the relationships between the near-surface (0-5 cm depth) layer and layers at greater depths in the soil profile decrease with depth. Higher correlations are depicted by layers adjacent to each other. The coefficients of determination are significant at either the 1% or 5% level of significance. It can therefore be deduced from these results that it is feasible to infer the average soil water contents to greater depths in the soil profile from the weighted-average soil water content to the 5 cm depth. However, accurate determination of the weighted-average soil water content to the 5 cm depth, whether directly or indirectly, is necessary for obtaining of better results. The correlation coefficients are however generally low as exemplified by the results of this subsection.

Table 7.1 **Simple coefficients of determination, r^2, for the relationships between weighted-average soil water contents (W_{AVG}) to different depths.**

Depth (cm)	5	15	30	45
5	1.00	0.94	0 54	0.32
15		1 00	0.72	
30			1.00	0.87
45				1 00

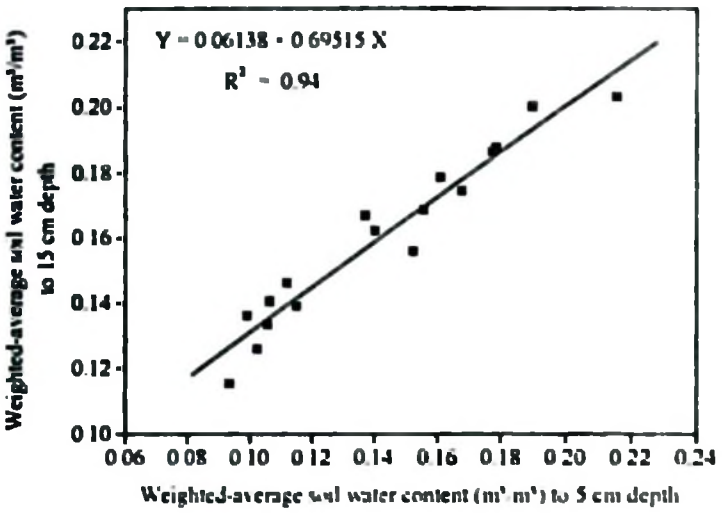

Fig. 7.34 Weighted-average soil water content to 15 cm depth vs that to 5 cm depth

7.3 Model simulation

7.3.1 Model calibration

The term "calibration" as used in modelling works means a process where some of the model parameter values are adjusted to better approximate the measured values (Chung and Austin, 1987). Generally, model parameters which cannot be determined or are hard to estimate can be approximated through the calibration process. Estimation of model parameters can be done either by trial and error or by optimization (Chung and Austin, 1987). A trial and error method was applied in this study. Each parameter was assigned an initial value based on field measurements or data from literature, and then varied over a reasonable range. The differences between the observed and simulated (e.g., soil water content and soil temperature) values for each set of parameter values were compared. This procedure was continued until the differences were within a satisfactory range. The parameter values for the minimum difference were then selected.

The parameters calibrated following the above procedure were the surface roughness length, residual soil water content, saturated soil water content, day length, solar noon, albedo, critical soil water content in the albedo-soil water content relationship, van Genuchten parameters (n), reference temperature for the temperature correction of the pressure head and unsaturated hydraulic conductivity functions, maximum value of water detention depth, and saturated hydraulic conductivity. Additionally, time step size and space step size were also varied. A total of about 70 simulations were run along with model improvement. Model calibration was done for

the period of the experiment during which gravimetric soil water content measurements were also conducted. Gravimetrically determined soil water content data were used during model calibration to initialize the model and as bottom boundary condition. This was done because they are more accurate than those obtained from either the gypsum blocks or the Watermark sensors. The model was also calibrated against field soil temperature measurements. In each simulation, the SUAHEAT model was run beginning at 0000 h local time (LT), DOY 140 (2400 h LT DOY 139) to 2400 h LT, DOY 214, of 1997

7.3.1.1 Comparison with measured soil water contents

7.3.1.1.1 Qualitative comparison

Fig. 7.35 shows the time series of both the model simulated and observed soil water content at the 5 cm depth (more accurately at the 5-10 cm depth). A section of the graph for DOY 176 to DOY 191 is shown in **Fig. 7.36**. As can be seen, the model could predict fairly well the temporal changes in soil water content at the 5 cm depth. Generally, some overpredictions by the model can be noted, especially when the model predicts soil saturation. Sharp rising peaks can be seen from the graph indicating state of soil saturation. The discrepancy between model simulated and observed soil water content values can be attributed to the errors in the estimation of the model input parameters, e.g., soil physical and thermal properties. The observed soil water content data are also based on measurement of matric potential and therefore these possess some errors resulting from the calibration process. In addition, the model was initialized using gravimetrically determined profile soil water content data. This partly explains the discrepancy between model simulated and observed soil water content values at the beginning of the simulation. However, it can be assumed that the model simulations become independent of the initial conditions after the first occurrence of substantial rainfall (**see Fig. 7.35**). Overestimation by the model, for example on DOY 192 (**see Fig. 7.35**), could probably be attributed to an underestimation of soil evaporation.

Similar trends are depicted by time series of model simulated and observed soil water contents at other depths of the soil. **Fig. 7.37** shows a sample model simulation of soil water content for the upper 10 cm layer of the soil. As can be seen from the graph, the model could also simulate the occurrences of high rainfall events (the high rainfall events exactly correspond to the peaks in soil water contents). This indicates that the model can simulate the effects of soil-water-atmosphere interactions reasonably well. Admittedly, the accuracy attained in the simulation of surface as well as subsurface soil moisture dynamics is limited, even in cases where extensive data on physical soil properties are available. This is especially so where wetting and drying alternate. The results presented in this subsection serve to illustrate this fact

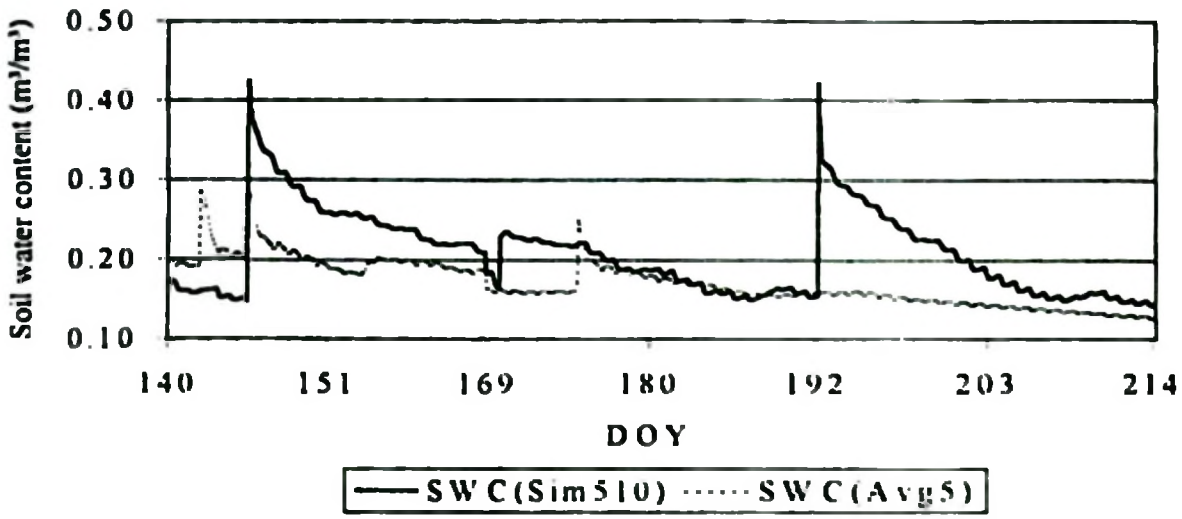

Fig. 7.35 Time series of model simulated, SWC(Sim510), and observed, SWC(Avg5), soil water content at the 5 cm depth - calibration phase.

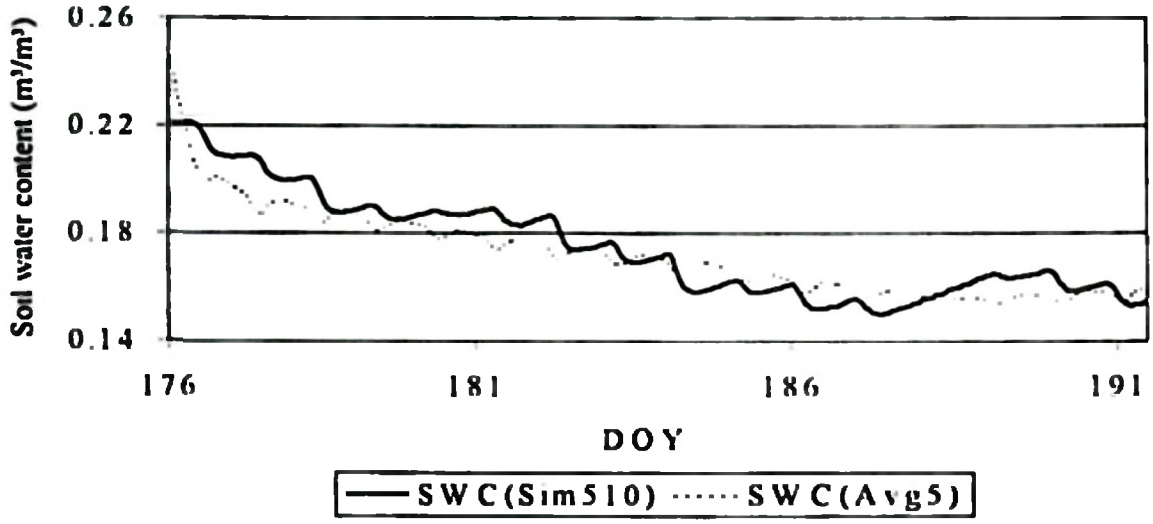

Fig. 7.36 A section of Fig. 7.35 showing in detail DOY 176 to DOY 191.

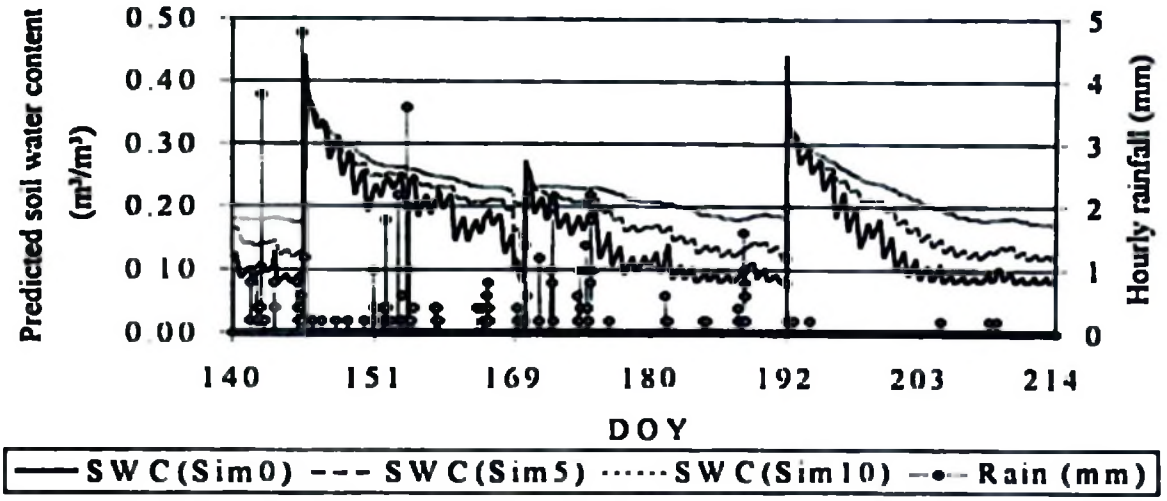

Fig 7.37 An example of the model simulation illustrating the model performance in simulating soil water content at 0, 5, and 10 cm depths - calibration phase.

7.3.1.1.2 Quantitative comparison

As already mentioned, the accuracy attained in the simulation of soil moisture dynamics is limited, especially so where wetting and drying alternate. The wetting and drying cycles were therefore considered separately in performing the quantitative model evaluation in this study. A drying cycle ranging from DOY 176 to DOY 191 (see Fig. 7.36) has therefore been used to illustrate the comparison between model simulated and observed soil water contents. Detailed quantitative model performance data are given in Table A11.3 in Appendix 11. As can be seen from Table 7.2, the model simulated soil water content values are very well correlated with the observed soil water content values for DOY 176 to DOY 191. A coefficient of determination of approximately 0.86 is obtained (see Table A11.3). For the chosen drying cycle, the MAD value of 0.006 m^3/m^3 is relatively low, indicating closeness of the model simulated to the observed soil water content data. This is also reflected by the low value of the RMSD. It can therefore reasonably be deduced from these results that the model can simulate soil water content values fairly well during a drying cycle provided that the model does not attain a state of soil saturation. This example serves to illustrate this.

Values of the MAD as well as the RMSD range from about 0.04 m^3/m^3 to about 0.07 m^3/m^3 for the other drying cycles and depths (see Table 7.2). Notwithstanding this, the error statistics indicate that the model performed well as far as the simulation of soil water content data is concerned. In addition, the model easily satisfies the criterion for model acceptance set by the

Predictive Exposure Assessment Workshop (Hedden, 1986 as cited by Clemente et al., 1994), which recommends that a model should be able to replicate field data within an order of magnitude for general applications and within a factor of 2 for site specific applications. It can therefore be concluded that the model is of acceptable accuracy for simulating soil water content in the soil profile.

Table 7.2 Quantitative measures of model performance for simulation of profile soil water content - calibration phase.

DOY	TIME			N	MAD	RMSD
192	100	SWC(Sim510)	SWC(Avg5)	543	0.057	0.073
to	to					
214	2400					
176	100	SWC(Sim510)	SWC(Avg5)	384	0.006	0.008
to	to					
191	2400					
147	100	SWC(Sim510)	SWC(Avg5)	360	0.056	0.061
to	to					
161	2400					
192	100	SWC(Sim1520)	SWC(Avg15)	543	0.072	0.076
to	to					
214	2400					
176	100	SWC(Sim1520)	SWC(Avg15)	384	0.040	0.041
to	to					
191	2400					
146	100	SWC(Sim1520)	SWC(Avg15)	932	0.054	0.058
to	to					
191	2400					
192	100	SWC(Sim3035)	SWC(Avg30)	543	0.048	0.049
to	to					
214	2400					
192	100	SWC(Sim4550)	SWC(Avg45)	543	0.025	0.026
to	to					
214	2400					

7.3.1.2 Comparison with measured surface soil temperatures

7.3.1.2.1 Qualitative comparison

Fig. 7.38 shows model simulated surface soil temperature and observed surface soil radiant temperature. As can be seen from the graph, the model simulated surface soil temperature can follow the variation of the observed surface soil radiant temperature fairly well. Generally the model tends to overpredict both the maximum and minimum surface soil temperatures. This is however to be expected taking into account the nature of the input weather data used. Higher resolution input weather data, at hourly time resolution, would admittedly produce more accurate simulation of the surface soil temperature. In any case, it is also not easy to take into account the ever-changing solar radiation which has a significant influence on the temporal variation of the surface soil temperature. Soil physical properties and the state of the soil surface have also a big influence on the surface soil temperature. Therefore accurate simulation of the surface soil temperature depends to a large extent on the accurate determination of both the soil physical properties and surface soil state as well as accurate and high resolution input weather data. Such type of data are difficult to obtain. Therefore simulation models will continue to depend on "deficient" data sets.

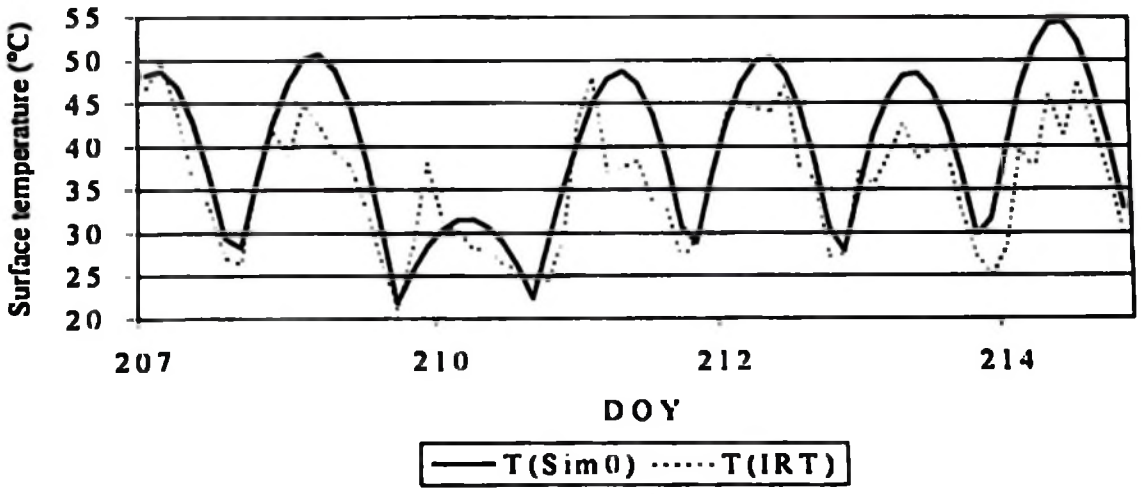

Fig.7.38 Comparison between model simulated, T(Sim0), surface soil temperature and observed surface soil radiant temperature, T(IRT).

7.3.1.2.2 Quantitative comparison

Table 7.3 shows the quantitave measures of model performance for the simulation of surface soil temperature. As can be seen from the table, the model was able to simulate fairly well the surface soil temperature. A MAD value of 4.1 °C was obtained. Similarly, a value of 5.2 °C was obtained for the RMSD. A value of 0 54 was obtained for the coefficient of determination in the first case where the "y-intercept" was included in fitting the regression equation. In setting the "y-intercept" to zero, a value of 0.48 was obtained for the coefficient of determination. Although the coefficient of determination (r^2) decreases from 0.54 to 0.48 for the "zero y-intercept" case, the simulated and observed surface soil temperatures attain a nearly "one-to-one" relationship in the latter case as reflected by the value of 1.01 for the slope (see the group of numbers at the bottom right hand side of the table) It is worthwhile to note that the coefficients of determination obtained are relatively low. Similarly, the MAD and RMSD values are also relatively high. Admittedly, the soil surface is not easy to simulate due to the continuous atmospheric forcing on the surface. The soil surface is very sensitive to the continuous changes in the weather parameters and other soil biophysical characteristics Clearly more accurate simulation of the soil surface temperature would have been obtained if higher resolution input weather data were used rather than the daily weather input data used in this study.

Table 7.3 Quantitative measures of model performance for simulation of surface soil temperature.

T(Sim0)	T(IRT)	N	MAD	RMSD	0 7537264	9.0024351
		564	4.1	5 2	0.029431	1.045806
					r^2 = 0.54	4.8777409
					655 8716	562
					15604 73	13371.304
					25.60999	
					1.0124104	0
					0 0313888	#N/A
					r^2 = 0.48	5.2022209
					508.68414	562
					28154.189	15209.463
					32.253899	

7.3.1.3 Comparison with measured profile soil temperatures

7.3.1.3.1 Qualitative comparison

Figs 7.39 and 7.40 show the temporal variations of both model simulated and observed soil temperatures at 15 cm depth. As can be seen from the graphs, the model could simulate very well the soil temperature. Both model underpredictions and overpredictions of about 1 to 2 °C can be noticed from the temporal variations of the soil temperatures. However, the model does respond very well to the diurnal as well as daily variations of the profile soil temperatures comparable to the observed soil temperatures. The model simulated soil temperatures are in phase with the observed soil temperatures. This trend is consistently maintained from the beginning to the end of the simulation as can be observed from the graphs. Similar trends were observed for the other measurement depths, i.e., at 5, 30, and 45 cm

The utility of model simulation is hereby exemplified. While, through model simulations, it might not be possible to exactly simulate the soil temperatures, it is, however, possible to at least obtain the general trend of the temporal variations of soil temperatures. This is very important for counterchecking the measurements. Low correlation between the model simulated and observed values should lead to questioning of either the model simulations or the measurements. Model simulations should, if feasible, therefore be treated as a crucial part of any measurement exercise, especially in the field where measurements are susceptible to many sources of errors.

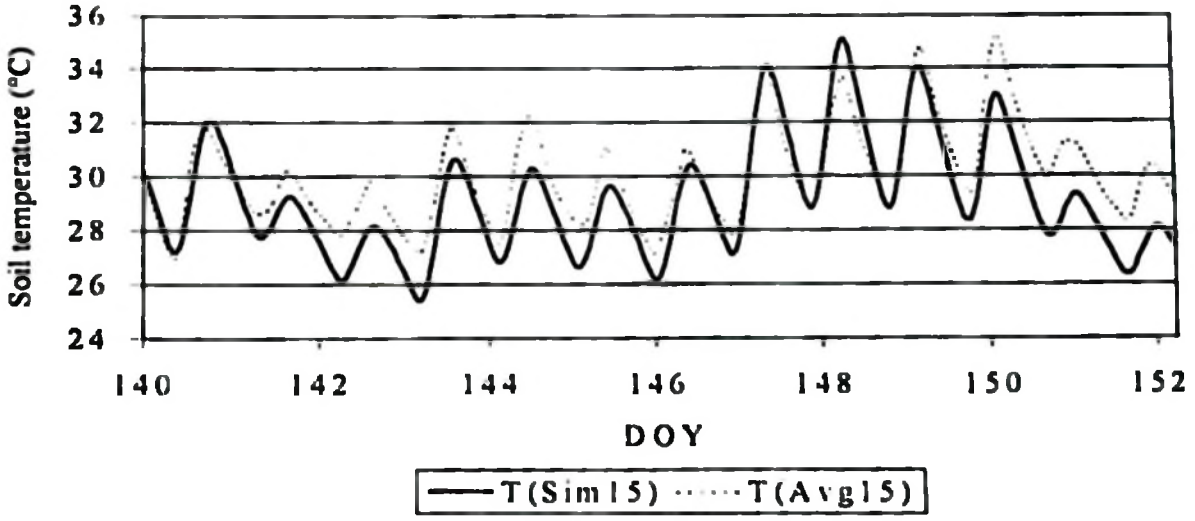

Fig.7.39 Comparison between model simulated, T(Sim15), and observed, T(Avg15), soil temperature at 15 cm depth for the first 12 days of model simulation - calibration phase.

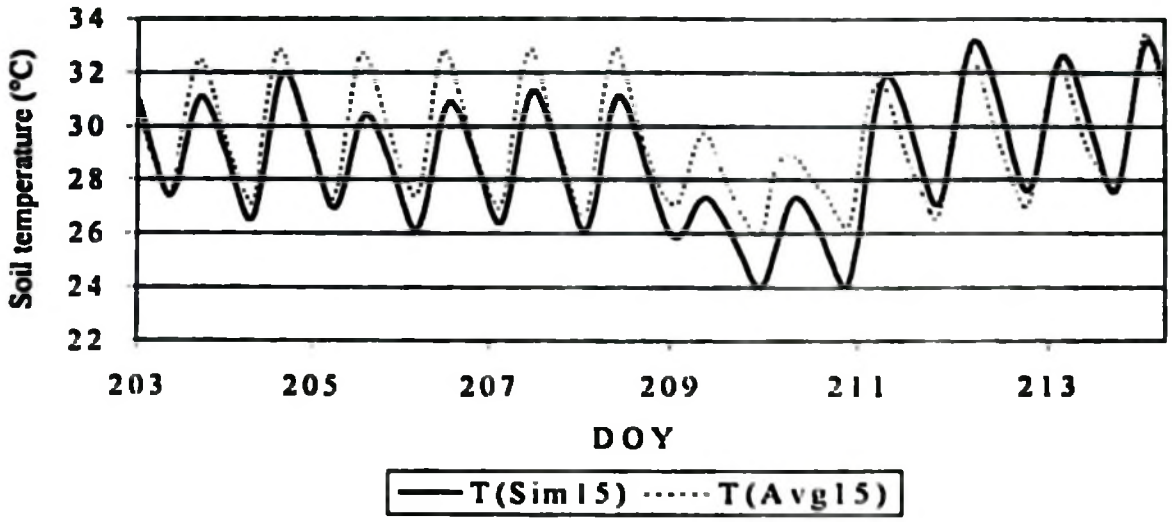

Fig.7.40 Comparison between model simulated, T(Sim15), and observed, T(Avg15), soil temperature at 15 cm depth for the last 11 days of model simulation - calibration phase

7.3.1.3.2 Quantitative comparison

Table A11.2 in Appendix 11 shows in detail the quantitave measures of model performance for the simulation of profile soil temperatures at different depths of the soil. **Table 7.4** shows an example for the 5 cm depth. As can be seen from **Table A11.2**, the model was able to simulate very well the profile soil temperatures at the depths of 5, 15, 30, and 45 cm. The MAD varies from 2.8 °C at 5 cm to 0.3 °C at 45 cm, with the degree of accuracy of the model simulation increasing with increasing depth. A similar trend is also shown by the values of the RMSDs. Also shown in the table are the coefficients of determination, both for the "nonzero y-intercept" and "zero y-intercept" cases. For the "nonzero y-intercept" case, these do follow the decreasing trend starting with a coefficient of determination of 0.83 at the 5 cm depth to one of 0.68 at the 30 cm depth. A higher coefficient of determination of 0.85 is however obtained at the 45 cm depth. This can partly be explained by the small variation in the soil temperatures at the 45 cm depth. This is also reflected by the low values of MAD and RMSD at this depth. On the other hand, for the "zero y-intercept" case, the coefficients of determination vary from a value of 0.71 at the 5 cm depth to one of 0.68 at the 30 cm depth. A higher vale of 0.84 is obtained at the 45 cm depth. Of much interest is probably the values of the slope. This is approximately equal to 0.99 for all the depths, showing a nearly one-to-one relationship between the model simulated and observed soil temperatures. Admittedly the near-surface (5 cm) layer of the soil is not easy to simulate due to

the atmospheric forcing on the layer. While the near-surface layer is very sensitive to the continuous changes in the weather parameters and other soil biophysical characteristics, the subsurface layers (15 - 45 cm) are less affected by these changes. Clearly more accurate simulation of the near-surface layer requires higher resolution input weather data than the daily weather data used in this study.

Table 7.4 Quantitative measures of model performance for simulation of profile soil temperatures - calibration phase.

T(Sim5)	T(Avg5)	N	MAD	RMSD	1.5868613	-17.10275
		1619	2.8	3.5	0.0177118	0.5116435
					$r^2 = 0.83$	2.6610186
					8026.9866"	1617
					56839.251	11450.009
					89.593451	-33.42708
					0.9894316	0
					0.023118	#N/A
					$r^2 = 0.71$	3.4732518
					4043.8267"	1617
					22097.617	19506.644
					42.799106	

7.3.2 Model validation

Validation of the SUAHEAT model was done using data obtained from DOY 91 to DOY 139. This period was frequented by rains. Both soil water content and soil temperature data were used for validation of the SUAHEAT model. **Fig. 7.41** shows sample model simulation of the soil water contents at selected depths in the soil.

7.3.2.1 Comparison with measured soil water contents

7.3.2.1.1 Qualitative comparison

Fig. 7.42 shows the time series of the measured and simulated soil water content at the 5 cm depth. Large discrepancy between the model simulated and measured values of the soil water content can be observed. This can be attributed to the overprediction arising from the calibration equation used to derive soil water content values from the measured matric potential data. The calibration equation was developed using relatively low values of soil water content obtained

gravimetrically during the period between DOY 140 and DOY 214, 1997.

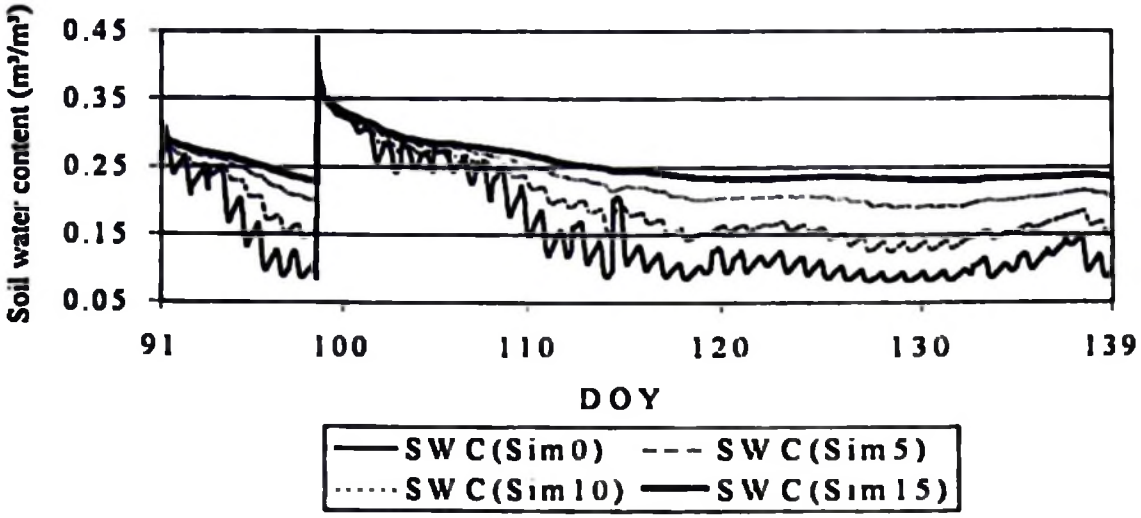

Fig. 7.41 Example of model simulation of the soil water content at 0 cm depth, SWC(Sim0), 5 cm depth, SWC(Sim5), 10 cm depth, SWC(Sim10), and 15 cm depth, SWC(Sim15)- validation phase.

7.3.2.1.2 Quantitative comparison

For the validation phase, as summarized in Table 7.5, the average MAD values of soil water content were 0.09, 0.05, 0.08, and 0.17 m^3/m^3 for the 5, 15, 30, and 45 cm depths, respectively. The corresponding average RMSD values for the same depths were 0.12, 0 08, 0 10, and 0 19 m^3/m^3, respectively. The unusually large errors (at the 45 cm depth) during the validation phase could be attributed to the overestimation of soil water content values during very wet conditions arising from the calibration equation used **Table A11.5 in Appendix 11** gives a summary of detailed statistical analysis. Notwithstanding this, the error statistics indicate that the model performed well as far as the simulation of soil water content data is concerned. In addition, the model easily satisfies the criterion for model acceptance set by the Predictive Exposure Assessment Workshop (Hedden, 1986 as cited by Clemente et al , 1994), which recommends that a model should be able to replicate field data within an order of magnitude for general applications and within a factor of 2 for site specific applications

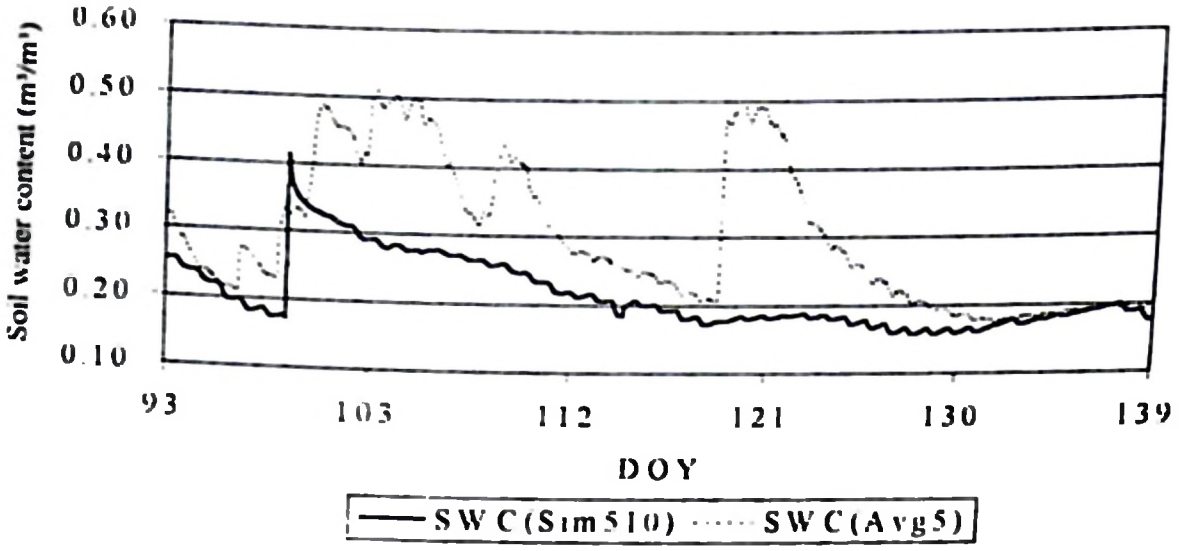

Fig. 7.42 Time series of model simulated, SWC(Sim510), and observed, SWC(Avg5), soil water content at the 5 cm depth - validation phase.

Table 7.5 Quantitative measures of model performance for simulation of profile soil water content - validation phase.

		N	MAD	RMSD
SWC(Sim510)	SWC(Avg5)	1101	0.09	0.12
SWC(Sim1520)	SWC(Avg15)	1101	0.05	0.08
SWC(Sim3035)	SWC(Avg30)	1101	0.08	0.10
SWC(Sim4550)	SWC(Avg45)	1101	0.17	0.19
SWC(Sim5560)	SWC(Avg60)	1101	0.00	0.00

7.3.2.2 Comparison with measured soil temperatures

7.3.2.2.1 Qualitative comparison

Figs 7.43 and 7.44 show the temporal variations of both model simulated and observed soil temperatures at the 5 and 15 cm depths, respectively. As can be seen from the graphs, the model could simulate very well the soil temperatures. Both model underpredictions and overpredictions of about 1 to 2 °C can be observed from the temporal variations of the soil temperatures. Similar trends were observed for the other measurement depths, i.e., at 30 and 45 cm.

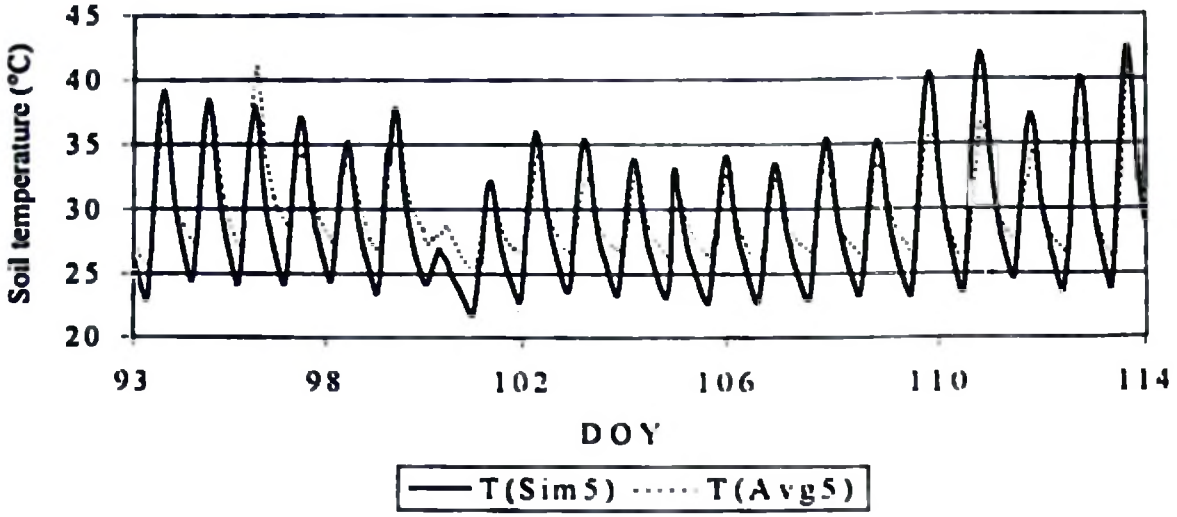

Fig. 7.43 Comparison between model simulated, T(Sim5), and observed, T(Avg5), soil temperature at 5 cm depth - validation phase.

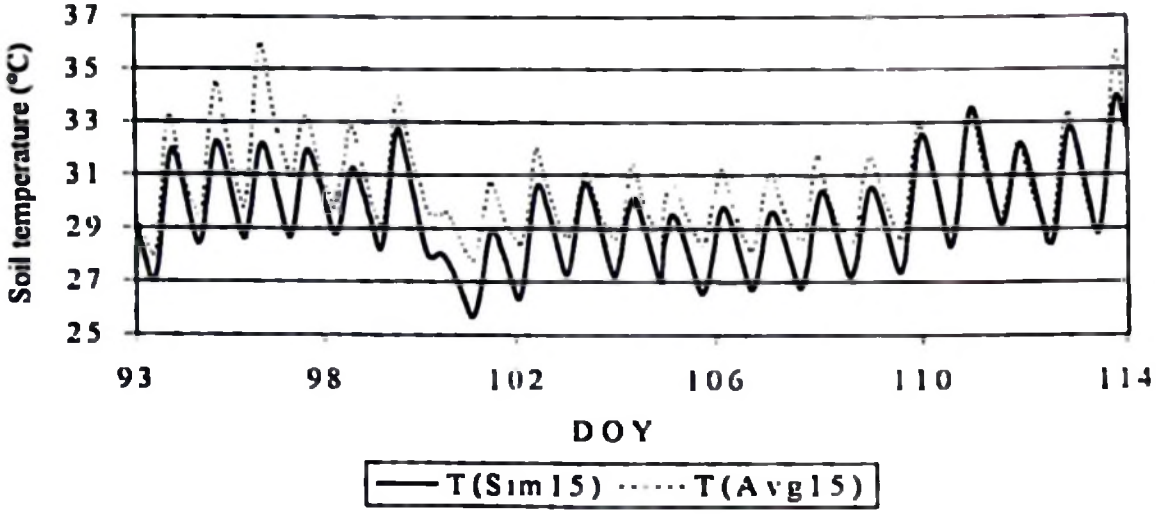

Fig. 7.44 Comparison between model simulated, T(Sim15), and observed, T(Avg15), soil temperature at 15 cm depth - validation phase.

7.3.2.2.2 Quantitative comparison

For the validation phase, the MAD values for the 5, 15, 30, and 45 cm depths were 2.3, 1.2, 0.7, and 0.4 °C, respectively. The corresponding RMSD values for the same depths were 2.7, 1.4, 0.8, and 0.5 °C, respectively. Again , the errors obtained with the use of the SUAHEAT model are generally comparable to values obtained by other researchers elsewhere using similar models. Table 7.6 gives a summary of the errors. Table A11.4 in Appendix 11 gives a detailed summary of the statistical analysis.

Table 7.6 Quantitative measures of model performance for simulation of profile soil temperatures - validation phase.

		N	MAD	RMSD
T(Sim5)	T(Avg15)	1101	2.3	2.7
T(Sim15)	T(Avg15)	1101	1.2	1.4
T(Sim30)	T(Avg30)	1101	0.7	0.8
T(Sim45)	T(Avg45)	1101	0.4	0.5

7.4 Integration of measurements with the model

7.4.1 Use of infrared thermometry derived near-surface soil moisture content and surface soil temperature as initial conditions to drive the model

As outlined under sections 4.5 and 4.6 of chapter 4, integration of remote sensing measurements with modelling provides a more flexible alternative for the estimation of profile soil water content. One of the major obstacles in using the conventional hydrological models with remotely-sensed data is the fact that these models were not meant to utilize remotely-sensed data. A continuous operational system for the monitoring of the temporal (and spatial) evolution of profile soil water content based on remotely-sensed data necessitates the incorporation of routines in the hydrological models which can serve as an interface between the conventional hydrological models and the remotely-sensed information. Remotely-sensed data can then be used to initialize or update the so-modified hydrological models.

This work attempts to illustrate a conceptual framework of a "remotely-sensed-soil water content driven soil heat and water flow model". Despite the fact that the general framework of the model is illustrated using thermal infrared remote sensing derived soil water content and

temperature data, it does allow the use of any other method of estimation of surface soil water content. A combined use of microwave measurements and thermal infrared remote sensing for the estimation of near-surface (0-5 cm depth) soil water content and soil surface radiant temperature, respectively, could be more appropriate in order to measure both the profile soil water contents and temperatures which are required for the initialization of the model.

Thermal infrared derived near-surface soil moisture contents and surface soil temperatures were used to initialize the model. The near-surface soil moisture content was calculated using the relationship between the near-surface soil moisture content and the TDMax derived from the experimental data. Soil water contents at greater depths were then calculated using the regression equations obtained between the near-surface soil moisture content and the the soil water contents at different depths. Similarly, soil temperatures at greater depths of the soil profile were calculated using the regression equations between the surface soil temperature and the soil temperatures at different depths of the soil profile.

The model was run using the infrared thermometry derived initial conditions for soil moisture content and soil temperature. Figs 7.45, 7.46, and 7.47 show the results of the model simulation for weighted-average soil water contents, soil temperatures, and soil water contents, respectively, for different depths.

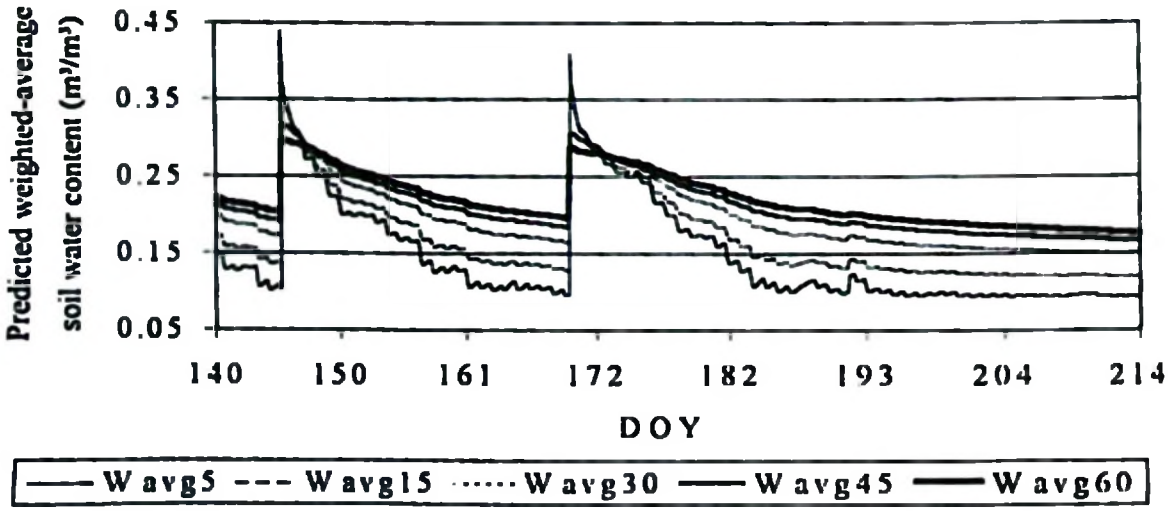

Fig. 7.45 Example of model simulation of the weighted-average soil water contents to the 5, 15, 30, 45, and 60 cm depths.

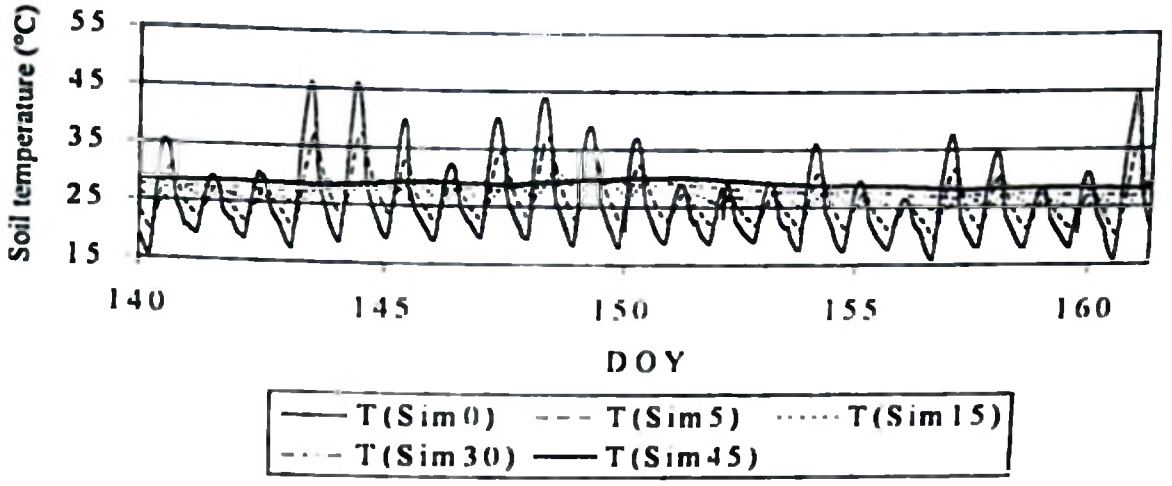

Fig. 7.46 Example of model simulation of the soil temperatures at the 0, 5, 15, 30, and 45 cm depths

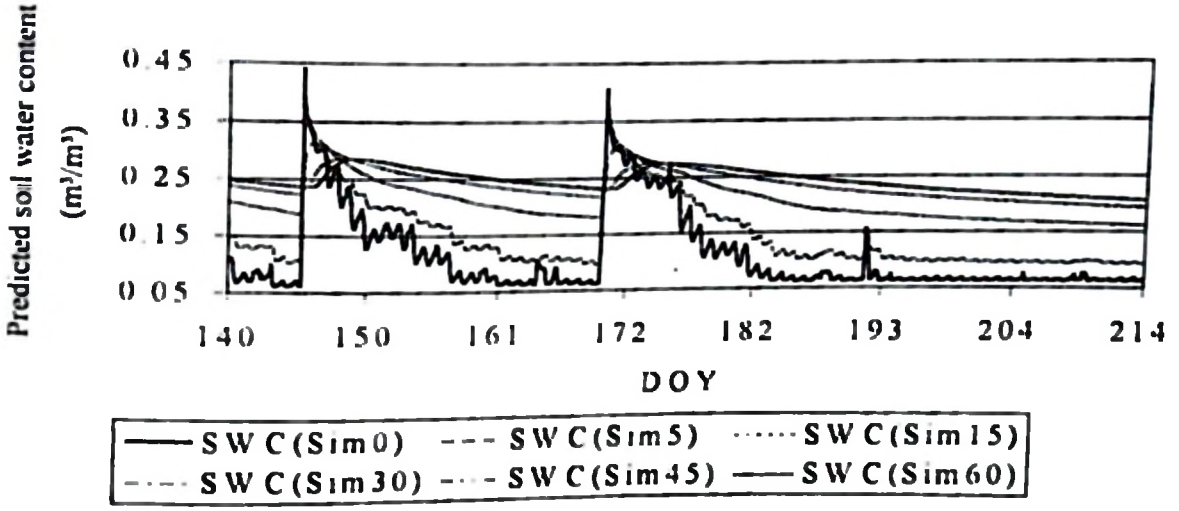

Fig. 7.47 Example of model simulation of the soil water contents at the 0, 5, 15, 30, 45, and 60 cm depths

Comparison of the model simulation using the infrared thermometry derived initial conditions and measured (standard) initial conditions shows that it is possible to use the infrared thermometry measurements to initialize or update the model. A continuous operational system for estimation of root-zone soil water content based on the intermittent thermal infrared near-surface measurements of the soil water content was therefore shown to be feasible

7.4.2 Inferring of soil water content in deeper layers of the soil from near-surface measurements

Based on the results outlined under section 7 4 1, soil water contents in deeper layers of the soil profile were estimated from the surface values using simple regression analysis. **Figs 7.48, 7.49, and 7.50** show the relationship between the surface (assumed to be at 0 cm) soil water content and the soil water contents for the 5, 10, and 15 cm depths, respectively, of the soil profile. **Table A11.7** in **Appendix 11** gives a summary of statistics for the relationship between the surface soil water content and soil water contents at different depths of the soil profile. As can be seen from the table, the correlation coefficients (given in terms of coefficients of determination) between the surface soil water content and the soil water content in different depths decrease with the increase in soil depth. The coefficients of determination (r^2) range from about 0.957 for the relationship between the surface soil water content and the soil water content at 5 cm depth, to about 0.231 for the relationship between the surface soil water content and the soil water content at 60 cm depth. Reasonable good correlation between the surface soil water content and soil water content at greater depths ceases beyond the 30 cm depth, at which a coefficient of determination of about 0.712 is obtained It can be deduced from the results that it is reasonably possible to estimate soil water contents up to the depth of 30 cm from the surface soil water content values.

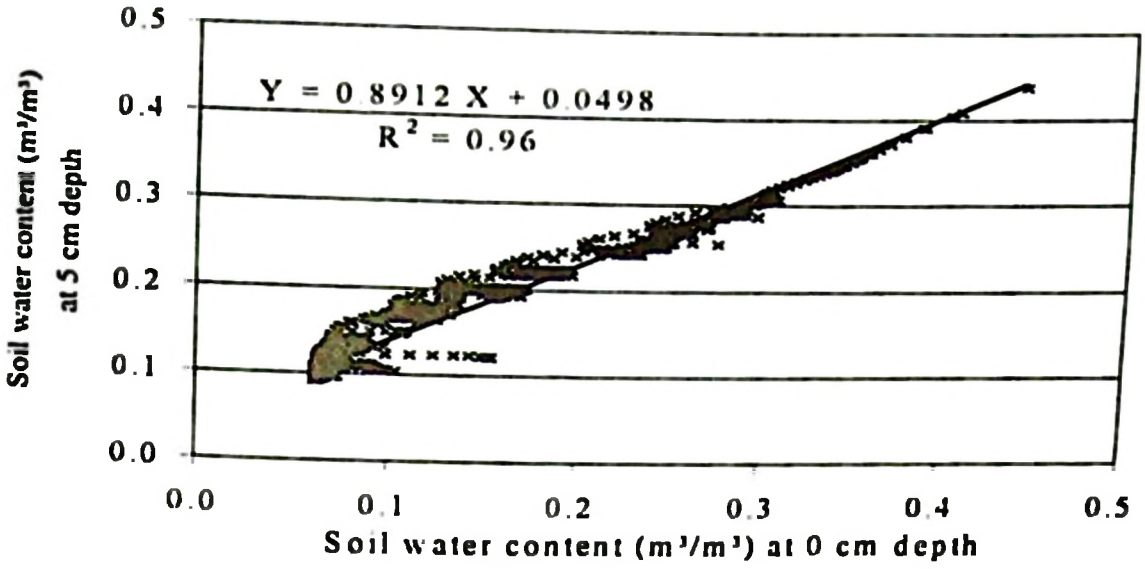

Fig. 7.48 Relationship between soil water content at 5 cm depth and that at 0 cm depth.

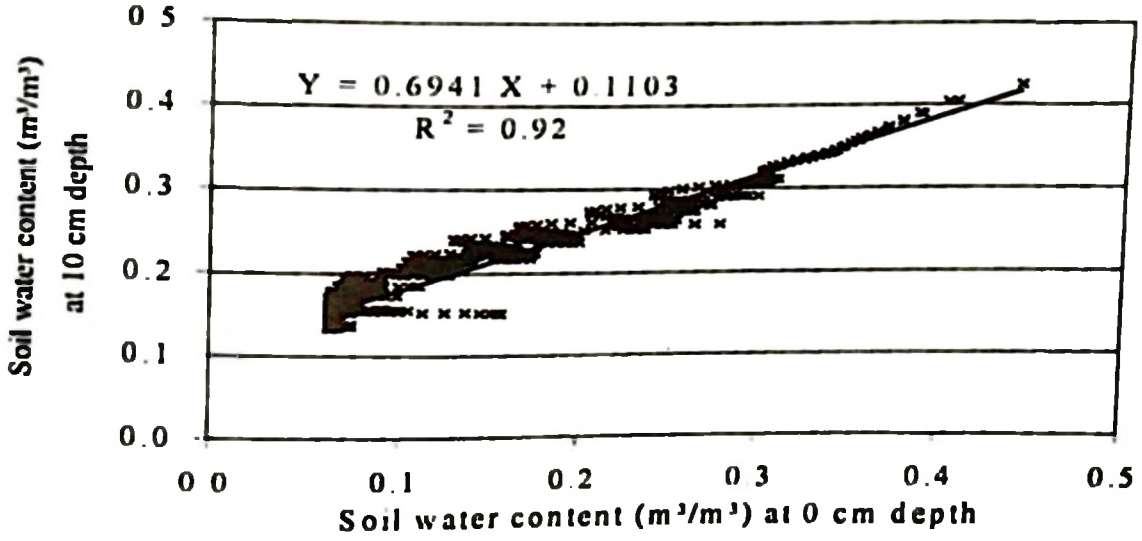

Fig. 7.49 Relationship between soil water content at 10 cm depth and that at 0 cm depth.

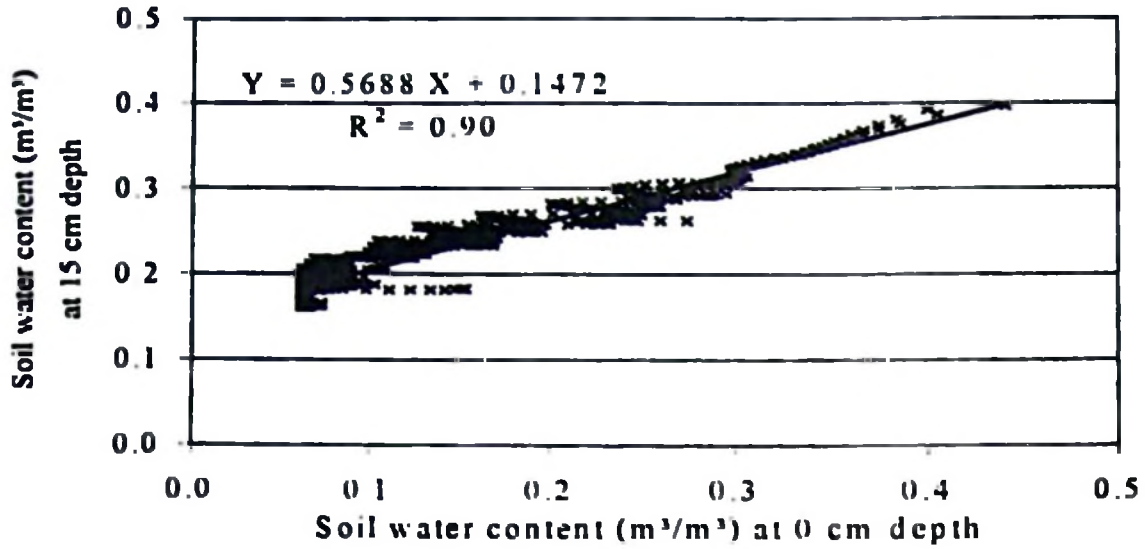

Fig. 7.50 Relationship between soil water content at 15 cm depth and that at 0 cm depth.

7.4.3 Predicting of root-zone weighted-average soil water content from near-surface measurements

One of the outputs of the model is the variable root-zone weighted-average soil water content **Fig. 7.51** shows a sample model simulation of the weighted-average soil water content for selected depths in the soil profile The root-zone can be defined as 0-5 cm, or 0-10 cm, or 0-15 cm, and so on in steps of 5 cm up to the 0-60 cm. The 0-5 cm layer is taken as the near-surface layer and its soil water content related to the other layers. **Figs 7.52 and 7.53** show the relationships between the near-surface (0-5 cm) layer soil water content and the weighted-average soil water contents for the 0-10 cm and 0-15 cm layers, respectively. The linear regressions between the near-surface soil water content (0-5 cm layer) and the variable root-zone weighted-average soil water contents for different profile depths are given in **Table A11.6, Appendix 11.** The table shows regressions with nonzero-intercepts and zero-intercepts. For the case of nonzero intercept regressions, the coefficients of determination range from about 0.998 for the 0-5 cm and 0-10 cm layer soil water content relationship to about 0 913 for 0-5 cm and 0-60 cm layer soil water content relationship. The zero intercept regression fails beyond the 0-25 cm layer, with only about 42% of the variation of the weighted-average soil water content at the 0-25 cm layer accounted for by the zero-constrained linear relationship with the 0-5 cm layer soil water content. As can be seen from the table, the correlations between the near-surface soil water content and the weighted-average soil water contents for the different soil layers are reasonably good The coefficients of determination decrease with increasing depth, as can be expected.

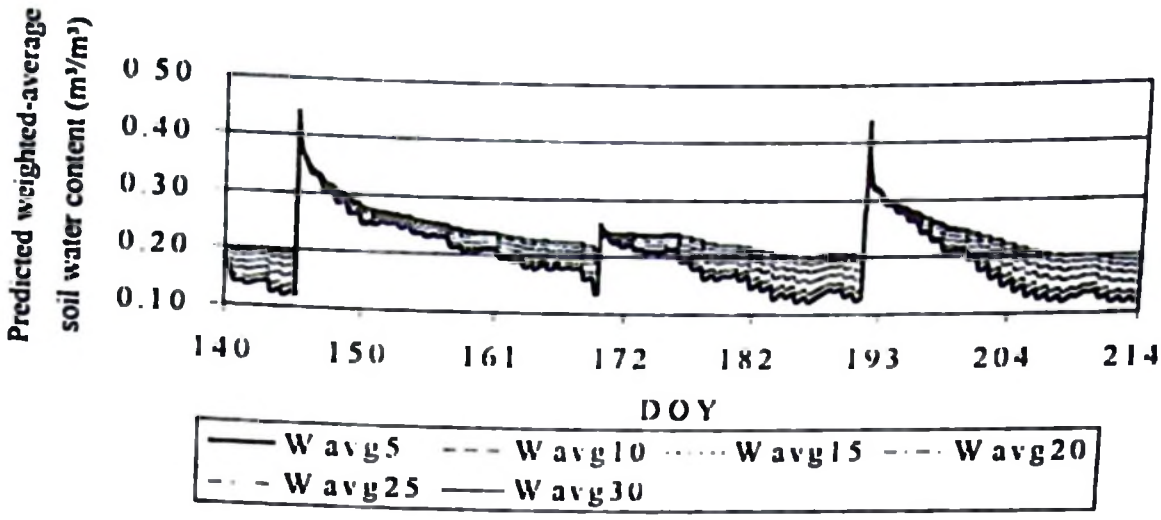

Fig. 7.51 Example of model simulation of the weighted-average soil water content to the 5, 10, 15, 20, 25, and 30 cm depths

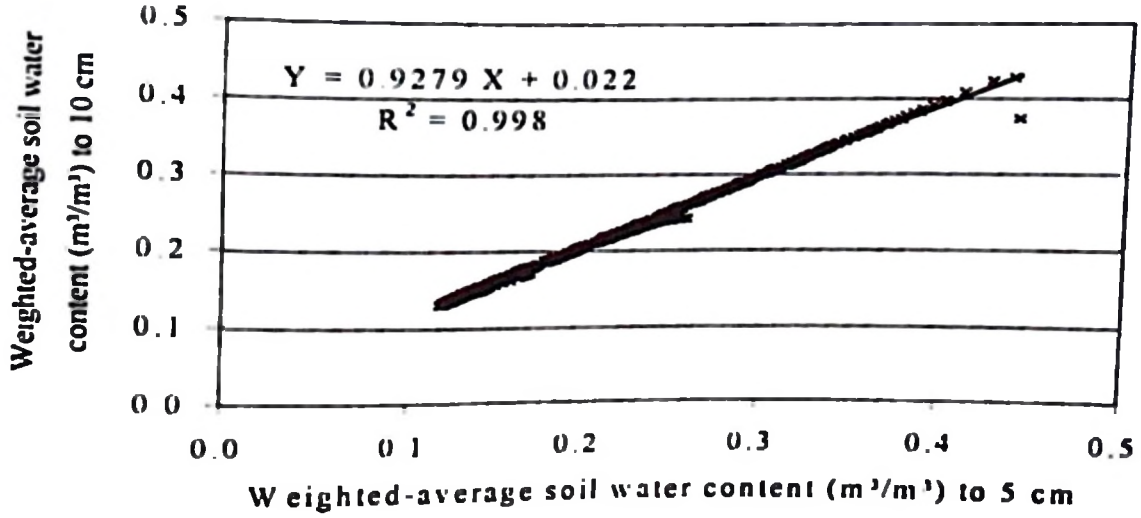

Fig. 7.52 The relationship between 0-10 cm layer weighted-average soil water content and weighted-average soil water content of the 0-5 cm layer.

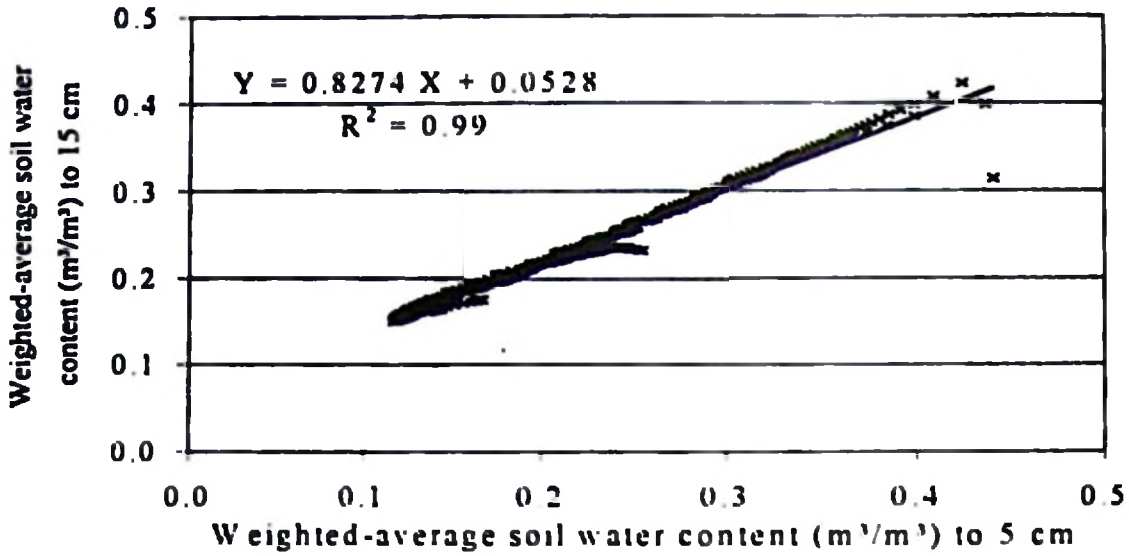

Fig. 7.53 The relationship between 0-15 cm layer weighted-average soil water content and weighted-average soil water content of the 0-5 cm layer.

It can therefore be deduced from the results that the zero-intercept regressions can be used up to the 0-20 cm layer, with about 70% of the variation explained by the zero-constrained linear relationship. The regression of these layers, especially using the nonzero intercept, shows a good linear fit with strong coefficients of determination. It is therefore reasonable to conclude that it is feasible to use slopes to compute (variable) weighted-average soil water contents in deeper layers of the soil from the near-surface layer (0-5 cm) soil water content values.

7.5 Sensitivity analysis

The term 'sensitivity analysis' has been used in the literature on modelling to indicate a wide range of activities related to the study of model or system behaviour. The results of sensitivity analyses could be looked at from two different viewpoints. If a model is intended to be used for prediction purposes, the sensitivity of the model result (the output variable) to a certain parameter indicates how precisely this parameter must be known in order to achieve a certain accuracy of the model result. If it is intended to simulate an experiment with a model and to obtain (by inverse modelling) an estimate of a certain parameter from comparison of calculated values of the output variable with measured data, a sensitivity analysis can help to find out if such a parameter identification is possible.

The mathematical model of coupled heat and water flow in unsaturated porous media contains a large variety of parameters. It is therefore particularly important to find out to which

parameters simulation results are most sensitive. This section will therefore focus on aspects of system sensitivity that may be relevant to the coupled flow of heat and water in the soil. A general sensitivity, i.e., one that is valid for all conditions, is not possible to determine. Sensitivity depends highly on the problem setup, i e , boundary conditions, parameters, time and location of interest, etc

Several functions can be used to express the sensitivity of systems. The most common expressions for the local sensitivity of some output variable y(z,t), e g., soil water content, to changes in a system parameter q, e.g., saturated hydraulic conductivity, are the absolute sensitivity $\delta y(z,t)/\delta q$ and the relative sensitivity $(\delta y(z,t)/y)/(\delta q/q)$

A detailed theoretical background on sensitivity analysis is beyond the scope of this work. However, interested readers may refer to the literature (e g. ten Berge, 1990). A rather simple method was used in this study whereby the difference between the output variable y computed with a 'standard' parameter set and y computed with another parameter set was calculated for specific points in space or time. These differences are highly dependent on the chosen 'standard' parameter set. Parameters were varied by specific value(s) either upwards or downwards.

A sensitivity analysis was carried out to test the model sensitivity to changes in various parameters. The model was found to be sensitive to the values of saturated hydraulic conductivity, the van Genuchten "EN" parameter, the soil hydraulic and thermal properties (albedo, emissivity, roughness length, thermal conductivity, and heat capacity). Proper determination of the van Genuchten (1980) fitting parameters is very important for obtaining more accurate simulation results. In this study this aspect was not investigated in detail. A value of 1.5 was assumed for the "EN" parameter of the van Genuchten curve

Different values of the saturated hydraulic conductivity were used to test the model sensitivity to the choice of this parameter. **Fig. 7.54** shows an example of model simulations. No substantial differences in the simulated values of soil water contents can be observed for the 0.2×10^{-5} m/s (...c02) and 0.3×10^{-5} m/s (...c03) values of the saturated hydraulic conductivity at the 5 and 15 cm depths. Choice of the 0.2×10^{-5} m/s value for the saturated hydraulic conductivity however led to the model predicting a state of total soil saturation on DOY 192 **(see Fig. 7.54)**.

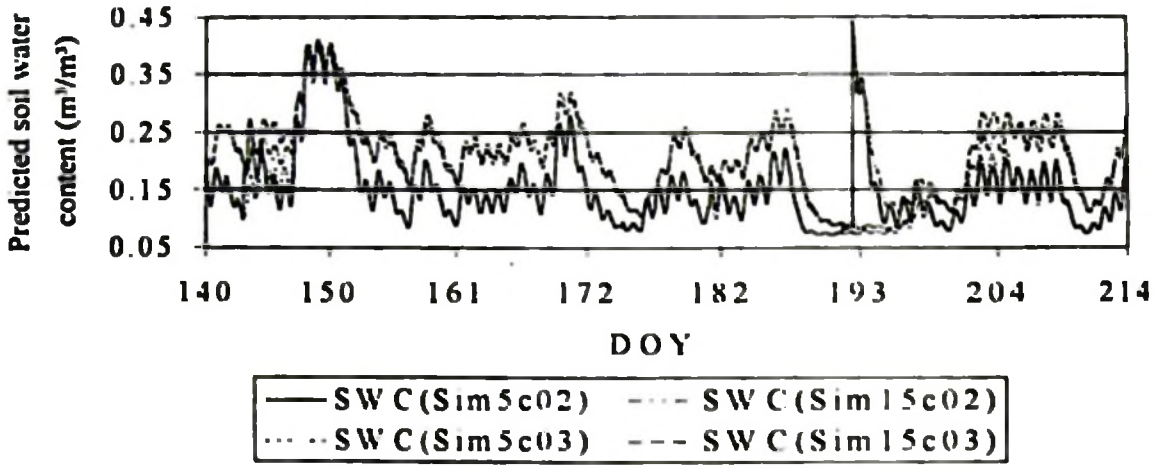

Fig. 7.54 Sensitivity of the SUAHEAT model simulation to different values of the saturated hydraulic conductivity.

7.5.1 Choice of the vertical space step size, Δz

Although space(depth)-intensive soil water content data were not available for this study, the decoupling phenomenon of the soil surface from the deeper layers (Capehart and Carlson, 1994; Carlson et al., 1995; Capehart et al., 1997) is worth a mention. In arid and semi-arid environments, careful selection of the vertical space step, Δz , is very important because of the dessication of the surface layer. This has a bearing on the utility of the thermal infrared method for estimation of surface soil water content. Capehart and Carlson (1994) and Capehart et al (1997) addressed in detail the dessication and decoupling phenomenon, respectively, and questioned the utility of the thermal infrared method in estimation of surface soil water content. Capehart et al. (1997) cautioned the blind incorporation of thermal infrared derived surface soil water content data in hydrologic models.

In this study, a vertical space step size of 5 cm was chosen This was dictated by the data availability both for model initialization, calibration, and validation Clearly better simulation results of the surface soil water content could have been obtained with a finer vertical space step size, e.g , 2 5 cm. But this would have required at least profile soil water content and soil temperature data at each of the depths to initialize the model simulation.

7.5.2 Choice of the time step size, Δt

The sensitivity of the model to the choice of the time step size was also tested. **Fig. 7.55** shows an example of model simulation for volumetric soil water content at 0 and 5 cm depths for Δt values of 240 s and 300 s. No substantial differences between the model simulated soil water contents for the different depths can be observed for the two values of time step sizes up to DOY 192. On DOY 192, differences occur in the model prediction of the soil state of "saturation" The use of the time step size of 300 s led to the model predicting total soil saturation for the layers considered in this example. When the time step size of 240 s was used, the model did not predict total soil saturation. However, model simulations come closer with the lapse of time, and as can be observed from the graph, the model simulations become nearly equal after about ten days (after DOY 204).

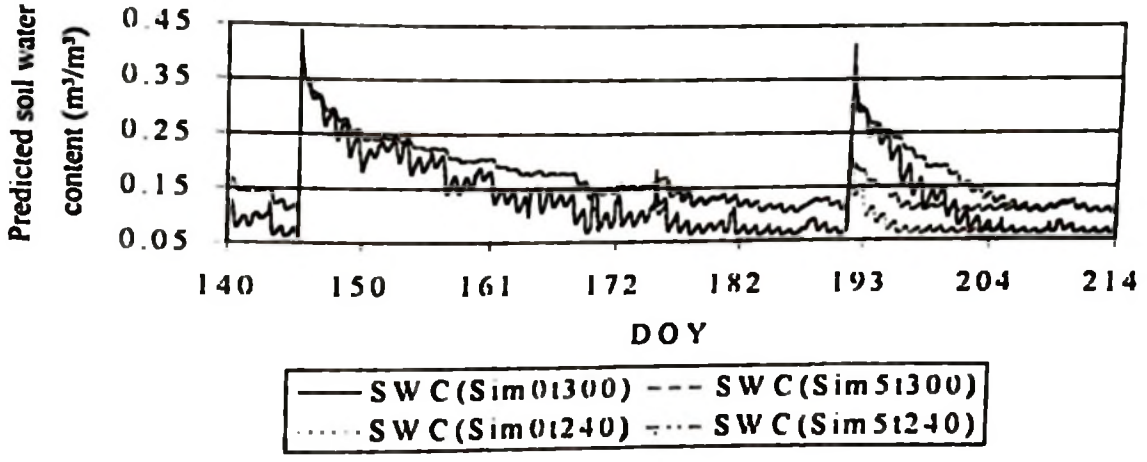

Fig. 7.55 Sensitivity of the SUAHEAT model simulation to different values of the time step size.

7.6 Simulation of the soil surface energy balance

Model simulations of the soil surface energy balance were also done. **Fig. 7.56** shows an example of the model simulation of the cummulative surface fluxes. **Fig. 7.57** shows the comparison between the model simulated, Rn(Sim), and observed, Rn(Avg), net radiation from a sample simulation. Both model under- and over-predictions can be observed from **Fig. 7.57**. The model could simulate the general trend of the diurnal and daily variation of the net radiation fairly well. Clearly, better results could have been obtained with more optimization of the model parameters

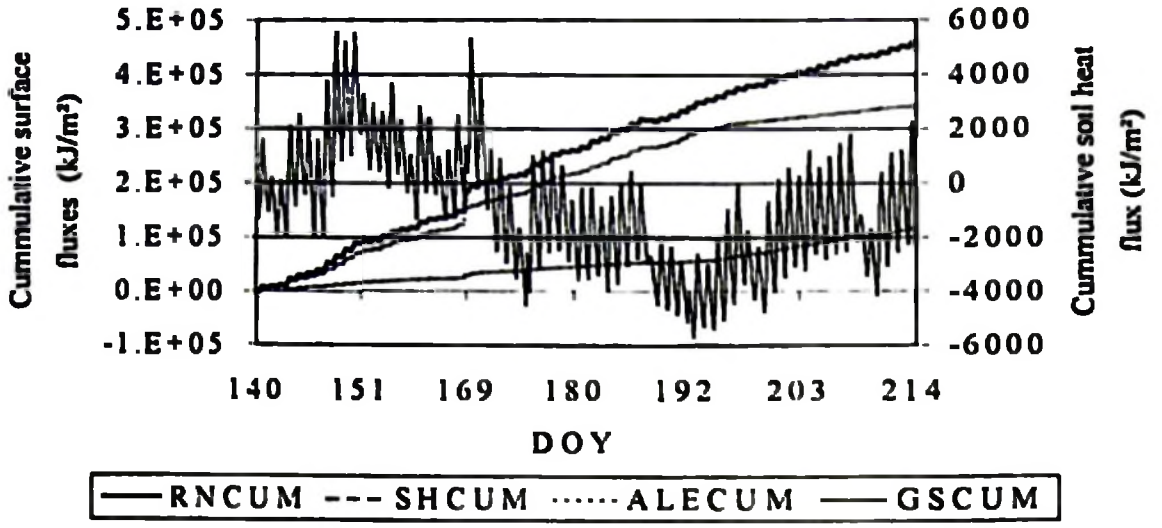

Fig. 7.56 Model simulated cummulative soil surface fluxes· RNCUM - cummulative net radiation; SHCUM - cummulative sensible heat flux; ALECUM - cummulative latent heat flux; and GSCUM - cummulative soil heat flux.

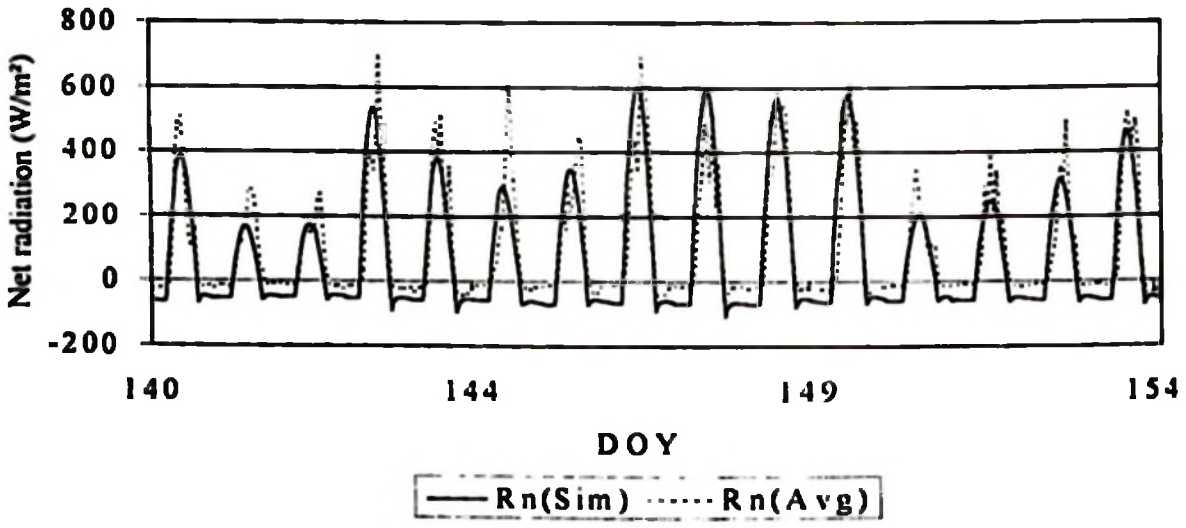

Fig 7.57 Comparison between model simulated, Rn(Sim), and measured, Rn(Avg), net radiation.

8 SUMMARY AND CONCLUSIONS

8.1 Summary

Soil moisture plays a very crucial role in land surface processes. It should therefore be monitored with the same accuracy and frequency as other important environmental variables Two approaches are used for estimation of soil moisture content, namely, modelling and measurement, either in-situ or remote. In-situ measurements are based on relatively small volumes of soil and since soil moisture content is highly variable in space and time, good estimates of the average moisture content of large areas require extensive and expensive observation Remote sensing methods, on the other hand, generally perform areal integration directly in the observation process. Their main disadvantage is their inability to sense beyond the surface (0 to 10 cm depth) soil layer. Many applications also require an estimate of root zone soil moisture. Four basic approaches for extrapolating surface measurements of soil water content to root-zone values have been described in this study that vary in sophistication and data requirements, regression, knowledge-based, inversion, and model-data combinations. Integration of modelling and measurements may provide the best solution towards estimation of profile soil moisture content.

This study looks at modelling and measurement of soil moisture content based on "ground" thermal infrared remote sensing measurement of surface soil temperature. The study was stimulated by the continuing need for development of methods for profile soil moisture estimation from remote sensing measurements of near-surface (0-5 cm depth) soil moisture content (see for example, Rawls and Jackson, 1997). The main focus of the research was to study the relationship between the surface radiant temperature and near-surface soil water content under natural semi-arid agricultural conditions at field scale. Extrapolation of these surface measurements to root-zone values through coupling of field measurements with modelling approaches was the ultimate goal of the study bearing in mind the utility of subsurface soil water content values for agronomical applications.

In this study, the utility of ground-based thermal infrared remote sensing method for the estimation of near-surface soil water content was tested under tropical semi-arid agricultural conditions in Morogoro, Tanzania, East Africa. Field experiments were conducted between

January and August, 1997 at a bare soil site. Regression relationships between the daily maximum surface soil temperature minus air temperature (TDMax) and weighted-average soil water contents to different depths in the soil profile were developed based on the measured data. Better correlations were obtained for the top 0-5 and 0-15 cm layers of the soil, with coefficients of determination of 0.81 and 0.78, respectively. Use of "Normalized TDMax" as well as cloudness-cover-corrected "Normalized TDMax" (TDaMax) resulted in even better coefficients of determination (e.g., 0.95 for the 0-5 cm soil layer).

A physically based model of coupled flow of heat and water in the soil (SUAHEAT) was developed, calibrated, and validated in this study. The SUAHEAT model can be applied confidently to predict values of water content near the soil surface, e.g., 0 to 5 cm, to be used to supplement or verify measurements obtained with a remote sensing technique. An important feature of the SUAHEAT model is that it can calculate the values of soil water content and/or temperature for any required time during the entire simulation period. This realistic dynamicism is important as the model is meant to be used to supplement measurements of soil water content by a remote sensing technique, in which time of observation is typically not controlled, nor constant.

The SUAHEAT model was tested by comparing its simulated soil water contents and soil temperatures with those measured at the bare soil site. Both qualitative as well as quantitative methods were used to evaluate the model performance, for the calibration and validation phases. For the calibration phase, the average values of the mean absolute difference (MAD) of soil water content were 0.06, 0.05, 0.05, and 0.03 m^3/m^3 for the 5, 15, 30, and 45 cm depths, respectively. The corresponding average values of the root mean square difference (RMSD) of soil water content were 0.07, 0.06, 0.05, and 0.03 m^3/m^3 for the same depths, respectively. As for the validation phase, the average MAD values of soil water content were 0.09, 0.05, 0.08, and 0.17 m^3/m^3 for the same depths, respectively. The corresponding average RMSD values for the same depths were 0.12, 0.08, 0.10, and 0.19 m^3/m^3, respectively. The unusually large errors (at the 45 cm depth) during the validation phase could be attributed to the overestimation of soil water content values during very wet conditions arising from the calibration equation used

The performance of the model in the simulation of surface, near-surface, and profile soil temperatures was also both qualitatively and quantitatively evaluated. In the calibration phase, the MAD values were 2.8, 1.1, 0.5, and 0.3 °C for the 5, 15, 30, and 45 cm depths, respectively. The corresponding RMSD values for the same depths were 3.5, 1.3, 0.6, and 0.4 °C, respectively. For the validation phase, the MAD values for the same depths were 2.3, 1.2, 0.7, and 0.4 °C, respectively. The corresponding RMSD values for the same depths were 2.7, 1.4, 0.8, and 0.5 °C, respectively. Generally, the errors obtained with the use of the SUAHEAT model are comparable to values obtained by other researchers elsewhere using similar models.

Use of empirical methods (based on statistical analysis) for the estimation of profile soil water content from surface measurements has been demonstrated in this study. Higher correlations were obtained for the soil layers adjacent to each other. Results obtained using these methods are however site-specific. Use of simulation models provides a more flexible alternative. Development of methods of coupling remote sensing data with hydrological and flux models is necessary towards solving the problem of extrapolating remote-sensing-derived surface state variables (e.g., soil water content and temperature) to subsurface or root zone values.

Use of the physically based soil heat and water flow model (SUAHEAT) to extrapolate near-surface soil water content values to root-zone values has been demonstrated in this study. Integration of the model with remotely sensed surface soil water content and temperature data was effected through use of the initial profiles of soil water content and temperature derived from the regression relationships between TDMax and near-surface soil water content on the one hand, and between the surface and profile soil temperatures on the other. It could be deduced from the results obtained that it is feasible to estimate profile soil water contents to the depth of 30 cm from the surface measurements. Furthermore, profile weighted-average soil water contents to the 0-25 cm soil layer can be reasonably estimated from the near-surface (0-5 cm soil layer) values.

The utility of small-scale field experiments under natural agricultural conditions has been demonstrated in this study. Realistic model calibrations and validations require measurements under representative conditions of the process being simulated. Furthermore, major

developments in spaceborne and airborne remote sensing techniques will continue to rely on ground-based measurements for data calibration.

8.2 Conclusions

The following conclusions can be drawn from this study

- Results of field experiments have shown that it is feasible to estimate soil water content from the measurement of TDMax to the depth of 15 cm under tropical semi-arid conditions. This is evidenced by the relatively high coefficients of determination obtained at the 5 and 15 cm depths. Use of "Normalized TDMax" and "Normalized maximum equilibrium temperature difference (TDaMax)" led to even better correlations.

- The performance of the SUAHEAT model in simulating surface and profile soil water content was fairly good. Discrepancies between the measured and simulated values were observed. This can partly be explained by the errors in the values of the measured data as these were derived from measurement of matric potential. Admittedly, the accuracy attained in the simulation of surface soil moisture dynamics is limited, even in cases where extensive data on physical soil properties are available. This is especially so where wetting and drying alternate. The results obtained in this study serve to illustrate this fact. The performance of the model in simulating profile soil temperature was good. Relatively low values of the MADs and RMSDs obtained support this fact. Generally the model performance was of comparable level to results from the literature obtained using similar models.

- Model simulation results obtained using the remotely sensed initial conditions indicated that it is feasible to use remotely sensed data (one value of TDMax per day) to initialize the model. Prior knowledge of the empirical relationships required for model initialization is however necessary.

- Extrapolation of the remotely sensed near-surface (0-5 cm depth) soil water content to values at greater depths in the soil profile by integrated use of modelling and remotely sensed data was also shown to be feasible.

8.3 Recommendations for further research

- The use of infrared thermometry for estimation of surface soil moisture content is greatly influenced by the occurrence of clouds. There is therefore a need to conduct further research in order to develop methods of correcting for the effects of clouds in order for the method to also be applicable under cloudy conditions.

- Further field experiments in different climatic and soil conditions are necessary in order to develop empirical relationships needed for the integration of the thermal infrared method with modelling.

- Coupling of field measurements with modelling provides an ideal combination for the estimation of the profile moisture content from the surface measurements. However, high spatial and temporal resolution data are required for the validation of models.There is therefore a real need for collecting high quality data for this purpose.

- Field research is also required to further explore profile soil moisture estimation methods based on remote sensing observations.

- Accurate knowledge of soil hydraulic and thermal properties is crucial for accurate simulation of soil water movement. The possibility of deriving such parameters from remote sensing techniques would be an interesting topic for further research.

REFERENCES

Altendorf, C.T., M.L. Stone, and R.L. Elliot, 1992. Using a Neural Network for Soil Moisture Predictions. ASAE Paper No. 92-3557, pp. 17

Altendorf, C T., M.L. Stone, R.L Elliot, and M.A. Kizer, 1992 Determining Soil Moisture using Soil Thermal Properties. ASAE Paper No. 92-3020, pp. 19.

Amer, S A., T.O. Keefer, M.A. Weltz, D C. Goodrich, and L.B Bach, 1994. Soil Moisture Sensors for Continuous Monitoring. Water Resources Bulletin, 30(1), 69-83

Anderson, M.C., J.M. Norman, G.R. Diak, W.P. Kustas, and J.R Mecikalski, 1997. A Two-Source Time-Integrated Model for Estimating Surface Fluxes Using Thermal Infrared Remote Sensing. Remote Sensing of Environment 60(2) 195-216

Arya, L.M., J.C. Richter, and J.F. Paris, 1983. Estimating Profile Water Storage from Surface Zone Soil Moisture Measurements under Bare Field Conditions Water Resourc. Res., 19(2), 403-412.

Asrar, G., 1989. Introduction. In: Asrar, G. (ed) Theory and applications of optical remote sensing. John Wiley & Sons, New York, pp. 1-13.

Bach, L.B., 1992. Soil water movement in response to temperature gradients: Experimental measurements and model evaluation. Soil Sci Soc Am J 56, 37-46.

Barrett, E.C., 1990 The use of satellites in rainfall monitoring Proc. Intl Symp. Remote sensing and water resources, Enschede, 39-52.

Barrett, E.C., 1989 An hierarchy of techniques for satellite - improved monitoring of rainfall, with special reference to the role of passive microwave satellite imagery, WMO-IAHS-ETH, Intl Workshop on Precipitation Measurement, St Moritz, Switzerland, 425-430.

Bastiaanssen, W.G.M , 1990 Mapping vapour and heat transport coefficients in soil and air using Landsat observations in arid regions Proc. IGARSS 1990 at Univ of Maryland, USA, May 20-24. 1845-1849

Bastiaanssen, W.G.M., 1991 Derivation of areal soil physical data from satellite measurements. In: Kienitz, G., P.C.D. Milly, M.Th. Van Genuchten, D. Rosbjerg, and W J. Shuttleworth (eds), Hydrological interactions between atmosphere, soil and vegetation. IAHS Publication No. 204, pp. 95-105.

Bell, K.R., B.J. Blanchard, T.J. Schmugge, and M.W Witczak, 1980. Analysis of Surface Moisture Variations within Large-Field Sites. Water Resourc. Res , 16(4), 796-810.

Ben Mehrez, M., O. Taconet, D. Vidal-Madjar, and C Valencogne, 1992b. Estimation of canopy stomatal resistance and canopy evaporation during HAPEX-MOBILHY experiment. Agric. For. Meteorol., 58: 285-313.

Ben Mehrez, M., O. Taconet, D. Vidal-Madjar and Y. Sucksdorff, 1992 Calibration of an Energy Flux Model over Bare Soils during the HAPEX-MOBILHY Experiment. Agric. For. Meteorol. 58: 257-283

Ben-Asher, J., A.D. Matthias, and A.W. Warrick, 1983 Assessment of Evaporation from Bare Soil by Infrared Thermometry. Soil Sci. Soc. Am J. 47. 185-191.

Ben-Asher, J., A.W. Warrick, and A.D Matthias, 1984. Bare-Soil Evaporation Determined in situ by Infrared Thermometry Journal of Hydrology, 69: 1-4, 325-334.

Benjamin, J.G., M.R Ghaffarzadeh, and R.M Cruse, 1990. Coupled water and heat transport in ridged soils Soil Sci Soc. Am. J. 54: 963-969.

Berge, H.F.M ten, L. Stroosnijder, P.A. Burrough, A.K. Bregt, and M.J de Heus, 1983. Spatial Variability of Physical Soil Properties Influencing the Temperature of the Soil Surface. Agric. Water Management, 6, 213-226.

Berge, H.F.M ten, 1990 *Heat and Water Transfer in Bare Topsoil and the Lower Atmosphere* Wageningen: Pudoc. -111. - (Simulation Monographs ISSN 0924-8439; 33)

Bernard, R., J.V Soarés, and D. Vidal-Madjar, 1986 Differential Bare Field Drainage Properties from Airborne Microwave Observations. Water Resourc. Res 22(6): 869-875.

Bernard, R., M Vaucli, and D. Vidal-Madjar, 1981. Possible Use of Active Microwave Remote Sensing Data for Prediction of Regional Evaporation by Numerical Simulation of Soil Water Movement in the Unsaturated Zone Water Resourc Res., 17(6), 1603-1610.

Beven, K.J. and J Fiher, 1996. Remote sensing and scaling in hydrology. In: Stewart, J.B., E.T. Engman, R.A Feddes, and Y. Kerr (eds.). Scaling up in Hydrology using Remote Sensing. John Wiley & Sons, Chichester, pp. 1-18.

Boissard, P., G Guyot, and R.D Jackson, 1990 Factors Affecting the Radiative Temperature of a Vegetative Canopy. In: *Steven, M.D. and J.A. Clark (Eds). Applications of Remote Sensing in Agriculture. Butterworths. London. 1990. pp. 45-72.*

Briggs, L.J., 1897. The Mechanics of Soil Moisture. U.S Dept Agric Div. of Soils Bull. 10.

Bristow, K.L., G.S. Campbell, R.I Papendick, and L.F. Elliott, 1986. Simulation of Heat and Moisture Transfer Through a Surface Residue-Soil system. Agric For. Meteorol., 36, 193-214.

Bruckler, L., H. Witono, and P. Stengel, 1988. Near Surface Soil Moisture Estimation from Microwave Measurements. Remote Sens. Environ. 26. 101-121.

Bruckler, L. and H Witono, 1989. Use of Remotely Sensed Soil Moisture Content as Boundary Conditions in Soil-Atmosphere Water Transport Modeling 2. Estimating Soil Water Balance Water Resourc. Res., 25(12), 2437-2447.

Buchan, G.D., 1991. Soil Temperature Regime: In Smith, K.A and C.E. Mullins (ed.), pp 551-612. *Soil Analysis: Physical Methods*. (Books in Soils, Plants, and the Environment). Marcel Dekker, Inc., New York.

Businger, J.A., J.C. Wyngaard, Y. Izumi, and E.F. Bradley, 1971. Flux profile relationships in the atmospheric surface layer. J. Atmos. Sci. 28. 181-189.

Camillo, P.J., R.J. Gurney, and T.J. Schmugge, 1983. A Soil and Atmospheric Boundary Layer Model for Evapotranspiration and Soil Moisture Studies. Water Resourc. Res., 19(2), 371-380.

Camillo, P. and T.J. Schmugge, 1983. Estimating Soil Moisture Storage in the Root Zone from Surface Measurements. Soil Sci. 135: 245-264.

Camillo, P.J. and R.J. Gurney, 1986. A Resistance Parameter for Bare-Soil Evaporation Models. Soil Science, Vol. 141, No 2, 95-105.

Campbell, G.S., 1985. *Soil Physics with BASIC: Transport Models for Soil-Plant Systems* (Developments in Soil Science 14). Elsevier, Amsterdam, 1985. pp. 150.

Campbell Scientific Ltd., 1996. Calculating Dew Point from RH and Air Temperature. Technical Note 16, Issued 08.10.1996.

Campbell, G.S. and J.M. Norman, 1990. Estimation of Plant Water Status from Canopy Temperature: An Analysis of the Inverse Problem. In *Steven, M.D. and J.A. Clark (Eds). Applications of Remote Sensing in Agriculture. Butterworths. London. 1990. pp. 255-271.*

Capehart, W.J., 1996. Issues Regarding the Remote Sensing and Modeling of Soil Moisture for Meteorological Applications (Drying). PhD Dissertation pp. 240, The Pennsylvania State University (0176).

Capehart, W.J. and T.N. Carlson, 1997. Decoupling of Surface and Near-Surface Soil Water Content: A Remote Sensing Perspective. Water Resourc. Res. 33(6): 1383-1395.

Capehart, W.J. and T.N. Carlson, 1994. Estimating Near-Surface Soil Moisture Availability Using a Meteorologically Driven Soil-Water Profile Model. Journal of Hydrology 160: 1-20.

Carlson, T.N., F.G. Rose, and E.M. Perry, 1984. Regional-Scale Estimates of Surface Moisture Availability from GOES Infrared Satellite Measurements. Agron. J. 76: 972-978.

Carlson, T.N., 1986. Regional-scale Estimates of Surface Moisture Availability and Thermal Inertia using Remote Thermal Measurements. Remote Sens. Rev., 1(2), 197-247.

Carlson, T.N., O. Taconet, A. Vidal, R.R. Gillies, A. Olioso, and K. Humes, 1995. An Overview of the Workshop on Thermal Remote Sensing Held at La Londe les Maures, France, September 20-24, 1993. Agric. For. Meteorol. 77: 141-151.

Carlson, T.N., J.K. Dodd, S.G. Benjamin, and J.N. Cooper, 1981. Satellite Estimation of the Surface Energy Balance, Moisture Availability and Thermal Inertia. Journal Appl. Meteorol., 20, 67-87.

Carlson, T.N., E.M. Perry, and T.J. Schmugge, 1990. Remote Estimation of Soil Moisture Availability and Fractional Vegetation Cover for Agricultural Fields. Agric. For. Meteorol., 52(1), 45-69.

Cass, A., G.S. Campbell, and T.L. Jones, 1984. Enhancement of Thermal Water Vapor Diffusion in Soil. Soil Sci. Soc. Am. J. 48: 25-32.

Celia, M.A., E.T. Bouloutas, and R.L. Zarba, 1990. A general mass-conservative numerical solution for the unsaturated flow equation. Water Resourc. Res., 26(7), 1483-1496.

Chanasyk, D.S. and M.A. Naeth, 1996. Field Measurement of Soil Moisture using Neutron Probes. Can. J. Soil Sci. 76: 317-323.

Chanzy, A. and L. Bruckler, 1993. Significance of Soil Surface Moisture with Respect to Daily Bare Soil Evaporation. Water Resourc. Res., 29 4, 1113-1125.

Choudhury, B.J. and J.L. Monteith, 1988. A four-layer model for the heat budget of homogeneous land surfaces. Q. J. R. Meteorol. Soc. 114: 373-398.

Choudhury, B.J. and S.B. Idso, 1984. Simulating Sunflower Canopy Temperatures to Infer Root-Zone Soil Water Potential. Agric. For. Meteorol., 31: 69-78.

Choudhury, B.J., 1989. Estimating Evaporation and Carbon Assimilation using Infrared Temperature Data: Vistas in Modeling. In: Asrar, Ghassem (ed), *Theory and Applications of Optical Remote Sensing*, John Wiley & Sons, New York, pp. 628-690.

Chung, S.-O. and T.A. Austin, 1987. Modelling saturated-unsaturated water flow in soils. J. Irrig. Drain. Eng., Vol. 113(2), 233-250.

Chung, S.-O. and R. Horton, 1987. Soil Heat and Water Flow with a Partial Surface Mulch. Water Resourc. Res. 23(12): 2175-2186.

Cihlar, J., 1980. Soil water and plant canopy effects on remotely measured surface temperatures. International Journal of Remote Sensing, 1: 167-173.

Clemente, R.S., R. De Jong, H.N. Hayhoe, W.D. Reynolds, and M. Hares, 1994. Testing and comparison of three unsaturated soil water flow models. Agricultural Water Management, 25, 135-152.

Colwell, R.N. (ed), 1983. Manual of remote sensing. 2nd edition, Virginia: American society of photogrammetry, Falls Church.

Cosby, B J., G M. Hornberger, R B. Clapp, and T.R. Ginn, 1984 A Statistical Explanation of the Relationship of Soil Moisture Characteristics to the Physical Properties of Soils. Water Resourc. Res. 20(6): 682-690.

Costello, T A. and W.J. Horst, 1991. Soil Temperature Sensor Installation: A Comparison of Two Methods. Transactions of the ASAE, 34(3), 904-908.

Daamen, C.C., L.P. Simmonds, J.S. Wallace, K.B. Laryea, and M.V.K. Sivakumar, 1993. Use of Microlysimeters to Measure Evaporation from Sandy Soils. Agric. For. Meteorol., 65: 159-173.

Daamen, C.C. and L.P. Simmonds, 1996. Measurement of Evaporation from Bare Soil and its Estimation using Surface Resistance. Water Resourc. Res., 32(5). 1393-1402.

Danson, F.M. and S.E. Plummer (eds), 1995. *Advances in Environmental Remote Sensing*. John Wiley & Sons, Chichester [a.o.], 1995, pp. 184.

Davis, J.B., 1977. Simulation of heat and moisture movement during drying of a two-dimensional soil profile, PhD Diss. Clemson Univ., Clemson, SC. Diss. Abstr. (DDK77-29688).

de Vries, D.A., 1975. Heat transfer in soils. In: de Vries, D.A. and N. Afgan (eds), Heat and Mass Transfer in the Biosphere, I. Transfer Processes in the Plant Environment. Scripta Book Company, Washington, D.C., 5-28.

De Vries, D.A., 1958. Simultaneous Transfer of Heat and Moisture in Porous Media. Transactions, American Geophysical Union 39(5). 909-916.

De Jong, R. and A. Bootsma, 1996. Review of Recent Developments in Soil Water Simulation Models. Can. J. Soil Sci. 76: 263-273.

De Vries, D.A., 1963. Thermal properties of soils. In: Van Wijk, W.R. (ed), Physics of plant environment. John Wiley & Sons, Inc., New York, 210-235.

De Pauw, E.F., 1984. Soils, Physiography and Agroecological Zones of Tanzania. Crop Monitoring and Early Warning Systems. Ministry of Agriculture, Dar es Salaam/FAO, Rome. Consultant's Final Report.

Deardorff, J.W., 1978. Efficient Prediction of Ground Surface Temperature and Moisture, with Inclusion of a Layer of Vegetation. J. Geophy. Res., 83(C4). 1889-1903.

Dirmeyer, P.A. and J. Shukla, 1993. Observational and modelling studies of the influence of soil moisture anomalies on atmosphere circulation (review). In: Shukla, J. (ed). Prediction of interannual climate variations. Springer-Verlag, Berlin, pp. 1-23.

Dirmeyer, P A., and J. Shukla, 1993 Observational and Modeling Studies of the Influence of Soil Moisture Anomalies on Atmospheric Circulation (Review). In Shukla, J. (ed), *Prediction of Interannual Climate Variations*. (NATO ASI Series I: Global Environmental Change, Vol 6). Springer-Verlag, 1993. p. 1-23

Durar, A A., J.L. Steiner, S.R. Evett, and E.L. Skidmore, 1995 Measured and Simulated Surface Soil Drying. Agron. J. 87: 235-244.

Dyer, A.J., 1967. The turbulent transport of heat and water vapour in an unstable atmosphere. Quart. J. Roy Meteorol Soc. 93 501-508.

El-Swaify, S.A., E.W. Dangler, and C.L. Armstrong, 1982. *Soil erosion by water in the tropics*. Research Extension Series 024, Univ. of Hawaii, Institute of Tropical Agriculture and Human Resources, Honolulu, Hawaii.

El-Swaify, S.A., P. Pathak, T.J. Rego, and S. Singh, 1985. Soil Management for Optimized Productivity under Rainfed Conditions in the Semi-Arid Tropics. In Stewart, B.A. (ed), *Advances in Soil Science*, Volume 1, Springer-Verlag, 1985. p. 1-64

Eldredge, E.P., C.C. Shock, and T.D. Stieber, 1993 Calibration of Granular Matrix Sensors for Irrigation Management. Agron. J. 85. 1228-1232

Engman, E.T. and R.J. Gurney, 1991. Remote sensing in hydrology. Chapman & Hall, London

Entekhabi, D., H. Nakamura, and E.G. Njoku, 1994. Solving the Inverse Problem for Soil Moisture and Temperature Profiles by Sequential Assimilation of Multifrequency Remotely Sensed Observations. IEEE Trans. Geosci. Remote Sensing, 32(2) 438-448.

Evett, S.R., A.D. Matthias, and A.W. Warrick, 1994. Energy Balance Model of Spatially Variable Evaporation from Bare Soil. Soil Sci. Soc. Am. J. 58: 1604-1611.

Farouki, O.T., 1986. Thermal properties of soils, Series on rock and soil mechanics, Vol. 11. Trans Tech. Publications.

Feddes, R.A., M. Menenti, P. Kabat, and W.G.M. Bastiaanssen, 1993. Is large-scale inverse modelling of unsaturated flow with areal average evaporation and surface soil moisture as estimated from remote sensing feasible? Journal of Hydrology, 143: 125-152.

Feddes, R.A., P.J. Kowalik and H. Zarady, 1978. Simulation of field water use and crop yield. Simulation Monographs, Pudoc, Wageningen, The Netherlands. p. 189.

Feddes, R.A., M. Menenti, P. Kabat, and W.G.M. Bastiaanssen, 1993. Is Large-Scale Inverse Modelling of Unsaturated Flow with Areal Average Evaporation and Surface Soil Moisture as Estimated from Remote Sensing Feasible? Journal of Hydrology 143: 125-152.

Forsythe, W.E., 1964. Smithsonian physical tables. Smithsonian Inst. Publ. 4169. Washington, DC.

Fox, D.G., 1981. Judging air quality model performance: A summary of the AMS workshop on dispersion model performance, Woods Hole, MA. 8-11 Sept. 1980. Bull. Am Meteorol. Soc. 62: 599-609.

Fuchs, M. and C.B. Tanner, 1967. Evaporation from a drying soil J. Appl. Meteorol. 6: 852-857.

Fuchs, M and C.B. Tanner, 1968. Surface Temperature Measurements of Bare Soils. J. Appl Meteorol. 7: 303-305

Gardner, B.R., D.C. Nielsen, and C.C. Shock, 1992a. Infrared Thermometry and the Crop Water Stress Index. II. Sampling Procedures and Interpretation. J. Prod. Agric., 5(4): 466-475.

Gardner, B R., D.C. Nielsen, and C.C. Shock, 1992b. Infrared Thermometry and the Crop Water Stress Index. I. History, Theory, and Baselines. J. Prod Agric., 5(4) 462--466

Goodrich, D.C., T.J. Schmugge, T.J. Jackson, C.L. Unkrich, T O Keefer, R. Parry, L B Bach, and S.A. Amer, 1994. Runoff Simulation Sensitivity to Remotely Sensed Initial Soil Water Content Water Resourc. Res., 30(5). 1393-1405.

Gupta, S.C., J.K. Radke, and W.E. Larson, 1981 Predicting temperature of bare and residue covered soils with and without a corn crop. Soil Sci. Soc. Am. J. 45 405-412.

Haefner, H. and P. Pampaloni, 1992 Water resources. Intl J. Remote Sensing, 13(6/7). 1277-1303.

Hanks, R.J., D.D. Austin, and W.T. Ondrechen, 1971 Soil temperature estimation by a numerical method. Soil Sci. Soc. Am. Proc. 35: 665-677.

Hares, M.A., J. Ben-Asher, A.D Matthias, and A.W. Warrick, 1985. A Simple Method to Evaluate Daily Positive Soil Heat Flux. Soil Sci. Soc. Am. J., 49. 45--47.

Haverkamp, R., M. Vauclin, J. Touma, P.J. Wierenga, and G. Vachaud, 1977 A Comparison of Numerical Simulation Models for One-Dimensional Infiltration Soil Sci. Soc. Am. J. 41. 285-294.

Haverkamp, R. and M. Vauclin, 1979. A Note on Estimating Finite Difference Interblock Hydraulic Conductivity Values for Transient Unsaturated Flow Problems. Water Resourc. Res. 15(1): 181-187.

Heilman, J.L. and D.G. Moore, 1980. Thermography for estimating near-surface soil moisture under developing crop canopies. Journal of Applied Meteorology, 19: 324-328.

Hillel, D., 1980. Introduction to Soil Physics. Academic Press, Inc. Harcourt Brace Jovanovich, Publishers. Orlando, Florida.

Hillel, D., 1971. *Soil and Water: Physical Principles and Processes*, Academic Press, New York (Kozlowski, T T. (ed). *Physiological Ecology: A Series of Monographs, Texts, and Treatises*).

Hipel, K.W., A.I. McLeod, and W.C. Lennox, 1977. Advances in Box-Jenkins Modeling. 1. Model Construction. Water Resourc. Res., 13(3): 567-575.

Hipel, K.W., 1985 Time series analysis in perspective Water Resourc. Bull. 21: 609-624.

Hornung, U. and W Messing, 1983. Truncation errors in the numerical solution of horizontal diffusion in saturated/unsaturated media. Adv Water Resourc 6, 165-168.

Horton, R., and S.-O. Chung, 1991. Soil Heat Flow. In Hanks, J , and J T. Ritchie (co-eds), 1991. *Modeling Plant and Soil Systems*. AGRONOMY No. 31, ASA,CSSA,SSSA, Madison, Wisconsin USA, p. 397-438

Horton, R., O. Aguirre-Luna, and P.J Wierenga, 1984a. Observed and Predicted Two-Dimensional Soil Temperature Distributions under a Row Crop. Soil Sci Soc. Am. J 48: 1147-1152.

Horton, R., 1989 Canopy Shading Effects on Soil Heat and Water Flow. Soil Sci Soc. Am. J 53: 669-679.

Horton, R., O. Aguirre-Luna, and P J Wierenga, 1984b Soil Temperature in a Row Crop with Incomplete Surface Cover Soil Sci Soc Am. J 48 1225-1232.

Huband, N D S , 1985. An Infrared Radiometer for Measuring Surface Temperature in 'the Field Part II Calibration and Performance. Agric For. Meteorol., 34: 227-233.

Huband, N D S., 1985. An Infrared Radiometer for Measuring Surface Temperature in 'the Field. Part I Design and Construction. Agric. For Meteorol , 34 215-226.

Humes, K S , W P Kustas, M S. Moran, W D Nichols, and M A. Weltz, 1994 Variability of Emissivity and Surface Temperature over a Sparsely Vegetated Surface Water Resourc Res 30(5): 1299-1310

Humes, K S., W P. Kustas, and M.S. Moran, 1994. Use of Remote Sensing and Reference Site Measurements to Estimate Instantaneous Surface Energy Balance Components over a Semiarid Rangeland Watershed. Water Resourc. Res 30(5) 1363-1373.

Idso, S.B , T.J Schmugge, R.D. Jackson, and R J. Reginato, 1975a. The Utility of Surface Temperature Measurements for the Remote Sensing of Surface Soil Water Status J. Geophy. Res., 80(21), 3044-3049.

Idso, S.B., 1981 A Set of Equations for Full Spectrum and 8- to 14-μm and 10.5- to 12.5-μm Thermal Radiation from Cloudless Skies Water Resourc Res , 17(2), 295-304.

Idso, S.B., 1982. Non-Water-Stressed Baselines: A Key to Measuring and Interpreting Plant Water Stress. Agric. Meteorol., 27: 59-70.

Idso, S.B., R.D. Jackson, P.J. Pinter, Jr., R.J. Reginato, and J.L. Hatfield, 1981. Normalizing the Stress-Degree-Day Parameter for Environmental Variability. Agric. Meteorol., 24: 45-55

Idso, S.B., R.D. Jackson, R.J. Reginato, B.A. Kimball, and F.S. Nakayama, 1975b The Dependence of Bare Soil Albedo on Soil Water Content. J. Appl. Meteorol. 14, 109-113.

Idso, S.B. and R.J. Reginato, 1974. Assessing soil water status via albedo measurements. Proceedings Arizona Section of the American Water Resources Association and Hydrology section of the Arizona Academy of Science.

Ijjas, G. and Y.S. Rao, 1992. Passive microwave remote sensing of soil moisture from aircraft in Hungary. International Journal of Remote Sensing, 13, 471-479.

Jackson, T.J. and T.J. Schmugge, 1989. Passive microwave remote sensing for soil moisture: some supporting research. I.E.E.E. Transactions on Geoscience and Remote Sensing. GE-27, 225-235.

Jackson, R.D. and D. Kirkham, 1958. Method of measurement of the real thermal diffusivity of moist soil. Soil Sci. Soc. Am. Proc. 22: 479-482.

Jackson, T.J., 1993. Measuring surface soil moisture using passive microwave remote sensing, Hydrological Processes, 7: 139-152.

Jackson, T.J., 1980. Profile soil moisture from surface measurements J. Irrig. Drainage Div. ASCE, 106: 81-92.

Jackson, T.J., M.E. Hawley, and P.E. O'Neil, 1987. Preplanting soil moisture using passive microwave sensors. Water Resourc. Bull., 23(1): 11-19

Jackson, R.D., R.J. Reginato, and S.B. Idso, 1977. Wheat Canopy Temperature: A Practical Tool for Evaluating Water Requirements. Water Resourc. Res., 13(3). 651-656.

Jackson, R.D., S.B. Idso, R.J. Reginato, and P.J. Pinter, Jr., 1981. Canopy Temperature as a Crop Water Stress Indicator. Water Resourc. Res., 17(4), 1133-1138.

James, M.L., G.M. Smith, and J.C. Wolford, 1977. Applied numerical methods for digital computation with FORTRAN and CSMP. Harper and Row Publishers, New York.

John, B., 1992. Soil moisture detection with airborne passive and active microwave sensors. International Journal of Remote Sensing, 13, 481-491.

Jury, W.A. and B. Bellantuoni, 1976b. Heat and water movement under surface rocks in a field soil: II. Moisture effects. Soil Sci. Soc. Am. J. 40. 509-513.

Jury, W.A. and B. Bellantuoni, 1976a. Heat and water movement under surface rocks in a field soil: I. Thermal effects. Soil Sci. Soc. Am. J. 40: 505-509.

Kaaya, A.K., B.M. Msanya, and J.P. Mrema, 1994. Soils and Land Evaluation of Part of the Sokoine University of Agriculture Farm (Tanzania) for Some Crops under Rainfed Conditions. African Study Monographs, 15(2): 97-117.

Kaaya, A.K., 1989. Soil Survey and Land Suitability Evaluation of the Central Part of Sokoine University of Agriculture (SUA) Farm for Rain-fed Crops. M.Sc. Thesis Submitted to SUA, Morogoro, Tanzania.

Kalma, J.D. and D.L.B. Jupp, 1990. Estimating Evaporation from Pasture using Infrared Thermometry: Evaluation of a One-Layer Resistance Model. Agric. For. Meteorol., 51. 223-246.

Kimball, B.A., R.D. Jackson, R.J. Reginato, F.S. Nakayama, and S.B. Idso, 1976. Comparison of Field-Measured and Calculated Soil-Heat Fluxes. Soil Sci. Soc. Am. J., 40, 18-25.

Kluitenberg, G.J. and R. Horton, 1990. Analytical solution for two-dimensional heat conduction beneath a partial surface mulch. Soil Sci. Soc. Am. J. 54: 1197-1206.

Kolev, N.V., K. Penev, Y. Kirkova, B. Krustanov, N. Poushkarov, T. Nazurski, E. Pumenina, G. Kamenov, and C. Levchev, 1994. Remote Sensing and Synchronous Land Surface Measurements for Estimation of Soil Moisture and Temperature. In: Stein, T.I. (ed), *IGARSS'94 (1994 International Geoscience and Remote Sensing Symposium), Surface and Atmospheric Remote Sensing: Technologies, Data Analysis and Interpretation*, California Institute of Technology, Pasadena, California USA, August 8-12, 1994. Volume III, p. 1442-1444.

Kondo, J., N. Saigusa, and T. Sato, 1990. A Parameterization of Evaporation from Bare Soil Surfaces. J. Appl. Meteorol. 29. 385-389.

Kondratyev, K.Ya., V.V. Malentyev, Yu.I. Rabinovich, and E.M. Shulgina, 1977. Passive microwave remote sensing of soil moisture. 11th Symp. on Remote sensing of the environment, Environ. Res. Inst. Mich., Ann Arbor, MI, pp. 1641-1661.

Kostov, K. and T.J. Jackson, 1993. Estimating Profile Soil Moisture from Surface Layer Measurements: A Review. Proceedings of SPIE Symposium on Ground Sensing, Orlando, Florida, April 1993, SPIE 1941, p. 125-136.

Krishnan, A., 1975. Some climatological features of the semi-arid tropical regions of the world. Trans. Intl. Workshop on Farming Systems, ICRISAT, Hyderabad, India, Nov. 18-21, 1974. pp. 53-124.

Kuittinen, R., 1992. Remote sensing for hydrology: Progress and prospects, WMO Operational Hydrology Rep. No. 36.

Lagouarde, J.-P., 1991. Use of NOAA AVHRR data combined with an agrometeorological model for evaporation mapping. Intl. J. Remote Sensing, 9: 1853-1864.

Landsberg, H.E., H. Lippman, K.H. Paffe, and C. Troll 1963. *World maps of climatology*. Springer, Berlin.

Lascano, R.J. and C.H.M. van Bavel, 1983. Experimental Verification of a Model to Predict Soil Moisture and Temperature Profiles. Soil Sci. Soc. Am. J. 47: 441-448.

Lin, J.D., 1980. On the Force-Restore Method for Prediction of Ground Surface Temperature. J. Geophysical Res., 85, No. C6, 3251-3254.

Mahrer, Y. and J. Katan, 1981. Spatial Soil Temperature Regime under Transparent Polyethylene Mulch. Numerical and Experimental Studies. Soil Science, 131(2): 82-87.

Mahrer, Y., 1982. A Theoretical Study of the Effect of Soil Surface Shape upon the Soil Temperature Profile. Soil Sci. 134: 381-387.

Makungu, P.S.J.J., 1991. Prediction of Tillage Parameters for Moisture Conservation in the Semi-arid Tropics. PhD Thesis Submitted to the University of Newcastle upon Tyne, U.K.

Mattikalli, N.M., E.T. Engman, L.R. Ahuja, K. Johnsen, and T.J. Jackson, 1996. Spatial variability of saturated soil hydraulic conductivity derived from remotely-sensed data. In: Stewart, J.B., E.T. Engman, R.A. Feddes, and Y. Kerr (eds.). Scaling up in Hydrology using Remote Sensing. John Wiley & Sons, Chichester, pp. 194-205.

McCann, I.R., D.C. Kincaid, and D. Wang, 1992. Operational Characteristics of the Watermark Model 200 Soil Water Potential Sensor for Irrigation Management. Applied Engineering in Agriculture 8(5): 603-609.

McCumber, M.C. and R.A. Pielke, 1981. Simulation of the Effects of Surface Fluxes of Heat and Moisture in a Mesoscale Numerical Model. I. Soil Layer. J. Geophy. Res., 86(C10): 9929-9938.

Menenti, M., W.G.M. Bastiaanssen and D. Van Eick, 1989a. Determination of hemispherical reflectance with Thematic Mapper measurements. Final Workshop NASA TM Science Program, Remote Sensing Environment (special issue) 28, 327-337.

Menenti, M., 1983. A new geophysical approach using remote sensing techniques to study groundwater table depths and regional evaporation from aquifers in deserts. ICW Rep. 9 Wageningen, Netherlands.

Menenti, M., W.G.M. Bastiaanssen, D. Van Eick, and M.H. Abd El Karim, 1989b. Linear relationships between surface reflectance and temperature and their application to map actual evaporation of groundwater. Adv. Space Res., Vol 9(1), 165-176.

Menenti, M., and B.J. Choudhury, 1993. Parameterization of Land Surface Evaporation by means of Location Dependent Potential Evaporation and Surface Temperature Range. In: Bolle, H.J., R.A. Feddes, and J.D. Kalma (eds), *Exchange Processes at the Land Surface for a Range of Space and Time Scales*, IAHS Publ. No. 212, pp. 561-575.

Miller, W. and E. Millis, 1989. Estimating evapotranspiration from Utah's Great Salt Lake using thermal infrared satellite imagery. Water Resources Bulletin, 25(3): 541-550.

Milly, P.C.D. and J. Kabala, 1986. "Integrating Modeling and Remote Sensing of Soil Moisture," in *Hydrologic Applications of Space Technology (Proc. Cocoa Beach Workshop*, FL, Aug. 1985), IAHS Publ. 160, pp. 331-339.

Milly, P.C.D., 1982. Moisture and Heat Transport in Hysteretic, Inhomogeneous Porous Media: A Matric Head-Based Formulation and a Numerical Model. Water Resourc. Res., 18(3), 489-498.

Milly, P.C.D., 1984. A Linear Analysis of Thermal Effects on Evaporation from Soil. Water Resourc. Res., 20(8), 1075-1085.

Milly, P.C.D. and P.S. Eagleson, 1982. Parameterization of moisture and heat fluxes across the land surface for use in atmospheric general circulation models. Tech. Rep. No. 279. Ralph M. Parsons Lab., Dept. Civil Eng., Mass. Inst. of Technology, Cambridge.

Milly, P.C.D. and P.S. Eagleson, 1980. The coupled transport of water and heat in a vertical soil column under atmospheric excitation. Report No. 258, Ralph M. Parsons Laboratory for Water Resources and Hydrodynamics, Dept. of Civil Engineering, Massachusetts Institute of Technology.

Mkrtchjan, F.A., E.A. Reutov, A.M. Shutko, K.G. Kostov, M.A. Michalev, N.M. Nedeltchev, A.Y. Spasov, and B.I. Vichev, 1988. Microcomputer-based radiometer data acquisition and processing system for large area mapping of soil moisture content in the top one metre layer. Proc. IGARSS '88 Symp., Edinburgh, 13-16 September 1988. ESA Publication Division, ESTEC, Nordwijk, pp. 1563-1564.

Mohanty, B.P., P.J. Shouse, and M.T. van Genuchten, 1998. Spatio-temporal dynamics of water and heat in a field soil. Soil & Tillage Research, 47: 133-143.

Monin, A.S. and A.M. Obukhov, 1954. Dimensionless characteristics of turbulence in the surface layer. Akad. Nauk. SSSR Geofiz. Inst. Tr. 24: 163-187.

Moran, M.S., T.R. Clarke, W.P. Kustas, M.A. Weltz, and S.A. Amer, 1994. Evaluation of Hydrologic Parameters in a Semiarid Rangeland Using Remotely Sensed Spectral Data. Water Resourc. Res., 30: 5, 1287-1297.

Moran, M.S., W.P. Kustas, A. Vidal, D.I. Stannard, J.H. Blanford, and W.D. Nichols, 1994. Use of Ground-Based Remotely Sensed Data for Surface Energy Balance Evaluation of a Semiarid Rangeland. Water Resourc. Res. 30(5): 1339-1349.

Moran, M.S., A.F. Rahman, J.C. Washburne, D.C. Goodrich, M.A. Weltz, and W.P. Kustas, 1996. Combining the Penman-Monteith Equation with Measurements of Surface Temperature and Reflectance to Estimate Evaporation Rates of Semiarid Grassland. Agric. For. Meteorol., 80: 87-109.

Msanya, B.M. and J.P. Magoggo, 1993. Review of Soil Surveys (Soil Resource Inventories) in Tanzania. *Ecology and Development Paper No.6*, Ecology and Development Programme, Agricultural University of Norway.

Mualem, Y., 1976. A New Model for Predicting the Hydraulic Conductivity of Unsaturated Porous Media. Water Resourc. Res. 12(3): 513-522.

Mualem, Y., 1976b. Hysteretical model for prediction of the hydraulic conductivity of unsaturated porous media. Water Resourc. Res. 12, 1248-1254.

Mualem, Y., 1976a. A new model for predicting the hydraulic conductivity of unsaturated porous media. Water Resourc. Res. 12, 513-522.

Murray, F.W., 1967. On the Computation of Saturation Vapor Pressure. J. Appl. Meteorol. 6 203-204.

Myhre, B.E. and S.F. Shih, 1990. Using Infrared Thermometry to Estimate Soil Water Content for a Sandy Soil. Transactions of the ASAE, 33(5), 1479-1486.

Nash, M.S., P.J. Wierenga, and A. Gutjahr, 1991. Time Series Analysis of Soil Moisture and Rainfall along a Line Transect in Arid Rangeland. Soil Science 152(3): 189-198.

Nassar, I.N. and R. Horton, 1989a. Water transport in unsaturated nonisothermal salty soil: I. Experimental results. Soil Sci. Soc. Am. J. 53: 1323-1329.

Nassar, I.N. and R. Horton, 1989a. Water transport in unsaturated nonisothermal salty soil: II. Theoretical development. Soil Sci. Soc. Am. J. 53. 1330-1337.

Newton, R.W., J.L. Heilman, and C.H.M. van Bavel, 1983. Integrating Passive Microwave Measurements with a Soil Moisture/Heat Flow Model. Agric. Water Management 7. 379-389.

Newton, R.W., Q.R. Black, S. Makanvand, A.J. Blanchard, and B.R. Jean, 1982. Soil moisture information and thermal microwave emission. IEEE Trans. Geosci. Remote Sensing, GE-20 275-281.

Nieuwenhuis, G.J.A., 1986. "Integration of Remote Sensing with a Soil Water Balance Simulation Model (SWATRE)," in *Hydrologic Applications of Space Technology (Proc. Cocoa Beach Workshop*, FL, Aug. 1985), IAHS Publ. 160, pp. 119-128.

Nieuwenhuis, G.J.A., 1986b. Integration of remote sensing with a water balance simulation model (SWATRE), ICW Tech. Bulletins 59, Wageningen, Netherlands.

Nieuwenhuis, G.J.A., 1985. Integration of remote sensing with a soil water balance simulation model (SWATRE). Paper presented at International Workshop on Hydrologic Applications of Space Technology, August 1985, Florida.

Nieuwenhuis, G.J.A., 1986a. Thermography: Principles and application in the Oost-Gelderland remote sensing study project, ICW Tech. Bulletins 55, Wageningen, Netherlands.

Njoku, E.G., S.J. Hook, and A. Chehbouni, 1996. Effects of surface heterogeneity on thermal remote sensing of land parameters. In: Stewart, J.B., E.T. Engman, R.A. Feddes, and Y. Kerr (eds.). Scaling up in Hydrology using Remote Sensing. John Wiley & Sons, Chichester, pp. 19-37.

Norman, J.M. and F. Becker, 1995. Terminology in Thermal Infrared Remote Sensing of Natural Surfaces. Agric. For. Meteorol. 77: 153-166.

Norman, J.M., M. Divakarla, and N.S. Goel, 1995. Algorithms for Extracting Information from Remote Thermal-IR Observations of the Earth's Surface. Remote Sensing of Environment 51(1) 157-168.

Ottlé, C., D. Vidal-Madjar, and G. Girard, 1989. Remote sensing applications to hydrological modelling. Journal of Hydrology, 105: 369-384.

Ottlé, C., D. Vidal-Madjar, A.L. Cognard, C. Loumagne, and M. Normand, 1996. Radar and optical remote sensing to infer evapotranspiration and soil moisture. In: Stewart, J.B., E.T. Engman, R.A. Feddes, and Y. Kerr (eds.). Scaling up in Hydrology using Remote Sensing. John Wiley & Sons, Chichester, pp. 221-233.

Ottlé, C. and D. Vidal-Madjar, 1994. Assimilation of Soil Moisture Inferred from Infrared Remote Sensing in a Hydrological Model over the HAPEX-MOBILHY Region. Journal of Hydrology 158: 241-264.

Ottlé, C., D. Vidal-Madjar, and G. Girard, 1989. Remote Sensing Applications to Hydrological Modeling. Journal of Hydrology 105: 369-384.

Parlange, M.B., A.T. Cahill, D.R. Nielsen, J.W. Hopmans, and O. Wendroth, 1998. Review of heat and water movement in field soils. Soil & Tillage Research, 47: 5-10.

Parlange, M.B., G.G. Katul, R.H. Cuenca, M.L. Kavvas, D.R. Nielsen, and M. Mata, 1992. Physical Basis for a Time Series Model of Soil Water Content. Water Resourc. Res., 28(9), 2437-2446.

Parton, W.J., 1984. Predicting soil temperatures in a shortgrass steppe. Soil Sci. 138: 93-101.

Paulson, C.A., 1970. The Mathematical Representation of Wind Speed and Temperature Profiles in the Unstable Atmospheric Surface Layer. J. Appl. Meteorol. 9: 857-861.

Pennington, D.A. and L. Heatherly, 1989. Effects of Changing Solar Radiation on Canopy-Air Temperatures of Cotton and Soybean. Agric. For. Meteorol., 46: 1-14.

Perera, L.K. and R. Tateishi, 1995. Do Remote Sensing and GIS have a Practical Applicability in Developing Countries? (Including Some Sri Lankan Experiences) Int. J. Remote Sensing, 16(1): 35-51.

Perry, E.M., and M.S. Moran, 1994. An Evaluation of Atmospheric Corrections of Radiometric Surface Temperatures for a Semiarid Rangeland Watershed Water Resourc Res 30(5): 1261-1269.

Perry, E.M. and T N. Carlson, 1988. Comparison of Active Microwave Soil Water Content with Infrared Surface Temperatures and Surface Moisture Availability. Water Resourc. Res. 24(10): 1818.

Persaud, N. and A.C. Chang, 1984. Analysis of the stochastic component in observed soil profile temperature. Soil Sci. 138: 326-334

Philip, J.R. and D.A de Vries, 1957. Moisture Movement in Porous Materials under Temperature Gradients. Transactions, American Geophysical Union 38(2): 222-232.

Pratt, D A. and C.D Ellyett, 1979 The Thermal Inertia Approach to Mapping of Soil Moisture and Geology. Remote Sens. Environ. 8. 151-168.

Press, W H , B.P. Flannery, S.A. Teukolsky, and W T. Vetterling, 1988. *Numerical recipes: The art of scientific computing*. Cambridge University Press, Cambridge. p. 818

Prevot, L , R. Bernard, O. Taconet, D. Vidal-Madjar, and J.L. Thony, 1984. Evaporation from Prevot, L., R Bernard, O. Taconet, D. Vidal-Madjar, and J L. Thony, 1984 Evaporation from a Bare Soil Evaluated using a Soil Water Transfer Model and Remotely Sensed Surface Soil Moisture Data. Water Resourc. Res , 20(2), 311-316.

Price, J.C., 1989. Quantitative Aspects of Remote Sensing in the Thermal Infrared. In: Asrar, Ghassem (ed), *Theory and Applications of Optical Remote Sensing*, John Wiley & Sons, New York, pp. 578-603.

Price, J.C., 1980 The Potential of Remotely Sensed Thermal Infrared Data to Infer Surface Soil Moisture and Evaporation. Water Resourc Res., 16(4), 787-795

Raes, D , 1982. A summary simulation model of the water budget of a cropped soil (BUDGET). PhD thesis. Laboratory of Land Management. K.U. Leuven, Belgium, p. 110.

Ragab, R. And J.D. Cooper, 1993. Variability of Unsaturated Zone Water Transport Parameters: Implications for Hydrological Modelling. 2. Predicted vs. In Situ Measurements and Evaluation of Methods Journal of Hydrology 148: 133-147.

Ragab, R., 1995. Towards a Continuous Operational System to Estimate the Root-Zone Soil Moisture from Intermittent Remotely Sensed Surface Moisture. Journal of Hydrology 173. 1-25.

Ragab, R And J D. Cooper, 1993 Variability of Unsaturated Zone Water Transport Parameters: Implications for Hydrological Modelling. 1 In Situ Measurements. Journal of Hydrology 148: 109-131.

Ragab, R , 1992. Assessment of the relationship between remotely sensed topsoil moisture content and profile moisture content. In: Eley, F.J. (ed), Soil moisture modelling and monitoring for regional planning, Environment Canada, Saskatoon, Sask., pp 141-154.

Rango, A., 1990 Remote sensing of water resources: accomplishments, challenges, and relevance to global monitoring. Proc. Intl Symp Remote sensing and water resources, Enschede, 3-16.

Rango, A., 1987. New technology for hydrological data acquisition and applications. Proc. Rome symposium, April, 1987, IAHS Publication No 164, pp 511-517.

Rawls, W J , D L Brakensiek, and K.E Saxton, 1982. Estimation of Soil Water Properties. Transactions of the ASAE, 25: 1316-1320

Rawls, W J , T.J. Gish, and D L Brakensiek, 1991. Estimating soil water retention from soil physical properties and characteristics In Stewart, B A (ed), Advances in Soil Science. Volume 16. Springer-Verlag, New York. pp 213-234

Rawls, W J and D L. Brakensiek, 1989 Estimation of soil water retention and hydraulic properties In: H J. Morel-Seytoux (ed), Unsaturated flow in hydrologic modelling theory and practice NATO ASI Series, Series c Mathematical and physical science, Vol. 275. Kluwer Academic, Dordrecht, pp. 275-300

Reginato, R.J , S.B Idso, J.F. Vedder, R.D Jackson, M.B Blanchard, and R Goettelman, 1976. Soil Water Content and Evaporation Determined by Thermal Parameters Obtained from Ground-Based and Remote Measurements. J Geophy Res., 81(9): 1617-1620.

Reutov, E.A and A M Shutko, 1986 Prior-knowledge based soil-moisture determination by microwave radiometry. Sov. J. Remote Sensing, 5(1): 100-125.

Robinson, J.M. and K.G. Hubbard, 1990. Soil water assessment model for several crops in the High Plains. Agron J. 82: 1141-1148.

Rosema, A., 1981. Thermal sensing of soil moisture, evaporation and crop yield In. Berg, A (ed) Application of remote sensing to agricultural production forecasting, A.A. Balkema, Rotterdam, 213-233.

Rosema, A , 1986. Results of the Group Agromet Monitoring Project (GAMP), ESAJ., 10: 17-41.

Rosema, A., 1990. Comparison of Meteosat-based rainfall and evapotranspiration mapping in the Sahel region, Intl J. Remote Sensing, 12: 2299-2309.

Ryan, J.G. M. von Oppen., K.V. Subrahmanyam, and M Asokan, 1974. Socio-economic aspects of agricultural development in the semi-arid tropics. International Workshop on Farming Systems. ICRISAT, Patancheru, AP, India, November, 1979

Saha, S.K., 1995. Assessment of Regional Soil Moisture Conditions by Coupling Satellite Sensor Data with a Soil-Plant System Heat and Moisture Balance Model. Int. J. Remote Sensing 16(5): 973-980.

Salisbury, J.W. and D.M. D'Aria, 1992. Emissivity of terrestrial materials in the 8-14 μm atmospheric window. Remote sensing Environment, 42: 83-106.

Sanchez, P.A., 1976. *Properties and Management of Soils in the Tropics*. John Wiley & Sons, New York, 618 pp.

Schaap, M.G., F.J. Leij, and M.Th. Van Genuchten, 1998 Neural network analysis for hierarchical prediction of soil hydraulic properties Soil Sci Soc. Am J 62: 847-855

Schmugge, T.J., F. Becker, and Z.-L. Li, 1991. Spectral emissivity variations observed in airborne surface temperature measurements. Remote sensing Environment, 35. 95-104.

Schmugge, T.J., T.J. Jackson, and H.L. McKim, 1980. Survey of Methods for Soil Moisture Determination. Water Resourc. Res., 16(6), 961-979.

Schmugge, T., 1978. Remote Sensing of Surface Soil Moisture. J Appl. Meteorol 17: 1549-1557.

Schmugge, T., 1990. Measurements of Surface Soil Moisture and Temperature In Hobbs, R.J., and H.A. Mooney (eds), *Remote Sensing of Biosphere Functioning* (Ecological Studies 79) Springer-Verlag, 1990. p 31- 63.

Schmugge, T.J., 1980. Microwave Approaches in Hydrology Photogram. Eng. and Remote Sensing, 46: 495-507.

Schmugge, T.J., E.G. Njoku, E Peack, and F.T. Ulaby, 1978. Microwave and gamma radiation observations of soils misture *Soil moisture workshop* (Johnson Space Centre, Pasadena: NASA), pp. 2073- 2084

Schmugge, T., 1985. Remote sensing of soil moisture. In: Anderson, M.G. and T.P. Burt (eds). Hydrological forecasting. John Wiley & Sons, pp. 101-124

Schmugge, T.J. and T.J. Jackson, 1996. Soil moisture variability. In: Stewart, J.B., E.T. Engman, R.A. Feddes, and Y. Kerr (eds.). Scaling up in Hydrology using Remote Sensing. John Wiley & Sons, Chichester, pp. 183-192.

Schmugge, T., P. O'Neill, and J.R. Wang, 1986. Passive microwave soil moisture research. *IEEE Trans.* Geosci. Remote Sensing, G7-24(1): 12-22.

Schultz, G.A., 1988. Remote sensing in hydrology. Journal of Hydrology, 100: 239-265.

Schultz, G.A. and E.C. Barrett, 1989. Advances in remote sensing for hydrology and water resources management. IHP-III Project 5.1.b., UNESCO, Paris.

Schultz, G.A., 1989. Remote sensing of watershed characteristics and rainfall input. In: Morel-Seytoux, H.J. (ed). Unsaturated flow in hydrologic modelling: Theory and practice, Kluwer Academic Publication, pp. 301-323.

Seguin, B., M. Savane, and B. Guillot, 1990. Estimation of large area evaporation from thermal infrared meteorological satellite data: A case study with Meteosat and NOAA for France. Proc. Intl. Symp. Remote sensing and water resources, Enschede, 215-228.

Seguin, B. and B. Itier, 1983. Using midday surface temperature to estimate daily evaporation from satellite thermal IR data. Int. J. Remote Sensing, 4(2), 371-383.

Serafini, Y.V., 1987. Estimation of the evapotranspiration using surface and satellite data. Intl. J. Remote Sensing, 8(10): 1547-1562.

Shao, M. and R. Horton, 1998. Integral method for estimating soil hydraulic properties. Soil Sci. Soc. Am. J. 62: 585-592.

Sheets, K.R. and J.M.H. Hendrickx, 1995. Noninvasive Soil Water Content Measurement Using Electromagnetic Induction. Water Resourc. Res. 31(10): 2401.

Shih, S.F. and J.D. Jordan, 1992. Landsat Mid-Infrared Data and GIS in Regional Surface Soil Moisture Assessment. Water Resources Bulletin, 28(4), 713-719.

Shih, S.F., D.S. Harrison, A.G. Smajstrla, and F.S. Zazueta, 1986. Using Infrared Thermometry Data in Soil Water Content Estimation. ASAE Paper No. 86-2121.

Smith, R.C.G., S.A. Prathapar, H.D. Barrs, and P. Slavich, 1989. Use of a Thermal Scanner Image of a Water Stressed Crop to Study Soil Spatial Variability. Remote Sens. Environ. 29:111-120.

Smith, M.R. and R.W. Newton, 1983. The prediction of root zone soil moisture with a water balance-microwave emission model. AgRISTARS Rep. SM-T3-04425.

Smith, R.C.G., H.D. Barrs, and J.L. Steiner, 1986. Alternative models for predicting the foliage-air temperature difference of well irrigated wheat. I. Derivation of parameters. II. Accuracy of predictions. Irrigation Science, 7, 225-236.

Soares, J.V., R. Bernard, and D. Vidal-Madjar, 1987. Spatial and temporal behaviour of a large agricultural area as observed from airborne C-band scatterometer and thermal infrared radiometer. International Journal of Remote Sensing, 8, 981-996.

Soarés, J.V., R. Bernard, O. Taconet, D. Vidal-Madjar, and A. Weill, 1988. Estimation of Bare Soil Evaporation from Airborne Measurements. Journal of Hydrology 99: 281-296

Soer, G.J.R., 1977. The Tergra Model - A Mathematical Model for the Simulation of Daily Behaviour of Crop Surface Temperature and Actual Evapotranspiration (Delft, Netherlands). Netherlands Interdepartmental Working Community for the Application of Remote Sensing Techniques (NIWARS).

Soer, G.J.R., 1980. Estimation of Regional Evapotranspiration and Soil Moisture Conditions Using Remotely Sensed Crop Surface Temperatures. Remote Sens. Environ. 9: 27-45.

Soil Survey Staff, 1975. *Soil Taxonomy, Agric. Handbook No. 436*, USDA U.S. Government Printing Office: Washington, D.C.

Sophocleous, M., 1979. Analysis of water and heat flow in unsaturated-saturated porous media. Water Resourc. Res., 15, 1195-1206.

Spaans, E.J.A. and J.M. Baker, 1992. Calibrating of Watermark Soil Moisture Sensors for Soil Matric Potential and Temperature. Plant and Soil. 143: 213-217.

Stafford, J.V., 1988. Remote, Non-contact and in-situ Measurement of Soil Moisture Content: A Review. J. agric. Engng Res., 41, 151-172.

Stroosnijder, L., R.J. Lascano, R.W. Newton, and C.H.M. van Bavel, 1984. Estimating net rainfall, evaporation and water storage of a bare soil from sequential L-band emissivities. Proc. IGARSS'84 Symposium, Strasbourg 27-30 August 1984.

Su, Z., 1996. *Remote Sensing Applied to Hydrology: The Sauer River Basin Study*. Schriftenreihe 15, Hydrologie/Wasserwirtschaft, Ruhr-Universitat Bochum. pp. 190.

Swindale, L.D., 1982. Distribution and use of arable soils in the semi-arid tropics. In: *Managing Soil Resources, Plenary Session Papers, Trans. 12th Intl. Congr. Soil Sci.*, New Delhi. pp. 67-100.

Taconet, O., T. Carlson, R. Bernard, and D. Vidal-Madjar, 1986. Evaluation of a Surface/Vegetation Parameterization using Satellite Measurement of Surface Temperature. J. Climate and Appl. Meteorol. 25: 1752-1767.

Taconet, O., A. Olioso, M. Ben Mehrez, and Brisson, 1995. Seasonal Estimation of Evaporation and Stomatal Conductance over a Soybean Field Using Surface IR Temperatures. Agric. For. Meteorol., 73: 321-337.

Takakura, T., K.A. Jordan, and L.L. Boyd, 1971. Dynamic simulation of plant growth and environment in the greenhouse. Trans. ASAE 14: 964-971

Tappan, G G., D.G. Moor, and W I Knausenberger, 1991. Monitoring grasshopper and locust habitats in Sahelian Africa using GIS and remote sensing technology. International Journal of Geographical Information Systems, 5, 123-135.

Ten Berge, H F.M., L Stroosnijder, P.A Burrough, A K Bregt, and M J. de Heus, 1983. Spatial Variability of Physical Soil Properties Influencing the Temperature of the Soil Surface Agric. Water Management, 6, 213-226

Ten Berge, H.F M , 1990. *Heat and Water Transfer in Bare Topsoil and the Lower Atmosphere* Wageningen: Pudoc -111. - (Simulation Monographs ISSN 0924-8439, 33).

Thadei, S.Y., 1992 Evaluation of Effective Rainfall by a Physically-Based Soil-Water Balance Model PhD Thesis Submitted to the University of Newcastle upon Tyne, U.K

Thomas, G.W , R.L. Blevins, and S H Phillips, 1984 No-tillage in the tropics In R E Phillips and S H. Phillips (eds) No-tillage agriculture Principles and practices. Van Nostrand Reinhold Co Inc. New York, N Y., pp. 270-301.

Thompson, B. 1965. *The climate of Africa* Oxford University Press, London

Thomson, S J. and C F. Armstrong, 1987 Calibration of the Watermark Model 200 Soil Moisture Sensor. Applied Engineering in Agriculture, 3(2) 186-189

Thomson, S J , T Younos, and K. Wood, 1996 Evaluation of Calibration Equations and Application Methods for the Watermark® Granular Matrix Soil Moisture Sensor. Applied Engineering in Agriculture 12(1) 99-103

Thunholm, B , 1990 A Comparison of Measured and Simulated Soil Temperature using Air Temperature and Soil Surface Energy Balance as Boundary Conditions. Agric For Meteorol., 53.59-72

Thunnissen, H A.M and G.J A Nieuwenhuis, 1989 An Application of Remote Sensing and Soil Water Balance Simulation Models to Determine the Effect of Groundwater Extraction on Crop Evapotranspiration Agric Water Management, 15 315-332.

Topp, G.C., M Watt and H.N. Hayhoe, 1996 Point Specific Measurement and Monitoring of Soil Water Content with an Emphasis on TDR Can J. Soil Sci. 76 307-316.

Troll, C., 1965. Seasonal climates of the Earth In *World maps of climatology*, E. Rodenwaldt and H. Jusatz, eds Springer-Verlag, Berlin

Ulaby, F.T., C.T. Allen, and G Eger, 1984. Relating the microwave backscattering coefficient to leaf area index Remote Sensing Environ , 17: 113-133.

Ulaby, F.T., P.P. Batlivala, and M C Dobson, 1978 Microwave backscattering dependence on surface roughness, soil moisture, and soil texture: Part I - Bare soil. IEEE Trans. Geosci. Electron , GE-16. 286-295.

van de Griend, A A., M. Owe, M. Groen, and M P. Stoll, 1991. Measurement and Spatial Variation of Thermal Infrared Surface Emissivity in a Savanna Environment. Water Resourc. Res. 27(3): 371-379.

Van Oevelen, P.J., D.H. Hoekman, and R A. Feddes, 1996. Errors in estimation of areal soil water content from SAR data. In: Stewart, J.B., E.T. Engman, R A. Feddes, and Y. Kerr (eds.). Scaling up in Hydrology using Remote Sensing. John Wiley & Sons, Chichester, pp. 207-220.

Van Keulen, H. and G.E.M. van Beek, 1971. Water movement in layered soils. A simulation model. Neth. J. Agric. Sci. 19: 138-153.

Van de Griend, A.A., P.J. Camillo, and R.J. Gurney, 1985. Discrimination of Soil Physical Parameters, Thermal Inertia, and Soil Moisture from Diurnal Surface Temperature Fluctuations. Water Resourc. Res., 21(7), 997-1009.

Van Genuchten, M.TH., 1980. A Closed-Form Equation for Predicting the Hydraulic Conductivity of Unsaturated Soils. Soil Sci. Soc. Am. J. 44: 892-898.

Van de Griend, A.A. and J.H. van Boxel, 1989. Water and Surface Energy Balance Model with a Multilayer Canopy Representation for Remote Sensing Purposes. Water Resourc. Res., 25(5), 949-971.

Van Bavel, C.H.M. and D.I. Hillel, 1975. A simulation study of soil heat and moisture dynamics as affected by a dry mulch. In: Proceedings 1975 Summer Computer Simulation Conference, San Francisco, CA, pp. 815-821. Simulation Councils, Inc., La Jolla, California.

Van Bavel, C.H.M. and R. Lascano, 1979. CONSERVB. A numerical method to compute soil water content and temperature profiles under a bare surface.

Van Bavel, C.H.M. and D.I. Hillel, 1976. Calculating potential and actual evaporation from a bare soil surface by simulation of concurrent flow of water and heat. Agric. Meteorol., 17: 453-476.

Vleck, J. and D. King, 1983. Detection of Subsurface Soil Moisture by Thermal Sensing: Results of Laboratory, Close-Range, and Aerial Studies. Photogram. Eng. and Remote Sensing, 49. 1593-1597.

Vyas, A.D., A.J. Trivedi, O.P.N. Calla, S.S. Rana, S.B. Sharma, and A.B. Vora, 1990. Experimental Data for Separation of Vegetation and Soil and Estimation of Soil Moisture using Passive Microwaves. Int. J. Remote Sensing, 11(8), 1421-1438.

Wang, J.R., J.C. Shiue, T.J. Schmugge, and E.T. Engman, 1989. Mapping Surface Soil Moisture with L-Band Radiometric Measurements. Remote Sens. Environ. 27: 305-312.

Wang, J.R., J.C. Shiue, T.J. Schmugge, and E.T. Engman, 1990. The L-band PBMR measurements of surface soil moisture in FIFE. IEEE Trans. Geosci. Remote Sensing, 28(5). 906-914.

Wang, J R , 1987. Passive microwave sensing of soil moisture. the frequency dependence of microwave penetration depth. IEEE Trans Geosci Remote Sensing GE-25: 616-622.

Wanjura, D.F., D.R Upchurch, and J.R. Mahan, 1992 Automated Irrigation based on Threshold Canopy Temperature. Transactions of the ASAE 35(5) 1411-1417.

Wanjura, D.F and D.R Upchurch, 1990. Considerations in Applying Infrared Thermometry to Crop Canopy Temperature Measurement ASAE Paper No. 90-4041.

Wanjura, D F. and D.R. Upchurch, 1991. Infrared Thermometer Calibration and Viewing Method Effects on Canopy Temperature Measurement Agric For. Meteorol., 55, 309-321.

Webb, E K., 1970. Profile relationships The log-linear range, and extension to strong stability Quart. J Roy Meteorol. Soc 96: 67-90

Wetzel, P J. and R H Woodward, 1987 Soil Moisture Estimation Using GOES-VISSR Infrared Data: A Case Study with a Simple Statistical Method. J. Climate Appl Meteor , 26, 107-117.

Wierenga, P.J and C T. De Wit, 1970. Simulation of heat flow in soils Soil Sci. Soc. Am. Proc. 34: 845-848.

Wilheit, T.T., 1978 Radiative transfer in a plane stratified dielectric. IEEE Trans. Geosci Electron. GE-16 138-143

Willmott, C J., 1981. On the validation of models Phys Geogr. 2 184-194

Willmott, C J , 1982. Some comments on the evaluation of model performance Bull. Am Meteorol. Soc 63. 1309-1313

Witono, H and L. Bruckler, 1989 Use of Remotely Sensed Soil Moisture Content as Boundary Conditions in Soil-Atmosphere Water Transport Modeling 1. Field Validation of a Water Flow Model. Water Resourc. Res , 25(12), 2423-2435

Woebbecke, D., A Al-Faraj, and G E. Meyer, 1994. Calibration of Large Field-of-View Thermal and Optical Sensors for Plant and Soil Measurements. TRANSACTIONS of the ASAE, 37(2), 669-677

Wu, L., W.A Jury, A C. Chang, and R.R Allmaras, 1997. Time Series Analysis of Field-Measured Water Content of a Sandy Soil. Soil Sci Soc Am J 61: 736-742.

Wu, Y., K.B Perry, and J.B. Ristaino, 1996 Estimating Temperature of Mulched and Bare Soil from Meteorological Data Agric For Meteorol. 81. 299-323.

Zaidel, J. and D. Russo, 1992. Estimation of finite difference interblock conductivities for simulation of infiltration into initially dry soils Water Resourc. Res. 28, 2285-2295.

Zetterqvist, L., 1991. Statistical estimation and interpretation of trends in water quality time series. Water Resourc. Res., 27: 1637-1648.

Zotova, E.N. and A.G. Geller, 1985. Soil moisture content estimation by radar survey data during the sowing campaign. Int. J. Remote Sensing, 6(2): 353-364.

APPENDIX 1. THE SUAHEAT PROGRAM

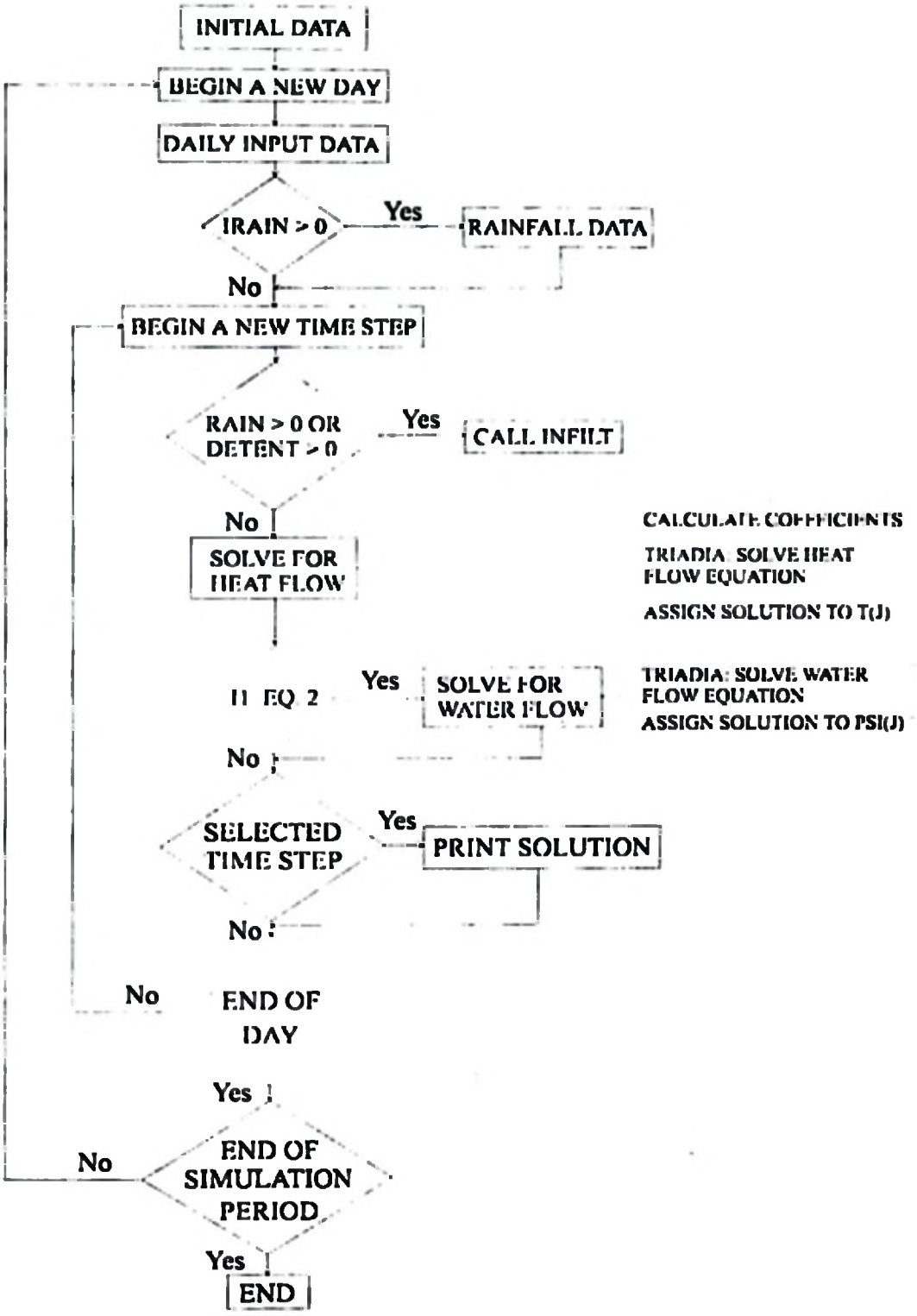

Fig. A1.1 Flow chart of the SUAHEAT program

Table A1.1 User Manual for the SUAHEAT Program

User Manual

Title:	One-dimensional soil heat and water flow model (SUAHEAT).
Programmer:	Baanda A. Salim, Institut fuer Landtechnik, University of Bonn, Germany.
Date:	September, 1998.
Language:	FORTRAN 77.
Computer:	IBM PC or Compatibles.
Potential users:	Soil scientists, soil-water management specialists, and remote sensing scientists.
Description:	Determine soil temperature and water content in the soil profile. Weighted-average profile soil water contents for variable profile depths can also be determined. User can choose from several different options for flow type (heat flow only, or heat and water flow), soil type, and boundary condition input data type. Standard or remote sensing-derived initial conditions for both the profile soil temperature and profile soil water content may be used. Energy balance equation may be used to determine the soil surface boundary conditions. Implicit finite-difference method with explicit linearization is used.
Algorithm:	The conductive soil heat flow equation and the pressure-head based, soil-water flow equation are used in this program. The vapour flow is not included, except at the soil surface. Temperature dependence of both the unsaturated hydraulic conductivity and pressure head are included. The current state of the computer program excludes the stability correction functions. Computational procedure is described in detail in the text.
Modification:	This program can be easily modified. For different flow domain depths, the DIMENSION declaration and input/output FORMAT statements must be modified accordingly. In the current state of the computer program, one can simulate up 150 cm depth using a vertical step size of at least 5 cm or up to 75 cm depth using a vertical step size of at least 2.5 cm. In either case, the maximum number of nodes is 31.
Input:	At least one input data file is needed in this program, depending on whether one uses standard or remote sensing-derived initial conditions. Use of keyboard input format is also possible by modifying the input statements. The SI units are used for the input data. Input data are as follows, see Appendix 2 for description of I's:

Line 1

- I1: Flow indicator
- I2: Soil type indicator
- I3: Input data type indicator
- I4: Temperature top B.C. indicator

I5 Temperature bottom B.C. indicator
I6: Soil water top B.C. indicator
I7: Soil water bottom B.C. indicator
I8: Initial condition indicator (standard or remotely-sensed)
I9. Stability correction functions indicator

Line 2
Depth of flow region
Step size in z-direction
Roughness length, zo

Line 3
Simulation length in days
Time step size in seconds (> 40)

Line 4
Time interval for output in hours

Line 5
Length of daytime in hours
Solar noon in hours

Line 6
Only if (I2 = 4)
Coefficients in soil thermal conductivity Equation
Saturated soil water content
Residual soil water content
Fraction of solid in soil
Fraction of organic matter in soil

Line 7
Only if (I2 = 4)
α_1 , and n in Van Genuchten's (1980) retention Equation
Saturated hydraulic conductivity

Line 8
Temperature initial condition (can be more than one line)

Line 9
Pressure-head or soil water content initial condition (for I1 = 2 only)

Line 10
Rainfall indicators for the simulation days (number of events per day)

Line 11
Top boundary condition for heat flow.
IF (I4 = 1) number of inputs per day and next line has sequential temperature values
IF (I4 = 2) daily maximum and minimum surface temperatures for a day
IF (I4 = 3) weather data for each day

Line 12
Bottom boundary condition for heat flow
IF (I5 = 1) a constant temperature value
IF (I5 = 2) number of inputs per day and next line has sequential temperature values
IF (I5 = 3) computer determines the flux condition

Line 13
Top boundary condition for soil water flow (I1 = 2 only):
IF (I6 = 1) number of inputs per day and next line has sequential pressure

head or soil water content values
IF (I6 = 2) number of inputs per day and next line has sequential flux values in a day
IF (I6 = 3) no data needed

Line 14 — Bottom boundary condition for soil water flow (I1 = 2 only):
IF (I7 = 1) number of inputs per day and next line has sequential pressure head or soil water content values
IF (I7 = 2 or I7 = 3) no input is needed

Line 15 — Rainfall starting time, ending time, and amount if rainfall indicator is not zero (a set for each rain event)

Repeat — Line 11 to Line 15 for each day

Output: The following output data files are generated in this program (all file names are user specified).

1. Soil surface energy partitioning
2. Soil temperature
3. ***Surface soil-minus-air temperature differential (TD)***
4. Regression coefficients - correction for changing solar radiation
5. Soil water content
6. Pressure head
7. ***Weighted-average profile soil water content***
8. Weighted-average profile pressure head
9. Moisture availability. **NB:** (5, 6, 7, 8, and 9 are for I1 = 2 only).

List of files

SUAHEAT.FOR	=	source file
SUAHEAT.OBJ	=	object file
SUAHEAT.EXE	=	executable file
INPUT.DAT	=	input data file (user specified)
OUT1.DAT	=	ouput data file for soil surface energy partitioning (user specified) Line 1. heat flux density and cumulative heat flux of net radiation, sensible heat, latent heat, and soil heat
OUT2.DAT	=	Temperature at each node in the soil (user specified)
OUT3.DAT	=	Surface soil minus air temperature differential (user specified)
OUT4.DAT	=	Regression coefficients (user specified)
OUT5.DAT	=	Soil water content (user specified)
OUT6.DAT	=	Pressure head (user specified)
OUT7.DAT	=	Weighted-average soil water content (user specified)
OUT8.DAT	=	Weighted-average pressure head (user specified)
OUT9.DAT	=	Moisture availability (user specified)

Variable description: See Appendix 2.

Subprogram description:

1. PARAM. Determines the values of soil parameters for a given representative soil type.

2. TRIDIA: Solves tridiagonal matrix problem without pivotting. Thomas algorithm, which is a special case of Gauss elimination method, is used in this subroutine and the diagonally dominant matrices are safe (Press et al., 1988, p. 40).

3 STORE. Determines volume of soil water stored in the one-dimensional flow region.

4. COEFNT: Computes the coefficient values in the flow equations.

5. BARE. Determines soil surface temperature and evaporation rate on the bare soil surface by using the energy balance equation. The bisect root-finding method is used in this subroutine and computation is done by iteratively calling subroutine BISEC

6 BISEC Computes residual in the energy balance equation at the bare soil and atmospheric interface

7 INFILT: Determines soil surface infiltration rate using a Darcy's law-based flow equation

8 RAINFL Determines rainfall amount during each time step period.

9. STABIL Calculate stability correction parameters

How to run:

1. Boot on.
2. Insert or copy SUAHEAT EXE file in the default disk drive.
3. Type SUAHEAT on the keyboard and return, then supply file names as indicated
4. Outputs will be displayed on the screen and stored on the diskette/hard disk in the user specified drive.

Example input and output files:

Example of input and output files for the SUA Field experiments are used for illustration. A 75-day long simulation of heat and water flow was performed. A one-hour time interval was used for output printing. Weather data were used for the soil-surface boundary condition. Measured lower boundary temperature was used for each day. Measured soil water content data were used for the bottom boundary condition for each day. No data were input for the top boundary conditions for soil water flow.

APPENDIX 2: VARIABLES IN SUAHEAT PROGRAM

VARIABLE	DESCRIPTION		
AALPA	COEFFICIENT ALPHA IN THE VAN GENUCHTEN'S RETENTION EQUATION		
ALES	LATENT HEAT FLUX DENSITY		
ALECUM	CUMULATIVE LATENT HEAT FLUX		
ALH	VOLUMETRIC LATENT HEAT OF VAPORIZATION		
ALPA	SOIL THERMAL DIFFUSIVITY		
B1, B2, B3	COEFFICIENTS IN THE SOIL THERMAL CONDUCTIVITY EQUATION		
CAPA	VOLUMETRIC SOIL HEAT CAPACITY		
COEF	ELEMENTS OF TRIDIAGONAL MATRIX		
COND	HYDRAULIC CONDUCTIVITY		
CONDS	SATURATED HYDRAULIC CONDUCTIVITY		
DAYL	DAY LENGTH		
DELZ	SPACE STEP SIZE IN Z-DIRECTION		
DELT	TIME STEP SIZE ADJUSTED FOR A RAINSTORM		
DETENT	WATER DETENTION DEPTH ON THE SOIL.		
DETMAX	MAXIMUM VALUE OF WATER DETENTION		
DWDP	SPECIFIC WATER CAPACITY		
EMIS	EMISSIVITY OF SURFACE		
EN	COEFFICIENT 'N' IN VAN GENUCHTEN'S RETENTION EQUATION		
FILE1	NAME OF ENERGY PARTITIONING OUTPUT FILE		
FILE2	NAME OF TEMPERATURE OUTPUT FILE		
FILE3	NAME OF WATER CONTENT OUTPUT FILE		
FILE4	NAME OF PRESSURE HEAD OUTPUT FILE		
FILE5	NAME OF AVERAGE WATER CONTENT FILE		
FILE6	NAME OF TEMPERATURE DIFFERENCE FILE		
FILE7	NAME OF REGRESSION COEFFICIENTS FILE		
FILE8	NAME OF AVERAGE PRESSURE HEAD FILE		
FILE9	NAME OF MOISTURE AVAILABILITY FILE		
FILE10	NAME OF CALCULATED INITIAL TEMP. & SWC OUTPUT FILE		
FLUX1	WATER FLUX BOUNDARY CONDITION ACROSS SOIL SURFACE		
GS	SOIL HEAT FLUX DENSITY		
GSCUM	CUMULATIVE SOIL HEAT FLUX		
HA	ABSOLUTE HUMIDITY OF AIR		
I1	FLOW INDICATOR		1 FOR HEAT FLOW ONLY 2 FOR HEAT AND WATER FLOW
I2	SOIL TYPE INDICATOR		1 SAND 2 LOAM 3 CLAY 4 USER SUPPLIED SOIL TYPE
I3	INPUT DATA TYPE.		1 PRESSURE HEAD 2 WATER CONTENT
I4	TEMP TOP B.C..	1	READ SEQUENTIAL TEMP VALUES FOR A DAY
		2	READ DAILY MAX AND MIN TEMP
		3	READ DAILY WEATHER DATA AND USE ENERGY BALANCE EQUATION
I5	TEMP BOTTOM B.C .	1	READ CONSTANT VALUE
		2	READ SEQUENTIAL TEMP VALUES FOR A DAY
		3	FLUX BOUNDARY - CALCULATED BY COMPUTER PROGRAM
I6	WATER TOP B.C :	1	READ SEQUENTIAL THETA OR PSI FOR A DAY

		2	READ SEQUENTIAL FLUX VALUES FOR A DAY
		3	NO DATA NEEDED. USE ENERGY BALANCE AS OF HEAT FLOW
I7	WATER BOTTOM B C ·	1	READ SEQUENTIAL THETA OR PSI VALUES FOR A DAY
		2	NO FLUX - NO DATA NEEDED
		3	UNIT GRADIENT FLUX - NO DATA NEEDED
I8	INITIAL CONDITIONS	1	MEASURED INITIAL CONDITIONS
		2	REMOTE SENSING-DERIVED INITIAL CONDITIONS
I9	STABILITY CORRECTION	1	EXCLUDE STABILITY
		2	INCLUDE STABILITY CORRECTION FUNCTIONS

IDAY	NUMBER OF SIMULATION DAYS
IDOY	DAY OF THE YEAR
INFIL	FILE NAME FOR THE INPUT FILE
INFIL1	FILE NAME FOR REMOTELY-SENSED TEMPERATURE COEFFICIENTS
INFIL2	FILE NAME FOR REMOTELY-SENSED SOIL WATER COEFFICIENTS
ISTEP	NUMBER OF TIME STEPS IN A DAY
N	NUMBER OF NODES IN THE Z DIRECTION
OMEGA	PERIOD OF SINE FUNCTION USED (2*PI/86400)
ORGAN	FRACTION OF ORGANIC MATTER IN THE SOIL
PSI	PRESSURE HEAD IN M OF WATER
PSIO	PRESSURE HEAD AT THE IMAGINARY POINTS ABOVE SOIL SURFACE
RA	AERODYNAMIC BOUNDARY LAYER RESISTANCE
RHS	RIGHT HAND SIDE OF THE MATRIX
RS	SOIL SURFACE RESISTANCE
RAMDA	SOIL THERMAL CONDUCTIVITY
RGD	DAILY GLOBAL SOLAR RADIATION
RN	NET RADIATION HEAT FLUX DENSITY
RNCUM	CUMULATIVE NET RADIATION HEAT FLUX
SOLID	FRACTION OF SOLID IN THE SOIL
SIGMA	STEFAN-BOLTZMANN CONSTANT
SKY	LONGWAVE SKY IRRADIANCE
SNOON	SOLAR NOON
SH	SENSIBLE HEAT FLUX DENSITY
SHCUM	CUMULATIVE SENSIBLE HEAT FLUX
T	TEMPERATURE
TAIR	AIR TEMPERATURE
TAVE	AVERAGE DAILY AIR TEMPERATURE
TAMP	AMPLITUDE OF DAILY TEMPERATURE VARIATION
TD	SOIL SURFACE MINUS AIR TEMPERATURE DIFFERENCE
TDRN	TD DIVIDED BY RN
TDEW	DEW POINT TEMPERATURE
TDEWA	AVERAGE DAILY DEW POINT TEMPERATURE
TDAMP	AMPLITUDE OF DAILY DEW POINT TEMPERATURE VARIATION
TDRAIN	CUMULATIVE DRAINAGE ACROSS THE BOTTOM BOUNDARY
TEVAP	CUMULATIVE EVAPORATION ACROSS THE TOP BOUNDARY
THETA	VOLUMETRIC WATER CONTENT
THETAS	SATURATION WATER CONTENT
THETAR	RESIDUAL WATER CONTENT
TIME1	TIME INTERVAL OF OUTPUT PRINTING AND STORAGE OF DATA FOR LINE CURVE
TMAX	DAILY MAXIMUM SOIL SURFACE TEMPERATURE
TMIN	DAILY MINIMUM SOIL SURFACE TEMPERATURE
TOL	TOLERANCE
TS	TEMPERATURE ON THE SOIL SURFACE NODES

VKAR	VON KARMAN'S CONSTANT
WSPEED	WIND SPEED
ZO	SOIL SURFACE ROUGHNESS LENGTH
ZM	MEASUREMENT HEIGHT

APPENDIX 3 SUAHEAT PROGRAM LISTING

```
$LARGE
*****************************************************************************
*                                                                           *
*                          SUAHEAT                                          *
*                                                                           *
*                                                                           *
*                    SOIL HEAT AND WATER FLOW MODEL.                        *
*                       September 1998                                      *
*                          by                                               *
*                    Baanda A. Salim                                        *
*           Institut fuer Landtechnik, University of Bonn, Germany          *
*                                                                           *
*                                                                           *
*          THIS PROGRAM SOLVES ONE-DIMENSIONAL TRANSIENT HEAT AND WATER FLOW *
*          PROBLEMS BY USING IMPLICIT FINITE DIFFERENCE METHOD WITH          *
*          EXPLICIT LINEARIZATION.  ONE CAN USE THIS PROGRAM FOR HEAT AND    *
*          WATER FLOW. USERS MAY NEED TO CHANGE DIMENSION DECLARATION        *
*          AND INPUT/OUTPUT FORMAT FOR DIFFERENT FLOW REGION.                *
*                                                                           *
*****************************************************************************
      PROGRAM SUAHEAT6
      IMPLICIT REAL*8 (A-H, O-Z)
      COMMON/WETHFR/SIGMA,TAIR,TDEW,ZO,TOL,DELZ,DELT,SKY,HA,RG,RA,RS,T0
      COMMON/SOIL/THETAS,THETAR,SOLID,ORGAN,CONDS,AALPA,EN,B1,B2,B3,
     $          C3,C5
      COMMON TIME,OMEGA,PI,ZM,VKAR
      DIMENSION COEF(30,3),RHS(30),T(30),RAMDA(30),Z(31)
      DIMENSION THETA(2880),CAPA(2880),ALPA(2880)
      DIMENSION COND(2880),PSI(2880),DWDP(2880),THETAN(2880)
      DIMENSION T1(2880),TN(2880),PSI1(2880),PSIN(2880),FLUX1(2880)
      DIMENSION IRAIN(125),TIMEB(96),TIMEE(96),AMOUNT(96)
      DIMENSION TT1(2880),TTN(2880),PSI11(2880),PSINN(2880)
      DIMENSION THETNN(2880),FLUX11(2880),THET11(2880)
C
      DIMENSION WAVGNT(31),WAV(31),WAVGN(31),WAVGS(31),WAVG(31)
      DIMENSION PAVGNT(31),PAV(31),PAVGN(31),PAVGS(31),PAVG(31)
C
      DIMENSION DTD(96),RND(96),RNEQ(96),TDA(96),TDD(96),AVAILM(31)
      DIMENSION AT(30),BT(30),AW(30),BW(30),TM(30),THETAM(30)
C
      DIMENSION IDOY1(125),SUNHR(125),TENN(30),TENS(30),TENSN(30),
     $          VISCO(30)
C
      CHARACTER*10 INFIL,FILE1,FILE2,FILE3,FILE4,FILE5,FILE6,FILE7,
     $          FILE8,FILE9,FILE10,INFIL1,INFIL2,FILE11,FILE12
C
      WRITE(*,1)
    1 FORMAT(///,25X,'SOIL HEAT AND WATER FLOW MODEL'/)
      WRITE(*,2)
    2 FORMAT(15X,'1-DIMENSIONAL TRANSIENT HEAT AND WATER FLOW PROGRAM')
      WRITE(*,3)
    3 FORMAT(15X,'SOLVE PROBLEM WITH IMPLICIT FINITE DIFFERENCE METHOD')
      WRITE(*,4)
    4 FORMAT(/,35X,'Written by')
      WRITE(*,5)
    5 FORMAT(/,33X,'Baanda A. Salim')
      WRITE(*,6)
    6 FORMAT(//,24X,'SOIL PHYSICS & REMOTE SENSING')
      WRITE(*,7)
    7 FORMAT(26X,'Institut fuer Landtechnik')
```

```
      WRITE(*,8)
    8 FORMAT(31X,'University of Bonn')
      WRITE(*,9)
    9 FORMAT(36X,'D-53115')
      WRITE(*,10)
   10 FORMAT(38X, 'Bonn')
      WRITE(*,11)
   11 FORMAT(26X,'Federal Republic of Germany')
C
C     Open Input and Output Files
C
      WRITE(*,*)' '
   12 FORMAT(A10)
      WRITE(*,*)'Enter Name of the Input File       >'
      READ(*,12)INFIL
      WRITE(*,*)'Enter Name of Energy Partition File >'
      READ(*,12)FILE1
      WRITE(*,*)'Enter Name of Temperature File     >'
      READ(*,12)FILE2
      WRITE(*,*)'Enter Name of Temperature Difference File  >'
      READ(*,12)FILE6
      WRITE(*,*)'Enter Name of Regression Coeff File  >'
      READ(*,12)FILE7
      WRITE(*,*)'Enter Name of Sunshine Hours Input File  >'
      READ(*,12)FILE11
      WRITE(*,*)'Enter Name of Sunshine Hours Output File  >'
      READ(*,12)FILE12
C
C     Open Input and Output Files
C
      OPEN(30,FILE=INFIL,STATUS='OLD')
      OPEN(31,FILE=FILE1,STATUS='NEW')
      OPEN(32,FILE=FILE2,STATUS='NEW')
      OPEN(36,FILE=FILE6,STATUS='NEW')
      OPEN(37,FILE=FILE7,STATUS='NEW')
C
      OPEN(25,FILE=FILE11,STATUS='OLD')
      OPEN(26,FILE=FILE12,STATUS='NEW')
C
C     Read Flow, Soil, and Boundary Conditions Indicators
C
      READ(30,*)I1,I2,I3,I4,I5,I6,I7,I8,I9
C
      IF (I1.EQ.2) THEN
        WRITE(*,*)'Enter Name of Water Content File     >'
        READ(*,12)FILE3
        WRITE(*,*)'Enter Name of Pressure Head File     >'
        READ(*,12)FILE4
        WRITE(*,*)'Enter Name of Average Water Content File  >'
        READ(*,12)FILE5
        WRITE(*,*)'Enter Name of Average Pressure Head File  >'
        READ(*,12)FILE8
        WRITE(*,*)'Enter Name of Moisture Availability File  >'
        READ(*,12)FILE9
        OPEN(33,FILE=FILE3,STATUS='NEW')
        OPEN(34,FILE=FILE4,STATUS='NEW')
        OPEN(35,FILE=FILE5,STATUS='NEW')
```

```
      OPEN(38,FILE=FILE8,STATUS='NEW')
      OPEN(39,FILE=FILE9,STATUS='NEW')
    END IF
C
    IF (I8.EQ.2) THEN
      WRITE(*,*)'Enter Name of Remotely-sensed Temp Coeff File >'
      READ(*,12)INFIL1
      WRITE(*,*)'Enter Name of Remotely-sensed SW Cont Coeff File>'
      READ(*,12)INFIL2
      WRITE(*,*)'Enter Name of Initial Temp & SWC Output File>'
      READ(*,12)FILE10
      OPEN(28,FILE=INFIL1,STATUS='OLD')
      OPEN(29,FILE=INFIL2,STATUS='OLD')
      OPEN(40,FILE=FILE10,STATUS='NEW')
    END IF
C
C   READ SUNSHINE HOURS FOR THE SIMULATION DAYS
C
    READ(25,*)IDAY1
    DO 175 J=1,IDAY1
      READ(25,*) IDOY1(J),SUNHR(J)
      WRITE(26,176) IDOY1(J),SUNHR(J)
175 CONTINUE
176 FORMAT(1X,I4,F6.2)
C
    READ(30,*)ZLENG,DELZ,ZO
    READ(30,*)IDAY,DELT
    READ(30,*)TIME1
    READ(30,*)DAYL,SNOON
C
    WRITE(*,13)I1,I2,I3,I4,I5,I6,I7,I8,I9
    WRITE(*,14)ZLENG
    WRITE(*,15)DELZ
    WRITE(*,16)ZO
    WRITE(*,17)IDAY
    WRITE(*,18)DELT
    WRITE(*,19)TIME1
    WRITE(*,20)DAYL
    WRITE(*,21)SNOON
C
C   Assign Parameter Values
C   Read Length of Flow Region and Spatial Step Size
C   Read Length of Simulation and Time Step Size
C   Read Time in Hours at which Output to be Stored
C   Read Day Length and Solar Noon in Hours
C
 13 FORMAT(1X,'I1 =',I3,5X,'I2 =',I3,5X,'I3 =',I3,5X,'I4 =',I3,
   $     5X,'I5 =',I3,5X,'I6 =',I3,5X,'I7 =',I3,'I8 =',I3,/)
 14 FORMAT(1X,'LENGTH OF FLOW REGION IS',2X,F7.3,' METRE')
 15 FORMAT(1X,'SPATIAL STEP SIZE IS',2X,F7.3,' METRE')
 16 FORMAT(1X,'ZO =',2X,F7.4,' METRE')
 17 FORMAT(1X,'LENGTH OF SIMULATION IS',2X,I4,' DAYS')
 18 FORMAT(1X,'TIME STEP SIZE IS',2X,F7.2,' SECONDS')
 19 FORMAT(1X,'OUPUT TIME INTERVAL IS',2X,F7.2,3X,'HOURS')
 20 FORMAT(1X,'DAY LENGTH IS',2X,F7.3,3X,'HOURS')
 21 FORMAT(1X,'SOLAR NOON IS',2X,F7.3,3X,'HOURS')
C
```

```
      TIME1=TIME1*3600.0D0
      DAYL=DAYL*3600.0D0
      SNOON=SNOON*3600.0D0
      ISTEP=IDNINT(86400.0D0/DELT)
      N=IDNINT(DINT((ZLENG+0.001D0)/DELZ))+1
      NM1=N-1
      OMEGA=7.2722D-5
      SIGMA=5.67D-8
      TOL=0.01D0
      PI=4.0D0*DATAN(1.0D0)
      DETMAX=0.01D0
      DZ2DT=DELZ*DELZ/DELT
      T0=28.75D0
      ZM=2.0D0
      VKAR=0.4D0
C
C     Determine Soil Parameters
C
      CALL PARAM(I2)
*****************************************************************************
C     STEP 1: ASSIGN INITIAL VALUES                                          *
*****************************************************************************
C
      IF (I8 .EQ. 1) THEN
       READ(30,*)(T(J),J=1,N)
       WRITE(*,22)(T(J),J=1,N)
      ELSE
       READ(28,*) TSM
       TM(1) = TSM
       READ(28,*) (AT(J), J=2,N)
       READ(28,*) (BT(J), J=2,N)
       DO 555 J = 2,N
         TM(J) = AT(J) + BT(J)*TM(J-1)
  555  CONTINUE
C
       READ(30,*)(T(J),J=1,N)
       DO 556 J = 1,N
         T(J) = TM(J)
  556  CONTINUE
       WRITE(*,22)(T(J),J=1,N)
       WRITE(40,22)(T(J),J=1,N)
      END IF
C
      IF (I1 EQ.2) THEN
       IF (I8 .EQ. 1) THEN
         IF (I3.EQ.1) THEN
           READ(30,*)(PSI(J),J=1,N)
           WRITE(*,23)(PSI(J),J=1,N)
         ELSE
           READ(30,*)(THETA(J),J=1,N)
           WRITE(*,24)(THETA(J),J=1,N)
           DO 100 J=1,N
             PSI(J)=-(((THETA(J)-THETAR)/(THETAS-THETAR))**
     $            (EN/(1.0D0-EN))-1.0D0)**(1.0D0/EN)/(AALPA)
  100      CONTINUE
       END IF
      ELSE
```

```
      IF (I3 EQ 1) THEN
        READ(30,*)(PSI(J),J=1,N)
        WRITE(*,23)(PSI(J),J=1,N)
      ELSE
        READ(29,*) (AW(J), J=1,N)
        READ(29,*) (BW(J), J=1,N)
        THETAM(1) = AW(1) + BW(1)*TM(1)
        DO 557 J = 2,N
          THETAM(J) = AW(J) + BW(J)*THETAM(J-1)
557       CONTINUE
C
        READ(30,*)(THETA(J),J=1,N)
        DO 558 J = 1,N
          THETA(J) = THETAM(J)
558       CONTINUE
        WRITE(*,24)(THETA(J),J=1,N)
        WRITE(40,24)(THETA(J),J=1,N)
        DO 101 J=1,N
          PSI(J)=-(((THETA(J)-THETAR)/(THETAS-THETAR))**
     $          (EN/(1.0D0-EN))-1.0D0)**(1.0D0/EN)/(AALPA)
101       CONTINUE
      END IF
    END IF
  END IF
C
 22 FORMAT(24F6.2)
 23 FORMAT(8E10.2,/8E10.2)
 24 FORMAT(24F6.2)
C
  TINFIL=0.0D0
  TEVAP=0.0D0
  TDRAIN=0.0D0
  RNCUM=0.0D0
  SHCUM=0.0D0
  ALECUM=0.0D0
  GSCUM=0.0D0
C
C   Determine Initial Water Storage in the System
C
  CALL STORE(THETA,N,DELZ,VOL)
  VOLUM1=VOL
C
C   Read Rainfall Indicator for Each Day
C
  DO 170 I=1,IDAY
    READ(30,*)IRAIN(I)
170 CONTINUE
C
  WRITE(*,25)(IRAIN(I),I=1,IDAY)
 25 FORMAT('IRAIN IS ',1X,65I3,/65I3)
C
C   Do Loop for the Length of the Simulation in Days
C
  DO 1000 III=1,IDAY
C
C   Determine Boundary Condition Values for a Day
C
```

```
      IF (I4.EQ.1) THEN
        READ(30,*)NO
        READ(30,*)(TT1(J), J=1,NO)
        WRITE(*,26)NO
   26   FORMAT(1X,'NO =',3X,I4)
        WRITE(*,22)(TT1(J), J=1,NO)
        NOINT=ISTEP/NO
        DO 181 J=1,NO
        DO 181 JK=1,NOINT
          K=(J-1)*NOINT+JK
          T1(K)=TT1(J)
  181   CONTINUE
      END IF
C
C     Use SINE FUNCTION to Determine Soil Surface Temperature.
C     Assume Maximum Temperature Occurs 2 Hours After the SOLAR NOON
C
      IF (I4.EQ.2) THEN
        READ(30,*)TMAX,TMIN
        WRITE(*,27)TMAX,TMIN
   27   FORMAT(1X,'TMAX =',3X,F6.3,5X,'TMIN =',3X,F6.3)
        DO 182 K=1,ISTEP
          T1(K)=(TMAX+TMIN)/2.0D0+(TMAX-TMIN)/2.0D0*
     $        DSIN(PI/2.0D0+(DBLE(K)*DELT-SNOON-7200.0D0)*OMEGA)
  182   CONTINUE
      END IF
C
      IF (I4.EQ.3) THEN
        READ(30,*)IDOY,TAVE,TAMP,TDEWA,TDAMP,WSPEED,RGD
        WRITE(*,505)IDOY,TAVE,TAMP,TDEWA,TDAMP,WSPEED,RGD
        RA=(DLOG(ZM/Z0))**2/((VKAR**2)*WSPEED)
      END IF
C
      IF (I5.EQ.1) THEN
        READ(30,*)TNC
        WRITE(*,29)TNC
   29   FORMAT('TNC =',F6.2)
      END IF
C
      IF (I5.EQ.2) THEN
        READ(30,*)NO
        READ(30,*)(IDOY,TTN(J),J=1,NO)
        WRITE(*,26)NO
        WRITE(*,22)(TTN(J),J=1,NO)
        NOINT=ISTEP/NO
        DO 183 J=1,NO
        DO 183 JK=1,NOINT
          K=(J-1)*NOINT+JK
          TN(K)=TTN(J)
  183   CONTINUE
      END IF
C
      IF (I1.EQ.1) GO TO 2000
C
C     If Heat Flow Uses Energy Balance Method, Use That for Water Also
C
      IF (I4.EQ.3) I6=3
```

```
C
      IF (I6.EQ.1) THEN
        IF (I3.EQ.1) THEN
          READ(30,*)NO
          READ(30,*)(PSI1(J), J=1,NO)
          WRITE(*,*)'NO =',NO
          WRITE(*,23)(PSI1(J),J=1,NO)
          NOINT=ISTEP/NO
          DO 184 J=1,NO
          DO 184 JK=1,NOINT
            K=(J-1)*NOINT+JK
          PSI(K)=PSI1(J)
  184     CONTINUE
        ELSE
          READ(30,*)NO
          READ(30,*)(THETA1(J),J=1,NO)
          WRITE(*,26)NO
          WRITE(*,24)(THETA1(J),J=1,NO)
          NOINT=ISTEP/NO
          DO 200 J=1,NO
          DO 200 JK=1,NOINT
            K=(J-1)*NOINT+JK
            THETA(K)=THETA1(J)
            PSI(K)=-(((THETA(K)-THETAR)/(THETAS-THETAR))**
     $           (EN/(1.0D0-EN))-1.0D0)**(1.0D0/EN)/(AALPA)
C
C     TEMPERATURE CORRECTION FOR MATRIC HEAD
C
          TEN0 = ((-0.15301D0*(T0+273.16D0))+117.528D0)*10**(-3.0D0)
          TENS(K) = ((-0.15301D0*(T(K)+273.16D0))+117.528D0)*
     $           10**(-3.0D0)
          PSI(K) = (TENS(K)/TEN0)*PSI(K)
  200     CONTINUE
        END IF
      END IF
C
      IF (I6.EQ.2) THEN
        READ(30,*) NO
        READ(30,*)(FLUX1(J), J=1,NO)
        WRITE(*,26) NO
        WRITE(*,31) (FLUX1(J), J=1,NO)
   31   FORMAT(8D12.4,/8D12.4)
        NOINT=ISTEP/NO
        DO 210 J=1,NO
        DO 210 JK=1,NOINT
          K=(J-1)*NOINT+JK
          FLUX(K)=FLUX1(J)
  210   CONTINUE
      END IF
C
      IF (I7.EQ.1) THEN
        IF (I3.EQ.1) THEN
          READ(30,*) NO
          READ(30,*) (IDOY,PSINN(J), J=1,NO)
          WRITE(*,26) NO
          WRITE(*,23) (PSINN(J), J=1,NO)
          NOINT=ISTEP/NO
```

```
          DO 250 J=1,NO
          DO 250 JK=1,NOINT
            K=(J-1)*NOINT+JK
            PSIN(K)=PSINN(J)
  250     CONTINUE
        ELSE
          READ(30,*) NO
          READ(30,*) (IDOY,THETNN(J), J=1,NO)
          WRITE(*,26) NO
          WRITE(*,24) (THETNN(J), J=1,NO)
          NOINT=ISTEP/NO
          DO 300 J=1,NO
          DO 300 JK=1,NOINT
            K=(J-1)*NOINT+JK
            THETAN(K)=THETNN(J)
            PSIN(K)=-(((THETAN(K)-THETAR)/(THETAS-THETAR))**
     $           (EN/(1.0D0-EN))-1.0D0)**(1.0D0/EN)/(AALPA)
  C
  C   TEMPERATURE CORRECTION FOR MATRIC HEAD
  C
          TENNT0 = ((-0.15301D0*(T0+273.16D0))+117.528D0)*10**(-3.0D0)
          TENN(K) = ((-0.15301D0*(T(K)+273.16D0))+117.528D0)*
     $          10**(-3.0D0)
          PSIN(K) = (TENN(K)/TENNT0)*PSIN(K)
  300     CONTINUE
        END IF
      END IF
  C
  2000 CONTINUE
      NUMRN=IRAIN(III)
      IF (NUMRN.NE.0) THEN
  C
        DO 151 I=1,NUMRN
          READ(30,*)IDOY,TIMEB(I),TIMEE(I),AMOUNT(I)
   151  CONTINUE
  C
        DO 152 I=1,NUMRN
          WRITE(*,507)IDOY,TIMEB(I),TIMEE(I),AMOUNT(I)
   152  CONTINUE
  C
        DO 153 I=1,NUMRN
          TIMEB(I)=TIMEB(I)*3600.0D0
          TIMEE(I)=TIMEE(I)*3600.0D0
          AMOUNT(I)=AMOUNT(I)/1000.0D0
   153  CONTINUE
  C
      END IF
  C
  C   DO LOOP FOR THE TIME STEPS IN A DAY
  C
      TIME=0.0D0
      ICOUNT = 0
      RNSUM = 0.0D0
      TDSUM = 0.0D0
      TDA(0) = 0.0D0
      TDD(0) = 0.0D0
      TDASUM = 0.0D0
```

```
      RNSQS = 0.0D0
      TDSQS = 0.0D0
      TDASQS = 0.0D0
      RNTDS = 0.0D0
      RNTDAS = 0.0D0
C
 3000 IF (TIME.LT.86400.0D0) THEN
        TIME=TIME+DELT
        K=IDNINT(DINT((TIME+0.1D0)/DELT))
        RAIN=0.0D0
C
        IF (NUMRN .NE. 0 .AND. TIME .GT. TIMEB(NUMRN) .AND.
     $     TIME .LE. TIMEE(NUMRN)) THEN
C
C     DETERMINE RAINFALL AMOUNT FOR THIS TIME STEP
C
        CALL RAINFL(TIME,DELT,NUMRN,TIMEB,TIMEE,AMOUNT,RAIN)
        END IF
C
C     Compute Values of Coefficients by SUBROUTINE COEFNT
C
        CALL COEFNT(N,PSI,THETA,DWDP,COND,CAPA,RAMDA,ALPA,
     $          T,TENSN,VISCO)
C
C*************************************************************************
C     STEP 2- FOR HEAT FLOW
C*************************************************************************
C
C     Set up Coefficient Matrix for the Top Boundary Conditions
C
        COEF(1,1)=0.0D0
        COEF(1,2)=1.0D0
        COEF(1,3)=0.0D0
        IF (I4 .NE. 3) THEN
          RHS(1)=T1(K)
        ELSE
          TAIR=TAVE+TAMP*DSIN(OMEGA*TIME+PI)
          IF (DETENT .GT. 0.0D0 .OR. RAIN .GT. 0.0D0) THEN
            CALL INFILT(RAIN,DETENT,DETMAX,PSI(2),CONDS,COND(2),
     $              DELZ,DELT,FLUX1(K))
            RHS(1)=TAIR
            TINFIL=TINFIL+FLUX1(K)*DELT
          ELSE
            TDEW=TDEWA+TDAMP*DSIN(OMEGA*TIME+PI)
C
C     CORRECTION FOR CLOUDINESS
C
C           LATITD = -0.1194D0
C           DR = 1.0D0 + 0.033D0*DCOS(((2.0D0*PI)/365)*IDOY)
C           SOLDEC = 0.4093D0*DSIN(2.0D0*PI*((IDOY+284)/365))
C           OMEGAS = DACOS(-DTAN(LATITD)*DTAN(SOLDEC))
C           RADEXT = 435.0D0*DR*(OMEGAS*DSIN(LATITD)*
C     $           DSIN(SOLDEC)+DCOS(LATITD)*DCOS(SOLDEC)
C     $           *DSIN(OMEGAS))
C           RADEXT = RADEXT*86400.0D0
C           AS = 0.25D0
C           BS = 0.50D0
```

```
C          AC = 1.35D0
C          BC = -0.35D0
C          RGBSUN = (AS + BS)*RADEXT
C          FCLOUD = AC*(RGD/RGBSUN) + BC
C
          HA=1.323D0*DEXP(17.27D0*TDEW/(237.3D0+TDEW))
     $       /(TAIR+273.16D0)
C
C          SKY = FCLOUD*(SIGMA*(TAIR+273.16D0)**4*(0.605D0+1.777D0
C     $          *DSQRT(HA)))
C
C    CORRECTION FOR CLOUD COVER
C
C          FCLOUD = 0.9D0*(SUNHR(III)/DAYL)+0.1D0
C          SKY = FCLOUD*(SIGMA*(TAIR+273.16D0)**4*(0.605D0+1.777D0
C     $          *DSQRT(HA)))
C
          SKY = SIGMA*(TAIR+273.16D0)**4*(0.605D0+1.777D0
     $          *DSQRT(HA))
          TIMESH=(TIME-SNOON+DAYL/2.0D0)/DAYL
          IF (TIMESH .LE. 0.0D0 .OR. TIMESH .GE. 1.0D0) THEN
            RG=0.0D0
          ELSE
            RG=PI*(9.0D0/16.0D0)*RGD/DAYL*DSIN(TIMESH*PI)
          END IF
          IF ((I9 .EQ. 1)) THEN
            CALL BARE(THETA(1),T(1),T(2),PSI(1),CAPA(1),CAPA(2),
     $       ALPA(1),ALPA(2),FLUX1(K),TS,RN,SH,ALES,GS,RA)
            RHS(1)=TS
          ELSEIF ((I9 .EQ. 2)) THEN
            IF((III .EQ. 1) .AND. (TIME .EQ. DELT)) THEN
              CALL BARE(THETA(1),T(1),T(2),PSI(1),CAPA(1),CAPA(2),
     $         ALPA(1),ALPA(2),FLUX1(K),TS,RN,SH,ALES,GS,RA)
              RHS(1)=TS
            END IF
          END IF
C
C INCLUDE STABILITY CORRECTION FUNCTIONS
C
      IF ((I4 .EQ. 3) .AND. (I9 .EQ. 2)) THEN
        IF ((III .EQ. 1) .AND. (TIME .EQ. DELT)) THEN
          FVEL = (WSPEED*0.4D0)/(DLOG(2.0D0/ZO))
          CAPAA = 1154.8D0+303.16D0/(TAIR+273.16D0)
          OBLEN = -((FVEL**3.0D0)*CAPAA*TAIR)/(0.4D0*9.813D0*SH)
          X = (1.0D0 - 16.0D0*(2.0D0/OBLEN))**(0.25D0)
          P1 = 0.0D0
          P2 = 0.0D0
        ELSE
          CALL STABIL(OBLEN,FVEL,X,P1,P2,WSPEED,RA,TS)
          CALL BARE(THETA(1),T(1),T(2),PSI(1),CAPA(1),CAPA(2),
     $       ALPA(1),ALPA(2),FLUX1(K),TS,RN,SH,ALES,GS,RA)
          RHS(1) = TS
        END IF
      END IF
C
C   COMPUTE CUMULATIVE EVAPORATION
C
```

```
          TEVAP=TEVAP+FLUX1(K)*DELT
          RNCUM=RNCUM+RN*DELT
          SHCUM=SHCUM+SH*DELT
          ALECUM=ALECUM+ALES*DELT
          GSCUM=GSCUM+GS*DELT
        END IF
      END IF
C
C   FOR THE INTERMEDIATE NODES
C
      DO 400 J=2,NM1
        COEF(J,1)=-0.5D0*(ALPA(J-1)+ALPA(J))
        COEF(J,3)=-0.5D0*(ALPA(J)+ALPA(J+1))
        COEF(J,2)=DZ2DT-COEF(J,1)-COEF(J,3)
        RHS(J)=DZ2DT*T(J)
  400 CONTINUE
C
C   FOR THE BOTTOM BOUNDARY POINTS
C
      IF (I5 .NE. 3) THEN
        COEF(N,1)=0.0D0
        COEF(N,2)=1.0D0
        COEF(N,3)=0.0D0
        IF (I5 .EQ. 1) RHS(N)=TNC
        IF (I5 .EQ. 2) RHS(N)=TN(K)
      ELSE
        HFLUX=-RAMDA(N)*(T(N)-T(N-1))/DELZ
        COEF(N,1)=-2.0D0*0.5D0*(ALPA(N-1)+ALPA(N))
        COEF(N,2)=DZ2DT-COEF(N,1)
        COEF(N,3)=0.0D0
        RHS(N)=DZ2DT*T(N)+0.5D0*(ALPA(N)+ALPA(N-1))
     $       *HFLUX*DELZ*2.0D0/RAMDA(N)
      END IF
C
C   SOLVE FOR THE HEAT FLOW BY CALLING TRIDIA
C
      CALL TRIDIA(N,COEF,RHS)
C
C   ASSIGN THE SOLUTION TO T(J)
C
      DO 500 J=1,N
        T(J)=RHS(J)
  500 CONTINUE
C
C   SKIP WATER FLOW PART IF THE PROBLEM IS ONLY FOR HEAT FLOW
C
      IF (I1 .EQ. 1) GO TO 4000
C
C**********************************************************************
C   STEP 3. FOR WATER FLOW
C**********************************************************************
C
C   SET UP COEFFICIENT MATRIX FOR THE TOP BOUNDARY CONDITION
C
      IF (I6 .EQ. 1) THEN
        COEF(1,1)=0.0D0
        COEF(1,2)=1.0D0
```

```
      COEF(1,3)=0.0D0
      RHS(1)=PSI1(K)
    ELSE IF (DETENT .GT. 0.0D0) THEN
      COEF(1,1)=0.0D0
      COEF(1,2)=1.0D0
      COEF(1,3)=0.0D0
      RHS(1)=DETENT
    ELSE
      TERMS=DWDP(1)*DELZ/(2.0D0*DELT)
      CBAR=0.5D0*(COND(1)+COND(2))
      PSI0=((FLUX1(K)-CBAR+CBAR*PSI(2)/DELZ)+PSI(1)*TERMS)
     $     /(TERMS+CBAR/DELZ)
      COEF(1,1)=0.0D0
      COEF(1,2)=1.0D0
      COEF(1,3)=0.0D0
      RHS(1)=PSI0
    END IF
C
C   For the Intermediate Rows
C
    DO 600 J=2,NM1
      COEF(J,1)=-0.5D0*(COND(J-1)+COND(J))
      COEF(J,3)=-0.5D0*(COND(J)+COND(J+1))
      COEF(J,2)=DWDP(J)*DZ2DT-COEF(J,1)-COEF(J,3)
      RHS(J)=DWDP(J)*DZ2DT*PSI(J)-DELZ/2.0D0*
     $     (COND(J+1)-COND(J-1))
  600 CONTINUE
C
C   FOR THE BOTTOM BOUNDARY NODES
C
    FLUXN=DSQRT(COND(NM1)*COND(N))*(1.0D0-(PSI(N)-PSI(NM1))/DELZ)
    TDRAIN=TDRAIN+FLUXN*DELT
    IF (I7 .EQ. 1) THEN
      COEF(N,1)=0.0D0
      COEF(N,2)=1.0D0
      COEF(N,3)=0.0D0
      RHS(N)=PSIN(K)
    ELSE IF (I7 .EQ. 2) THEN
      COEF(N,1)=-1.0D0
      COEF(N,2)=1.0D0
      COEF(N,3)=0.0D0
      RHS(N)=DELZ
    ELSE
      COEF(N,1)=-1.0D0
      COEF(N,2)=1.0D0
      COEF(N,3)=0.0D0
      RHS(N)=0.0D0
    END IF
C
C   SOLVE FOR THE WATER FLOW BY CALLING TRIDIA
C
    CALL TRIDIA(N,COEF,RHS)
C
C   ASSIGN THE SOLUTION TO PSI(J)
C
    DO 700 J=1,N
      PSI(J)=RHS(J)
```

```
 700 CONTINUE
4000 CONTINUE
C
C   PRINT SOLUTION ON THE SCREEN WHILE CALCULATIONS PROCEED
C   AND CREATE USER SPECIFIED  OUTPUT FILES
C
    IF (DMOD(TIME,TIME1) .EQ. 0.0D0) THEN
      WRITE(*,99) III, TIME/3600.0D0
 99   FORMAT(' DAY =',2X,I3,10X,'TIME =',2X,F5.2)
      WRITE(*,118) RN,RNCUM
      WRITE(*,120) SH,SHCUM
      WRITE(*,122) ALES,ALECUM
      WRITE(*,124) GS,GSCUM
      WRITE(*,111) (T(J), J=1,N)
      WRITE(32,111) (T(J), J=1,N)
C
      IF (I4 .EQ. 3) THEN
C
        TD = TS - TAIR
        TDRN = TD/RN
        WRITE(36,132)TS,T(1),TAIR,TD,TDRN
C
C       IF (RN .GE. 0.0D0 .AND. TD .GE. 0.0D0) THEN
        IF (RN .GE. 0.0D0) THEN
          ICOUNT = ICOUNT + 1
          TDSUM = TDSUM + TD
          RNSUM = RNSUM + RN
          TDD(ICOUNT) = TD
          RND(ICOUNT) = RN
        END IF
C
        IF (TIME .EQ. 86400.0D0) THEN
          RNBAR = RNSUM/ICOUNT
          TDBAR = TDSUM/ICOUNT
          DO 70 I = 1,ICOUNT
            RNSQR = (RND(I)-RNBAR)**2
            TDSQR = (TDD(I)-TDBAR)**2
            RNTD = (RND(I)-RNBAR)*(TDD(I)-TDBAR)
            RNSQS = RNSQS + RNSQR
            TDSQS = TDSQS + TDSQR
            RNTDS = RNTDS + RNTD
 70       CONTINUE
C
          BETA1 = RNTDS/RNSQS
          ALPHA1 = TDBAR - BETA1*RNBAR
C
          DO 71 I = 1,ICOUNT
            RNEQ(I) = (TDD(I)-ALPHA1)/BETA1
            IF (I .EQ. 1) RNEQ(0) = RNEQ(1)
            DTD(I) = (RND(I)-RNEQ(I-1))*BETA1
            TDA(I) = 0.7D0*DTD(I)+TDD(I)
            TDASUM = TDASUM + TDA(I)
            TDABAR = TDASUM/ICOUNT
            TDASQ = (TDA(I)-TDABAR)**2
            RNTDA = (RND(I)-RNBAR)*(TDA(I)-TDABAR)
            TDASQS = TDASQS + TDASQ
            RNTDAS = RNTDAS + RNTDA
```

```
 71       CONTINUE
C
      BETA2 = RNTDAS/RNSQS
      ALPHA2 = TDABAR - BETA2*RNBAR
C
      END IF
C
      WRITE(37,133)III,BETA1,ALPHA1,BETA2,ALPHA2,TDD(ICOUNT),
     $          TDA(ICOUNT)
C
C      WRITE(36,132)TS,T(1),TAIR,TD,TDRN,FCLOUD
C
     END IF
C
     WRITE(31,127)RN,RNCUM,SH,SHCUM,ALES,ALECUM,GS,GSCUM
     IF (II .EQ. 2) THEN
      CALL STORE(THETA,N,DELZ,VOL)
      BALANS=VOL-VOLUM1-TEVAP+TDRAIN-TINFIL
      WRITE(*,114) VOL,BALANS
      WRITE(*,116) FLUXN,TDRAIN
      WRITE(*,126) FLUX1(K),TEVAP,TINFIL
      WRITE(*,131) (THETA(J), J=1,N)
      WRITE(*,113) (PSI(J), J=1,N)
C
      DO 899 J=1,N
       AVAIL.M(J) = THETA(J)/THETAS
 899   CONTINUE
C
      J = 1
      Z(J) = 0.0D0
      DO 900 J=2,N
       Z(J) = Z(J-1) + DELZ
 900   CONTINUE
      Z(N) = ZLENG
C
      DO 901 M = 2,N
       WAVGS(M) = 0.0D0
       WAVGN(M) = 0.0D0
       PAVGS(M) = 0.0D0
       PAVGN(M) = 0.0D0
 901   CONTINUE
C
      M = 2
      WAVGNT(M) = 0.5D0*(Z(2) - Z(1))*THETA(2)
      WAV(M) = 0.5D0*(Z(M) - Z(M-1))*THETA(M)
      WAVGN(M) = (WAVGNT(M) + WAV(M))/(Z(M) - Z(1))
C
      PAVGNT(M) = 0.5D0*(Z(2) - Z(1))*PSI(2)
      PAV(M) = 0.5D0*(Z(M) - Z(M-1))*PSI(M)
      PAVGN(M) = (PAVGNT(M) + PAV(M))/(Z(M) - Z(1))
C
      DO 920 M = 3,N
      WAVGNT(M) = 0.5D0*(Z(2) - Z(1))*THETA(2)
      PAVGNT(M) = 0.5D0*(Z(2) - Z(1))*PSI(2)
       DO 903 J=2,M-1
       WAVG(J) = 0.5D0*(Z(J+1) - Z(J-1))*THETA(J)
       WAVGS(M) = WAVG(J) + WAVGS(M)
```

```
          PAVG(J) = 0.5D0*(Z(J+1) - Z(J-1))*PSI(J)
          PAVGS(M) = PAVG(J) + PAVGS(M)
903         CONTINUE
          WAV(M) = 0.5D0*(Z(M) - Z(M-1))*THETA(M)
          WAVGN(M) = (WAVGNT(M) + WAVGS(M) + WAV(M))/(Z(M) - Z(1))
          PAV(M) = 0.5D0*(Z(M) - Z(M-1))*PSI(M)
          PAVGN(M) = (PAVGNT(M) + PAVGS(M) + PAV(M))/(Z(M) - Z(1))
920       CONTINUE
C
          WRITE(33,131) (THETA(J), J=1,N)
          WRITE(39,131) (AVAIL.M(J), J=1,N)
          WRITE(34,113) (PSI(J), J=1,N)
C
          WRITE(35,131) (WAVGN(M), M=2,N)
          WRITE(38,113) (PAVGN(M), M=2,N)
        END IF
      END IF
      GO TO 3000
      END IF
 1000 CONTINUE
C
  131 FORMAT(31F6.3)
  132 FORMAT(3F6.2,1X,F6.2,E10.3)
  133 FORMAT(I4,1X,4F10.3,1X,2F6.2)
C 132 FORMAT(3F6.2,1X,F6.2,E10.3,1X,F6.2)
  111 FORMAT(31F6.2)
C 113 FORMAT(16E10.2,/15E10.2)
  113 FORMAT(31E10.2)
  114 FORMAT(' STORAGE =',F8.6,' BALANCE =',F12.6)
  116 FORMAT(' FLUXN(M/S) =',D12.4,'CUM. DRAINAGE =',D12.4)
  118 FORMAT(' NET RADIATION (W/M*M) =',F12.0,'CUM. NET RAD =',F12.0)
  120 FORMAT(' SENSIBLE HEAT FLUX   =',F12.0,'CUM. SEN. HEAT=',F12.0)
  122 FORMAT(' EVAP. HEAT FLUX      =',F12.0,'CUM. EVAP HEAT=',F12.0)
  124 FORMAT(' SOIL HEAT FLUX(W/M*M) =',F12.0,'CUM. SOIL HEAT=',F12.0)
  126 FORMAT(' FLUX1(M/S)=',D12.4,' TEVAP=',D12.4,'  TINFIL=',D12.4)
C 127 FORMAT(8D10.3)
  127 FORMAT(8E10.3)
  501 FORMAT(20I2)
  502 FORMAT(24F5.1)
  503 FORMAT(24F6.2)
  504 FORMAT(24F6.3)
  505 FORMAT(I4,5F6.2,E10.4)
  506 FORMAT(24F5.2)
  507 FORMAT(I4,2X,2F7.3,2X,F6.3)
  508 FORMAT(I3,F5.0)
  509 FORMAT(F4.1)
  510 FORMAT(24F5.1)
  511 FORMAT(24F5.2)
  512 FORMAT(24F5.2)
C
C  CLOSE ANY FILES WHICH ARE OPEN
      CLOSE (25)
      CLOSE (26)
      CLOSE (28)
      CLOSE (29)
      CLOSE (30)
      CLOSE (31)
```

```
      CLOSE (32)
      CLOSE (33)
      CLOSE (34)
      CLOSE (35)
      CLOSE (36)
      CLOSE (37)
      CLOSE (38)
      CLOSE (39)
      CLOSE (40)
      STOP
      END
C
C*****************************************************************
C   THIS SUBROUTINE DETERMINES THE VALUES OF SOIL PARAMETERS FOR *
C   A GIVEN REPRESENTATIVE SOIL TYPE                             *
C*****************************************************************
C
      SUBROUTINE PARAM(I2)
      IMPLICIT REAL*8 (A-H,O-Z)
      COMMON/SOIL/THETAS,THETAR,SOLID,ORGAN,CONDS,AALPA,EN,B1,B2,B3,
     $       C3,C5
C
      IF (I2 .EQ. 1) THEN
        AALPA = 3.28D0
        EN    = 1.54D0
        CONDS = 2.5D-5
        B1    = 0.228D0
        B2    = -2.406D0
        B3    = 4.909D0
        THETAS= 0.44D0
        THETAR= 0.00D0
        SOLID = 0.56D0
        ORGAN = 0.0D0
C
C     SOIL TYPE INDICATOR 2 HAS BEEN USED IN THIS STUDY.
C     VALUES ARE USER SUPPLIED INSTEAD OF READING FROM
C     INPUT DATA FILE.
C
C     ELSE IF (I2 .EQ. 2) THEN
C       AALPA = 1.55D0
C       EN    = 1.5D0
C       CONDS = 0.7D-5
C       B1    = 0.243D0
C       B2    = 0.393D0
C       B3    = 1.536D0
C       THETAS= 0.48D0
C       THETAR= 0.01D0
C       SOLID = 0.52D0
C       ORGAN = 0.0D0
      ELSE IF (I2 .EQ. 2) THEN
        AALPA = 2.5D0
        EN    = 1.5D0
        CONDS = 0.5D-5
        B1    = 0.243D0
        B2    = 0.393D0
        B3    = 1.536D0
        THETAS= 0.48D0
```

```
      THETAR= 0.07D0
      SOLID = 0 52D0
      ORGAN = 0 0D0
C
C     SOIL TYPE INDICATOR 3 HAS BEEN USED IN THIS STUDY.
C     VALUES ARE USER SUPPLIED INSTEAD OF READING FROM
C     INPUT DATA FILE
C
C     ELSE IF (I2 .EQ. 3) THEN
C       AALPA = 0.432D0
C       EN    = 1.36D0
C       CONDS = 0.2D-5
C       B1    = -0 197D0
C       B2    = -0.962D0
C       B3    = 2 521D0
C       THETAS= 0 52D0
C       THETAR= 0.04D0
C       SOLID = 0.48D0
C       ORGAN = 0.0D0
      ELSE IF (I2 .EQ. 3) THEN
        AALPA = 2.0D0
        EN    = 1 5D0
        CONDS = 0 2D-5
C       B1    = -0 197D0
C       B2    = -0.962D0
C       B3    = 2 521D0
        THETAS= 0 44D0
        THETAR= 0 07D0
        SOLID = 0.56D0
        ORGAN = 0.0D0
C
        CLAY = 0 51D0
        PQ = 0 27D0
        PNQ = 0 29D0
        C2 = 2 8D0*(PQ + PNQ)*THETAS
        C1 = ((0 57D0+1 73D0*PQ+0.93D0*PNQ)/(1 0D0-0.74D0*PQ
     S       -0.49D0*PNQ))-C2*THETAS
        C3 = THETAS + (2.6D0*THETAS)/(CLAY**0 5D0)
        C4 = 0.03D0 + 0 7D0*(PQ + PNQ)**2
        C5 = 4
        B1 = C1
        B2 = C2
        B3 = C1 - C4
      ELSE
C
C     Read User Supplied Soil Parameters from Input Data File
C
        READ(30,*)B1,B2,B3,THETAS,THETAR,SOLID,ORGAN
        READ(30,*)AALPA,EN,CONDS
      END IF
      WRITE(*,100)B1,B2,B3,THETAS,THETAR,SOLID,ORGAN
      WRITE(*,200)AALPA,EN,CONDS
  100 FORMAT(7F8.3)
  200 FORMAT(2F8 3,E13.4)
      RETURN
      END
C
```

```
C*********************************************************************
C   THIS SUBROUTINE COMPUTES VOLUME OF WATER STORED IN THE          *
C   ONE-DIMENSIONAL DOMAIN AT A GIVEN TIME                          *
C*********************************************************************
C
      SUBROUTINE STORE(THETA,N,DELZ,VOL)
      IMPLICIT REAL*8 (A-H,O-Z)
      DIMENSION THETA(30)
C
      NM1 = N-1
      VOL1 = THETA(1)*DELZ/2.0D0
      VOLN = THETA(N)*DELZ/2.0D0
      VOL  = 0.0D0
      DO 10 J=2,NM1
        VOL = VOL+THETA(J)*DELZ
   10 CONTINUE
      VOL = VOL+VOL1+VOLN
      RETURN
      END
C
C*********************************************************************
C   SUBROUTINE RAINFL DETERMINES THE RAINFALL AMOUNT DURING         *
C   EACH TIME STEP                                                  *
C*********************************************************************
C
      SUBROUTINE RAINFL(TIME,DELT,IRAIN,TIMEB,TIMEE,AMOUNT,RAIN)
      IMPLICIT REAL*8 (A-H,O-Z)
      DIMENSION TIMEB(96),TIMEE(96),AMOUNT(96)
C
      IF (TIME .LE. TIMEE(1)) THEN
        RAIN = AMOUNT(1)/(TIMEE(1)-TIMEB(1))*DELT
      ELSE
        DO 10 I=2,IRAIN
          IF (TIME .GT. TIMEB(I) .AND. TIME .LE. TIMEE(I)) THEN
            RAIN = AMOUNT(I)/(TIMEE(I)-TIMEB(I))*DELT
            IF (RAIN .GT. 0.0D0) RETURN
          END IF
   10   CONTINUE
      END IF
      RETURN
      END
C
C*********************************************************************
C   THIS SUBROUTINE COMPUTES THE VALUES OF THE FLOW EQUATION        *
C   COEFFICIENTS FOR BOTH HEAT AND WATER FLOW                       *
C   INPUTS ARE N, AND PSI, AND THE REST ARE OUTPUTS                 *
C*********************************************************************
C
      SUBROUTINE COEFNT(N,PSI,THETA,DWDP,COND,CAPA,RAMDA,ALPA,
     $                  T,TENSN,VISCO)
      IMPLICIT REAL*8 (A-H,O-Z)
      DIMENSION PSI(30),THETA(30),DWDP(30),COND(30),CAPA(30)
      DIMENSION RAMDA(30),ALPA(30)
      DIMENSION T(30),TENSN(30),VISCO(30)

      COMMON/WETHER/SIGMA,TAIR,TDEW,ZO,TOL,DELZ,DELT,SKY,HA,RG,RA,RS,T0
      COMMON/SOIL/THETAS,THETAR,SOLID,ORGAN,CONDS,AALPA,EN,B1,B2,B3,
```

```
     $       C3,C5
C
C    USE STATEMENT FUNCTION FOR THE SOIL HEAT CAPACITY,
C    HYDRAULIC CONDUCTIVITY AND SPECIFIC WATER CAPACITY
C
     CAPACT(SOLID,ORGAN,WATER)
     $       = 1.92D6*SOLID+2.51D6*ORGAN+4.18D6*WATER
     CONDUC(CONDS,AALPA,EN,PRE)
     $       = CONDS*(1.0D0-(-AALPA*PRE)**(EN-1.0D0)*(1.0D0+
     $        (-AALPA*PRE)**EN)**((1.0D0-EN)/EN))**2/(1.0D0
     $        +(-AALPA*PRE)**EN)**((EN-1.0D0)/EN/2.0D0)
C
     FUN(WACON,THETAS,THETAR,EN,PRE)
     $       = (EN-1.0D0)*(WACON-THETAR)*(1.0D0-((WACON-THETAR)/
     $        (THETAS-THETAR))**(EN/(EN-1.0D0)))/(-PRE)
C
C    CONDT(B1,B2,B3,THTA) = B1+B2*THTA+B3*DSQRT(THTA)
     CONDT(B1,B2,B3,C3,C5,THTA) = B1+B2*THTA-B3*DEXP(-(C3*THTA)**C5)
     THET(THETAS,THETAR,AALPA,EN,PRE)
     $    = THETAR+(THETAS-THETAR)*(1.0D0+(-AALPA*PRE)**EN)
     $       **((1.0D0-EN)/EN)
C
C    TEMPERATURE CORRECTION FOR HYDRAULIC CONDUCTIVITY AND MATRIC HEAD
C
     TENST0 = ((-0.15301D0*(T0+273.16D0))+117.528D0)*10**(-3.0D0)
     VISCT0 = 1.0681D0*10**(-3.0D0)*DEXP(-0.02372D0*(T0+273.16D0))
     DO 100 J = 1,N
      TENSN(J) = ((-0.15301D0*(T(J)+273.16D0))+117.528D0)*10**(-3.0D0)
      PSI(J) = (TENSN(J)/TENST0)*PSI(J)
      VISCO(J) = 1.0681D0*10**(-3.0D0)*DEXP(-0.02372D0*
     $       (T(J)+273.16D0))
      VISCO(J) = VISCT0/VISCO(J)
C
      IF (PSI(J) .GT. -0.01D0) THEN
        THETA(J) = THETAS
        DWDP(J)  = 0.01D0
        COND(J)  = CONDS
      ELSE
        THETA(J) = THET(THETAS,THETAR,AALPA,EN,PSI(J))
        DWDP(J)  = FUN(THETA(J),THETAS,THETAR,EN,PSI(J))
        CONDX(J) = CONDUC(CONDS,AALPA,EN,PSI(J))
        COND(J)  = COND(J)*VISCO(J)
      END IF
C
      CAPA(J) = CAPACT(SOLID,ORGAN,THETA(J))
      RAMDA(J)= CONDT(B1,B2,B3,C3,C5,THETA(J))
      ALPA(J) = RAMDA(J)/CAPA(J)
  100 CONTINUE
     RETURN
     END
C

C*****************************************************************
C    THIS SUBROUTINE DETERMINES SOIL SURFACE INFILRATION WATER   *
C    FLUX CONDITION                                              *
C*****************************************************************
C
```

```
      SUBROUTINE INFILT(RAIN,DETENT,DETMAX,PSI2,CONDS,COND2,DELZ,
     $              DELT,FLUX1)
      IMPLICIT REAL*8 (A-H,O-Z)
C
      PSI1 = 0.0D0
      IF (DETENT .GT. 0.0D0) PSI1 = DETENT
      CAP = ((PSI1-PSI2)/DELZ+1.0D0)*0.5D0*(CONDS+COND2)*DELT
      IF (RAIN+DETENT .LE. CAP) THEN
        RINFIL = RAIN + DETENT
        DETENT = 0.0D0
      ELSE
        RINFIL = CAP
        DETENT = DETENT+RAIN-RINFIL
        IF (DETENT .GT. DETMAX) DETENT=DETMAX
      END IF
      FLUX1 = RINFIL/DELT
      RETURN
      END
C
C*****************************************************************
C   THIS SUBROUTINE DETERMINES SOIL SURFACE TEMPERATURE AND      *
C   EVAPORATION RATE USING ENERGY BALANCE EQUATION BY BISECT     *
C   ROOT FINDING METHOD                                          *
C*****************************************************************
C
      SUBROUTINE BARE(THETA1,T1,T2,PSI1,CAP1,CAP2,ALP1,ALP2,
     $           FLUX1,TS,RN,SH,ALES,GS,RAH)
      IMPLICIT REAL*8 (A-H,O-Z)
      COMMON/WETHER/SIGMA,TAIR,TDEW,ZO,TOL,DELZ,DELT,SKY,HA,RG,RA,RS,T0
      COMMON /SOIL/THETAS,THETAR,SOLID,ORGAN,CONDS,AAI PA,EN,B1,B2,B3,
     $          C3,C5
C
      CAPAS = 0.5D0*(CAP1+CAP2)
      RAMDA = 0.5D0*(ALP1*CAP1+ALP2*CAP2)
C     EMIS  = 0.9D0 + 0.18D0*THETA1
C
      EDRY = 0.90D0
      EWET = 0.94D0
      EMIS = EDRY + (THETA1/THETAS)*(EWET - EDRY)
C
C     COMPUTE ALBEDO FOR THE GIVEN TOP WATER CONTENT
C
      AWET = 0.06D0
      ADRY = 0.12D0
      THETACR = 0.23D0
C
      IF (THETA1 .GE. THETACR) THEN
        ALBE = AWET
      ELSE
        ALBE = AWET + ((THETACR - THETA1)/THETACR)*(ADRY - AWET)
      END IF
C
C     IF (THETA1 .GE. 0.25D0) THEN
C       ALBE = 0.1D0
C     ELSE IF (THETA1 .LE. 0.1D0) THEN
C       ALBE = 0.25D0
C     ELSE
```

```
C      ALBE = 0.35D0 - THETA1
C    END IF
C
     CAPAA = 1154.8D0+303.16D0/(TAIR+273.16D0)
C
     A = T1
     B = T1
     RAH = RA
     DO 100 J=1,50
       A = A-0.5D0
       B = B+0.5D0
       CALL BISEC(A,T1,T2,PSH,CAPAS,CAPAA,RAMDA,
    $           EMIS,ALBE,RES,EVAP,RN,SH,ALES,GS,THETA1,RAH)
       FA = RES
       CALL BISEC(B,T1,T2,PSH,CAPAS,CAPAA,RAMDA,
    $           EMIS,ALBE,RES,EVAP,RN,SH,ALES,GS,THETA1,RAH)
       FB = RES
       IF (FA*FB .LT. 0.0D0) GO TO 200
  100 CONTINUE
C
     WRITE(*,*)' ITERATION LIMIT EXCEEDED IN BARE'
C
  200 DO 300 J=1,50
       AMID=(A+B)/2.0D0
       IF ((AMID-A) .LE. TOL) GO TO 500
       CALL BISEC(AMID,T1,T2,PSH,CAPAS,CAPAA,RAMDA,
    $           EMIS,ALBE,RES,EVAP,RN,SH,ALES,GS,THETA1,RAH)
       FMID = RES
       IF ((FA*FMID) .GT. 0.0D0) THEN
         A = AMID
       ELSE
         B = AMID
       END IF
  300 CONTINUE
C
     WRITE(*,*)' ITERATION LIMIT EXCEEDED IN SUBROUTINE BISEC'
C
  500 TS = AMID
     FLUX1 = -EVAP
     RETURN
     END
C
C*************************************************************************
C    THIS SUBROUTINE SOLVES TRIDIAGONAL MATRIX WITHOUT PIVOTING        *
C    DIAGONALLY DOMINANT MATRICES ARE SAFE                             *
C*************************************************************************
C
     SUBROUTINE TRIDIA(N,W,B)
     IMPLICIT REAL*8 (A-H,O-Z)
     DIMENSION W(30,3),B(30)
C
C    FF IS MULTIPLIER FOR THE FORWARD ELIMINATION STEP
C
     DO 10 J=2,N
       FF = W(J,1)/W(J-1,2)
       W(J,2) = W(J,2) - FF*W(J-1,3)
       W(J,1) = FF
```

```
  10 CONTINUE
C
C    FORWARD ELIMINATION STEP
C    B: ON INPUT, VECTOR OF RIGHT HAND SIDES
C    ON EXIT, SOLUTION VECTOR
C
     DO 20 J=2,N
       B(J) = B(J) - W(J,1)*B(J-1)
  20 CONTINUE
C
C    BACK SUBSTITUTION LOOP
C
     B(N) = B(N)/W(N,2)
  100 DO 30 J=2,N
       JB = N-J+1
       B(JB)=(B(JB)-W(JB,3)*B(JB+1))/W(JB,2)
  30 CONTINUE
     RETURN
     END
C
C*****************************************************************************
C    THIS SUBROUTINE DETERMINES THE RESIDUAL OF THE ENERGY                    *
C    BALANCE  EQUATION FOR SUBROUTINE: BARE                                   *
C    UNITS USED ARE JOULE, METRE, AND SECOND                                  *
C*****************************************************************************
C
     SUBROUTINE BISEC(TS,T1,T2,PSI1,CAPAS,CAPAA,RAMDA,EMIS,
    $            ALBE,RES,EVAP,RN,SH,ALES,GS,THETA1,RA1)
     IMPLICIT REAL*8 (A-H, O-Z)
     COMMON /WETHER/SIGMA,TAIR,TDEW,ZO,TOL,DELZ,DELT,SKY,HA,RG,RA,RS,T0
     COMMON /SOIL/THETAS,THETAR,SOLID,ORGAN,CONDS,AALPA,EN,B1,B2,B3,
    $         C3,C5
     COMMON TIME, OMEGA,PI,ZM,VKAR
C
C    RN = (1.0D0-ALBE)*RG+SKY-EMIS*SIGMA*(TS+273.16D0)**4
C
C    CORRECTION OF GLOBAL RADIATION FOR HOURLY VARIATION OF WEATHER
C
     CONS1 = 1.0D0
     CONS2 = 1.0D0
     CONS3 = 0.75D0*(TS/TAIR)
C
     IF (CONS3 .LE. 1.0D0) THEN
     RN = (1.0D0-ALBE)*(RG*CONS1)+SKY*EMIS-EMIS*SIGMA*(TS+273.16D0)**4
     ELSE
       IF ((TIME .GE. 39600.0D0) .AND. (TIME .LE. 54000.0D0)) THEN
         RN = (1.0D0-ALBE)*(RG*(MIN(CONS2,CONS3)))+SKY*EMIS-EMIS*
    $        SIGMA*(TS+273.16D0)**4
       ELSE
         RN = (1.0D0-ALBE)*(RG*CONS1)+SKY*EMIS-EMIS*
    $        SIGMA*(TS+273.16D0)**4
       END IF
     END IF
C
     RA = RA1
     SH = CAPAA*(TS-TAIR)/RA
     HO = 1.323D0*DEXP(17.27D0*TS/(TS+237.3D0))/(TS+273.16D0)
```

```
      IF (PSII .GT. 0.0D0) PSII=0.0D0
      HS = HO*DEXP(PSII/(46.97D0*(TS+273.16D0)))
      RS = (3.0D0*(10**10.0D0))*((THETAS-THETAT)**16.6D0)
      EVAP = (HS-HA)/((RA+RS)*1000.0D0)
      ALH = 2.49463D9-2.247D6*TS
      ALES = EVAP*ALH
      GS = RAMDA*(TS-T2)/DELZ+(TS-T1)*CAPAS*DELZ/DELT/2.0D0
      RES = RN-SH-ALES-GS
      RETURN
      END
C     ******************************************************************
      SUBROUTINE STABIL(OBLEN,FVEL,X,P1,P2,WSPEED,RAH,TS)
      IMPLICIT REAL*8 (A-H, O-Z)
      COMMON /WETHER/SIGMA,TAIR,TDEW,ZO,TOL,DELZ,DELT,SKY,HA,RG,RA,RS,T0
      COMMON /SOIL/THETAS,THETAR,SOLID,ORGAN,CONDS,AALPA,EN,B1,B2,B3,
     $     C3,C5
      COMMON TIME, OMEGA, PI,ZM,VKAR
      CAPAA = 1154.8D0+303.16D0/(TAIR+273.16D0)
      OBLEN = -((FVEL**3.0D0)*CAPAA*TAIR)/(0.4D0*9.813D0*SH)
       X = (1.0D0 - 16.0D0*(2.0D0/OBLEN))**(0.25D0)
       P1 = 2.0D0*DLOG((1.0D0 + X)/2.0D0) + DLOG((1.0D0 + X**2)
     $    /2.0D0) - 2.0D0*DATAN(X) + PI/2.0D0
       P2 = 2.0D0*DLOG((1.0D0 + X**2)/2.0D0)
       FVEL = (WSPEED*0.4D0)/(DLOG(2.0D0/ZO) - P1)
       OBLEN = -((FVEL**3.0D0)*CAPAA*TAIR)/(0.4D0*9.813D0*SH)
C
       IF (TS .EQ. TAIR) THEN
        RAH = ((DLOG(ZM/ZO))**2)/((VKAR**2)*WSPEED)
        RA = RAH
       ELSE
        IF ((TS .GT. TAIR) .AND. (OBLEN .LT. 0.0D0)) THEN
         RAH = ((DLOG(ZM/ZO) - P1)*(DLOG(ZM/ZO) - P2))/
     $       ((VKAR**2)*WSPEED)
         RA = RAH
        ELSE
         IF ((TS .LT. TAIR) .AND. (OBLEN .GT. 0.0D0)) THEN
          IF (OBLEN .GT. 2.0D0) THEN
           RAH = ((DLOG(ZM/ZO) + 4.7D0*(ZM/OBLEN))**2)/
     $          ((VKAR**2)*WSPEED)
           RA = RAH
          ELSE
           IF ((OBLEN .GT. 0.0D0) .AND. (OBLEN .LE. 2.0D0)) THEN
            RAH = ((DLOG(ZM/ZO) + 4.7D0 + 4.7D0*DLOG(ZM/
     $          OBLEN))**2)/((VKAR**2)*WSPEED)
            RA = RAH
           END IF
          END IF
         END IF
        END IF
       END IF
      RETURN
      END
```

APPENDIX 4: DATA PROCESSING PROGRAMS

```
C Program irtemp.for for sorting infrared temperature data
C
    IMPLICIT REAL*8 (A-H, O-Z)
    CHARACTER*10 IRTMIN,IRTMOU,PROTMP
  10 FORMAT(A10)
    WRITE(*,*)'Enter the name of the IR Input File'
    READ(*,10)IRTMIN
    WRITE(*,*)'Enter the name of the Temp. Input File'
    READ(*,10)PROTMP
    WRITE(*,*)'Enter the name of the IR Output File'
    READ(*,10)IRTMOU
    OPEN(15,FILE=IRTMIN,STATUS='OLD')
    OPEN(16,FILE=PROTMP,STATUS='OLD')
    OPEN(17,FILE=IRTMOU,STATUS='NEW')
    M=5000
    N=8000
    DO 20 J=1,M
     READ(15,*)IDOY,ITIME,TMPIR
     IF (TMPIR .EQ. 9999.0D0) GO TO 55
      DO 19 I=1,N
       READ(16,*)IDOY1,ITIME1,TEMP1
       IF((IDOY .EQ. IDOY1) .AND. (ITIME .EQ. ITIME1)) THEN
       WRITE(17,25)IDOY,IDOY1,ITIME,ITIME1,TMPIR,TEMP1
       GO TO 20
       END IF
 19    CONTINUE
 20  CONTINUE
 25  FORMAT(1X,2I4,2I6,1X,2F6.2)
    CLOSE(15)
    CLOSE(16)
    CLOSE(17)
 55  END
```

```
C Program irtemp1.for for sorting infrared temperature data
C
    IMPLICIT REAL*8 (A-H, O-Z)
    CHARACTER*10 IRTMIN,IRTMOU,PROTMP,IRPAOU
 10 FORMAT(A10)
    WRITE(*,*)'Enter the name of the IR Input File'
    READ(*,10)IRTMIN
    WRITE(*,*)'Enter the name of the Temp. Input File'
    READ(*,10)PROTMP
    WRITE(*,*)'Enter the name of the IR Output File'
    READ(*,10)IRTMOU
    WRITE(*,*)'Enter the name of the IR Partial Output File'
    READ(*,10)IRPAOU
    OPEN(15,FILE=IRTMIN,STATUS='OLD')
    OPEN(16,FILE=PROTMP,STATUS='OLD')
    OPEN(17,FILE=IRTMOU,STATUS='NEW')
    OPEN(18,FILE=IRPAOU,STATUS='NEW')
    M=5000
    N=8000
    DO 25 J=1,M
     READ(15,*)IDOY,ITIME,TMPIR
     IF (TMPIR .EQ. 9999.0D0) GO TO 55
      DO 19 I=1,N
```

```
      READ(16,*)IDOY1,ITIME1,TEMP1
      IF (TEMP1 .EQ. 9999.0D0) GO TO 55
      IF((IDOY .EQ. IDOY1) .AND. (ITIME .EQ. ITIME1)) THEN
       WRITE(17,30)IDOY,IDOY1,ITIME,ITIME1,TMPIR,TEMP1
       GO TO 20
      END IF
19     CONTINUE
20    IF((ITIME .GE. 1100) .AND. (ITIME .LE. 1500)) THEN
      WRITE(18,30)IDOY,IDOY1,ITIME,ITIME1,TMPIR,TEMP1
     END IF
25   CONTINUE
30   FORMAT(1X,2I4,2I6,1X,2F6.2)
     CLOSE(15)
     CLOSE(16)
     CLOSE(17)
     CLOSE(18)
55   END
*****************************************************************************************

C Program netrud.for for sorting net radiation data
C
     IMPLICIT REAL*8 (A-H, O-Z)
     CHARACTER*10 RNMES,RNSIM,RNOUT,RNPAT
  10 FORMAT(A10)
     WRITE(*,*)'Enter the name of the Measured RN Input File'
     READ(*,10)RNMES
     WRITE(*,*)'Enter the name of the Simulated RN Input File'
     READ(*,10)RNSIM
     WRITE(*,*)'Enter the name of the Combi RN Output File'
     READ(*,10)RNOUT
     WRITE(*,*)'Enter the name of the Partial RN  Output File'
     READ(*,10)RNPAT
     OPEN(15,FILE=RNMES,STATUS='OLD')
     OPEN(16,FILE=RNSIM,STATUS='OLD')
     OPEN(17,FILE=RNOUT,STATUS='NEW')
     OPEN(18,FILE=RNPAT,STATUS='NEW')
     M=5000
     N=8000
     DO 25 J=1,M
      READ(15,*)IDOY,ITIME,RNAVG,RNMAX,RNMIN,RNINS
      IF (RNINS .EQ. 9999.0D0) GO TO 55
       DO 19 I=1,N
        READ(16,*)IDOY1,ITIME1,RN,RNCUM,SH,SHCUM,ALES,ALECUM,
     $          GS,GSCUM
        IF (GSCUM .EQ. 111.0D0) GO TO 55
        IF((IDOY .EQ. IDOY1) .AND. (ITIME .EQ. ITIME1)) THEN
         WRITE(17,30)IDOY,IDOY1,ITIME,ITIME1,RN,RNCUM,SH,SHCUM,
     $             ALES,ALECUM,GS,GSCUM
         GO TO 20
        END IF
  19    CONTINUE
  20   IF((ITIME .GE. 600) .AND. (ITIME .LE. 1900) .AND. (RNAVG .GE
     $ 0.0D0)) THEN
       WRITE(18,31)IDOY,IDOY1,ITIME,ITIME1,RNAVG,RNMAX,RNMIN,RNINS,
     $          RN,RNCUM
      END IF
  25  CONTINUE
```

```
 30  FORMAT(1X,2I4,2I6,1X,4(F7.1,F15.1))
 31  FORMAT(1X,2I4,2I6,1X,5F7.1,F15.1)
     CLOSE(15)
     CLOSE(16)
     CLOSE(17)
     CLOSE(18)
 55  END
```

```
C Program protmp.for for sorting profile temperature data
C
     IMPLICIT REAL*8 (A-H, O-Z)
     CHARACTER*10 PROTMES,PROTSIM,PROTOUT,PROTPAT
  10 FORMAT(A10)
     WRITE(*,*)'Enter the name of the Measured Temp  Input File'
     READ(*,10)PROTMES
     WRITE(*,*)'Enter the name of the Simulated Temp. Input File'
     READ(*,10)PROTSIM
     WRITE(*,*)'Enter the name of the Combi Temp. Output File'
     READ(*,10)PROTOUT
     WRITE(*,*)'Enter the name of the Partial Temp.  Output File'
     READ(*,10)PROTPAT
     OPEN(15,FILE=PROTMES,STATUS='OLD')
     OPEN(16,FILE=PROTSIM,STATUS='OLD')
     OPEN(17,FILE=PROTOUT,STATUS='NEW')
     OPEN(18,FILE=PROTPAT,STATUS='NEW')
     M=5000
     N=8000
     DO 25 J=1,M
      READ(15,*)IDOY,ITIME,TMP05,TMP15,TMP30,TMP45
      IF (TMP45 .EQ. 9999.0D0) GO TO 55
       DO 19 I=1,N
        READ(16,*)IDOY1,ITIME1,T0,T5,T10,T15,T20,T25,T30,T35,T40,
     $          T45,T50,T55,T60
        IF (T60 .EQ. 9999.0D0) GO TO 55
        IF((IDOY .EQ. IDOY1) .AND. (ITIME .EQ. ITIME1)) THEN
         WRITE(17,30)IDOY,IDOY1,ITIME,ITIME1,T0,T5,T10,T15,T20,T25,
     $           T30,T35,T40,T45,T50,T55,T60
         GO TO 20
        END IF
  19    CONTINUE
  20    IF((ITIME .GE. 1100) .AND. (ITIME .LE. 1500)) THEN
        WRITE(18,31)IDOY,IDOY1,ITIME,ITIME1,TMP05,T0,T5
       END IF
  25  CONTINUE
  30  FORMAT(1X,2I4,2I6,1X,13F6.2)
  31  FORMAT(1X,2I4,2I6,1X,3F6.2)
     CLOSE(15)
     CLOSE(16)
     CLOSE(17)
     CLOSE(18)
 55  END
```

C Program *suaswc.for* for sorting soil water content data

```
C
      IMPLICIT REAL*8 (A-H, O-Z)
      CHARACTER*10 SWCMES,SWCSIM,SWCOUT,SWCPAT
   10 FORMAT(A10)
      WRITE(*,*)'Enter the name of the Measured SWC Input File'
      READ(*,10)SWCMES
      WRITE(*,*)'Enter the name of the Simulated SWC Input File'
      READ(*,10)SWCSIM
      WRITE(*,*)'Enter the name of the Combi SWC Output File'
      READ(*,10)SWCOUT
      WRITE(*,*)'Enter the name of the Partial SWC  Output File'
      READ(*,10)SWCPAT
      OPEN(15,FILE=SWCMES,STATUS='OLD')
      OPEN(16,FILE=SWCSIM,STATUS='OLD')
      OPEN(17,FILE=SWCOUT,STATUS='NEW')
      OPEN(18,FILE=SWCPAT,STATUS='NEW')
      M=5000
      N=8000
      DO 25 J=1,M
       READ(15,*)IDOY,ITIME,SW02,SW05,SW510,SW1015,SW1520,SW2030,SW3035
       IF (SW3035 .EQ. 9999.0D0) GO TO 55
        DO 19 I=1,N
         READ(16,*)IDOY1,ITIME1,W0,W5,W10,W15,W20,W25,W30,W35,W40,
     S          W45,W50,W55,W60
         IF (W60 .EQ. 9999.0D0) GO TO 55
         IF((IDOY .EQ. IDOY1) .AND. (ITIME .EQ. ITIME1)) THEN
          WRITE(17,30)IDOY,IDOY1,ITIME,ITIME1,W0,W5,W10,W15,W20,W25,
     S             W30,W35,W40,W45,W50,W55,W60
          GO TO 20
         END IF
   19    CONTINUE
   20   IF((ITIME .GE. 600) .AND. (ITIME .LE. 1100)) THEN
        WRITE(18,31)IDOY,IDOY1,ITIME,ITIME1,SW02,SW05,W0,W5
       END IF
   25  CONTINUE
   30  FORMAT(1X,2I4,2I6,1X,13F6.3)
   31  FORMAT(1X,2I4,2I6,1X,4F6.3)
      CLOSE(15)
      CLOSE(16)
      CLOSE(17)
      CLOSE(18)
   55  END
*****************************************************************************************
```

C Program *wmaswc.for* for sorting soil water content data

```
C
      IMPLICIT REAL*8 (A-H, O-Z)
      CHARACTER*10 SWCMES,SWCSIM,SWCOUT,SWCPAT
   10 FORMAT(A10)
      WRITE(*,*)'Enter the name of the Measured SWC Input File'
      READ(*,10)SWCMES
      WRITE(*,*)'Enter the name of the Simulated SWC Input File'
      READ(*,10)SWCSIM
      WRITE(*,*)'Enter the name of the Combi SWC Output File'
      READ(*,10)SWCOUT
      WRITE(*,*)'Enter the name of the Partial SWC  Output File'
```

```
      READ(*,10)SWCPAT
      OPEN(15,FILE=SWCMES,STATUS='OLD')
      OPEN(16,FILE=SWCSIM,STATUS='OLD')
      OPEN(17,FILE=SWCOUT,STATUS='NEW')
      OPEN(18,FILE=SWCPAT,STATUS='NEW')
      M=8000
      N=8000
      DO 25 J=1,M
       READ(15,*)IDOY,ITIME,WMSW05,WMSW15,WMSW30,WMSW45
       IF (WMSW45 .EQ. 9999.0D0) GO TO 55
        DO 19 I=1,N
         READ(16,*)IDOY1,ITIME1,W0,W5,W10,W15,W20,W25,W30,W35,W40,
     $          W45,W50,W55,W60
         IF (W60 .EQ. 9999.0D0) GO TO 55
         IF((IDOY .EQ. IDOY1) .AND. (ITIME .EQ. ITIME1)) THEN
          WRITE(17,30)IDOY,IDOY1,ITIME,ITIME1,W0,W5,W10,W15,W20,W25,
     $             W30,W35,W40,W45,W50,W55,W60
          GO TO 20
         END IF
19      CONTINUE
20     IF((IDOY .EQ. IDOY1) .AND. (ITIME .EQ. ITIME1)) THEN
        WRITE(18,31)IDOY,IDOY1,ITIME,ITIME1 WMSW05,WMSW15,WMSW30,
     $          WMSW45
       END IF
25    CONTINUE
30    FORMAT(1X,2I4,2I6,1X,13F6.3)
31    FORMAT(1X,2I4,2I6,1X,4F6.3)
      CLOSE(15)
      CLOSE(16)
      CLOSE(17)
      CLOSE(18)
55    END
*******************************************************************************
C Program wmheem.for for sorting pressure head data
C
      IMPLICIT REAL*8 (A-H, O-Z)
      CHARACTER*10 HEADMES,HEADSIM,HEADOUT,HEADPAT
 10   FORMAT(A10)
      WRITE(*,*)'Enter the name of the Measured Prel lead Input File'
      READ(*,10)HEADMES
      WRITE(*,*)'Enter the name of the Simulated Prel lead Input File'
      READ(*,10)HEADSIM
      WRITE(*,*)'Enter the name of the Combi Prel lead Output File'
      READ(*,10)HEADOUT
      WRITE(*,*)'Enter the name of the Partial Prel lead  Output File'
      READ(*,10)HEADPAT
      OPEN(15,FILE=HEADMES,STATUS='OLD')
      OPEN(16,FILE=HEADSIM,STATUS='OLD')
      OPEN(17,FILE=HEADOUT,STATUS='NEW')
      OPEN(18,FILE=HEADPAT,STATUS='NEW')
      M=8000
      N=8000
      DO 25 J=1,M
       READ(15,*)IDOY,ITIME,WMCM05,WMCM15,WMCM30,WMCM45,WMCM60
       IF (WMCM60 .EQ. 9999.0D0) GO TO 55
        DO 19 I=1,N
```

```
      READ(16,*)IDOY1,ITIME1,H0,H5,H10,H15,H20,H25,H30,H35,H40,
     $          H45,H50,H55,H60
      IF (H60 .EQ. 9999.0D0) GO TO 55
      IF((IDOY .EQ. IDOY1) .AND. (ITIME .EQ. ITIME1)) THEN
       WRITE(17,30)IDOY,IDOY1,ITIME,ITIME1,H0,H5,H10,H15,H20,H25,
     $           H30,H35,H40,H45,H50,H55,H60
       GO TO 20
      END IF
19    CONTINUE
20    IF((IDOY .EQ. IDOY1) .AND. (ITIME .EQ. ITIME1)) THEN
      WRITE(18,31)IDOY,IDOY1,ITIME,ITIME1,WMCM05,WMCM15,WMCM30,
     $           WMCM45,WMCM60
     END IF
25   CONTINUE
30   FORMAT(1X,2I4,2I6,1X,13F10.2)
31   FORMAT(1X,2I4,2I6,1X,5F10.2)
     CLOSE(15)
     CLOSE(16)
     CLOSE(17)
     CLOSE(18)
55   END
*****************************************************************************************
```

C Program *wmswcp.for* for sorting soil water content data

```
C
     IMPLICIT REAL*8 (A-H, O-Z)
     CHARACTER*10 SWCMES,SWCSIM,SWCOUT,SWCPAT,SWCMON,SWCMOS
  10 FORMAT(A10)
     WRITE(*,*)'Enter the name of the Measured SWC Input File'
     READ(*,10)SWCMES
     WRITE(*,*)'Enter the name of the Simulated SWC Input File'
     READ(*,10)SWCSIM
     WRITE(*,*)'Enter the name of the Combi SWC Output File'
     READ(*,10)SWCOUT
     WRITE(*,*)'Enter the name of the Partial SWC  Output File'
     READ(*,10)SWCPAT
     WRITE(*,*)'Enter the name of the Partial Morning SWC Output File'
     READ(*,10)SWCMON
     WRITE(*,*)'Enter the name of the Partial Morning SIM Output File'
     READ(*,10)SWCMOS
     OPEN(15,FILE=SWCMES,STATUS='OLD')
     OPEN(16,FILE=SWCSIM,STATUS='OLD')
     OPEN(17,FILE=SWCOUT,STATUS='NEW')
     OPEN(18,FILE=SWCPAT,STATUS='NEW')
     OPEN(19,FILE=SWCMON,STATUS='NEW')
     OPEN(20,FILE=SWCMOS,STATUS='NEW')
     M=8000
     N=8000
     DO 25 J=1,M
      READ(15,*)IDOY,ITIME,WMSW05,WMSW15,WMSW30,WMSW45
      IF (WMSW45 .EQ. 9999.0D0) GO TO 55
       DO 19 I=1,N
        READ(16,*)IDOY1,ITIME1,W0,W5,W10,W15,W20,W25,W30,W35,W40,
     $           W45,W50,W55,W60
       IF (W60 .EQ. 9999.0D0) GO TO 55
       IF((IDOY .EQ. IDOY1) .AND. (ITIME .EQ. ITIME1)) THEN
```

```
      WRITE(17,30)IDOY,IDOY1,ITIME,ITIME1,W0,W5,W10,W15,W20,W25,
     $          W30,W35,W40,W45,W50,W55,W60
      GO TO 20
     END IF
19   CONTINUE
20   IF((IDOY EQ IDOY1) AND (ITIME EQ ITIME1)) THEN
     WRITE(18,31)IDOY,IDOY1,ITIME,ITIME1,WMSW05,WMSW15,WMSW30,
     $          WMSW45
     END IF
     IF((ITIME GE 900) AND (ITIME LE 1100)) THEN
     WRITE(19,31)IDOY,IDOY1,ITIME,ITIME1,WMSW05,WMSW15,WMSW30,
     $          WMSW45
     WRITE(20,30)IDOY,IDOY1,ITIME,ITIME1,W0,W5,W10,W15,W20,W25,
     $          W30,W35,W40,W45,W50,W55,W60
     END IF
25   CONTINUE
30   FORMAT(1X,2I4,2I6,1X,13F6.3)
31   FORMAT(1X,2I4,2I6,1X,4F6.3)
     CLOSE(15)
     CLOSE(16)
     CLOSE(17)
     CLOSE(18)
     CLOSE(19)
     CLOSE(20)
55   END
```

APPENDIX 5: PREVAILING CONDITIONS DURING THE EXPERIMENTAL PERIOD

Table A5.1 Calculated "potential evapotranspiration" (ETo) and soil evaporation (Esoil).

DOY	ETo (mm): Kp = 0.8	Rain recurrence interval (days)	Kc	KpKc	Esoil (mm)	Esoil (W/m²)
94	0 66	2	1.00	0.80	0.528	14.96
95	4.32	2	0.90	0.72	3.110	88.16
96	5.28	2	0.85	0.68	3.590	101.76
97	1.08	2	1.10	0.88	0.950	26.94
98	1.02	2	1.10	0.88	0.898	25.44
111	3.42	2	0.90	0.72	2.462	69.79
112	0.78	2	1.10	0.88	0.686	19.45
113	0.24	2	1.10	0.88	0 211	5.99
114	3.60	2	0.90	0.72	2 592	73.46
115	1 20	2	1.00	0.80	0.960	27.21
116	2.16	2	1.00	0.80	1 728	48.98
117	2.70	2	0.90	0.72	1.944	55.10
118	2.94	2	0.90	0.72	2.117	60.00
123	0.12	2	1.10	0.88	0.106	2.99
125	4.02	7	0.50	0.40	1.608	45.58
126	3.72	7	0.50	0.40	1.488	42.17
127	3.96	7	0.50	0.40	1.584	44.89
128	3.90	7	0.50	0.40	1.560	44.21
129	2 76	7	0.55	0.44	1.214	34.42
130	3.06	7	0.50	0.40	1.224	34.69
131	2.28	7	0.60	0.48	1.094	31.02
157	2.28	2	0.95	0.76	1.733	49.11
202	3.24	20	0.25	0.20	0.648	18.37
203	3.30	20	0.25	0.20	0.660	18.71
204	3.66	20	0.25	0.20	0.732	20.75
205	3 42	20	0.25	0.20	0.684	19.39
206	4.20	20	0.20	0.16	0.672	19.05
207	4.08	20	0.20	0.16	0.653	18.50
208	4.86	20	0.20	0.16	0.778	22.04
212	5.22	20	0.20	0.16	0.835	23.67
213	2.70	20	0.30	0.24	0.648	18.37
214	3.12	20	0.20	0.16	0.499	14.15

APPENDIX 6: CORRECTION FOR CHANGES IN SOLAR RADIATION

Table A6.1 Measured TDMax, calculated TDaMax and TDrMax, and the corresponding means and standard deviations (STD). Calculated as detailed under section 6.6 of chapter 6 for each day.

DOY	Max (TDa)	Max (TDr)	Max (TD)	Mean (TDa)	Mean (TDr)	Mean (TD)	STD (TDa)	STD (TDr)	STD (TD)
91	13.0	8.2	9.50	4.3	4.3	4.4	2.7	1.1	2.2
94	17.8	12.3	15.9	9.0	9.0	8.9	3.8	1.3	4.1
95	22.8	16.8	20.6	11.4	11.4	11.4	5.4	2.0	4.6
96	26.1	19.8	23.8	14.2	14.2	14.3	6.3	2.3	5.8
97	8.8	5.9	8.8	4.9	4.9	5.0	2.1	0.6	2.0
98	16.8	11.0	13.1	7.4	7.4	7.5	3.1	1.0	2.8
99	13.7	10.0	12.1	7.7	7.7	7.7	3.4	0.8	3.4
111	17.9	12.5	17.6	8.9	8.9	8.8	3.9	1.4	3.8
113	15.4	11.6	16.5	9.4	9.4	9.4	3.8	1.1	3.8
114	24.9	18.1	23.6	15.0	15.0	15.0	5.2	1.3	6.2
115	13.9	10.3	12.5	7.8	7.8	7.8	2.8	1.2	2.7
116	20.7	14.6	18.7	10.3	10.3	10.3	4.1	1.5	3.5
117	23.2	15.5	21.9	12.5	12.5	12.4	5.3	1.3	5.7
118	21.9	17.9	21.3	12.6	12.6	12.6	3.4	1.5	3.7
125	21.2	13.8	17.9	8.5	8.5	8.5	4.2	1.7	3.3
126	18.7	15.4	18.3	12.0	12.0	12.0	4.1	1.4	4.3
127	23.4	18.7	22.7	14.0	14.0	14.0	5.4	2.0	5.0
128	22.1	15.7	20.7	12.8	12.8	12.8	4.3	1.2	4.7
129	19.6	15.2	19.3	10.5	10.5	10.4	3.1	1.3	3.8
137	12.4	7.5	11.0	5.5	5.5	5.6	2.9	0.7	2.7
138	15.6	11.3	15.2	8.3	8.3	8.2	3.3	1.6	3.0
140	22.0	14.0	20.3	10.7	10.7	10.7	4.4	1.2	4.7
143	13.8	10.6	13.0	8.0	8.0	8.0	2.8	1.1	2.7
144	20.1	15.1	19.3	10.5	10.5	10.5	3.9	1.8	4.1
147	20.5	16.2	22.0	13.1	13.1	13.1	4.8	1.6	5.6
149	23.5	18.4	23.5	14.3	14.3	14.3	4.8	1.7	5.1
150	24.0	19.4	23.7	14.9	14.9	14.8	5.6	1.6	6.2
154	13.7	11.1	10.9	8.3	8.3	8.3	1.9	1.2	1.7
155	20.8	12.0	18.1	7.0	7.0	7.0	4.8	1.4	4.4
156	9.1	5.7	7.5	4.5	4.5	4.5	1.5	0.4	1.6
157	21.4	17.3	20.8	13.4	13.4	13.3	4.0	1.8	4.6
158	20.5	16.3	17.5	9.7	9.7	9.7	3.6	1.8	3.3
169	21.9	19.0	20.8	13.1	13.1	13.0	5.5	3.2	5.5
170	15.8	12.4	16.0	7.6	7.6	7.6	3.5	1.6	3.8
171	8.5	6.4	8.7	4.3	4.3	4.3	2.0	1.0	2.4

172	13 4	9.2	12 9	6 3	6.3	6.2	3 9	1.4	4.5
173	12 7	10.2	11.1	6 6	6.6	6.5	2.2	1.2	2.2
177	19 2	13.2	17.6	10.0	10.0	9.9	4.9	1.8	5.2
178	19.1	14.1	18.0	10.2	10.2	10.2	4.2	1.6	4.6
179	21 8	14 0	15.5	7.8	7.8	7 8	3.7	1.8	3.4
180	10 6	6.6	10.7	5.3	5.3	5 3	2.2	0.7	2.3
181	19 5	12.7	16.3	7.5	7 5	7 5	3 5	1.4	3.6
182	19 9	13.6	18 4	10 0	10.0	10.0	4 5	1 5	4.6
183	15.5	11.4	14 7	8 1	8 1	8.0	3 6	1 4	3.6
184	24 7	16.6	22.2	11.5	11.5	11.5	5 5	2.2	5.2
185	17 8	13 9	16 3	8 3	8.3	8.3	3.8	1 8	3.8
186	25 9	19.1	22 1	11.9	11 9	11.9	6.6	2.8	5.4
187	22 8	17.3	21 9	11.4	11.4	11.4	4 0	1.8	4.2
189	4 8	3 0	4 4	1.9	1 9	1 8	1 5	0.5	1 6
190	15.5	9 9	12.5	5 3	5 3	5.3	2.9	1.4	2 6
191	17.3	9 4	15 1	6.2	6 2	6 2	5 0	1 4	5.3
193	16.6	11 2	13 9	7 1	7 1	7 0	3 7	1.7	3.9
194	21 6	13 5	22 4	8.2	8 2	8.2	4 8	1 6	4.9
195	19.9	16 4	19 4	12 2	12 2	12 4	5.1	2.0	4.7
196	21.7	17.1	21 7	11 5	11 5	11.5	5.1	1.9	4.8
197	28.1	19.6	22 7	13 0	13 0	13 0	6 3	2 5	5 8
198	23 9	26 6	19 3	9.4	9.4	9.4	6.5	4 9	5.8
199	10 8	8.4	9.4	6.4	6 4	6 6	2 5	0.7	2 2
200	26.4	18.1	22.1	11.7	11 7	11 7	6.1	2 7	5.8
201	30.1	22.6	23 7	13.8	13.8	13.9	6.8	3.2	5.3
202	28 0	19 4	22.9	12.9	12 9	12.9	5.6	1.9	5 0
203	22 3	15.9	18.6	11 5	11 5	11.5	4.4	1.6	4.2
204	31 2	19.4	24 8	11 9	11 9	11.9	7.1	2.2	6.6
205	23 1	16 5	21.7	11.2	11.2	11 2	5.1	1.8	5 1
206	27.1	16.6	24.4	11 4	11.4	11.4	7.2	2.5	6.4
207	21.7	17.8	22.0	12.1	12 1	12.2	6.0	2 3	5.6
208	23 1	15.7	22.7	12 8	12 8	12 9	5.7	1.5	5.7
210	15.7	9.0	16 3	5 5	5.5	5.5	3 4	1 2	3.4
211	21 5	12.6	21.5	9.9	9.9	9.9	5.3	1.4	5.2
212	19.8	17.2	20.2	12.3	12.3	12.4	4.9	2 0	4.7
213	19.4	15.7	18.7	10.9	10.9	10 9	4.3	1 5	4.0
214	21.7	16.4	21 5	12.1	12 1	12.1	5.7	1.9	5.6

APPENDIX 7: SOIL PHYSICAL PROPERTIES

Table A7.1 Calculation of soil water content (SWC) using the Rawls and Brakensiek (1989) model based on soil physical properties.

Rawls and Brakensiek (1989) Model: Van Genuchten (1980)										
DEPTH (cm)	% CLAY	% SAND	Porosity (θ_s)	ψ_s (cm)	λ	θ_r (v/v)	Ks (cm/h)	a (1/cm)	n (=λ+1)	m (=λ/n)
0-2	43.3	45.7	0.517	14.460	0.191	0.124	1.0954	0.069	1.191	0.161
0-5	43.3	45.7	0.462	21.763	0.166	0.117	0.2480	0.046	1.166	0.142
5-10	40.5	51.0	0.506	10.829	0.196	0.122	1.7909	0.092	1.196	0.164
10-15	46.0	44.0	0.490	20.274	0.167	0.121	0.3766	0.049	1.167	0.143
15-20	53.0	38.5	0.505	29.039	0.145	0.122	0.1902	0.034	1.145	0.127
20-30	56.5	38.0	0.500	34.259	0.126	0.119	0.1113	0.029	1.126	0.112
30-35	55.0	37.6	0.480	40.036	0.120	0.115	0.0567	0.025	1.120	0.107
35-45	56.0	37.0	0.441	59.377	0.092	0.102	0.0095	0.017	1.092	0.084
45-50	55.0	38.0	0.419	66.456	0.082	0.096	0.0044	0.015	1.082	0.075
50-60	56.5	36.0	0.389	101.674	0.059	0.081	0.0006	0.010	1.059	0.056
Average	**50.5**	**41.1**	**0.471**	**39.817**	**0.134**	**0.112**	**0.388**	**0.039**	**1.134**	**0.117**

	Depth: 0-2 cm		Depth: 0-5 cm		Depth: 5-10 cm		Depth: 10-15 cm		Depth: 15-20 cm	
SWP (cm)	RHS	SWC (vol fr)	RHS	SWC (vol fr)	RHS	SWC (vol fr)	RHS	SWC (vol fr)	RHS	SWC (vol fr)
10	0.9232	0.4867	0.9529	0.4461	0.8993	0.4673	0.9494	0.4715	0.9678	0.4931
20	0.8647	0.4637	0.9124	0.4321	0.8313	0.4412	0.9068	0.4558	0.9384	0.4818
30	0.8221	0.4470	0.8802	0.4210	0.7846	0.4233	0.8734	0.4435	0.9139	0.4724
40	0.7893	0.4341	0.8541	0.4120	0.7500	0.4100	0.8466	0.4336	0.8931	0.4644
50	0.7631	0.4238	0.8324	0.4045	0.7227	0.3996	0.8244	0.4254	0.8754	0.4576
60	0.7413	0.4152	0.8138	0.3981	0.7005	0.3910	0.8055	0.4185	0.8600	0.4517
70	0.7228	0.4079	0.7978	0.3926	0.6818	0.3839	0.7893	0.4125	0.8463	0.4465
80	0.7068	0.4017	0.7836	0.3877	0.6657	0.3777	0.7750	0.4072	0.8342	0.4418
90	0.6927	0.3961	0.7710	0.3833	0.6517	0.3723	0.7623	0.4025	0.8233	0.4376
100	0.6802	0.3912	0.7597	0.3794	0.6392	0.3675	0.7509	0.3983	0.8133	0.4338
.....										
13900	0.2686	0.2295	0.3430	0.2356	0.2453	0.2165	0.3369	0.2456	0.4090	0.2788
14000	0.2683	0.2293	0.3426	0.2355	0.2450	0.2164	0.3365	0.2455	0.4086	0.2786
14100	0.2679	0.2292	0.3422	0.2353	0.2447	0.2162	0.3361	0.2453	0.4082	0.2785
14200	0.2675	0.2290	0.3418	0.2352	0.2443	0.2161	0.3357	0.2452	0.4078	0.2783
14300	0.2672	0.2289	0.3414	0.2351	0.2440	0.2160	0.3353	0.2450	0.4073	0.2782
14400	0.2668	0.2288	0.3410	0.2349	0.2437	0.2159	0.3349	0.2449	0.4069	0.2780
14500	0.2665	0.2286	0.3406	0.2348	0.2433	0.2157	0.3345	0.2447	0.4065	0.2778
14600	0.2661	0.2285	0.3402	0.2347	0.2430	0.2156	0.3341	0.2446	0.4061	0.2777
14700	0.2658	0.2283	0.3398	0.2345	0.2427	0.2155	0.3338	0.2445	0.4057	0.2775
14800	0.2654	0.2282	0.3394	0.2344	0.2423	0.2154	0.3334	0.2443	0.4053	0.2774
14900	0.2651	0.2281	0.3390	0.2343	0.2420	0.2152	0.3330	0.2442	0.4049	0.2772
15000	0.2648	0.2279	0.3387	0.2341	0.2417	0.2151	0.3326	0.2440	0.4045	0.2771

Table A7.2 Soil analysis data for SUA Field Experiments 1996/97

SOIL ANALYSIS DATA: SUA FIELD EXPERIMENTS 1996/97													
FIELD REFERENCE. KEY: P.D. = Particle Density; C = Clay; and SC = Sandy Clay													
DSGN.	DATE	DEPTH (cm)	LAB NO	% CLAY	%F. SILT	%C. SILT	% SAND	T. CLASS	P.D (g/cm³)	DEPTH (cm)	% CLAY	% SAND
B	27 07 97	0-07	422	37	5	6	52	SC	2 58	0-07	37	52
A	23 07 97	0-07	424	52	5	4	39	SC	2 56	0-07	52	39
A	25 07 97	0-07	436	41	4	9	46	SC	2 56	0-07	41	46
	24 07 97	03-08	429	41	4	5	50	SC	2 54	03-08	41	50
Mean		4		43	4	6	47		2.56	4	43	47
	20 05 97	05-10	415	40	2	6	52	SC	2 56	05-10	40	52
B	27 07 97	07-14	423	45	3	8	44	C	2 58	07-14	45	44
A	23 07 97	07-14	425	45	3	8	44	C	2 51	07-14	45	44
A	25 07 97	07-15	421	47	5	4	44	C	2 58	07-15	47	44
Mean		10		44	3	6	46		2.56	10	44	46
	20 05 97	10-20	419	46	2	8	44	C	2 53	10-20	46	44
	24 07 97	11-26	418	52	4	6	38	C	2 53	11-26	52	38
B	27 07 97	14-24	427	53	3	4	40	C	2 54	14-24	53	40
A	23 07 97	14-24	420	52	3	5	40	C	2 57	14-24	52	40
A	25 07 97	15-26	432	55	1	8	36	C	2 55	15-26	55	36
Ah	26 11 96	0-25	412	47	1	8	44	C	2.55	0-25	47	44
Mean		15		51	2	6	40		2.54	15	51	40
	20 05 97	20-30	414	55	2	5	38	C	2 55	20-30	55	38
B	27 07 97	24-35	417	58	0	4	38	C	2 57	24-35	58	38
A	23 07 97	24-40	435	55	3	4	38	C	2 56	24-40	55	38
B1	26 11 96	25-50	411	55	3	4	38	C	2 56	25-50	55	38
A	24 07 97	26-34	426	55	3	6	36	C	2 52	26-34	55	36
A	25 07 97	26-39	428	53	3	4	40	C	2 54	26-39	53	40
Mean		30		55	2	4	38		2.55	30	55	38
	20 05 97	30-45	416	57	1	6	36	C	2.5	30-45	57	36
A	24 07 97	34-40	431	57	3	6	34	C	2.54	34-40	57	34
B	27 07 97	35-48	413	55	2	3	40	C	2 58	35-48	55	40
Mean		40		56	2	5	37		2.54	40	56	37
	20 05 97	45-55	434	57	3	4	36	C	2 51	45-55	57	36
B	27 07 97	48-59	430	53	3	4	40	C	2 41	48-59	53	40
Mean		50		55	3	4	38		2.46	50	55	38
B2	26 11 96	50-75	410	55	3	4	38	C	2 26	50-75	55	38
B3	26 11 96	75-100	433	58	2	6	34	C	2 49	75-100	58	34
Mean		75		56	2	5	36		2.38	75	56	36

Table A7.3 Estimation equations for the Brooks and Corey parameters according to Rawls and Brakensiek (1989)

ψ_e - Brooks and Corey air entry water potential (cm)

$$\psi_e = \exp[5.3396739 + 0.184038(C) - 2.4839454(\theta_s) - 0.00213853(C^2) - 0.04356349(S)(\theta_s) - 0.617445089(C)(\theta_s) + 0\ 00143598(S^2)(\theta_s^2) - 0.00855375(C^2)(\theta_s^2) - 0.00001282(S^2)(C) + 0.00895359(C^2)(\theta_s) - 0.00072472(S^2)(\theta_s) + 0.0000054(C^2)(S) + 0.50028060(\theta_s^2)(C)]$$

λ - Brooks and Corey pore size distribution index

$$\lambda = \exp[-0.7842831 + 0.0177544(S) - 1.062498(\theta_s) - 0.00005304(S^2) - 0.00273493(C^2) + 1.11134946(\theta_s^2) - 0.03088295(S)(\theta_s) + 0.00026587(S^2)(\theta_s^2) - 0.00610522(C^2)(\theta_s^2) - 0.00000235(S^2)(C) + 0.00798746(C^2)(\theta_s) - 0.00674491(\theta_s^2)(C)]$$

θ_r - Brooks and Corey residual water content (vol fraction)

$$\theta_r = - 0.0182482 + 0.00087269(S) + 0.00513488(C) + 0.02939286(\theta_s^2) - 0.00015395(C^2) - 0.0010827(S)(\theta_s) - 0.00018233(C^2)(\theta_s^2) + 0\ 00030703(C^2)(\theta_s) - 0.0023584(\theta_s^2)(C)$$

K_s - Saturated hydraulic conductivity (cm h^{-1})

$$K_s = \exp[- 8.96847 + 19.52348(\theta_s) - 0.028212(C) + 0\ 00018107(S^2) - 0.0094125(C^2) - 8.395215(\theta_s^2) + 0\ 077718(S)(\theta_s) - 0.00298(S^2)(\theta_s^2) - 0.019492(C^2)(\theta_s^2) + 0.0000173(S^2)(C) + 0\ 02733(C^2)(\theta_s) + 0.001434(S^2)(\theta_s) - 0\ 0000035(C^2)(S)]$$

C - Percentage of clay ($5 < C < 60$), S - percentage of sand ($5 < S < 70$), θ_s - porosity (volume fraction).

Table A7.4 Soil survey and classification

DESCRIBED BY: Baanda A. Salim
DATE: 25.11.1996
WEATHER: Sunny, dry and calm, humid. Rained on 20.11.1996 after a long dry season.
LOCALITY: SUA campus, Morogoro, Tanzania
NE of SUA Meteorological Weather Station (MWS) (located at latitude 6°50'20"S and longitude 37°39'20"E); about 150 m from the MWS office.
North of SUA Primary School; about 100 m from the school.
NE of SUA Estates Department; about 150 m away.
ELEVATION: 525.8 m above mean sea level (msl).
RELIEF: Undulating
North of Uluguru Mountains
Upper Slope from an Interfluve
1.6° - 2.3° (eastern aspect)
Level to gently sloping (using PM Clinometer Height Meter (PM-5/360 PC), SUUNTO Co., Finland)
LAND USEAND VEGETATION: Fallow (grass covered)
Very few shrubs
Planted trees and sisal on the field boundary (with at least 50 m fetch on each side of the experimental field)
NATURAL VEGETATION:

PROFILE DESCRIPTION:

1. A_h Horizon (0 - 25 cm)

COLOUR: i. Slightly moist — 2.5YR 3/3 Dark Reddish Brown
ii. Moist — Same as for Slightly Moist

STONINESS: Stoneless

SOIL WATER STATE: Slightly Moist
SOIL STRUCTURE: Medium to Very Coarse Subangular Blocky
DEGREE OF PED DEVELOPMENT: Massive Appearance
Moderately Developed Peds
Compound Peds

VOIDS:
Porosity: Very Slightly Porous
Fissures: 1 - 3 mm
Fine fissures
Macropores: 20 mm (isolated case)
0.5 - 2 mm: fine macropores

Consistence: Very hard when dry
Friable when moist

Packing Density: About 1.4 g/cm^3 (medium packing density)
Stickiness: Slightly sticky
Plasticity: Moderately plastic

ROOTS & OTHER FLORA & PLANT REMAINS:
Very fine to fine fibrous roots
Many (25 - 200 roots/100 cm^2)

TYPES OF COATS: Indistinct clay coating on voids (surfaces)

BOUNDARY TO NEXT HORIZON: Clear smooth boundary

2. B1 Horizon 25 - 50 cm

COLOUR. i. Air dry 2.5 YR 4/6. Red
ii. Moist 2.5 YR 4/4 Reddish Brown

STONINESS: Stoneless
SOIL WATER STATE: Dry
SOIL STRUCTURE Same as for A_h
DEGREE OF PED DEVELOPMENT Massive Appearance
Moderately Developed Compound Peds

VOIDS.
Porosity: Very slightly porous
Fissures Very fine to fine fissures
Macropores: 0.5 - 2 mm. fine macropores
Packing Density: About 1 4 g/cm^3 (medium packing density)
Consistence: Hard when dry
Friable when moist
Stickiness. Same as for A_h
Plasticity: Same as for A_h

ROOTS: Very fine to fine fibrous roots
Many
CLAY COATS: Indistinct clay coats

BOUNDARY TO NEXT HORIZON. Not visible

3 B2 Horizon (50 - 75 cm)

COLOUR: i. Air Dry 2.5YR 4/6. Red
ii. Moist 2.5YR 4/4: Reddish Brown

STONELESS:
WATER STATUS: Dry

SOIL STRUCTURE: Same as B_1
DEGREE OF PED DEVELOPMENT: Same as for B_1

VOIDS
Porosity: Porous for all
Fissures: Very fine to fine fissures
Packing Density: approx. 1.4 g/cm^3 (medium packing density)
Consistence: hard when dry
friable when moist
STICKINESS: Same as for B_1
PLASTICITY: Same as for B_1
ROOTS, etc Common. Very fine to fine fibrous roots
COATING: Indistinct clay coating
BOUNDARY TO NEXT LAYER: Not there

4. B3 HORIZON (75 - 100 cm)

COLOUR: i. Dry 2.5YR 4/6: Red
ii. Moist 2.5YR 4/4: Reddish Brown

SOIL STRUCTURE: Same as for B_2

VOIDS:
Porosity: Porous
Fissures: Unobservable
Packing Density: approx. 1.4 g/cm^3 (medium packing density)
Macropores Very fine to fine macropores

CONSISTENCE: hard when dry
friable when moist

STICKINESS: Same as for B_2
PLASTICITY: Same as for B_2

ROOTS. Very fine fibrous roots
few

COATS

APPENDIX 8: EXAMPLE OF INPUT FILES

```
2,3,2,3,2,3,1,1
0.6,0.05,0.001
124,300.0
1.0
12.0,12.0
22.7,28.5,28.4,28.2,28.2,28.2,28.2,28.1,28.1,28.0,28.0,28.0,28.0
0.317,0.317,0.287,0.257,0.274,0.274,0.2919,0.287,0.287,0.282,0 282,0 282,0.282
5
1
4
0
0
0
11
91,25.3,4.5,22 5,1 0,0.99,15490000
1
91,30.4
1
91,0.285
91,4.25,4.50,0.199
91,4.50,4.75,0.398
91,4.75,5.00,3.582
91,5.00,5 25,1.791
91,5 25,5.50,0.199
92,24.9,4.5,22 3,0.7,0.88,15780000
1
92,30.4
1
92,0.285
92,15.00,15.25,0.398
93,23.9,4.1,22.1,0.9,0.80,11390000
1
93,30.0
1
93,0.285
93,13.25,13.50,1.194
93,13.50,13.75,0.199
93,14.00,14.25,5.771
93,14.25,14.50,0.796
94,25.2,6.0,21.6,1.2,0.81,18670000
1
94,30 7
1
94,0.285

95,26.1,5.2,22.0,0 9,0.94,17840000
1
```

95,31.1
1
95,0.284
96,26.0,5.9,21.2,1.0,1.22,20100000
1
96,31.6
1
96,0.283
97,25.4,4.7,22.2,1.5,1.00,16080000
1
97,32.1
1
97,0.281
97,6.50,6.75,1.99
97,6.75,7.00,2.189
97,7.00,7.25,2.786
97,7.25,7.50,1.791
97,7.50,7.75,0.199
97,8.25,8.50,0.199
97,8.50,8.75,0.597
97,8.75,9.00,0.597
97,9.00,9.25,0.199
97,23.25,23.50,0.199
97,23.50,23.75,0.199

APPENDIX 9: EXAMPLE OF *SUAHEAT MODEL* OUTPUT SCREEN

SOIL HEAT AND WATER FLOW MODEL

1-DIMENSIONAL TRANSIENT HEAT AND WATER FLOW PROGRAM
SOLVE PROBLEM WITH IMPLICIT FINITE DIFFERENCE METHOD

Written by

Baanda A. Salim

SOIL PHYSICS & REMOTE SENSING
Institut fuer Landtechnik
University of Bonn
D-53115
Bonn
Federal Republic of Germany

```
Enter Name of the Input File                          >
Enter Name of Energy Partition File                   >
Enter Name of Temperature File                        >
Enter Name of Temperature Difference File             >
Enter Name of Water Content File                      >
Enter Name of Pressure Head File                      >
Enter Name of Average Water Content File              >
Enter Name of Average Pressure Head File              >
Enter Name of Moisture Availability File              >
```

Optionally

```
Enter Name of Remotely-sensed Temp. Coeff. File       >
Enter Name of Remotely-sensed SW Cont. Coeff. File    >
Enter Name of Initial Temp. & SWC  Output File        >

I1 = 2   I2 = 3   I3 = 2   I4 = 3   I5 = 2   I6 = 3   I7 = 1 I8 = 1  I9 = 1
LENGTH OF FLOW REGION IS          600 METRE
SPATIAL STEP SIZE IS              .050  METRE
ZO =                              .0010 METRE
LENGTH OF SIMULATION IS           124  DAYS
TIME STEP SIZE IS                 300.00  SECONDS
OUPUT TIME INTERVAL IS            1.00  HOURS
DAY LENGTH IS                     12.000  HOURS
SOLAR NOON IS                     12.000  HOURS
  1.682   .690  1.433   .440   .070   .560   .000
  2.000  1.500   .2000E-05
22.70 28.50 28.40 28.20 28.20 28.20 28.20 28.10 28.10 28.00 28.00 28.00 28.00
  .32   .32   .29   .26   .27   .27   .29   .29   .29   28   .28   .28   .28
```

APPENDIX 10 DEFINITIONS OF "SURFACE TEMPERATURE"

Aerodynamic Temperature A temperature obtained by extrapolating the air temperature profile to an apparent canopy height given by the displacement height plus the roughness length, which is typically about 3/4 the canopy height. If the roughness length for momentum is used then the extrapolated temperature is a *momentum aerodynamic temperature*, and if the roughness for heat is used then the extrapolated temperature is a *thermal aerodynamic temperature* (T_{aero})

Canopy Temperature A general nonspecific term referring to aerodynamic temperature or directional infrared temperature, which usually is made from a view angle oblique to the surface so that vegetation dominates the Infrared Thermometer (IRT) field of view minimizing the effect of soil. Use of this term usually implies that directional and hemispherical, broadband and narrowband infrared temperatures, and aerodynamic temperature are all equal.

Directional Brightness Temperature A temperature that assumes the surface to be Lambertian Black Body. It is obtained by equating the measured radiance with the integral over wavelength of the Planck's Black Body function times the sensor response; then inverting this equation for the temperature in the Planck's function. This requires specification of wavelength interval, direction, and whether the observation is immediately above the surface or above the atmosphere from a satellite $T_B(\Theta)$

Directional Emissivity Emissivity of a surface from a particular view direction, which may be estimated as the ratio of the actual radiance from the surface to the radiance that would occur if all conditions were the same except that the elements of the surface were Black Bodies. This is appropriate for satellite observations (usually 10-12 μm) and ground observations (usually 8-14 μm), but care must be taken in comparing these because of atmospheric effects and wavelength differences. This is a property of the surface if conditions are isothermal. $\varepsilon(\Theta)$.

Directional Infrared Temperature The temperature from a given view direction that is calculated from the thermal radiance in a given wavelength interval considering appropriate surface emissivity and reflected thermal irradiance. It may be estimated by subtracting the reflected sky radiance from the measured radiance and setting this adjusted quantity equal to the integral over wavelength of the product of the Planck's function times the sensor response; then inverting the equation for the temperature in the Planck's function. $T_{IR}(\Theta)$.

Hemispherical Emissivity Integral of the directional emissivity over the hemisphere of view. A *narrowband* hemispherical emissivity can be defined for particular sensors, but it rarely is useful. For purposes of the thermal radiation in the surface energy budget, a *broadband* (3-100 μm) hemispherical emissivity is used (ε)

Hemispherical Infrared Temperature A temperature of the radiating surface that provides an estimate of the broadband emitted flux density when the temperature is raised to the fourth power and multiplied by the Stefan-Boltzman constant and broadband hemispherical emissivity. (T_{sh}).

Kinetic Temperature A weighted-average thermodynamic temperature of all elements comprising the surface. For a heterogeneous surface composed of objects with a range of temperatures, the kinetic temperature depends on the weighting and thus is not unique; further, the kinetic temperature of a canopy-soil system probably is not directly measurable except when it is near isothermal. For a Lambertian surface with a uniform temperature in thermodynamic equilibrium, the kinetic temperature, hemispherical infrared temperature and directional infrared temperature from any direction are identical. A *mean kinetic temperature* may be defined as the arithmetic average of the temperatures of all the objects, or an area weighted mean A *directional kinetic temperature* may weight the fourth power of temperatures of objects by the fraction of view they occupy from some particular view direction.

Skin Temperature A nonspecific term that may refer to the directional brightness or infrared temperature for a sensor with particular wavelength and view characteristics.

Surface Temperature A general, nonspecific term referring to the aggregate temperature of all objects, comprising the surface. It might be an infrared temperature, kinetic temperature, or aerodynamic temperature, or it may be directional or hemispherical.

APPENDIX 11: SUMMARY OF STATISTICAL ANALYSIS

Table A11.1 Relationships between TDMax/A5MR and weighted-average soil water contents.

TDMax	Wavg5	-0.006	0.241813	A5MR	Wavg5	-0.006	0.2370653
		0.001	0.01941			0.001	0.018171
		0.814212	0.01314			0.821724	0.012873
		35.05986	8			36.87422	8
		0.0061	0.0014			0.0061	0.00133
		-5.92114	12.45616			-6.07241	13.046582
TDMax	Wavg15	-0.005	0.243406	A5MR	Wavg15	-0.005	0.2405741
		0.001	0.01747			0.001	0.015649
		0.783356	0.01182			0.809561	0.011086
		28.92689	8			34.00822	8
		0.004	0.0011			0.0042	0.001
		-5.37837	13.93445			-5.83166	15.373248
TDMax	Wavg30	-0.004	0.257724	A5MR	Wavg30	-0.004	0.2558452
		0.001	0.01933			0.001	0.017726
		0.644523	0.01309			0.672609	0.012557
		14.50494	8			16.43564	8
		0.0025	0.0014			0.0026	0.00126
		-3.80854	13.33252			-4.05409	14.433457
TDMax	Wavg45	-0.005	0.295415	A5MR	Wavg45	-0.005	0.2897626
		0.0012	0.02466			0.0013	0.024253
		0.632639	0.01669			0.61088	0.017181
		13.77697	8			12.5592	8
		0.0038	0.0022			0.0037	0.00236
		-3.71173	11.97862			-3.5439	11.947688
TDMax	Wavg60	-0.01	0.391678	A5MR	Wavg60	-0.009	0.374086
		0.0022	0.04377			0.0024	0.046424
		0.706075	0.02963			0.63792	0.032888
		19.2178	8			14.09458	8
		0.01687	0.007			0.01525	0.00865
		-4.38381	8.947599			-3.75428	8.0579954

Table A11.2 Quantitative measures of model performance for simulation of profile soil temperatures at different depths in the soil - calibration phase.

T(Sim5)	T(Avg5)	SUMABS	N	MAD	SUMSQR	RMSD	1.5868613	-17.10275
		4497.8012	1619	2.8	19362.195	3.5	0.0177118	0.5116435
							0.8323307	2.6610186
							8026.9866**	1617
							56839.251	11450.009
							89.593451	-33.42708
							0.9894316	0
							0.023118	#N/A
							0.7143527	3.4732518
							4043.8267**	1617
							22097.617	19506.644
							42.799106	
T(Sim15)	T(Avg15)	SUMABS	N	MAD	SUMSQR	RMSD	1.0560503	-2.310205
		1743.9295	1619	1.1	2758.4529	1.3	0.0155021	0.4543184
							0.741601	1.11605
							4640.7647**	1617
							5780.3856	2014.0826
							68.123158	-5.084992
							0.9770646	0
							0.015626	#N/A
							0.7374524	1.1249734
							4541.884**	1617
							4948.0511	2046.4187
							62.528044	
T(Sim30)	T(Avg30)	SUMABS	N	MAD	SUMSQR	RMSD	0.9279982	1.7143732
		845.18091	1619	0.5	658.84742	0.6	0.0157998	0.4622322
							0.6808609	0.5009153
							3449.7563**	1617
							865.59952	405.73139
							58.734626	3.7089007
							0.9866211	0
							0.015867	#N/A
							0.6781439	0.5030431
							3406.9836**	1617
							978.41586	409.18566
							62.180835	

T(Sim45)	T(Avg45)	SUMABS	N	MAD	SUMSQR	RMSD	1.1265661	-4.008524
		509.02622	1619	0.3	230.84118	0.4	0.0118734	0.3492985
							0.8477339	0.238853
							9002.5638**	1617
							513.60317	92.251089
							94.881841	-11.47593
							0.9902873	0
							0.0123476	#N/A
							0.8353287	0.2483923
							8202.5602**	1617
							396.85943	99.766824
							80.201093	

* F-value significant (at the 5% probability level)
** F-value highly significant (at the 1% probability level)

KEY TO READING THE STATISTICAL ANALYSIS TABLES A11.1 - A11.7: The last two columns or the two columns immediately to the right of the Y- and X-variables.

Y-VARIABLE	X-VARIABLE				SLOPE	Y-INTERCEPT
					SE	SE
					r^2	SEY
					F-VALUE	df
					SSR	SSE
					t-VALUE	t-VALUE
					SLOPE	0
					SE	#N/A
					r^2	SEY
					F-VALUE	df
					SSR	SSE
					t-VALUE	t-VALUE

Table A11.3 Quantitative measures of model performance for simulation of profile soil water contents at different depths in the soil - calibration phase

DOY	TIME	SWC (Sim510)	SWC(Avg5)	SUMABS	N	MAD	SUMSQR	RMSD	4.9428651	-0.510725
192	100			31.220531	543	0.057	2.9117445	0.073	0.0935005	0.0135062
									0.8378135	0.0219817
214	2400								2794.6654	541
									1.3503683	0.2614085
									52.864595	
									1.4187509	0
									0.1784705	#N/A
									0.4090916	0.0419579
									374.53958	541
									0.1158282	0.9524124
									7.9494964	
DOY	TIME	SWC (Sim510)	SWC(Avg5)	SUMABS	N	MAD	SUMSQR	RMSD	1.1181786	-0.017541
176	100			2.4309755	384	0.006	0.023113	0.008	0.0222816	0.0038588
									0.8682953	0.0069868
191	2400								2518.4279	382
									0.1229377	0.0186474
									50.183941	
									1.0175038	0
									0.0228765	#N/A
									0.8611687	0.0071733
									2369.5402	382
									0.1018095	0.0196565
									44.478133	
DOY	TIME	SWC (Sim510)	SWC(Avg5)	SUMABS	N	MAD	SUMSQR	RMSD	2.1996422	-0.179271
147	100			20.263698	360	0.056	1.3544977	0.061	0.1153681	0.0226815
									0.5038279	0.0214214
161	2400								363.5239	358
									0.1668119	0.1642772
									19.066303	
									1.2894737	0
									0.1250305	#N/A
									0.4172356	0.0232155
									256.31342	358
									0.0574348	0.1929469
									10.313274	

DOY	TIME	SWC (Sim1520)	SWC(Avg15)	SUMABS	N	MAD	SUMSQR	RMSD		
192	100			39.13795	543	0.072	3.1133321	0.076	3.7529542	-0.420137
									0.0804711	0.0143987
									0.8008127	0.0130708
214	2400								2175.0369	541
									0.3715934	0.092427
									46.637291	
									1.4074695	0
									0.1291015	#N/A
									0.4873227	0.0209697
									514.24465	541
									0.0525895	0.2378927
									10.90204	
DOY	TIME	SWC (Sim1520)	SWC(Avg15)	SUMABS	N	MAD	SUMSQR	RMSD	1.282037	-0.014629
176	100			15.470024	384	0.040	0.6420613	0.041	0.0889839	0.0173296
									0.3520775	0.00693
191	2400								207.57668	382
									0.0099688	0.0183454
									14.407522	
									1.2069445	0
									0.0890668	#N/A
									0.3508688	0.0069364
									206.4789	382
									0.0088352	0.0183797
									13.550999	
DOY	TIME	SWC (Sim1520)	SWC(Avg15)	SUMABS	N	MAD	SUMSQR	RMSD	2.6640823	-0.282118
146	100			50.174169	932	0.054	3.1781655	0.058	0.0594434	0.0120132
									0.6835204	0.0166845
191	2400								2008.5777	930
									0.5591309	0.2588855
									44.817159	
									1.2702833	0
									0.075028	#N/A
									0.49582	0.0210587
									914.57921	930
									0.1276188	0.4124275
									16.930794	

DOY	TIME	SWC (Sim3035)	SWC(Avg30)	SUMABS	N	MAD	SUMSQR	RMSD	1.9861139	-0.17707
192	100			26.029562	543	0.048	1.2967628	0.049	0.0302416	0.0069045
									0.8885496	0.0055263
214	2400								4313.1782	541
									0.1317253	0.0165222
									65.674791	
									1.2112729	0
									0.0450167	#N/A
									0.7530445	0.0082263
									1649.6781	541
									0.0490338	0.0366105
									26.907167	
DOY	TIME	SWC (Sim4550)	SWC(Avg45)	SUMABS	N	MAD	SUMSQR	RMSD	1.0410006	0.0138277
192	100			13.620843	543	0.025	0.3733402	0.026	0.0341374	0.0090582
									0.632201	0.0088123
214	2400								929.91204	541
									0.0722146	0.0420127
									30.494459	
									1.0930344	0
									0.0342108	#N/A
									0.6306164	0.0088313
									923.60204	541
									0.0796148	0.0421937
									31.949954	

Table A11.4 Quantitative measures of model performance for simulation of profile soil temperatures at different depths in the soil - validation phase.

T(Sim5)	T(Avg5)	SUMABS	N	MAD	SUMSQR	RMSD	1.480561	-15.0777
		2485.1269	1101	2.3	7773.3421	2.7	0.0183472	0.5470668
							0.8556035	1.9812817
							6511.9898	1099
							25562.667	4314.0994
							80.696901	-27.56098
							0.9716411	0
							0.0239226	#N/A
							0.7545096	2.5833618
							3377.753	1099
							11009.486	7334.4602
							40.616025	
T(Sim15)	T(Avg15)	SUMABS	N	MAD	SUMSQR	RMSD	1.0525265	-2.627397
		1289.9463	1101	1.2	2054.7617	1.4	0.0160598	0.4861768
							0.7962638	0.8827489
							4295.2305	1099
							3347.0393	856.39087
							65.538008	-5.404202
							0.965597	0
							0.0162725	#N/A
							0.7908322	0.8944385
							4155.1552	1099
							2816.9981	879.22217
							59.339353	
T(Sim30)	T(Avg30)	SUMABS	N	MAD	SUMSQR	RMSD	1.0097019	-0.862905
		722.83279	1101	0.7	649.55819	0.8	0.0179731	0.5439503
							0.7417163	0.5159128
							3156.0118	1099
							840.0232	292.51649
							56.178392	-1.586368
							0.9811774	0
							0.0179937	#N/A
							0.7411244	0.5165037
							3146.2821	1099
							793.23166	293.1869
							54.528881	

T(Sim45)	T(Avg45)	SUMABS	N	MAD	SUMSQR	RMSD	1.1004588	-3.479784
		478.55043	1101	0.4	283.86345	0.5	0.0143766	0.4391877
							0.8420558	0.2913371
							5859.1529	1099
							497.30898	93.280134
							76.545104	-7.923227
							0.9865254	0
							0.0147817	#N/A
							0.8330298	0.2995459
							5483.0118	1099
							399.66419	98.610797
							66.739697	

Table A11.5 Quantitative measures of model performance for simulation of profile soil water contents at different depths in the soil - validation phase.

SWC (Sim510)	SWC (Avg5)	SUMABS	N	MAD	SUMSQR	RMSD	0.2963334	0.1244082
		94.247125	1101	0.09	15.300614	0.12	0.010951	0.0034426
							0.3998615	0.037799
							732.24395	1099
							1.0462014	1.570208
							27.060006	36.13789
							0.6532985	0
							0.0162676	#N/A
							-0.324326	0.0561502
							-269.1442	1099
							5.4614947	3.46498
							40.159393	
SWC (Sim1520)	SWC (Avg15)	SUMABS	N	MAD	SUMSQR	RMSD	0.2191568	0.1942802
		57.258909	1101	0.05	6.8081059	0.08	0.0067034	0.0020857
							0.4930492	0.0185899
							1068.8632	1099
							0.3693822	0.379797
							32.693473	93.148269
							0.8026001	0
							0.0200924	#N/A
							-3.554501	0.0557204
							-857.7002	1099
							5.368475	3.4121378
							39.945491	
SWC (Sim3035)	SWC (Avg30)	SUMABS	N	MAD	SUMSQR	RMSD	0.1179518	0.2456515
		89.310839	1101	0.08	11.638277	0.10	0.0033768	0.0012738
							0.5261062	0.0079608
							1220.0849	1099
							0.0773219	0.0696482
							34.929713	192.84901
							0.744437	0
							0.0200403	#N/A
							-15.69054	0.0472445
							-1033.154	1099
							3.2820534	2.4530106
							37.146983	

SWC (Sim4550)	SWC (Avg45)	SUMABS	N	MAD	SUMSQR	RMSD	0.1368579	0.242756
		187.14749	1101	0.17	37.867157	0.19	0.0021327	0.001036
							0.7893373	0.0060602
							4117.8716	1099
							0.1512342	0.0403622
							64.170644	234.31052
							0.61513	0
							0.0154	#N/A
							-9.983981	0.0437597
							-998.9452	1099
							3.2723882	2.1044911
							39.943623	
SWC (Sim5560)	SWC (Avg60)	SUMABS	N	MAD	SUMSQR	RMSD	0.9305264	0.0189709
		3.9166482	1101	0	0.0213848	0	0.0033026	0.0010696
							0.9863456	0.0022814
							79387.634	1099
							0.4131952	0.0057201
							281.75811	17.735846
							0.9888641	0
							0.0037459	#N/A
							0.9824337	0.0025876
							61464.118	1099
							0.4666429	0.0073588
							263.98645	

Table A11.6 Summary statistics for inferring variable root-zone weighted-average soil water contents from surface layer soil water content - model simulation results.

WAVG010	WAVG05	0.9279294	0.021984	WAVG015	WAVG05	0.827408	0.0527673
		0.0009947	0.0001989			0.0020524	0.0004103
		0.9979382	0.0024756			0.9890585	0.005108
		870273.03	1798			162530.86	1798
		5.333673.	0.0110195			4.2406845	0.0469126
		1.0309541	0			1.0746942	0
		0.0027824	#N/A			0.0065661	#N/A
		0.9838675	0.006925			0.888007	0.0163421
		109654.04	1798			14256.57	1798
		6.5932349	0.0862233			7.2087676	0.480181
WAVG020	WAVG05	0.742138	0.0790035	WAVG025	WAVG05	0.6711538	0.1008126
		0.0026415	0.0005281			0.002934	0.0005866
		0.9777287	0.0065743			0.9667805	0.0073023
		78933.858	1798			52326.814	1798
		3.411661	0.0777127			2.7902342	0.0958751
		1.1123762	0			1.1435972	0
		0.0097047	#N/A			0.012272	#N/A
		0.6993911	0.0241535			0.4188267	0.0305432
		4183.1925	1798			1295.7417	1798
		7.7869079	1.048937			8.2999323	1.6773296
WAVG030	WAVG05	0.6109137	0.1192688	WAVG035	WAVG05	0.5581846	0.1353239
		0.0030459	0.0006089			0.0030626	0.0006123
		0.9572175	0.0075807			0.9486517	0.0076224
		40228.535	1798			33217.745	1798
		2.3118319	0.1033265			1.9299777	0.1044652
		1.1698494	0			1.1923602	0
		0.014423	#N/A			0.016286	#N/A
		0.0407118	0.0358965			-0.452001	0.0405333
		76.306313	1798			-559.7092	1798
		8.7556102	2.316833			9.164974	2.954014

WAVG040	WAVG05	0.5120624	0.1493757	WAVG045	WAVG05	0.4709537	0.1619509
		0.0030122	0.0006022			0.0029436	0.0005885
		0.9414285	0.0074968			0.9343699	0.0073261
		28899.528	1798			25597.968	1798
		1.6242108	0.1010512			1.3738932	0.0965022
		1.2120897	0			1.2299131	0
		0.0179114	#N/A			0.0193677	#N/A
		-1.071053	0.0445788			-1.84125	0.0482033
		-929.8426	1798			-1165.18	1798
		9.5371015	3.5731091			9.8833121	4.177761
WAVG050	WAVG05	0.4347241	0.1731515	WAVG055	WAVG05	0.4027928	0.1832266
		0.0028758	0.0005749			0.0027836	0.0005565
		0.9270582	0.0071573			0.9209197	0.006928
		22851.785	1798			20938.37	1798
		1.1706416	0.0921072			1.004986	0.0862992
		1.2461731	0			1.2614573	0
		0.0206677	#N/A			0.0218357	#N/A
		-2.7675	0.0514387			-3.866106	0.0543457
		-1320.76	1798			-1428.505	1798
		10.206142	4.7574063			10.513809	5.3103097
WAVG060	WAVG05	0.3742147	0.1923758				
		0.0027168	0.0005432				
		0.9134333	0.0067618				
		18972.112	1798				
		0.8674375	0.0822076				
		1.2757557	0				
		0.0229007	#N/A				
		-5.150671	0.0569964				
		-1505.674	1798				
		10.805767	5.8409552				

Table A11 7 Summary statistics for inferring profile soil water contents from surface layer soil water content - model simulation results: model initialized from remotely-sensed data.

SWC(Sim5)	SWC(Sim0)	0.891218	0.0498208	SWC(Sim10)	SWC(Sim0)	0.6941438	0.1102995
		0.0044429	0.0005833			0.0047719	0.0006265
		0.9572272	0.01375			0.9216839	0.0147682
		40238.075	1798			21160.233	1798
		7.6075104	0.3399343			4.6150192	0.3921415
		1.1952272	0			1.3671978	0
		0.0100017	#N/A			0.0204042	#N/A
		0.7832381	0.0309535			-0.431898	0.0631476
		6496.8166	1798			-542.3237	1798
		14.180374	1.722703			20.342227	7.1697417
SWC(Sim15)	SWC(Sim0)	0.5687652	0.1471775	SWC(Sim20)	SWC(Sim0)	0.4862509	0.1693336
		0.0045141	0.0005927			0.0044142	0.0005795
		0.8982635	0.0139705			0.8709469	0.0136613
		15875.105	1798			12134.251	1798
		3.0984231	0.3509246			2.2646207	0.3355616
		1.466851	0			1.5195348	0
		0.0268533	#N/A			0.0307744	#N/A
		-2.600179	0.0831066			-5.272493	0.0952417
		-1298.58	1798			-1511.352	1798
		24.950646	12.418268			27.863329	16.309624
SWC(Sim25)	SWC(Sim0)	0.4107976	0.1856534	SWC(Sim30)	SWC(Sim0)	0.3413971	0.1985075
		0.0047209	0.0006198			0.0051191	0.0006721
		0.8081126	0.0146103			0.7121185	0.0158428
		7572.0782	1798			4447.6252	1798
		1.6163318	0.3838001			1.1163343	0.4512901
		1.543666	0			1.5527019	0
		0.0337235	#N/A			0.0360685	#N/A
		-8.792	0.1043687			-13.29152	0.111626
		-1614.381	1798			-1672.191	1798
		29.732632	19.585291			30.990474	22.403738
SWC(Sim35)	SWC(Sim0)	0.2793634	0.2088064	SWC(Sim40)	SWC(Sim0)	0.2273304	0.2168313
		0.0054525	0.0007159			0.0056783	0.0007455
		0.5935025	0.0168744			0.4713035	0.0175733
		2625.1512	1798			1602.8168	1798
		0.747504	0.5119752			0.4949824	0.5552589

		1.5535122	0			1.5504478	0
		0.0379495	#N/A			0.0394103	#N/A
		-18.69175	0.1174472			-24.46797	0.1219683
		-1706.693	1798			-1727.402	1798
		31.855468	24.801354			32.449064	26.747509
SWC(Sim45)	SWC(Sim0)	0.1858734	0.2228539	SWC(Sim50)	SWC(Sim0)	0.1559969	0.2269747
		0.0058371	0.0007663			0.0059587	0.0007823
		0.3606022	0.0180647			0.2759877	0.0184411
		1014.0209	1798			685.3831	1798
		0.3309094	0.5867483			0.233081	0.611453
		1.5457415	0			1.5410101	0
		0.0405051	#N/A			0.041256	#N/A
		-29.78951	0.1253565			-33.70741	0.1276806
		-1739.603	1798			-1746.195	1798
		32.840322	28.25423			33.072014	29.311584
SWC(Sim55)	SWC(Sim0)	0.1401275	0.2291009	SWC(Sim60)	SWC(Sim0)	0.1401275	0.2291009
		0.0060264	0.0007912			0.0060264	0.0007912
		0.2311881	0.0186506			0.2311881	0.0186506
		540.67341	1798			540.67341	1798
		0.1880708	0.6254262			0.1880708	0.6254262
		1.5381149	0			1.5381149	0
		0.0416442	#N/A			0.0416442	#N/A
		-35.71283	0.1288819			-35.71283	0.1288819
		-1749.025	1798			-1749.025	1798
		33.181012	29.865776			33.181012	29.865776

Lebenslauf

Persönliche Daten:

Name:	Baanda Ayub SALIM
Geburt:	27.08.1959 in Kikore, Kondoa, Tansania
Wohnort:	Sokoine Universität, Morogoro, Tansania
Familienstand:	verheiratet mit Zukra B A Salim, geb Abdulrahman Kibakaya zwei Töchter: Keja (9) und Hawa (6)
Eltern:	Salim Swalehe Baanda, Landwirt Mwanahamisi Salim, Landwirt

Schulbildung:	01.1967 - 10.1973	Grundschule, Kikore
	01.1974 - 11.1977	Secondary School, Songea
	05.1978 - 05.1980	High School, Pugu
Militärdienst:	07.1980 - 06.1981	
Studium:	07.1981 - 04.1985	Elektrotechnik-Studium an der Universität Dar es Salaam, Tansania
	09.1986 - 09.1987	Agrartechnik-Studium an der Universität Newcastle upon Tyne, Großbritannien
	10.1987 - 12.1987	Praktikum, Silsoe Research Institute (Sensors Group), Großbritannien
	06 1992 - 09.1992	EDV-Kurse, an der Universität Newcastle upon Tyne, Großbritannien
Berufstätigkeit:	04.1985 - 12.1987	"Tutorial Assistant" an der Sokoine Universität, Morogoro, Tansania
	01 1988 - 06.1991	"Assistant Lecturer" an der Sokoine Universität, Morogoro, Tansania
	07.1991 - zur Zeit	"Lecturer" an der Sokoine Universität, Morogoro, Tansania
	04.1994 - 09.1994	Deutschkurs am Goethe Institut Bremen
	10.1994 - zur Zeit	Promotion an der Universitat Bonn

19/8/99